

# Sheffield Hallam University

*The softening and melting of blast furnace burden materials.*

CLIXBY, George.

Available from the Sheffield Hallam University Research Archive (SHURA) at:

<http://shura.shu.ac.uk/19482/>

## A Sheffield Hallam University thesis

This thesis is protected by copyright which belongs to the author.

The content must not be changed in any way or sold commercially in any format or medium without the formal permission of the author.

When referring to this work, full bibliographic details including the author, title, awarding institution and date of the thesis must be given.

Please visit <http://shura.shu.ac.uk/19482/> and <http://shura.shu.ac.uk/information.html> for further details about copyright and re-use permissions.

SHEFFIELD CITY  
POLYTECHNIC LIBRARY  
POND STREET  
SHEFFIELD S1 1WB

6846

7924513019



**Sheffield City Polytechnic  
Eric Mensforth Library**

**REFERENCE ONLY**

This book must not be taken from the Library

PL/26

R5193

ProQuest Number: 10694363

All rights reserved

INFORMATION TO ALL USERS

The quality of this reproduction is dependent upon the quality of the copy submitted.

In the unlikely event that the author did not send a complete manuscript and there are missing pages, these will be noted. Also, if material had to be removed, a note will indicate the deletion.



ProQuest 10694363

Published by ProQuest LLC (2017). Copyright of the Dissertation is held by the Author.

All rights reserved.

This work is protected against unauthorized copying under Title 17, United States Code  
Microform Edition © ProQuest LLC.

ProQuest LLC.  
789 East Eisenhower Parkway  
P.O. Box 1346  
Ann Arbor, MI 48106 – 1346

THE SOFTENING AND MELTING OF BLAST FURNACE  
BURDEN MATERIALS

BY  
GEORGE CLIXBY

A THESIS SUBMITTED TO THE COUNCIL FOR NATIONAL ACADEMIC  
AWARDS IN PARTIAL FULFILMENT FOR THE DEGREE OF

DOCTOR OF PHILOSOPHY

SUBMITTED FEBRUARY 1981

COLLABORATING ESTABLISHMENT:-

British Steel Corporation  
Teesside Laboratories

SPONSORING ESTABLISHMENT:-

Department of Metallurgy  
Sheffield City Polytechnic  
Pond Street  
Sheffield.



7924513-01

## PREFACE

The work presented in this thesis was undertaken in the Ironmaking Department of the British Steel Corporation's Research Laboratories on Teesside in the period December 1976 to November 1980.

During the project the author attended a series of lectures, given to MSc course students, at Sheffield Polytechnic Metallurgy Department dealing with Heat and Mass Transfer.

Two papers have been published concerning certain aspects of the studies:-

- (a) "Simulated Blast Furnace Reduction of Acid Pellets in the Temperature Range 950-1350°C".  
Ironmaking and Steelmaking 7 (1980), 68-75.
- (b) "Softening and Melting of Superfluxed Sintors and Acid Pellets". 39th Meeting of the Ironmaking Proceedings of AIME, held in Washington DC, March 1980, 370-389. This conference was attended by the author.

The work described in this thesis is, to the best of my knowledge, original except where reference has been made to others, and no part of it has been submitted for an award at any college or university.

## ACKNOWLEDGEMENTS

I would like to thank Mr T A T Fray and Mr R E Thompson for the provision of the acid pellets and sinters used in the experimental studies. Acknowledgement is also due to Mr M G Tonks for his assistance with the writing of the computer program and to Mrs S Howard for her X-ray analyses contribution. I would also like to thank Dr L M Jukes for his help with the petrological aspects, and Mr K Abernethy and Dr S Butler for their assistance with the electron microscope. Acknowledgements are also due to my colleagues in the Research Organisation, especially the Ironmaking Department, for assistance with various aspects of this work.

I would also like to thank my tutors, Dr A W D Hills and Dr G Briggs of Sheffield Polytechnic Metallurgy Department, for their extremely helpful discussions and guidance throughout the supervision of this work.

A special mention of acknowledgement is required for Mr F B Traice, of the British Steel Corporation, for his guidance and assistance in making this project possible, for without his help this project would never have started.

Last, but not least, I would like to thank the Management of the British Steel Corporation Research Organisation for granting permission for the work to be carried out and for providing the necessary equipment and finances.

# THE SOFTENING AND MELTING OF BLAST FURNACE BURDEN MATERIALS

By: George Clixby

## Abstract

The conditions prevailing in the cohesive zone of the blast furnace have been determined from published data and applied in a study of burden materials on an experimental scale. The mechanism of softening and melting of burden materials has been evaluated and it was found that two opposing reactions are important, namely the liquid slag formation reaction and the gaseous reduction reaction. At high temperatures the permeability of burden materials was found to be strongly dependent upon the degree of reduction and the pertaining temperature. A concept, summarised by Temperature-Reduction-Isobar Diagrams, was developed to portray this relationship, each burden material having its own characteristic diagram which can be used to predict the permeability of materials at elevated temperatures.

The influence of gaseous sulphur and alkali vapour in the reducing gas upon the softening and melting behaviour of acid pellets has been evaluated. Sulphur is detrimental because of the formation of a low melting point Fe-S-O eutectic phase which hinders gaseous reduction and lowers the melt-down temperature. Alkali vapours increased the reduction rate of acid pellets, creating a rise in the melt-down temperature. Although the pellets absorbed alkali from the gas phase it had no discernable influence upon the liquid slag formation process. A joint sulphur/alkali study showed that the detrimental influence of sulphur was capable of eliminating the beneficial effect of alkali vapour.

The information accrued from the experimental studies has been used to explain the structure of the cohesive zone found in dissected blast furnaces and to suggest methods to improve the performance of existing furnaces.

## CONTENTS

	<u>Page No.</u>
PREFACE	i
ACKNOWLEDGEMENTS	ii
ABSTRACT	iii
<u>CHAPTER 1</u>	
<u>INTRODUCTION</u>	1
<u>CHAPTER 2</u>	
<u>LITERATURE REVIEW</u>	3
2.1    The Development of the Blast Furnace Process	3
2.1.1    Prepared Burdens	4
2.1.2    Blast Injectants	5
2.1.3    High Top Pressure	7
2.1.4    High Blast Temperature	8
2.1.5    Improvements in Burden Distribution	9
2.2    Iron Ore Pellets	9
2.2.1    Fluxed Pellets	11
2.2.2    Reduction Mechanisms Operating in Acid Pellets	12
2.2.2.1    Gaseous Reduction	12
2.2.2.2    Kinetic Considerations	14
2.2.2.3    Direct Reduction	17
2.2.3    Influence of Alkali upon Reduction	18
2.3    Iron Ore Sinters	19
2.3.1    Structure of Sinter	20
2.3.1.1    Reduction of Sinter	21
2.4    Burden Behaviour in the Blast Furnace	22
2.4.1    Japanese Dissection Studies	23

<u>CONTENTS (CONTINUED)</u>	<u>Page No.</u>
2.4.1.1 Reduction Levels	24
2.4.1.2 Temperature Profiles	25
2.4.1.3 Burden Layer Structure within the Cohesive Zone	25
2.4.1.4 Slag Composition Changes	27
2.4.1.5 Metal Composition Changes	28
2.4.1.6 Size Distribution	30
2.4.1.7 Influence of Gas Flow	31
2.5 Cohesive Zone Control	31
2.6 Melting Processes	32
2.7 Methods of Assessing Blast Furnace Burden Quality	33
2.7.1 Physical Tests	34
2.7.2 Reduction Tests	34
2.7.3 Softening Tests	36
<u>CHAPTER 3</u>	
<u>EXPERIMENTAL TECHNIQUES</u>	39
3.1 Sample Manufacture	39
3.1.1 Manufacture of the Acid Pellets	39
3.1.2 Manufacture of the Sinters	40
3.2 Reduction Procedure	40
3.2.1 Pre-Reduction Stage	41
3.2.2 High Temperature Test Procedure	42
3.2.2.1 Determination of the Critical Flow Rate	44
3.2.2.2 Selection of Heating Rate	45
3.2.2.3 Incorporation of Sulphur in the Reducing Gas	46
3.2.2.4 Incorporation of Alkali Vapour into the Reducing Gas	47

<u>CONTENTS (CONTINUED)</u>	<u>Page No.</u>
3.2.2.5    Incorporation of Sulphur and Alkali Vapour in the Reducing Gas	48
3.3            Initial Slag Formation Tests	48
3.3.1         Synthetic Acid Pellets	49
3.3.2         Heating Stage	49
3.4            Gases Used in the Test Procedure	50
3.5            Petrology	51
3.5.1         Sample Preparation	51
3.5.2         Microscope Techniques	52
 <u>CHAPTER 4</u>	
<u>RESULTS</u>	53
4.1            Critical Gas Flow Rate Tests	53
4.2            Reproducibility Tests	54
4.3            Experimental Studies with Acid Pellets	54
4.3.1         Optical and Electron Microprobe Examination of the Fully Oxidised Pellets	54
4.3.2         Initial Slag Formation Tests	55
4.3.2.1       Synthetic Acid Pellets	55
4.3.2.2       Pilot Plant Pellets	56
4.3.3         High Temperature Tests with Acid Pellets	56
4.3.3.1       Tests at a Heating Rate of $200^{\circ}\text{C.hr}^{-1}$	56
4.3.3.2       Tests at a Heating Rate of $400^{\circ}\text{C.hr}^{-1}$	57
4.3.3.3       Variation in Applied Load	57
4.3.3.4       Nitrogen Only Tests	58
4.3.3.5       Low Temperature Pre-Reduction Test	58
4.3.3.6       Interrupted Test	59
4.3.3.7       Tests Incorporating Sulphur in the Reducing Gas	59
4.3.3.8       Tests Incorporating Alkali Vapour in the Reducing Gas	61

# THE SOFTENING AND MELTING OF BLAST FURNACE BURDEN MATERIALS

By: George Clixby

## Abstract

The conditions prevailing in the cohesive zone of the blast furnace have been determined from published data and applied in a study of burden materials on an experimental scale. The mechanism of softening and melting of burden materials has been evaluated and it was found that two opposing reactions are important, namely the liquid slag formation reaction and the gaseous reduction reaction. At high temperatures the permeability of burden materials was found to be strongly dependant upon the degree of reduction and the pertaining temperature. A concept, summarised by Temperature-Reduction-Isobar Diagrams, was developed to portray this relationship, each burden material having its own characteristic diagram which can be used to predict the permeability of materials at elevated temperatures.

The influence of gaseous sulphur and alkali vapour in the reducing gas upon the softening and melting behaviour of acid pellets has been evaluated. Sulphur is detrimental because of the formation of a low melting point Fe-S-O eutectic phase which hinders gaseous reduction and lowers the melt-down temperature. Alkali vapours increased the reduction rate of acid pellets, creating a rise in the melt-down temperature. Although the pellets absorbed alkali from the gas phase it had no discernable influence upon the liquid slag formation process. A joint sulphur/alkali study showed that the detrimental influence of sulphur was capable of eliminating the beneficial effect of alkali vapour.

The information accrued from the experimental studies has been used to explain the structure of the cohesive zone found in dissected blast furnaces and to suggest methods to improve the performance of existing furnaces.

4.3.3.9	Inclusion of both Sulphur and Alkali Vapour in the Reducing Gas	62
4.3.3.10	Dropped Materials	63
4.4	Experimental Studies with Sinters	64
4.4.1	Examination of Sinters in the As-Received State	64
4.4.2	Initial Slag Formation Tests	65
4.4.3	High Temperature Tests with Sinters	65
4.4.3.1	Sinters Tested in the 'As-Received' State	65
4.4.3.2	Sinters Tested after Pre-Reduction	66
4.5	High Temperature Reduction Tests with Sinter/Pellet Mixtures	66
4.6	Photographic Plates	67
4.6.1	High Temperature Apparatus	67
4.6.2	Acid Pellets	67
4.6.2.1	Initial Slag Formation Tests with Acid Pellets	67
4.6.2.2	Structure after the High Temperature Test	68
4.6.2.3	Dropped Material	68
4.6.2.4	Microstructure of the Sample Bed after the High Temperature Test	69
4.6.3	Sinters	70
4.6.3.1	Initial Slag Formation Tests	70
4.6.3.2	Structure after the High Temperature Test	70
4.6.4	Sinter/Pellet Mixtures	70
4.6.5	EDAX Spectra	71
4.6.5.1	Acid Pellets in the Oxidised State	71
4.6.5.2	Acid Pellets in the Softened State	71
4.6.5.3	Icicles	71

4.6.5.4	Acid Pellets after the High Temperature Tests with Alkali Vapour in the Reducing Gas	71
---------	--	----

CHAPTER 5

	<u>DISCUSSION</u>	73
5.1	The Softening and Melting Process - Stage I	73
5.1.1	Melting Behaviour of Synthetic Acid Pellets	77
5.1.2	Quantity of Wustite/Residual Slag Reaction Sites	79
5.2	The Softening and Melting Process - Stage II	80
5.2.1	Temperature - Reduction - Isobar Diagrams	82
5.2.1.1	Nitrogen Only Tests	83
5.2.1.2	Reduction Test with Fully Oxidised Pellets	84
5.2.1.3	Gas Pressure Drop - Contraction Relationship	85
5.2.2	The Mechanism of the Softening and Melting Process in Burden Materials	88
5.2.2.1	Changes in Slag Composition During the High Temperature Reduction of Acid Pellets	91
5.2.2.2	Reduction Characteristics of Burden Materials	93
5.2.2.3	Reduction-Time-Temperature Considerations	95
5.3	Comparison of the Proposed Softening and Melting Mechanism with the Japanese Dissection Studies	97
5.4	Effect of Possible Modifying Phenomena on the Proposed Softening and Melting Mechanism	102
5.4.1	Effect of Applied Load	102
5.4.2	Effect of Pre-Reduction Temperature	103

<u>CONTENTS (CONTINUED)</u>		<u>Page No.</u>
5.4.3	Influence of Sulphur in the Reducing Gas	105
5.4.4	Influence of Alkali Vapour in the Reducing Gas	109
5.4.5	Influence of Both Sulphur and Alkali Vapour	112
5.5	Iron Carburisation	113
5.6	Combinations of Sinter and Pellets	115
5.7	Application to the Blast Furnace Process	116
5.7.1	Sinter Burdens	117
5.7.2	Acid Pellet Burdens	119
5.7.3	Acid Pellets and Superfluxed Sinter Burdens	122
 <u>CHAPTER 6</u>		
	<u>CONCLUSIONS</u>	124
 <u>CHAPTER 7</u>		
	<u>SUGGESTIONS FOR FURTHER WORK</u>	128
 <u>REFERENCES</u>		130
<u>TABLES</u>	1 - 41	138
<u>FIGURES</u>	1 - 110	165
<u>PLATES</u>	1 - 50	251
 <u>APPENDIX I</u>		AI
<u>APPENDIX II</u>		AII
<u>APPENDIX III</u>		AIII

INTRODUCTION

The blast furnace process for the production of iron is of paramount importance because it is the only process capable of supplying iron in the vast quantities required at an economic price. Blast furnaces have been in existence for *several* centuries, yet even today the reactions occurring inside the furnace are not fully understood. One of the major problems is the difficulty of obtaining samples from an operating furnace. Even if samples can be obtained they only represent a minute quantity of the volume of the furnace. The use of vertical and horizontal probes allow the sampling of gas, measurement of temperature and gas pressure. Over the years these techniques have added to the fund of knowledge of the blast furnace process. However, these probes are limited to the stack region of the furnace, generally covering the temperature range of 20 - 1000°C. In the early seventies the Japanese quenched several operating furnaces with water and systematically dissected their interiors producing a wealth of information on the temperature distribution, size distribution of the burden, degree of reduction of the burden and the recirculation of sulphur and alkalis within the furnace. One of the most interesting discoveries was the arrangement of the softening and melting or cohesive zone. Each furnace had a different arrangement of the cohesive zone depending upon the operating practice prior to the quenching operation. This observation developed into a new operating philosophy for blast furnaces in which control of the shape and size of the cohesive zone was vitally important if productivity and campaign life were to be maximised.

The work described in this thesis was undertaken to obtain a greater understanding of the softening and melting behaviour of blast furnace burdens. At the time of initiation of this study the British Steel Corporation's 14 m blast furnace was under

construction at the Redcar Works. The furnace was to operate with an acid pellet/superfluxed sinter burden, consequently these materials were selected for the experimental study in order that the work should have a specific application. Also at the time of initiation an experimental reduction under load apparatus was in the process of construction and it was planned to use this apparatus to study the influence of several variables upon the behaviour of acid pellets at elevated temperatures. The aspects selected for evaluation were heating rate, influence of the degree of reduction, variation in applied load and the influence of minor constituents in the reducing gas (sulphur and alkali).

The detailed studies with acid pellets were to provide the basis for a greater understanding of the behaviour of burden materials inside the cohesive zone of the blast furnace and the work was to be extended to include sinters and sinter/pellet mixtures, albeit studied to a lesser degree. Finally the information arising from the experimental studies was to be examined in relation to the findings of the Japanese dissection studies and applied to the improvement of blast furnace operation.

LITERATURE REVIEW

The blast furnace process for the manufacture of iron has been in existence for a considerable number of decades. The technological development of the process has led it from a small production unit, consuming large quantities of fuel to its present state where furnaces designed to produce 10,000 tonnes per day of iron are fairly common in several industrial countries, such as Japan, Italy, Germany and the UK. Even with this dramatic increase in size and output of the blast furnace, many of the reactions occurring within the furnace are still unknown.

Modern furnaces operate predominantly on sinter, pellets or sinter/pellet burdens. The type of sinter and/or pellets depends upon individual plants operating philosophy, thus the manufacture and reduction characteristics of these materials are of paramount importance to the blast furnace process.

2.1 The Development of the Blast Furnace Process

The developments that have taken place in blast furnace operation have been introduced gradually, eventually becoming standard operating practice. The majority of developments have occurred since the end of the Second World War and it is possible to list the major developments in an approximate chronological order<sup>1</sup>:-

- (a) Effective use of prepared burdens
- (b) Blast injectants
- (c) High top pressure
- (d) High blast temperature
- (e) Improved control of burden distribution

Occurring simultaneously with these developments has been the gradual increase in physical size of the blast furnace, culminating with today's 10,000 tonne per day units. An indication of the timing of these developments can be obtained from Figures 1 and 2<sup>2,3</sup>.

#### 2.1.1 Prepared Burdens

The first preparation of burden materials was merely the sizing of the iron ores charged to the furnace (Figure 2). The closer sizing of the burden improved the permeability of the furnace, allowing more wind to be blown, thus increasing furnace output. Additionally the efficiency of the reduction reactions also increased because of the removal of the larger ore lumps, thus decreasing the coke rate.

Sintering of iron ores prior to charging was the second important step in burden preparation, but sintering was originally developed to render such waste iron bearing materials as blast furnace flue dust, mill scale and ore fines into a usable blast furnace feed. This concept, however, changed rapidly after the success in Russia with self-fluxing sinter in the mid 50's,<sup>4</sup> allowing the fluxes to be removed from the charging procedure and to be incorporated within the sinter. Trials in the USA with a 100% self-fluxing sinter burden reduced the coke rate from 900 to ~600 kg/tonne whilst production increased to 975 tonnes per day from the 590 tonnes per day normally achieved with a 100% ore burden<sup>4</sup>. It was found that the limitation to production was the wide range of particle size charged, causing a restriction in wind volume. An attempt to overcome the limitation by close screening of the sinter during a trial period of six weeks proved successful in decreasing the coke rate and raising production (Table 1), but the cost of sizing the sinter made the operation uneconomic.

The current situation is that sinter is now an established burden component in modern blast furnace plants and it is still under continuous investigation by researchers in order to further improve its properties (refer to Section 2.3).

The depletion of readily available high grade ores made it necessary for suppliers to upgrade their product by means of beneficiation followed by the production of high grade iron ore pellets from the concentrate<sup>4</sup>. This process gained wide acceptance in the USA resulting in the burden charged to blast furnaces having a high iron content and a low gangue content, which in turn led to a further increase in production coupled with a fall in coke rate (Figures 3 and 4). Another improvement claimed with pellets was that the permeability of the burden increased due to the closer sizing (Table 2). In Japan and Europe the use of pellets is not as universal as in the USA and furnaces still operate predominantly on sinter burdens with pellets contributing a small proportion of the overall charge. Indeed Ishikawa<sup>3</sup> states that a high sinter ratio is essential for the stable operation of large blast furnaces because sinter has superior high temperature properties and better distribution properties (pellets roll easily, making control of distribution difficult). Also the use of sinter maintains a balance between lump coke and coke breeze in a steelworks with a minimum coke rate (blast furnace coke + breeze).

### 2.1.2 Blast Injectants

Three injectants are in general use: steam, hydrocarbons and oxygen. Injection of these species either singly or simultaneously affects the flame temperature, i.e. the temperature of the flame in the combustion zone of the tuyere. Steam and hydrocarbons lower the flame temperature whilst oxygen increases it.

The theoretical flame temperature can be calculated<sup>3</sup> and it is extremely important for maintaining smooth operation and raising productivity with large quantities of oxygen and fuel oil (Figure 5). A low flame temperature prevents reaction in the furnace and leads to furnace chilling. A high flame temperature may impair the permeability as a result of expansion of the melting zone and evaporation of alkalis and SiO<sub>2</sub> in the burden. In order to ensure a smooth operation it is necessary to control the theoretical flame temperature by varying the quantities of injectants<sup>5</sup>.

Looking at the three injectants separately; steam reacts with coke to produce hydrogen which increases the extent of reduction of burden materials, thus decreasing the fuel rate<sup>6</sup>. Hydrocarbons are the main injectants, the type of hydrocarbon depending upon local conditions. Fuel oil is probably used most, followed by natural gas, coke oven gas, fuel oil/coal slurry and in some instances pulverised coal<sup>4</sup>. Injection of hydrocarbons provides additional quantities of hydrogen and carbon monoxide in the blast furnace, increasing the degree of reduction of the burden, which in turn provides for a decrease in coke rate. Although the economics change with world events, coke has always been more expensive than fuel oil, thus the substitution of oil for coke has been economic, with additional pressure for the substitution coming from the diminishing supply of good quality coking coal<sup>3</sup>. As an example of the extent of oil injection relative to the overall fuel rate, some furnaces in Japan are operating with oil rates in excess of 70 kg per tonne and coke rates of ~ 450 kg per tonne, i.e. the oil is ~ 13% of the total fuel consumed. A problem with oil injection is ensuring complete combustion at the tuyere; incomplete combustion gives rise to soot formation which impairs furnace permeability, causing adverse effects upon furnace operation. Insufficient combustion can be remedied by providing sufficient excess oxygen in the blast and by burner design<sup>5,7</sup>.

Oxygen injection raises the quantity of excess oxygen and increases the flame temperature, which counteracts the drop in flame temperature caused by steam and hydrocarbon injection. It is also useful for decreasing the quantity of bosh gas, thus minimising the extent of channelling of the gas in the furnace and the extent of flooding and loading<sup>4</sup>. (The latter is the situation when the molten slag is prevented from descending due to the upward gas velocity. Eventually the weight of slag becomes sufficient to overcome the gas flow and it descends - flooding - causing irregular furnace operation). When the ratio of oxygen in the blast is gradually increased the volume of gas produced per tonne of iron decreases, causing a drop in the quantity of heat transfer from the gases to the solids in the shaft, hence a decrease in the temperature of the shaft. Furthermore, the increase in productivity through oxygen enrichment accelerates the burden descent rate, resulting in less time for heat transfer. Consequently burden materials enter the high temperature zone without being sufficiently pre-heated, thus chilling the furnace and causing slipping and hanging of the burden<sup>5</sup>.

The practice of using injectants requires careful control with regards to three limits: limit in heat transfer between gases and solids, limit of theoretical flame temperature and the limit of complete combustion of oil<sup>5</sup>. Control within these limits provides low fuel rates and high productivity.

### 2.1.3 High Top Pressure

Russia was the first country to introduce high top pressure on their furnaces on a wide scale as a means of rapidly increasing production following the end of World War II<sup>4</sup>. The benefit of high top pressure is that it reduces the gas velocity in the furnace, allowing more time for gaseous reduction, thus decreasing

the fuel rate. Dust losses also decrease because the lower gas velocity is insufficient to convey the coarser dust particles<sup>6</sup>. Alternatively one can blow more wind and thus raise production whilst maintaining the same gas velocity in the furnace, hence preventing channelling, flooding and loading.

The main disadvantage is that to accommodate the increased gas pressure, stronger construction is required throughout the blast furnace system, from stoves, through bustle pipe, furnace walls, top and gas cleaning plant, which is obviously expensive<sup>4</sup>. Indeed the furnace top alone needs special design in order to equalise gas pressure in the charging system and prevent wear of the furnace bells. Another disadvantage is the loss in energy in the high pressure top gas, although efforts to recover this energy are underway, e.g. Mizushima No.2 blast furnace in Japan was modified in 1974 to recover the energy in the top gas<sup>8</sup>. Although there are problems with the application of high top pressure from an engineering aspect, the operation of large blast furnaces requires the use of it to (a) lower the fuel ratio and (b) permit the expansion of the range of adjustment of productivity coefficient<sup>8</sup> (Figure 6).

#### 2.1.4 High Blast Temperature

The air entering the furnace through the tuyeres is heated by the combustion of the coke, consequently the hotter the incoming air, the less coke consumed in further heating inside the tuyere region. Pre-heating of the air is not a new innovation, indeed over 100 years ago furnace stoves were in existence<sup>9</sup>, however, it is only relatively recently that temperatures in excess of 1300°C have been obtained<sup>3</sup>. The achievement of higher temperatures is due to modifications to stove design<sup>1</sup>, i.e. increasing the area of heated surface of chequer work by alteration of the shape of the bricks; using a higher quality refractory able to withstand the higher temperatures and finally

providing external combustion chambers which also increases the heated surface area.

### 2.1.5 Improvements in Burden Distribution

Control of the distribution of burden materials is important for improving the gas utilisation and lowering the fuel rate (Figures 7 and 8). Correct distribution is also essential to control the shape of the cohesive zone of the blast furnace, thus maximising production and minimising the gas flow at the furnace wall, the latter prolonging the life of the furnace<sup>3</sup>.

As furnace size increased the distribution of burden material required to provide a stable gas distribution inside the furnace could not be maintained with conventional charging equipment due to differences in compiling angle, density and shape<sup>3</sup>. These problems were overcome by the installation of movable armour to control the distribution of material as it leaves the charging bell (Figure 9). A recent development in furnace charging is the bell-less top, which is a rotating chute capable of accurately distributing the charge to any position on the furnace stockline<sup>10</sup>.

### 2.2 Iron Ore Pellets

Consider now the manufacture and reduction properties of iron ore pellets. In their manufacture the iron ore is concentrated by crushing and removing the liberated gangue material. Generally some quartz is added in the manufacture of acid pellets in order to improve the pellet properties. The majority of pellets used at the moment are of the acid type, i.e. without any deliberate substantial flux addition. During manufacture acid pellets are fired at  $\sim 1300 - 1340^{\circ}\text{C}$ <sup>11</sup> in an

oxidising atmosphere which promotes bonding of the particles by:-

- (a) Sintering of the hematite grains
- (b) Oxidation and subsequent sintering of the magnetite grains
- (c) Slag bonding

The latter is caused by fusion of the small traces of gangue and the bentonite, used in the pelletising process to ensure sufficient wet strength. This slag phase consists essentially of lime, silica, ferric oxide and small traces of alkalis, magnesia, alumina, etc.<sup>12</sup>. An indication of the chemical composition of this slag phase can be obtained by referring to the CaO - SiO<sub>2</sub> - Fe<sub>2</sub>O<sub>3</sub> phase diagram<sup>13</sup> (Figure 10). A point worth mentioning is that equilibrium diagrams must be used carefully as in the majority of processes the reactions are rarely at equilibrium, nevertheless, such diagrams are extremely useful. Very little reaction, if any, occurs between the quartz grains and the hematite during firing and consequently acid pellets are comprised of hematite, quartz, a slag phase and in some cases, if insufficient firing has taken place, magnetite, originating from any magnetite ores in the pellet blend.

The manufacturing process for producing acid pellets is now well proven, such that almost every company operating blast furnaces use some of them in the furnace burden. The amount used in the burden depends upon the operating practice adopted. It is fair to state that some furnaces operate entirely on acid pellets as the source of iron units. The flux for the slag formation process arises from limestone and dolomite charged separately to the furnace.

### 2.2.1. Fluxed Pellets

In recent years there has been substantial interest in the use of fluxed pellets<sup>14-17</sup>, i.e. with the fluxes incorporated into the pellet, hence avoiding the necessity of charging them separately into the furnace. Fluxed pellets can be manufactured with lime additions, as the flux, or dolomite. As the basicity of the pellets rises with the flux additions the microstructure changes accordingly.

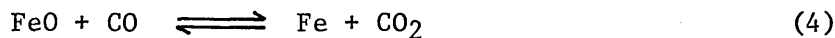
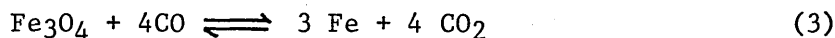
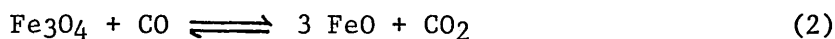
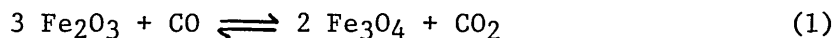
Considering lime fluxed pellets, the addition of lime has an influence on the slag composition and quantity, also the quantity of hematite. The addition of lime creates the possibility of a reaction between the hematite and the lime to produce calcium ferrites ( $\text{CaO} - \text{Fe}_2\text{O}_3$  or  $2 \text{CaO} \cdot \text{Fe}_2\text{O}_3$  depending upon the lime concentration (Figure 11)<sup>14,18</sup>. With limestone fluxed pellets the firing temperature is lower than that of acid pellets to avoid excessive slag formation occurring<sup>14</sup>. Consequently in limestone fluxed pellets one can expect to find grains of hematite surrounded by calcium ferrites caused by the chemical attack by lime. In some cases the original hematite grain may be fully digested, this obviously depending on the original hematite grain size. The effect of lime on the slag phase, as stated, is two-fold. Firstly a general increase in quantity of the slag and secondly a change in basicity. The exact composition naturally depends upon the quantity of phases reacting, but the possibilities can be surmised from Figure 10. The marked areas are those liquid at temperatures between the solidus and  $1300^\circ\text{C}$ <sup>14</sup>. One of the problems with limestone fluxed pellets is the relatively poor reduction properties. This deficiency of lime-fluxed pellets has led to the production of pellets fluxed with dolomite, instead of lime<sup>14</sup>.

The addition of magnesia to iron oxide results in a solid state reaction between the two and an increase in melting temperature<sup>17</sup> (Figure 12)<sup>19</sup>. Hence in dolomite fluxed pellets magnesio ferrites  $[MgO.Fe_2O_3 \text{ or } (Mg.Fe)O.Fe_2O_3]$  are produced. The quartz may not be fully assimilated in dolomite fluxed pellets because melting between magnesia and silica does not occur at the firing temperature<sup>14</sup>. Thus any reaction occurring is a solid state reaction (Figure 13)<sup>20</sup>.

## 2.2.2 Reduction Mechanisms Operating in Acid Pellets

### 2.2.2.1 Gaseous Reduction

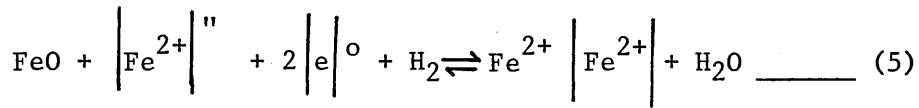
Acid pellets follow a reduction path illustrated in Figure 14<sup>21</sup>. As the oxygen is removed the iron oxide moves from hematite  $\rightarrow$  magnetite  $\rightarrow$  wustite (at temperatures greater than 560°C)  $\rightarrow$  metallic iron. These phase changes are represented by the following gaseous reactions, using carbon monoxide as the reducing agent.



The mechanism of hematite reduction has been extensively studied by numerous workers and the reduction of hematite does not take place in discrete steps, i.e. to magnetite, then to wustite, etc, but reduction produces a topochemical structure, provided the reduction potential of the gas is great enough, i.e.

one normally obtains a structure of a hematite particle, surrounded by a layer of magnetite, then wustite and finally an outer layer of metallic iron<sup>22</sup>.

Wustite as shown in Figure 14 is non-stoichiometric, i.e. it is deficient in iron ions. These vacancies are the important defects in the reduction behaviour of iron oxides as they make possible the diffusion of iron through the iron oxide lattice. The removal of oxygen from wustite produces a filling up of the iron ion vacancies at the oxide surface<sup>23</sup>, viz:-



where:-

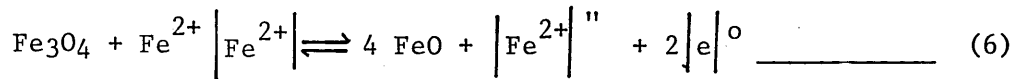
$\left| \text{Fe}^{2+} \right|''$  is an iron ion vacancy.

$\left| e \right|^{\circ}$  is an electron deficiency to maintain electrical neutrality.

$\text{Fe}^{2+} \left| \text{Fe}^{2+} \right|$  is a divalent iron ion in the normal lattice position for wustite.

The surface reduction sets in motion a diffusion of vacancies and electron defects from the interior of the oxide towards the reaction interface. Figure 15 shows diagrammatically the curves of equal concentration of vacancies in an oxide with a wavy surface and the corresponding flows  $j(\left| \text{Fe}^{2+} \right|'')$ , the magnitude of these being indicated by the thickness of the arrows. As  $j(\left| \text{Fe}^{2+} \right|'') \sim dy/dx$  the flow towards a depression has a higher value than the flow towards an elevated portion.

With the reduction of wustite the inward flow of metallic ions react with the magnetite layer, viz:-



so reducing the magnetite. The reaction (5) then takes place and the cycle repeats itself gradually reducing the magnetite.

#### 2.2.2.2 Kinetic Considerations

The kinetics of the reduction of iron oxides has been extensively examined by many workers, perhaps two of the best known being McKewan<sup>24</sup> and Edstrom<sup>25</sup>. Yet even today conflict still exists as to the rate controlling step. The process of gaseous reduction of iron oxides necessitates the following steps:-

- (a) Diffusion of the reacting gas from the bulk gas phase through the boundary layer.
- (b) Diffusion of the gas through the product layer to the reaction interface.
- (c) Adsorption of the gas onto the reaction interface.
- (d) Chemical reaction at the interface.
- (e) Desorption of the product gas from the reaction interface.
- (f) Diffusion of the gaseous reaction products away from the reaction interface to the particle surface.
- (g) Diffusion of the product gas through the boundary layer into the bulk gas phase.

Although great conflict exists as to the rate limiting step or steps, generally reduction of iron oxides conform to an equation derived by McKewan<sup>24</sup>.

$$K_1 = \frac{K_w}{d_o} = \frac{r_o [1 - (1-R)^{\frac{1}{3}}]}{t} \quad (7)$$

where:-

$K_1$  = rate of advance of the hematite/magnetite interface, mm.min.<sup>-1</sup>

$K_w$  = rate constant, g.mm.<sup>-2</sup> min.<sup>-1</sup>

$d_o$  = density of the pure iron oxide sphere, g.mm<sup>-3</sup>

$r_o$  = radius of iron oxide sphere, mm

$R$  = fractional conversion of hematite to magnetite and

$t$  = reaction time, minutes

McKewan claims that as the reduction rate of iron oxides conform to this equation the rate limiting step is the chemical reaction.

Hills<sup>26</sup> used mass transport principles to illustrate that a reaction controlled by mass transfer and diffusion alone can have the specific characteristics frequently used to identify a chemically controlled reaction, particularly the linearity of  $[1 - (1-R)^{\frac{1}{3}}]$  with time. Hills postulated that the reaction is controlled by both processes of (i) gas diffusion through the product layer and (ii) transport through the boundary layer

external to the particle. A form of Hills rate equation can be expressed as:-

$$3 \left[ 1 - (1-R)^{2/3} \right] - 2 R(1-B_m) = \beta_2 t \quad (8)$$

where:-

R = fractional reduction

t = reduction time, seconds

$B_m$  =  $DE/Kg r_0$ , Biot modulus for mass transfer, i.e. the ratio of the diffusion resistance within the product layer and mass transfer resistance outside the particle.  $DE$  = diffusion coefficient in the product layer,  $\text{mm}^2 \text{sec}^{-1}$ .  $Kg$  = mass transfer coefficient to the surface of the reacting sphere,  $\text{mm} \cdot \text{sec}^{-1}$ .  $r_0$  = radius of sphere, mm.

$\beta_2$  = a constant for a reduction reaction and depends upon the iron oxide sphere properties and experimental conditions.

Hills showed that equation (8) could be rearranged as:-

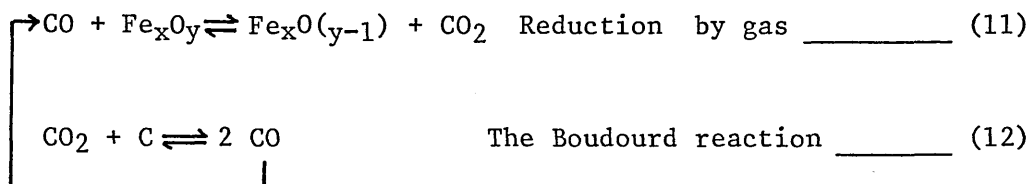
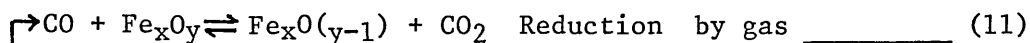
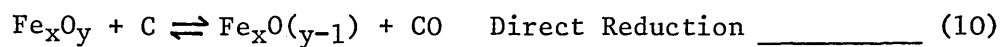
$$\left[ 1 - (1-R)^{2/3} \right] = f(\beta_2 t, B_m) \quad (9)$$

where  $B_m$  is a parameter, the value of which determines the shape of the curve,  $\left[ 1 - (1-R)^{2/3} \right]$  with  $\beta_2 t$ , and is a function of the make-up of the reduced layer.

In the case of reduction at temperatures of 800°C and upwards, an increase in temperature of gaseous reduction leads to a rise in the reaction rate, provided melting of the particles does not occur<sup>25,27</sup>. An increase in porosity also produces a rise in the reduction rate<sup>27</sup>.

### 2.2.2.3 Direct Reduction

The mechanism of direct reduction of iron oxides with carbon is extremely important in the blast furnace and Yun<sup>28</sup> found that direct reduction only occurred in appreciable quantities at temperatures in excess of 900°C. Baldwin<sup>29</sup> came to the conclusion that the direct reduction reaction (Equation (10)) could actually be split into equations (11) and (12).



where,

$$x = 1, 2 \text{ or } 3 \quad \text{and} \quad y = 1, 3 \text{ or } 4.$$

That is the direct reduction reaction actually occurs via an indirect reduction reaction, indicating that the direct reduction of solid oxides in industrial processes is of no importance with respect to the progress of the reaction.

The situation with liquid iron oxides reacting with carbon is of course quite different in that the area of contact between liquid oxide and solid carbon is much greater than that of solid oxide and solid carbon. Additionally, diffusion of reacting and product species in the liquid is much faster than that in the solid state. These effects lead to much higher reaction rates in liquid oxide/solid carbon systems than in solid oxide/solid carbon systems. The higher the reaction temperature the greater the degree of reduction<sup>30</sup> (Figure 16);

Borgianni<sup>30</sup> found that the rate limiting step for reduction of FeO rich slags changed with the extent of reduction. Nucleation of reduced iron and chemical reaction at the carbon/liquid interface appear to constitute the rate limiting step until a high degree of reduction is attained. At higher reduction levels the slowest step is the diffusion of oxygen through the slag boundary layer.

### 2.2.3 Influence of Alkali upon Reduction

Alkali recirculates inside the blast furnace by vaporisation in the high temperature zone and subsequent deposition on the burden and coke in the cooler regions. The deposited alkali then descends with the burden and coke to be eventually vaporised<sup>31,32</sup>. The nature of this recirculating effect is such that quite high levels of alkali can accumulate inside the blast furnace (refer to Section 2.6) which can influence the reduction of the burden materials. Numerous investigators have examined the influence of alkali on the reduction process<sup>22,31,33,34</sup> using the general techniques of impregnating the sample with alkali salts prior to reduction or by the inclusion of alkali compounds in the raw mix which was then formed into compacts and fired. Some researchers have incorporated alkali vapour into the reducing gas flowing over the sample<sup>35</sup>.

Alkali additions were found to increase the reduction rate of acid and basic pellets<sup>31,33,35</sup> whilst some researchers found that an optimum level of alkali additions existed, above which the reduction rate decreased due to extensive slag formation<sup>33,34</sup>. Takahashi et al<sup>35</sup> found that dolomite fluxed pellets showed a decrease in reduction rate when alkali was included in the reducing gas. Khalafalla and Weston Jr<sup>34</sup> found that the type of alkali species was important, i.e. sodium hydroxide was a better promoter of the reduction reaction than sodium chloride for the same concentration of the sodium cation. The increase in reduction rate that occurs when alkali is added to the iron oxide is caused by the increased swelling exposing a greater surface area to the reducing gas<sup>31</sup>. In addition the alkali causes non-topochemical reduction which means that the surface of the wustite is continually exposed to the reducing gas instead of being shielded by a layer of metallic iron<sup>22,31</sup>. Non-topochemical reduction is caused by the incorporation of alkali cations into the wustite lattice which causes inhomogenisation in the wustite activity, modifying the nucleation behaviour of iron, thus leading to non-topochemical reduction<sup>31,34</sup>.

Pellet swelling seems generally regarded as a symptom of excessive alkali content<sup>31,35</sup>, however, Bleifuss<sup>22</sup> using a reduction under load technique with compacts showed that the concentration and type of alkali compound present could have a significant influence on the reduction/deformation curves, e.g. in general sodium carbonate produced a larger degree of swelling in comparison with the other species of alkali used.

### 2.3 Iron Ore Sinters

Sinter is often the major component of the blast furnace burdens. The chemical composition of sinter depends upon the other components constituting the furnace burden. Generally the

sinter ranges from fluxed ( $\sim 1.2 \text{ CaO/SiO}_2$ ) to super-fluxed ( $1.8 - 2.2 \text{ CaO/SiO}_2$ ); the fluxed sinter being used when the majority of the furnace burden is sinter. Super-fluxed sinter is used when the rest of the burden is acidic in nature, thus balancing the slag chemistry to provide an acceptable slag composition. Compared to pellets, sinter is extremely heterogeneous due to the nature of the sintering process.

### 2.3.1 Structure of Sinter

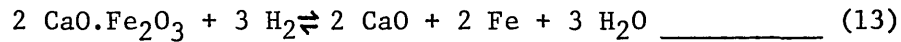
The fluxes, which are mixed with the iron ores, react during sintering, melt and attack the ore particles. Complete digestion of small ore particles may occur, but generally the larger particles only undergo surface attack. During cooling precipitation of different phases occurs within the slag matrix, the overall result being a mixture of phases that are far removed from an equilibrium state and a heterogeneous material whose phases depend upon the segregation of components in the initial mixing<sup>36</sup>, e.g. where particles of lime existed prior to sintering, a lime rich region will be formed. Overall the phases present depend upon the quantity of fluxing agents added. Self-fluxing sinter ( $1.2 \text{ CaO/SiO}_2$ ) is predominantly hematite and magnetite with small quantities of calcium ferrites, produced by a reaction between iron ore and lime<sup>36</sup>. Here the term ferrites refers to the combined quantities of the different species of ferrites which can be produced, depending upon the basicity and the ore particles in the reaction zone. An indication of the possible number of calcium ferrites that can be produced can be obtained from Figure 17<sup>37</sup>. As the basicity increases the proportion of ferrites increase<sup>38</sup> (Figure 18).

CRM workers<sup>39</sup> found that the ferrites were contaminated with silica and alumina and they christened them SFCA (silico ferrite of calcium and alumina). They found that the SCFA conformed to a general formula  $n_1(\text{Fe}_2\text{O}_3) \cdot n_2(\text{SiO}_2) \cdot n_3(\text{Al}_2\text{O}_3) \cdot 5 \cdot \text{CaO}$ , the sum of  $n_1 + n_2 + n_3 \sim 12$ . The calcium content was fairly constant at  $\sim 15$  wt. %. In industrial sinters the following ferrites are usually found:-  
7  $\text{Fe}_2\text{O}_3 \cdot 2 \cdot \text{SiO}_2 \cdot 3 \text{Al}_2\text{O}_3 \cdot 5 \text{CaO}$  and 9  $\text{Fe}_2\text{O}_3 \cdot 2 \text{SiO}_2 \cdot 0.5 \text{Al}_2\text{O}_3 \cdot 5 \text{CaO}$ .

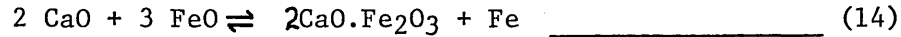
### 2.3.1.1 Reduction of Sinter

The type and quantity of ferrites present in sinter play an important role in the reduction properties. The reducibilities of the ferrites are not constant, but vary from one species to another, as indicated in Table 3<sup>23</sup>. It has been shown that the proportion of ferrites increases as the sinter basicity rises (Figure 18). However, the reducibility does not follow the same trend<sup>38</sup> (Figure 19). Between a basicity of 1.0 and 1.5 the reducibility rises due to the increase in ferrites of the type  $\text{CaO} \cdot 2 \text{Fe}_2\text{O}_3$  and  $\text{CaO} \cdot \text{FeO} \cdot \text{Fe}_2\text{O}_3$ . At a basicity of 1.4 - 1.5 the reducibility decreases due to a drop in the proportion of hematite present in the sinters and the disappearance of  $\text{CaO} \cdot 2 \text{Fe}_2\text{O}_3$  coupled with the appearance of the relatively irreducible  $2 \text{CaO} \cdot \text{Fe}_2\text{O}_3$ . Further increases in basicity again show an upward trend due to the appearance of  $\text{CaO} \cdot \text{Fe}_2\text{O}_3$  and  $\text{CaO} \cdot \text{FeO} \cdot \text{Fe}_2\text{O}_3$ .

The reduction behaviour of ferrites is complex in that they must decompose for reduction of the iron oxide to occur. Seth and Ross<sup>40</sup> explain reduction as follows. First the higher iron oxides and ferrites, rich in iron oxide, are reduced until only dicalcium ferrite and wustite still remain. The gas then attacks the dicalcium ferrite.



The liberated lime then immediately reacts with the wustite as depicted in equation (14).



The reaction then proceeds as equation (13) and so on.

However, microphotographs show that wustite is not present at the gas boundary and consequently a diffusion process between reactions (13) and (14) must intervene. Bogdandy<sup>23</sup> indicates that at the oxide surface the dicalcium ferrite is reduced. The liberated iron separates out in the oxide phase and the calcium diffuses in and reacts with the wustite and again the iron either separates out or diffuses into the  $\text{Fe}_3\text{O}_4$ . This is shown schematically in Figures 20 and 21.

#### 2.4 Burden Behaviour in the Blast Furnace

In the lifespan of the blast furnace process a considerable wealth of knowledge of the reduction characteristics of iron oxides, pellets and sinters has been accumulated, up to reaction temperatures of circa  $1000^\circ\text{C}$ <sup>23</sup>. At temperatures beyond this very little is known of the reactions occurring or their effect on the properties of blast furnace burden materials. Even with the vast quantity of information available on burden material behaviour at temperatures up to  $1000^\circ\text{C}$  it is not easy to apply it for the simple reason that internal examination of the blast furnace during operation is extremely difficult. The main 'tools' for obtaining samples from operating blast furnaces, e.g. gas probes, temperature probes, burden probes, etc. although useful cover only a minute volume of a blast furnace.

It is fair to state, however, that correlations between material behaviour during reduction and the blast furnace process have been reasonably established. For example, it is known that materials that exhibit a large degree of breakdown of physical size during low temperature reduction cause a decrease in furnace permeability in practice and highly reducible burden materials decrease the fuel rate. Also pellets that swell extensively during reduction lead to a loss of furnace permeability<sup>41</sup>.

#### 2.4.1 Japanese Dissection Studies

A major breakthrough concerning the behaviour of materials within the blast furnace came with the water quenching of several operating furnaces in Japan and the methodical dissection of their contents<sup>42-49</sup>. The distribution of the burden inside the blast furnace depends upon the charging sequence, charge weights, burden components and furnace operation and results in each furnace operating in a different manner. Figure 22 shows the arrangement in Kukioka No.4<sup>49</sup>. The ore and the coke layers are maintained until the softening-melting zone or cohesive zone is reached. The start of the cohesive zone during the dissection procedure was ascertained by the increased physical resistance to removal of the material by mechanical means<sup>48</sup>.

The cohesive zone is where the materials start to soften and eventually melt. The discovery that the cohesive zone was not in one region of the furnace, but distributed in a reasonably geometrical shape was one of the major insights to the reactions occurring within the blast furnace during operation. It was found that the structure of the cohesive zone varied depending upon furnace operation and, as an example, Figure 23<sup>49</sup> shows the structures found in three different furnaces. Hirohato No.1 shows the softened layers having a 'doughnut' shape arranged in an

inverted 'V' structure, whilst Kukioka No.4 has a 'W' shaped cohesive zone. Higashida No.5 reveals a distorted inverted 'V' caused by irregular furnace operation prior to the quenching operation.<sup>45</sup>

#### 2.4.1.1 Reduction Levels

The extent of reduction in each burden layer of Hirohato No.1 and Kukioka No.4 blast furnaces is shown in Figures 24 and 25 respectively<sup>47</sup>. One of the interesting features is the fact that very little reduction occurs until the burden reaches the cohesive zone, wherein reduction proceeds rapidly.

One of the major problems with water quenching is the possible reoxidation of burden material during the cooling period and laboratory tests were conducted to determine the extent of reoxidation that might occur<sup>46,47</sup>. K Sasaki<sup>46</sup> et al measured the reoxidation of sinter, in the laboratory, under the same cooling conditions existing during quenching of a blast furnace, using a series of different initial reduction levels (Figure 26). Shimomura et al<sup>47</sup> used another technique employing burden materials of various reduction degrees cooled from three different temperatures (400°C, 800°C and 1000°C) at a cooling rate of 200°C.hr<sup>-1</sup> in a nitrogen atmosphere. They found that although the reduction temperatures and reduction degrees were different, the final reoxidation degree was approximately constant at 20 - 25%, i.e. the reoxidation increased in proportion to the initial reduction degree. At temperatures below 300°C no reoxidation occurred (Figure 27). The result of these experiments is that the reduction levels in Figures 24 and 25 should possibly be increased, e.g. 10 - 30% should be 15 - 40%. These corrected levels are in agreement with the reduction levels found in Russian dissection studies on a nitrogen quenched furnace<sup>50</sup>.

#### 2.4.1.2 Temperature Profiles

The temperature isotherms within the furnaces were estimated by a combination of several methods<sup>49</sup>:- Tempil pellets encased in numerous graphite holders were charged prior to blowing out the furnaces. This technique allowed the estimation of the temperature within the range 200 - 1800°C, but one of the problems with this technique is that there was no method of controlling the distribution of the graphite holders within the furnace. The other methods employed were measurement of the extent of coke graphitisation, thus estimating the temperature between 1200°C and 1700°C. Measurement of the coke electrical resistance, which allowed temperature estimation between 1100°C and 1700°C and finally the degree of iron ore fusion was measured to estimate temperatures within the range 900 - 1400°C.

Comparing the isotherms with the distribution of the softening-melting burden layers (Figures 23 and 28) one finds that the cohesive zone exists over a temperature range of approximately 1100°C to 1500°C for furnaces operating predominantly on sinter burdens (Tables 4 and 5).

#### 2.4.1.3 Burden Layer Structure within the Cohesive Zone

The type of structure of an individual burden layer in the cohesive zone depends upon the position of the layer within the furnace. Two layers from Hirohato No.1 are shown in Figure 29<sup>51</sup>. Layer G-5 is near the apex of the cohesive zone, whilst layer G-19 is situated near the base of the cohesive zone. Layer G-5 has four distinct zones, two of which are lumpy or granular portions (C and D). Layer G-19, on the other hand, contains only one lumpy portion, D. Apart from the obvious shape differences between the layers the other main difference is the replacement of the 'icicles' in layer G-5 by a half-molten portion

just prior to melting down, A' in layer G-19.

As mentioned earlier a considerable amount of reduction occurs in the cohesive zone and this is validated by the reduction data for each portion<sup>51</sup> (Tables 6 and 7). These figures may be on the low side, as reoxidation, caused by the act of water quenching, will almost certainly have taken place. The reason for the high reduction level of portion C is attributed to the slightly lower reduction temperature whilst in contact with the coke<sup>48</sup>.

The thickness of the softening-melting layers in Hirohato No.1 ranged from 400 - 500 mm, in the case of the upper layers, to 70 - 100 mm for the layers near the base of the cohesive zone<sup>45</sup>. The diminishing thickness is due to compaction, caused by the pressure exerted by the weight of material above the layer and secondly, a natural thinning of material due to the increase in furnace diameter as one descends. In the softening portions iron ore granules were combined in contact with each other. Sinter particles in the layers deformed very little, unlike pellets, which exhibited signs of deformation<sup>48</sup>.

The process of pellet metallization may take place in one of three modes<sup>48</sup>:-

- (a) The metallic iron is uniformly distributed within a pellet.
- (b) A metallic shell is formed, leaving a wustite core, and
- (c) Wustite within the pellet reacts to form a slag and moves towards the metallic iron shell, leaving a central cavity.

The reason for these three possible modes is not connected with the distribution within the softening-melting layer, but may be due to differences between the pellets or uneven gas flow in the softening-melting layer<sup>48</sup>.

M Sasaki et al<sup>48</sup> found that the half molten portion consisted of highly compacted metallic iron and a small quantity of slag. Any limestone or olivine present remained unslagged. The icicles extend into the coke voids and consist of a metallic shell with a hollow interior, with small droplets of slag adhering to the iron. The higher the softening-melting layer within the furnace, the greater the length of the icicles, e.g. level G-1 produced some icicles of several ten centimetres in length, whilst the lower layers produced icicles only one to two centimetres long.

The structure of the softening-melting layers in Kukioka No.4 was basically identical to those described for Hirohato No.1, except the thinner burden layers made the structure less distinct and the icicles smaller<sup>47</sup>.

#### 2.4.1.4 Slag Composition Changes

The major chemical change of the slag phase in the softening-melting layers is a decrease in the FeO content as the slag trickles down from the melting portion. Although large differences were detected by x-ray microanalyses of slags in portion A, ranging from 2 wt. % to 20 wt. % FeO, depending upon the location; the FeO content of the slag immediately prior to separation from the softening-melting layer was only 2-3 wt. % (Table 8)<sup>42</sup>. The type of slag was not significantly different to that found in the normal sinter product, but in the ore granules a considerable quantity of fayalite was produced (Table 9)<sup>48</sup>.

Descent of the slag results in a gradual change in composition as depicted in Figure 30<sup>48</sup>. The gradual increase in the CaO/SiO<sub>2</sub> ratio is attributed to fluxing with limestone and a drop in the silica content, caused by silica reduction. The rise in alumina is created by the incorporation of coke ash into the descending slag.

#### 2.4.1.5 Metal Composition Changes

Turning now to the changes in metal composition as it descends the furnace; the carbon content of the metal in the half-molten portion of the softening-melting layer is approximately 0.2 wt. % in the upper part and 0.35 - 0.57 wt. % in the lower part (Table 10). The source of carbon in these half-molten layers is attributed to the carburising action of carbon monoxide, except for the metal in contact with coke<sup>48</sup>. Similar trends are evident in the layers found in Kukioka No.4 (Table 11). The rise in the carbon content of the icicles is attributed to the metal being in direct contact with particles of coke<sup>48</sup>.

M Sasaki<sup>48</sup> has identified two distinct processes operating for the separation of metallic iron from the layers:-

- (i) The first mechanism is via the icicles which form at 1350-1400°C and drip into the coke bed. Reduction of the iron oxides present in the icicles occurs rapidly to produce metallic iron.
- (ii) The second process occurs in layers in which no icicles form. In this situation, the metallic iron is carburised by the underlying coke until it reaches a carbon level such that melting can occur at the pertaining temperature. In this case the temperature of meltdown is approximately 1500°C.

The question of the mechanism of silicon pick-up by the metal within the furnace has been the subject of considerable debate. Workers using an experimental blast furnace at Liege<sup>52</sup> fitted with sampling probes found that the silicon level rose gradually from the melting zone to the hearth, such that ~ 75% of the final hot metal silicon was achieved by the time the metal reached the tuyere level. The Japanese dissection studies on the

other hand reveal that the silicon level of the metal at the tuyere level is far in excess of that of the tapped metal<sup>48</sup>. An explanation for this discrepancy between the two groups of workers may be that silicon pick-up occurred during the process of water quenching the Japanese furnaces. M Sasaki<sup>48</sup> and co-workers conducted laboratory experiments to determine the probability of silicon pick-up during quenching and found that silicon pick-up from any slag present could be a possibility. Consequently this must be borne in mind when analysing the Japanese dissection data.

The sulphur level of the metal within the softening-melting region is much higher than the concentration in the tapped metal. (Figures 30 and 31). The sulphur distribution within the furnace is shown in Figure 32. In the granular zones very little increase in sulphur level occurs, which may be due to the materials in the softening-melting zone absorbing the sulphur from the ascending gases, rather than a lack of absorption capacity by the burden in the granular zones<sup>53</sup>. Figure 33 illustrates the absorption of sulphur in relation to the temperature, but as stated the lack of substantial quantities of sulphur in the gas in the stack of the furnace could explain the horizontal profile at temperatures below 800°C.

The transfer of sulphur from the metal to the slag during their descent of the furnace is indicated by Figure 34. As the temperature and slag basicity rise, the distribution of sulphur between the slag and metal,  $(S)/[S]$  increases accordingly.

Finally, some idea of how sulphur recirculates within the blast furnace can be obtained from examination of Figure 35<sup>47</sup>.

#### 2.4.1.6 Size Distribution

The change in physical size of the burden components during their descent was determined from the quenched furnace data<sup>47</sup> and one of the major problems with this part of the investigation is that breakdown of material occurs during the quenching operation. Degradation of sinter reaches a maximum at temperatures of 400 - 600°C and increases with retention time<sup>43</sup> (Figures 36 and 37). At levels of reduction in excess of 30% very little degradation occurs (Figure 38). Estimation of the cooling pattern of Kokura No.2 blast furnace shows that the burden materials are exposed for a lengthy period of time to conditions that lead to considerable breakdown (Figure 39).

K Sasaki and his co-workers<sup>43</sup> calculated the effect of the water quenching operation on the degradation of sinter (Figure 40). Their work indicates that the sinter degradation increases with time after blow out and considerable degradation occurs in the region around the middle of the stack. Applying this to a centre working furnace (centre working means that the majority of the gas flows up the central axis of the furnace), K Sasaki states that the degradation of sinter in the central zone of the furnace, where the reduction degree is high, is principally caused by the reduction processes during operation. The situation in the peripheral zone is that the reduction degree is low and in this situation the breakdown is principally caused by the long residence time of materials around 500°C during blowing out of the furnace. This is illustrated in Figure 41 with the dissection results for the centre working Hirohato No.1 blast furnace. Another factor in maintaining the size of the burden materials is that in the central region of Hirohato No.1, cracks are generated and fused immediately because of the high temperatures and the rapid reduction taking place<sup>47</sup>.

Degradation is generally a problem of most concern with sinters, which Japanese furnaces operate predominately on. Examination of the size distribution of pellets revealed that they were hardly pulverised and maintained their original shape<sup>47</sup>, which is verified in Figure 42.

#### 2.4.1.7 Influence of Gas Flow

Kanbara<sup>45</sup>, as further proof that the determination of the shape of the cohesive zone is by the gas flow within the furnace, took core samples from Hirohato No.1 and Kukioka No.4 and determined their permeability. He then related their permeability to gas flow and produced gas velocity distribution profiles, which can be directly related to the softening-melting layer distribution (Figure 43). The gas flow in the lower part of the furnace is fast, 7-9 m. sec<sup>-1</sup>, but slows considerably in the softening-melting layers to 2-4 m.sec<sup>-1</sup>, thus indicating the poor permeability of the softening-melting layers. As the gas ascends the stack its velocity naturally decreases due to the drop in gas temperature.

#### 2.5 Cohesive Zone Control

It has been demonstrated that the shape of the cohesive zone varies from furnace to furnace and much attention needs to be devoted to its control. As mentioned previously, its control is very dependent upon burden distribution. For maximum production, at the expense of fuel rate, a strong centre working profile should be adopted, but if the fuel rate is to be minimised, then a less centre working practice should be sought. Indeed, this is extremely evident by comparing a strong centre working furnace, like Hirohato No.1 with a moderate centre working furnace, like Kukioka No.4 (Tables 4 and 5 and Figure 23). Omori and Takahashi<sup>44</sup> illustrated this point extremely well by relating productivity to

the height of the cohesive zone above the tuyeres (Figures 44 and 45). The higher the cohesive zone up the furnace the greater the productivity, although at the expense of an increase in fuel rate.

One final point concerning control of the cohesive zone is its effect on the refractory lining. If the wall temperature of the furnace is too high, then refractory wear is appreciable and one can expect a shortened furnace life. Consequently, to maintain refractory thickness it is necessary to control the cohesive zone such that the wall temperatures are maintained at minimum levels<sup>3</sup>.

## 2.6 Melting Processes

The role of sulphur in the melting process has been postulated by Hills<sup>54</sup> in a theory which necessitates a reaction between solid metallic iron and wustite in the burden with gaseous sulphur, in the ascending gases. These phases react to form a eutectic of chemical composition 24 wt.% S, 9 wt.% O and 67 wt.% Fe, possessing a melting point of 915°C (Figure 46<sup>55,56</sup>). Once formed this liquid gains temperature as it descends the furnace, dissolving solid metallic iron and wustite which cause a change in liquid composition along the line EM until at M the liquid splits into two conjugate liquid phases. Further increases in temperature cause liquid M to dissolve more solid iron, moving its composition along the line MB (Figure 46) whilst liquid S dissolves more iron oxide and moves along the composition line SC. Consequently we have the creation of a liquid metal phase, M, and a liquid slag phase, S. The presence of silica in the system does not appreciably alter this mechanism, indeed it moves the miscibility gap in Figure 46 towards point E. Hence the separation of the nascent liquid into liquid metal and liquid slag phases will occur at lower temperatures.

Once formed the two liquids will go their own separate ways; the liquid metal dissolving solid iron, carbon and sulphur to become the final metal phase. The slag during its descent dissolves alumina, silica and lime from the coke ash, burden gangue and fluxes to form the final slag phase. This final stage of the process is illustrated in Figure 47.

Orrebo<sup>57</sup> using experimental apparatus designed to simulate the conditions existing in the bosh of the blast furnace found that the presence of hydrogen sulphide, in a carbon monoxide/nitrogen gas mixture, lowered the melting point of iron ore sinters and pellets due to the formation of the liquid Fe-S-O phase.

Alkalis are also thought to be closely associated with the initial melting process in the blast furnace<sup>31</sup> and examination of the distribution of alkali in Hirohato No.1 (Figure 48<sup>47</sup>) shows that the alkali is concentrated in the softening-melting layers. The reason for this is that alkali compounds, inherent within the burden and coke charged into the furnace are reduced and at temperatures in excess of 800 - 900°C the alkalis vaporize, as a metallic element or as a cyanide, and are swept into the softening-melting layers where they concentrate<sup>31</sup>. As the softening-melting layers descend the alkali evaporates and continues the cycle (Figure 49).

## 2.7 Methods of Assessing Blast Furnace Burden Quality

This section describes some of the tests used for assessing the suitability of burden materials as blast furnace feed. The test procedures can be conveniently split into three distinct groups: physical tests, reduction tests and softening tests. With the majority of these tests no standard test procedure is adopted on a world-wide basis, but each country tends to select test procedures which suit their particular requirements, even though there have been some attempts made to standardise test procedures.

### 2.7.1 Physical Tests

The principal test is the drum test which is used for all burden materials. Although there are several versions of the drum test the basic principle is identical, namely the charging of a set weight of burden material, of a standardised size range, into a large rotating drum. After a set number of revolutions, the sample is screened and the degree of undersize is quoted as the test index, e.g. the ISO drum test<sup>58</sup> uses a 15 kg sample comprised of aliquots of material screened on 25, 16 and 10 mm screens (with pellets the sample is screened between 10 - 40 mm). The sample is then rotated in a drum having a diameter of 1000 mm for 200 revolutions. After tumbling the sample is screened on 10, 6.3, 2 mm and 500  $\mu\text{m}$  screens and the tumble index quoted as the %+6.3 mm, whilst the abrasion index is the %-500  $\mu\text{m}$ .

A test developed specifically for iron ore pellets is that of the compressive strength in which, as the name implies, the average individual compressive strength of a batch of pellets is determined, e.g. the JIS (Japanese Industrial Standard) test<sup>59</sup> measures the individual compressive strength of at least 100 pellets and the test index is expressed in the form of a histogram of compressive strength against frequency.

### 2.7.2 Reduction Tests

Over the last twenty years a multitude of reduction tests have been devised, but many of them never gained wide acceptance and gradually faded in popularity. Three basic types are in use throughout the world: low temperature degradation tests which simulate the hematite to magnetite transition stage in the upper stack of the blast furnace and measure the extent of degradation occurring during this phase transformation. The second category is reducibility tests which measure the ease of oxygen removal from the

sample at a temperature representing the lower stack region of the furnace. Finally the third category is pertinent to iron ore pellets only, namely the measurement of the degree to which pellets swell during reduction, again at temperatures representing the lower stack region of the furnace.

One of the earliest degradation tests was developed by Linder<sup>60</sup> and subsequently modified by the British Iron and Steel Research Association<sup>61</sup> to become the BISRA low temperature break-down test. The BISRA test procedure uses 500 g of sample, sized between 9.5 and 15.9 mm, which is heated in a rotating drum to the holding temperature of 600°C in a controlled N<sub>2</sub>/CO/CO<sub>2</sub> gas atmosphere which is in equilibrium with magnetite. At the end of the test the sample is screened and the test indices expressed as the % +6.35 mm and the % -500 µm.

Several reducibility tests have been employed; Gakushin<sup>62</sup>, VdE<sup>63</sup> and CNRM<sup>64</sup>, but these have given way to the ISO reducibility test<sup>65</sup> which is a modified VdE test procedure. In the ISO reducibility test, 500 g of sample sized between 10 and 12.5 mm is reduced isothermally with a 40% CO/60% N<sub>2</sub> gas mixture at 950°C and the weight loss continuously recorded. The test index is the gradient of the reduction-time curve at 40% reduction.

Pellet swelling tests are split into two distinct groups; free swelling in which, as the name implies, the pellets are not packed in a bed, but allowed to swell separately and secondly those tests in which a bed of pellets is utilised. The LKAB free swelling test<sup>66</sup> uses 18 pellets in the size range 10 - 12.5 mm which are reduced isothermally at 1000°C in a 40% CO/60% N<sub>2</sub> gas mixture. Expression of the test index is in the form of a % swelling - % reduction curve where the % swelling is determined by mercury displacement. The CNRM<sup>67</sup> test also uses a 40% CO/60% N<sub>2</sub> reducing gas mixture and an isothermal test temperature of 1000°C, but the sample weight is 60 g and is contained in a bed. As with the LKAB

test the result is expressed in the form of a % swelling - % reduction curve.

### 2.7.3 Softening Tests

Softening tests have been primarily research tools and not general routine quality control tests due to their complexity and often lengthy test procedure. Consequently there is no universal softening test procedure, nevertheless, there is one established test that is often classed as a softening test although the test temperature is relatively low, namely the reduction-under-load test, or as it is more commonly known the Burghardt test after one of its developers<sup>68</sup>. The Burghardt test is only used for iron ores and pellets; the test procedure adopted is that a 1200 g sample, sized between 9.2 and 12.7 mm, is reduced by a 40% CO/60% N<sub>2</sub> gas mixture at 1050°C. During the reduction procedure a physical load of 49 kN.m<sup>-2</sup> is applied to the sample and the contraction of the sample bed and the differential gas pressure drop across the bed measured. The weight loss is continuously measured throughout the test in order to determine the change in the degree of reduction. The test indices are the gas pressure drop at 80% reduction and the rate of oxygen removal with respect to time at 40% reduction.

The attainment of higher temperatures is required for the design of true softening tests and several tests have been developed. CRM in Belgium developed a test in which semi-reduced ferrous burden material is crushed to between 1.4 - 2.0 mm, packed in a steel crucible and slowly heated whilst maintaining a nitrogen atmosphere inside the crucible<sup>69</sup>. A load of 196 kN.m<sup>-2</sup> is applied and the contraction of the bed measured. The temperature at which 3% contraction of the bed occurs is arbitrarily defined as the start of softening, whilst the temperature

at which 25% contraction of the bed occurs is arbitrarily defined as the end of softening.

One of the earliest test procedures published by the Japanese was by Nakamura et al<sup>70</sup> who determined the apparent viscosity of semi-reduced burden material, in the form of a tablet manufactured from finely crushed ferrous burden material, by applying a load to the sample and measuring the extent of contraction at elevated temperatures. Another softening test developed in Japan utilising the contraction of a single iron ore pellet, whilst under load in a reducing atmosphere was reported by Sugiyama et al<sup>71</sup>. Narita et al<sup>72</sup> developed a test in which pre-reduced pellets were heated to  $\sim 1400^{\circ}\text{C}$  in a nitrogen atmosphere. During the heating procedure a load of  $59 \text{ kN.m}^{-2}$  was applied to the sample bed and the gas pressure drop across the sample bed and the extent of contraction of the bed measured.

Perhaps one of the most grandiose pieces of softening apparatus was developed by MEFOS in Sweden<sup>73</sup> (Figure 50). In the design of the apparatus they have attempted to simulate the gas flow conditions existing in the softening-melting region of the blast furnace as closely as possible. The sample (1200 g) is pre-reduced in a separate piece of apparatus to wustite by control of the  $\text{CO}/\text{CO}_2$  ratio in the reducing gas, cooled in nitrogen and transferred to the softening apparatus. In the softening apparatus the sample is heated to  $950^{\circ}\text{C}$  in nitrogen then heated at a rate of  $200^{\circ}\text{C.hr}^{-1}$  up to a maximum of  $1325^{\circ}\text{C}$ . Heating of the sample is carried out by heat transference from the pre-heated reducing gas as it passes through the sample bed. The reducing gas is composed of 40%  $\text{CO}/60\% \text{N}_2$  and flows at a rate of  $600 \text{ l.min}^{-1}$ . Simultaneously a load of  $49 \text{ kN.m}^{-2}$  is applied to the sample bed and the contraction of the bed along with the gas pressure drop across it are measured. Analysis of the inlet and outlet gases is used to monitor the progress of reduction.

The only other notable European softening test that has been documented is the one developed in Italy by CSM<sup>74</sup> (Figure 51) in which 500 g samples of burden materials, that have been previously reduced, are heated in a nitrogen atmosphere up to 1400°C whilst applying a load of 49 kN.m<sup>-2</sup> to the sample. Throughout the test the gas pressure drop across the bed and the contraction of the bed are measured.

Recent developments in softening studies show a move to even higher temperatures, complete melt-down of the sample and collection of the molten material dripping from the sample<sup>75,76</sup>. Kondo et al<sup>75</sup> constructed such a test in which 120 g of pre-reduced material, sandwiched between two layers of coke, is charged into a graphite crucible and heated to 1650°C under programmed conditions. During the test argon is purged through the sample and the molten products collected in magnesia crucibles. Recent development of the test<sup>77</sup> has included the measurement of the gas pressure drop across the bed, reduction of the bed and the extent of bed contraction whilst maintaining a programmed heating rate coupled with the use of reducing gas in place of argon.

## CHAPTER 3

### EXPERIMENTAL TECHNIQUES

#### 3.1 Sample Manufacture

The major material used for this work was acid pellets. Sinters and sinter/pellet mixtures were also examined, but to a lesser extent. All the materials were laboratory made using suitable pilot plant facilities.

##### 3.1.1 Manufacture of the Acid Pellets

The pellets were manufactured at the Teesside Laboratories of the British Steel Corporation in their 'pot-grate' pilot plant, from a blend of iron ores. A major investigation into the effect of pellet chemistry, blend and firing regime upon pellet properties was in progress at the time of the commencement of the cohesive zone studies. The pellets selected for the cohesive zone studies originated from this major programme and were typical of the blend, chemistry and quality expected to be fed to the Redcar blast furnace.

The blend of ores used, chemical analysis of the fired pellets, the firing conditions and the physical properties of the fired pellets are shown in Tables 12, 13 and 14. As part of the major programme the reduction properties of each batch of pellets were determined on a routine basis. These tests included ISO reducibility, Burghardt, low temperature breakdown and free swelling. Details of the test indices obtained for the acid pellets used in the cohesive zone studies are given in Table 15.

### 3.1.2 Manufacture of the Sinters

The sinters were also manufactured in the Teesside Laboratories of the British Steel Corporation sinter unit from a blend of materials typical of the anticipated feed for the Redcar blast furnace. The variation of lime/silica ratio was obtained by small changes to the proportions of the materials and by control of the limestone addition.

Tables 16, 17, 18 and 19 show the materials used, the chemical analyses, phase analyses and ISO reducibility indices of the sinters respectively.

### 3.2 Reduction Procedure

The general philosophy adopted for the experimental study of the behaviour of burden materials within the cohesive zone of the blast furnace was that of a reduction under load test using athermal conditions. During the test the gas pressure drop across the sample bed, contraction of the bed and extent of reduction were monitored.

Rather than attempt the complete temperature-time cycle and reducing gas composition-time cycle that may be anticipated inside the blast furnace, the procedure was simplified to span the changing conditions within the cohesive zone only. The reduction procedure was split into two distinct procedures; the first was to isothermally pre-reduce the material to the desired extent in one piece of apparatus. Finally the pre-reduced material was transferred to the high temperature apparatus for athermal reduction under load. In some cases the material under investigation was subjected to the high temperature athermal reduction under load procedure without the pre-reduction stage being carried out.

### 3.2.1 Pre-Reduction Stage

The technique adopted was to charge 900 g of pellets or 675 g of sinter, within the size range 10 - 12.5 mm, into the reaction vessel and heat the sample up to 950°C. During the heating procedure a nitrogen atmosphere was maintained inside the vessel. On attaining 950°C the nitrogen atmosphere was replaced by one of composition 40% carbon monoxide and 60% nitrogen, on a volume basis, at a flow rate of 50 l.min<sup>-1</sup>. Throughout the reduction process the weight loss was measured and when the necessary weight loss was attained, the reaction vessel was removed from the furnace and allowed to cool in air. During the cooling period a nitrogen atmosphere was maintained inside the reaction vessel to prevent reoxidation of the sample. When cold the sample was weighed in order to accurately determine the level of reduction attained.

Pre-reduction of sinter and pellets for the high temperature studies using a mixture of sinter and pellets was slightly different to that described. As the ISO reducibilities of the sinter and the pellets were different, the materials were reduced separately, under identical conditions, for the same length of time. Using this procedure the two materials could reduce at their own intrinsic rate as would occur in the blast furnace. For the lower level of reduction the time of reduction was thirty minutes, whilst for the higher level of reduction the time of reduction was sixty minutes.

In one case only, with a sample of acid pellets, a lower reduction temperature of 600°C was selected, but the gas flow and composition were identical to those used for reduction at 950°C.

Details of the pre-reduction apparatus are shown in Figure 52.

### 3.2.2 High Temperature Test Procedure

A schematic diagram of the apparatus is shown in Figure 53 and a photograph of the apparatus is shown in Plate 1. The apparatus consists of two distinct parts: a gas pre-heating section in the lower half and the actual sample holder in the upper half.

The graphite crucible was sealed to the graphite tube with 'Carbond' graphite cement and the space between the induction coil and the crucible packed with 'Triton Kaowool' ceramic fibre, to prevent excessive heat loss. A layer of coke was placed in the bottom of the crucible and the sample was loaded on top, followed by a second coke layer. The depths of the layers were maintained constant for every test and the weight of sample charged recorded. (An exception to this was during the critical gas flow rate tests - refer to Section 4.1). During the charging of the sample three inconel sheathed chromel/alumel thermocouples were embedded into the sample bed at the bottom, side and top of the layer to measure bed temperature. Actual measurement of temperature was with a multi-channel electronic digital indicator calibrated directly in degrees centigrade. A graphite ram, comprised of a perforated disc and connecting rod, was placed on top of the upper coke layer to transmit the pressure from the pneumatic cylinder during the reduction procedure. The method of calculating the gas pressure required in the pneumatic cylinder in order to provide the desired load on the sample bed is shown in Appendix I. The top of the ram and crucible was insulated with 'Triton Kaowool' to minimise heat loss.

Heating of the sample to 950°C was undertaken whilst maintaining a nitrogen atmosphere inside the apparatus. As mentioned earlier the heating process was via two stages; firstly from the hot gases leaving the pre-heat stage and secondly by the induction coil. The induction coil was arranged so that heating was concentrated around the bottom coke layer, thus the gases leaving the pre-heat stage were further heated within the coke bed. This

arrangement of the induction coil was found by a process of trial and error to minimise the induction heating effects at the periphery of the sample. The net effect was that virtually no melting of the periphery of the sample occurred. At 950°C the nitrogen gas was replaced with a carbon monoxide/nitrogen mixture of the desired flow rate and composition. (The selection of flow rate is dealt with in sections 3.2.2.1 and 4.1). In some cases nitrogen only was used instead of the reducing gas. Simultaneously with the introduction of the reducing gas a load was applied to the sample by means of the pneumatic cylinder.

The gas pressure drop across the bed was measured by a manometer calibrated in m.m. water gauge. Two pressure probes were used; one was situated beneath the crucible and the other one doubled up as the exit tube for the chromel/alumel thermocouples. Measurement of the contraction of the bed was with a conventional scale and pointer technique, although initially a linear displacement transducer coupled to a chart recorder was employed, but problems with the recorder caused the abandonment of this system. The change in reduction of the bed was monitored by measurement of the concentrations of CO and CO<sub>2</sub> in the inlet and outlet gases using two Grubb Parsons Infra Red Gas Analysers (model SB2), which allowed an oxygen mass balance to be calculated. (Details of the oxygen mass balance calculations are given in Appendix II).

Heating of the sample from 950°C was controlled at the selected heating rate by increasing the temperature of the pre-heat stage and by increasing the power to the induction coil. (The method of selecting the heating rate is discussed in section 3.2.2.2). Termination of the test occurred either when the chromel/alumel thermocouples failed or when the rate of increase of gas pressure drop became excessive. In some cases the test was intentionally interrupted at a stage prior to thermocouple failure or rapid increase in gas pressure drop. (These cases are dealt with in

Sections 4.3.3.6 and 4.3.3.8). After termination of the test the sample was allowed to cool in a nitrogen atmosphere, removed from the crucible and weighed. The lower coke bed and the top of the graphite chips within the pre-heat zone were examined for any traces of metal or slag that may have dripped from the sample bed.

The test conditions employed in the high temperature test are shown in Table 20 and were used in all tests unless specifically stated otherwise. An assessment of the errors involved in the test procedure is presented in Appendices I and II.

### 3.2.2.1 Determination of the Critical Flow Rate

Udy and Lorig<sup>78</sup> first illustrated the existence of a critical flow rate, above which little or no increase in reduction rate occurs. As long as reduction occurs in flow rates greater than the critical flow, then the reaction is not inhibited by the build-up of product gas in the bulk gas phase.

To determine the critical flow rate for the high temperature test, examination of one of the most demanding reduction situations was selected, i.e. an isothermal test at a high temperature, with a sample of zero pre-reduction, that possessed a high ISO reducibility index. The severity of these conditions ensured that if a critical flow rate was established, then the testing of materials having some pre-reduction would always be with a gas flow above the critical rate. A gas composition of 40 vol. % carbon monoxide and 60 vol. % nitrogen was selected because this composition was in standard use for burden quality tests, e.g. Burghardt test and the ISO reducibility test. It is also close to the composition of the gas produced in the blast furnace by the burning of coke at the tuyeres.

The material chosen for these tests was dolomite fluxed iron ore pellets commercially manufactured by LKAB of Sweden. Details of their chemical analysis and ISO reducibility index are given in Table 21.

A temperature of 1250°C was selected for these tests, which was within the temperature range encountered in the high temperature test. In all cases no load was applied to the sample bed.

### 3.2.2.2 Selection of Heating Rate

As the cohesive zone studies were primarily aimed towards the Redcar blast furnace, which was to be operated with the philosophy of a strong centre working practice, it was necessary to examine the Japanese quenched furnace data for a similar operating furnace. Such a furnace was Hirohato No.1, as shown by Figure 28, and Kanbara et al<sup>45</sup> published details of the burden that was charged to Hirohato No.1 just prior to the quenching operation (Tables 4 and 5). The Japanese dissection studies were very methodical and included the necessary detail for estimating the heating rates inside the cohesive zone. Making the assumption that the burden layers descend uniformly, one can look upon the burden layers as time intervals within the furnace, which allows an estimation of the heating rate within the cohesive zone to be made.

Redcar blast furnace was designed to operate at a production rate of  $2.38 \text{ t.m}^{-3}.\text{day}^{-1}$  which was almost achieved with Hirohato No.1 (Table 4). Using the burden weights shown in Table 5 one can calculate the weight of iron per charge entering the furnace. The ores and sinter contained 22 tonne of iron, the fluxes 0.13 tonne and the coke a negligible quantity of 0.077 tonne.

Assuming 94 wt.% Fe in the hot metal, the equivalent weight of hot metal per burden charge was 23.54 tonne. A production rate of  $2.34 \text{ t.m}^{-3} \cdot \text{day}^{-1}$  corresponded to a daily production rate of 3289 tonne (Table 4). Thus to achieve such a rate the furnace must have been charged viz:-

$$\frac{3289 \text{ t.day}^{-1}}{23.54 \text{ t.charge}^{-1}} \sim 139 \text{ times per day,}$$

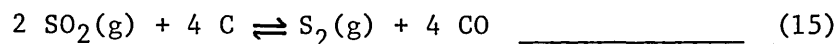
which is equivalent to a charge every 10 minutes. Hence the burden layers in Figures 24 and 28(b) represent 10 minute intervals. Using this time scale the burden near the walls was estimated to be exposed to a heating rate of  $\sim 200^{\circ}\text{C.hr}^{-1}$  and the burden towards the apex of the cohesive zone was exposed to a heating rate of  $\sim 300^{\circ}\text{C.hr}^{-1}$ .

An example of the method of estimation of heating rate is shown in Figure 54. Assuming uniform descent of the burden the heating rate near the apex of the cohesive zone is  $500^{\circ}\text{C.hr}^{-1}$  and near the base  $230^{\circ}\text{C.hr}^{-1}$ . It should be stressed that these heating rates are on a hypothetical furnace and are not to be taken as a true indication of actual heating rates in blast furnaces, but solely as an example of the method of estimation.

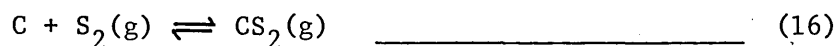
Consequently, for the experimental studies, two separate heating rates of  $200^{\circ}\text{C.hr}^{-1}$  and  $400^{\circ}\text{C.hr}^{-1}$  were selected, which represented the conditions towards the wall and centre of a strong centre working furnace respectively.

### 3.2.2.3 Incorporation of Sulphur into the Reducing Gas

Sulphur was introduced in selected cases at the start of the test ( $950^{\circ}\text{C}$ ) in the form of sulphur dioxide, which reacted with the graphite chips to form molecular sulphur gas viz:-



A second reaction is also thermodynamically possible:-



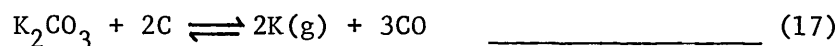
Two levels of addition were used: 0.28 and 0.75 vol.% calculated in terms of elemental sulphur. 0.28 vol.% was the calculated sulphur concentration in the gas within the bosh of the blast furnace arising from complete combustion of oil and coke at the tuyeres (Table 22). 0.75 vol.% was used in an attempt to represent the influence of recirculation of sulphur within the blast furnace.

Although sulphur dioxide injection produces carbon monoxide, no allowance was made for this extra carbon monoxide, i.e. the flow rates of nitrogen and carbon monoxide were maintained at their normal values. The error in this procedure was quite small as the inclusion of 0.75 vol.% elemental sulphur creates an increase in the carbon monoxide level by less than 1 vol.% and the total flow rate by less than 2%.

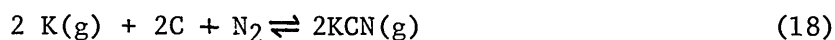
#### 3.2.2.4 Incorporation of Alkali Vapour into the Reducing Gas

Alkali vapour was introduced with the reducing gas by the incorporation of one or two expendable 'reaction cells' placed in the top layer of the graphite chips in the pre-heat stage. Each cell was manufactured by drilling lengthways a 23 mm diameter hole, to a depth of  $\sim 25 - 35$  mm into a piece of graphite rod (40 mm diameter and  $\sim 30 - 40$  mm long), thus forming a small crucible. Small 'vee' cuts were made around the lip of the crucible and a lid (40 mm diameter and  $\sim 4$  mm thick with several 4 mm diameter holes drilled in it) was added. The vee cuts and the holes in the lid were designed to allow the free circulation of the reducing

gas, thus ensuring the pick-up of the alkali vapour. Analar grade anhydrous potassium carbonate was placed in the reaction cell and during the test it reacted with the graphite to produce potassium and cyanide vapours, viz:-



A second reaction is thermodynamically possible:-



The quantities of potassium carbonate used were 5 g, 10 g and 15 g. In the case of the 15 g addition it was necessary to use two reaction cells in order to accommodate the volume of carbonate.

### 3.2.2.5 Incorporation of Sulphur and Alkali Vapour in the Reducing Gas

The test incorporating both species of addition was simply a combination of the procedures described in the previous two sections. A sulphur level of 0.75 vol.% elemental sulphur and an alkali loading of 15 g potassium carbonate were used. The possibility of a reaction between sulphur and potassium vapour during the test was examined and, although no data was available for  $\text{K}_2\text{S}(\text{g})$  formation, information for  $\text{Na}_2\text{S}(\text{g})$  was available<sup>79</sup> and showed that  $\text{Na}_2\text{S}(\text{g})$  could form during the high temperature test. Due to the similarity between potassium and sodium it is reasonable to assume that  $\text{K}_2\text{S}(\text{g})$  could be formed.

### 3.3 Initial Slag Formation Tests

A simple heating test procedure was developed to study the initial melting phenomena in acid pellets, sinters and in

synthetic pellets. The latter<sup>was</sup> produced specifically for this particular section of the experimental study.

### 3.3.1 Synthetic Acid Pellets

Several batches of synthetic pellets were manufactured from chemical reagent grade ferric oxide or MalMBERGET iron ore concentrate, which was particularly free from gangue. Silica additions were made as either silica flour, silica glass or silica sand. These silica additions increased the silica concentration to the same level as that in the acid pellets used in the high temperature studies. No bentonite was added, except in one special case when pellets were made from MalMBERGET and bentonite only. Sufficient quantities of iron oxide and silica (or bentonite) were mixed by hand to provide 50 g of mixture. The mix was then moistened, hand formed into pellets, placed in an alumina crucible and fired at either 1100°C for 3 hours or at 1300°C for 30 minutes in an oxidising atmosphere using a small laboratory vertical tube furnace.

Several fired pellets from each batch were reduced in a 40 vol.% CO/60 vol.% N<sub>2</sub> atmosphere at 950°C until approximately 40% reduced, using a small laboratory vertical tube furnace, then cooled in nitrogen.

### 3.3.2 Heating Stage

In the case of the materials used in the high temperature studies, the reduction stage mentioned in the last section was omitted as suitably reduced samples were obtainable from the pre-reduction procedure (Section 3.2.1.).

To study the initial slag forming reactions the partially reduced sample was placed in an iron crucible and heated in a small laboratory vertical tube furnace to the desired temperature, generally between 950°C and 1075°C for acid pellets and 1100°C for sinters. On attaining the desired temperature the sample was held at temperature for 30 minutes, then furnace cooled. Throughout the whole procedure a nitrogen atmosphere was maintained around the sample to prevent any oxidation occurring. This simple technique allowed the slag forming reactions to occur and be subsequently detected by microscopic examination.

#### 3.4 Gases used in the Test Procedures

The nitrogen was obtained from a commercial supply of liquid nitrogen, whilst the carbon monoxide and sulphur dioxide were obtained from cylinders of technical grade carbon monoxide and liquid sulphur dioxide respectively. Gas flow rate and composition were controlled using 'Flowbits' rotameters. In the case of the high temperature test, the rotameters were recalibrated for an operating pressure of 1.38 bar above atmospheric at a temperature of 15°C. As the permeability of the bed decreased during the test it created an increase in back pressure, but the rise in back pressure was however insignificant relative to the operating pressure of the rotameters, hence the gas flow rate and composition remained constant throughout the test procedure. In the case of experiments utilising sulphur dioxide the rotameters were pressurised to only 0.55 bar above atmospheric instead of the normal 1.38 bar and the calibration altered accordingly. This decrease in operating pressure was necessary because of the relatively low vapour pressure of sulphur dioxide. The maximum obtainable pressure from liquid sulphur dioxide is 1.74 bar above atmospheric at 20°C<sup>80</sup>, but because the gas cylinder was stored outside a temperature of 20°C was never attained.

### 3.5 Petrology

The samples for examination arose from several sources, e.g. pellets and sinter in the as-received state; pellets and sinter in the pre-reduced condition; pellets and sinter after the high temperature test; material that had dripped from the sample bed during the high temperature test and finally pellets used in the study of the initial melting process.

#### 3.5.1 Sample Preparation

All the samples for microscopic examination were vacuum impregnated in araldite compound made from araldite MY753 resin and HY951 hardener. Vacuum impregnation was carried out in a dessicator attached to a filter pump. Sectioning of the smaller sample blocks was undertaken using a diamond saw, whilst the larger blocks arising from the high temperature test samples were sectioned using a mechanical hacksaw. After sectioning the cut surface was ground flat using a rotary grinder, with a water-spray and a succession of silicon carbide waterproof grinding discs, i.e. 120, 220, 320, 400 and 600 grit. When smooth the surface was vacuum impregnated with resin again and reground using the procedure outlined. Polishing of the sample surface was carried out using a Kent Mk IIA automatic polisher and metron polishing discs impregnated with diamond polishing paste. The grades of paste used in succession were: 30  $\mu\text{m}$ , 15  $\mu\text{m}$ , 6  $\mu\text{m}$  and finally 1  $\mu\text{m}$ , whilst the polishing lubricant was Leitz P.M. lubricant. Some of the samples originating from the high temperature test were etched in 2% nital to reveal the microstructure of the metallic iron phase.

Samples for examination using the electron microscope were polished using the procedure previously stated. In the case of samples of the bed after the high temperature test further

sectioning, using the diamond saw, was necessary in order to reduce the sample size to that which could be accommodated in the stage of the microscope. The surface of the sample was coated with carbon using a vacuum coating unit and the sides of sample painted with electrically conductive silver paint to prevent build-up of electrostatic potential in the sample.

### 3.5.2 Microscope Techniques

Optical examination of the samples was undertaken using an Olympus reflected light microscope fitted with a 35 mm camera attachment. Phase analysis of the polished samples was carried out using the optical microscope in conjunction with a Swift Automatic point counter (Model E) and the associated electro-mechanical stage operating in 0.3 mm steps.

The electron microscope used was a Cambridge Stereoscan 600 SEM attached to an EDAX 711 microprobe unit which allowed qualitative analysis of the mineralogical phases to be made.

RESULTS

4.1 Critical Gas Flow Rate Tests

Initially a sample weight of 1000 g was selected and tests with gas flow rates of 60 and 75 l.min<sup>-1</sup> produced a discrepancy between the two, indicating that the critical flow rate was greater than 60 l.min<sup>-1</sup> (Figure 55). A problem existed with attempts to increase the flow rate above 75 l.min<sup>-1</sup>, in that cooling of the pre-heat stage was noticeable, i.e. the upper limit of electrical power input was reached. Another snag was that there was very little room left in the graphite crucible for the top coke layer. These problems resulted in the decision to decrease the sample weight to 800 g, whilst maintaining the gas flow rates at 60 and 75 l.min<sup>-1</sup>. Again the results are shown in Figure 55, but this time both flow rates produced almost identical reduction paths, indicating that 60 l.min<sup>-1</sup> was equal to or greater than the critical flow rate. Consequently a flow rate of 60 l.min<sup>-1</sup> was adopted for the high temperature test along with a constant initial bed height of 66 mm. The latter was the height of 800 g of unreduced pellets, which meant that with pre-reduced samples of pellets the sample weight was less than 800 g.

During the gas flow tests the gas pressure drop across the sample bed only increased by 3mm water gauge at the most.

Finally to give some indication what the flow rate selected is equivalent to, the gas flow conditions in the high temperature test and the Burghardt test are compared in Table 23. The latter test is recognised as a standard reduction under load test for assessing the quality of iron ores and pellets. It is evident that the high temperature test has superior gas flow characteristics to the established Burghardt test.

## 4.2 Reproducibility Tests

The reproducibility of the results obtained from the high temperature apparatus was examined with dolomite fluxed iron ore pellets from the same batch as used for the gas flow tests. These were selected because shortly after building the apparatus, LKAB in Sweden requested that BSC undertake some high temperature testwork on these particular pellets. The tests were carried out under the operating conditions requested by LKAB which were slightly different to the usual conditions. In this case the pre-reduction procedure was modified to that described in Section 3.2.1. That is the pre-reduction was carried out at 1000°C and the pellets reduced to wustite using a controlled nitrogen, carbon monoxide and carbon dioxide gas mixture. Cooling of the pellets was as described in Section 3.2.1. The high temperature test procedure was also modified slightly by altering the starting temperature to 1000°C from the normal 950°C. Apart from this the test procedure was identical to that described in Section 3.2.2. A heating rate of 200°C.hr<sup>-1</sup> was specified by LKAB for the tests.

The results are presented in Figures 56 and 57 and show that good agreement of the measured parameters was obtained between the two tests.

## 4.3 Experimental Studies with Acid Pellets

The majority of the experimental studies were undertaken using acid pellets and this section details the results of these studies.

### 4.3.1 Optical and Electron Microprobe Examination of the Fully Oxidised Pellets

Optical examination and electron probe analysis of the

acid pellets in the fully oxidised state showed that they consisted of hematite, quartz and a slag phase, along with minute traces of magnetite which had not oxidised completely during the firing stage. (Refer to Section 4.6 for photographic details and to Table 24 for the phase analysis). The electron probe studies revealed that the slag phase consisted essentially of calcium, silicon and iron with traces of magnesium, aluminium and potassium. (Again refer to Section 4.6 for EDAX details).

#### 4.3.2 Initial Slag Formation Tests

##### 4.3.2.1 Synthetic Acid Pellets

Microscopic examination revealed that the pellets manufactured from reagent grade ferric oxide generally had extensive slag formation in the fully oxidised state and contained fayalite in the partially reduced state, irrespective of the form of silica or the firing temperature. Pellets manufactured from MalMBERGET iron ore and silica sand (quartz), fired at 1300°C, contained no slag phase in the fully oxidised state or the partially reduced state after heat treatment. In contrast pellets manufactured from MalMBERGET iron ore and bentonite, also fired at 1300°C, had extensive slag formation both in the fully oxidised state and the partially reduced state. (Refer to Section 4.6 for details of photographic plates and to Table 25 for details of the studies undertaken with the synthetic acid pellets.) Electron probe analysis of the oxidised pellets containing bentonite revealed that the slag phase was composed of iron, calcium, potassium, silicon, aluminium and in some instances traces of sodium. The semi-reduced pellets containing bentonite contained two slag phases; the darker coloured phase was found to consist of iron, calcium, silicon, potassium and a trace of aluminium, whilst the lighter phase (the more abundant of the two) was found to contain iron and silicon plus traces of potassium, aluminium and calcium.

#### 4.3.2.2 Pilot Plant Pellets

After heat treatment the partially reduced pellets (44% reduced) contained two slag phases (Refer to Section 4.6 for photographic and EDAX details). The light coloured phase was found by electron probe analysis to consist of calcium, silicon and iron whilst the darker phase (the minor phase) was found to consist of iron, calcium and silicon, plus traces of potassium, aluminium and magnesium. Only iron was found in the wustite grains. A repeat of the experimental procedure using pellets reduced by 52% produced identical microstructures, thus ensuring that the phenomenon observed was not an isolated incident.

#### 4.3.3 High Temperature Tests with Acid Pellets

The major part of the experimental study of the reactions occurring within the cohesive zone of the blast furnace was carried out with acid pellets. All the principal factors that could influence the reactions taking place were examined, i.e. the effects of degree of pre-reduction, heating rate, pre-reduction temperature, applied load and the influence of sulphur and alkali vapours in the reducing gas. Table 26 lists the individual tests carried out.

##### 4.3.3.1 Tests at a Heating Rate of $200^{\circ}\text{C}\cdot\text{hr}^{-1}$

For this series of tests two levels of pre-reduction were investigated, namely 32 and 52% respectively.

The contraction-temperature; gas pressure drop-temperature and the reduction-temperature curves for these tests are shown in Figures 58, 59 and 60 respectively. The temperature at which 3% contraction of the initial bed height occurred was taken as the start of softening and was  $1010^{\circ}\text{C}$  and  $985^{\circ}\text{C}$  for the 32% and 52% pre-reduced samples respectively. 3% contraction of the bed was

the minimum initial change in bed height that could be detected (equivalent to a movement of 2 mm). Additionally the commencement of direct reduction was detected for the 32% pre-reduced sample and is marked on the reduction-temperature curve.

#### 4.3.3.2 Tests at a Heating Rate of $400^{\circ}\text{C}\cdot\text{hr}^{-1}$

Four levels of pre-reduction were examined at this heating rate: 0% (fully oxidised), 30%, 49% and 61%. The contraction-temperature, gas pressure drop-temperature and the reduction-temperature curves for the three pre-reduced samples are shown in Figures 61, 62 and 63 respectively. The 3% contraction temperatures for the 30%, 49% and 61% pre-reduced samples were  $985^{\circ}\text{C}$ ,  $1010^{\circ}\text{C}$  and  $985^{\circ}\text{C}$  respectively. Again, as with the slower heating rate tests, the commencement of direct reduction was detected in two cases and is marked on the appropriate reduction-temperature curves.

The contraction-temperature, gas pressure drop-temperature and reduction-temperature results for the 0% pre-reduced sample are shown in Figures 64 and 65. In this case the 3% contraction temperature was  $1095^{\circ}\text{C}$ .

#### 4.3.3.3 Variation in Applied Load

The 'standard' load used throughout the tests was  $49\text{ kN}\cdot\text{m}^{-2}$ , but it was naturally desirable to study the effect of variations in load on the high temperature properties of acid pellets. All the samples in this series of tests were pre-reduced to a reduction degree of 30% and subsequently subjected to high temperature reduction at the  $400^{\circ}\text{C}\cdot\text{hr}^{-1}$  heating rate. Three loads were selected:- 49, 78 and  $98\text{ kN}\cdot\text{m}^{-2}$ ; the results of these tests are shown in Figures 66 and 67.

#### 4.3.3.4 Nitrogen Only Tests

In the high temperature test the standard procedure adopted was to carry on the reduction reaction following the pre-reduction stage. This practice complicated the study of the reaction mechanism and because of this some high temperature tests were carried out in a nitrogen atmosphere only using a heating rate of  $400^{\circ}\text{C}\cdot\text{hr}^{-1}$ . All other variables were maintained at the levels shown in Table 20. Figure 68 shows the results for the four different levels of reduction studied, i.e. 26%, 44%, 47% and 65%. The contraction of the sample bed, with increase in temperature, for each reduction level studied is marked on the lines of constant reduction. The increase in gas pressure drop across the bed with rise in temperature for each reduction level is indicated in Figure 69 in a similar manner to the contraction levels.

#### 4.3.3.5 Low Temperature Pre-Reduction Test

As stated in Section 3.2.1, all pre-reduction was carried out at  $950^{\circ}\text{C}$ , which has the advantage of minimising the time required to reduce samples prior to the high temperature test, but it was recognised that this simple situation was not encountered in the blast furnace. In practice undoubtedly some reduction occurs at temperatures less than  $950^{\circ}\text{C}$ , albeit at a relatively slow rate. This shortcoming was remedied by a high temperature test using acid pellets that had been pre-reduced at  $600^{\circ}\text{C}$  to  $\sim 26\%$  reduction. The time for the pre-reduction stage was of the order of 2.5 hours compared with approximately 30 minutes for comparable reduction at  $950^{\circ}\text{C}$ . In fact the reduction process had for all practical purposes ceased after 2 hours. The subsequent reduction process in the high temperature test still commenced at  $950^{\circ}\text{C}$ , using a heating rate of  $400^{\circ}\text{C}\cdot\text{hr}^{-1}$ . Figures 70 and 71 show the contraction-temperature, gas pressure drop-temperature and reduction-temperature curves obtained. Commencement of the direct reduction reaction was detected and is marked on the reduction-temperature curve.

#### 4.3.3.6 Interrupted Test

The normal procedure for the high temperature test was to continue until the rate of rise of gas pressure drop became excessive or when the thermocouples failed. In order to study the reactions occurring inbetween the start and finish of the test, one test was prematurely terminated at a temperature of 1125°C. The technique adopted for this particular test was to pre-reduce the pellets at 950°C to a reduction level of 44%, carry out the high temperature test at a heating rate of 400°C.hr<sup>-1</sup> until 1125°C was attained, then stop the test. The final level of reduction achieved was 62%.

#### 4.3.3.7 Tests Incorporating Sulphur in the Reducing Gas

Sulphur is one of the major elements that recirculate in the blast furnace, either in elemental or compound form and it was essential to study its influence upon the softening-melting process.

In this series of tests all the samples of acid pellets were pre-reduced to a level of 30% and then tested at a heating rate of either 400°C.hr<sup>-1</sup> or 200°C.hr<sup>-1</sup>. The contraction-temperature and gas pressure drop-temperature curves for the three cases studied are shown in Figures 72 and 73 along with the base case of zero sulphur in the reducing gas for comparative purposes. Figure 74 shows the reduction-temperature curves for the two samples tested at the 400°C.hr<sup>-1</sup> heating rate with 0.28 and 0.75 vol. % elemental sulphur in the reducing gas along with the base case of zero sulphur in the reducing gas. The start of direct reduction was not detected with the test incorporating sulphur in the gas, but this does not necessarily mean that direct reduction did not occur. As stated in Appendix II, the start of direct reduction was calculated from the difference between the

CO/N<sub>2</sub> ratios of the inlet and outlet gases. This was a particularly sensitive method and small variations in the inlet and outlet carbon monoxide levels could upset the calculation. With sulphur dioxide injection the additional carbon monoxide, from the reduction of sulphur dioxide, although calculable, affected the mass balance sufficiently to make the start of direct reduction difficult to detect with any reasonable accuracy. Another problem was that the sulphur reacted with the wustite and metallic iron to produce a lot of fluid, iron oxide rich, liquid very early in the test, which could react with the underlying coke to produce additional carbon monoxide in the outlet gas, further complicating the mass balance.

Sulphur pick-up by the sample also affected the reduction calculation as the true decrease in the weight of the sample was impossible to calculate, i.e. although oxygen was removed some sulphur was absorbed. This behaviour lowered the accuracy of the reduction calculations, but in all cases but one the calculations cannot be said to be widely inaccurate. The exception was the test at a heating rate of 200°C.hr<sup>-1</sup> with 0.75 vol. % elemental sulphur in the reducing gas. In this case a large amount of liquid dripped from the sample bed into the gas pre-heat section, in fact 34 g of solidified material was found in the underlying coke bed and in the pre-heat stage. (Refer to Section 4.6 for photographic details). Unfortunately, it was impossible to detect how much extra molten material had penetrated further down the pre-heat stage. A good indication of the extent of direct reduction that occurred during this particular test can be obtained from the recorder trace of the carbon monoxide level in the outlet gas (Figure 75).

Phase, chemical and x-ray analyses of the sample beds with sulphur in the reducing gas were carried out and are given in Tables 27, 28 and 29 respectively.

#### 4.3.3.8 Tests Incorporating Alkali Vapour in the Reducing Gas

Three tests using acid pellets were carried out with alkali vapour in the reducing gas using three levels of alkali loading - 5, 10 and 15 g  $K_2CO_3$ , which was calculated as being approximately equivalent to 6, 12 and 18 kg  $(K_2O + Na_2O)$ .tonne of iron<sup>-1</sup>. These levels are roughly equal to the alkali level in the lumpy, softening-melting and the dropping zones of the blast furnace respectively (Figure 49).

The test conditions chosen were a pre-reduction level of 30% along with a heating rate of  $400^{\circ}C.hr^{-1}$ . Figures 76, 77 and 78 show the results of these tests as well as the base case with zero alkali loading for comparative purposes. A fourth test using the  $400^{\circ}C.hr^{-1}$  heating rate and a degree of pre-reduction equal to 30% coupled with an alkali loading of 15 g  $K_2CO_3$  was also undertaken. In this particular case, however, no load was applied to the bed and the test was interrupted at  $1106^{\circ}C$ . These particular test conditions were selected in order to study the influence of alkali vapour in the reducing gas upon the mode of reduction of the iron oxide grains. Another feature of this particular test was that the rate of evaporation of alkali from the reaction cell could be estimated. At the conclusion of the test the reaction cell had lost 8.1 g of  $K_2CO_3$  of the original 15 g. (This indicates that the alkali evaporation rate was fairly uniform throughout the test because the completed tests had 100% evaporation of the alkali). The change in the degree of reduction of the bed was as follows:  $950^{\circ}C/30.5\%$  reduced;  $1000/38$ ;  $1025/41.5$ ;  $1050/45.5$ ;  $1100/55$  and  $1106/57.1$ .

Optical microscopic examination of the sample bed from the interrupted test showed that the reduction mode had changed from the topochemical mode normally observed without alkali vapour to non-topochemical (Refer to Section 4.6 for photographic details).

Optical and electron probe examination of the sample beds from the completed tests showed that at the highest alkali loading the slag phase had precipitated within it olivine crystals (electron probe analysis showed that these crystals were composed of iron and silicon, plus traces of calcium and magnesium) and a needle-like phase, which was found, by electron probe analysis, to consist of iron, silicon, aluminium, calcium and potassium. The surrounding slag phase was found by electron probe analysis to consist of iron, silicon, aluminium and potassium (the potassium level was great enough to generate both  $K\alpha$  and  $K\beta$  lines - refer to Section 4.6 for photographic and EDAX details). Examination of the sample beds at the two lowest alkali loadings showed that the microstructure was gradually changing from that found with acid pellets without alkali vapour addition to that previously described.

As the alkali loading increased there was a tendency for the metallic shell of the pellets to take upon a finer structure and this observation is indexed in Section 4.6.

Chemical and x-ray analyses of the sample beds were undertaken and are given in Tables 30 and 31 respectively.

#### 4.3.3.9 Inclusion of both Sulphur and Alkali Vapour in the Reducing Gas

In this test the pellets were pre-reduced by 30% and subjected to the  $400^{\circ}\text{C}.\text{hr}^{-1}$  heating rate. The sulphur concentration was 0.75 vol. % S and the alkali load was 15 g  $\text{K}_2\text{CO}_3$ . Figures 79, 80 and 81 show the results of the test alongside the results of the tests using sulphur and alkali vapour alone for comparison. Partial chemical analysis of the sample bed was undertaken after the test and the results are shown in Table 32.

#### 4.3.3.10 Dropped Materials

In a few high temperature tests with acid pellets, material dripped from the sample bed to collect in the bottom of the crucible and in the upper layers of the pre-heat stage. It was fairly common to find small spheres of metallic iron (~2 mm diameter) in the bottom of the crucible and microscopic examination showed them to have a typical grey cast iron structure.

During one of the commissioning tests of the high temperature apparatus, using acid pellets manufactured from an identical blend of iron ores as the pellets used in these studies, a considerable quantity of material dripped from the bed. (The final degree of reduction of the bed was ~65%, the temperature ~1225°C and the gas pressure drop in excess of 400 mm water gauge. The shape of the dropped material was very similar to the icicles found in the Japanese dissection studies<sup>48</sup> and they were consequently christened with the same name. Some of the icicles were crushed to a powder, the majority of the metallic iron removed with a small magnet and the remaining powder subjected to x-ray and chemical analysis (Tables 33 and 34). The surface layers of some of the remaining icicles were abraded away by gently agitating them in a small polythene bag and the resulting powder x-rayed. (Table 33). Microscopic examination of the icicles revealed the presence of numerous phases within them (Refer to Section 4.6 for details of photographic plates). Electron probe analysis showed that the olivine crystals within the slag matrix consisted of iron, silicon, some calcium, plus traces of aluminium, titanium and manganese. The small crystals at the walls of the icicles were found by electron probe analysis to be grains of silica. The feathery structured phase, also near the walls, consisted of iron, silicon, calcium, aluminium, titanium, manganese, plus traces of vanadium and potassium, whilst the surrounding slag phase was found to be iron, silicon, calcium, aluminium, plus traces of titanium, manganese and potassium (refer to Section 4.6 for EDAX details).

A considerable quantity of dropped material was produced by the high temperature test with sulphur in the reducing gas at the  $200^{\circ}\text{C}.\text{hr}^{-1}$  heating rate. (Already referred to in Section 4.3.3.7). Optical and electron probe examination along with the chemical analysis (Table 35) showed that the material was rich in sulphur. (Refer to Section 4.6 for details of photographic plates). The slag phases were found by electron probe studies to be extremely variable in chemical composition, some areas were basically iron, calcium, silicon with in some instances traces of potassium and aluminium. Other areas were iron, aluminium and titanium. The metallic grains were found to be one of three possibilities; iron, ferrous sulphide or the Fe-O-S eutectic phase.

#### 4.4 Experimental Studies with Sinters

The major part of the research programme was directed towards the study of acid pellets. All the concepts and ideas derived from this study were tested using sinters. Consequently the depth of the investigation into sinter behaviour was not as great as that of the pellets.

##### 4.4.1 Examination of Sinters in the As-Received State

The mineralogical structure of the sinters studied can be conveniently split into two distinct groups; lime rich and lime deficient. Lime rich regions naturally exist where particles of lime or limestone were present prior to the sintering process - the greater the lime addition, the greater the quantity of lime rich areas. Consequently as the  $\text{CaO}/\text{SiO}_2$  ratio increases the number of lime rich regions also increase. Lime rich regions of sinter were found to consist of ferrites, which were shown by electron probe analysis to be composed of iron and calcium plus

in some instances silicon. The lime deficient regions of the sinters were found to consist of magnetite and/or hematite surrounded by a slag phase, which was found by electron probe microanalysis to be composed of calcium, silicon and iron, with in some instances traces of aluminium and potassium.

#### 4.4.2 Initial Slag Formation Tests

Heating of semi-reduced sinters to 1100°C caused partial melting to take place, which was subsequently detected by optical examination and Section 4.6 gives details of the photographic plates showing the typical structures obtained after heat treatment. Electron probe analysis revealed that the new slag phase in the lime deficient regions of the sinters was essentially calcium, iron and silicon, with in some instances a trace of potassium. In the lime rich regions, the new slag phase was found to be composed of calcium and iron, with in some cases combinations of aluminium, magnesium and silicon.

#### 4.4.3 High Temperature Tests with Sinters

The scope of the investigation into the behaviour of sinters at elevated temperatures was not as extensive as the investigation with pellets. Basically the sinters were tested in the as-received condition and after pre-reduction using the 400°C.hr<sup>-1</sup> heating rate. Table 36 lists the tests undertaken with sinters.

##### 4.4.3.1 Sinters Tested in the 'As-Received' State

Examination of the reduction behaviour of sinters in the as-received state is obviously not directly applicable to the

blast furnace process. However, such a study is extremely useful for providing information at the lower reduction levels. The gas pressure-drop temperature curves at a heating rate of  $400^{\circ}\text{C}\cdot\text{hr}^{-1}$  are shown in Figure 82 and the reduction-temperature curves are presented in Figure 83. No contraction-temperature curves are shown, but the temperatures at which 3% contraction of the bed occurred are given in Table 37.

#### 4.4.3.2 Sinters Tested After Pre-Reduction

Two levels of pre-reduction were chosen, 30% and 45%. The gas pressure drop-temperature curves and the reduction-temperature curves for the 30% pre-reduced samples are shown in Figures 84 and 85. Only the gas pressure drop-temperature curves are shown for the 45% pre-reduced samples (Figure 86) because the final level of reduction attained in each case was virtually 100%. The 3% bed contraction temperatures are shown in Table 37.

In the case of the high temperature tests using 2.4 CaO/SiO<sub>2</sub> sinter a white powdery deposit was found on the surface of the sample in isolated locations. X-ray analysis of this powder showed that it was mostly comprised of calcium silicates (mainly dicalcium silicate) (Table 38).

#### 4.5 High Temperature Reduction Tests with Sinter/Pellet Mixtures

For these tests a 50/50 sinter/pellet ratio on a weight basis was selected using the superfluxed sinter (2.4 CaO/SiO<sub>2</sub>) and the acid pellets. The 50/50 ratio was that of the materials in the as-received state. Three situations were examined:- low pre-reduction level with a fast heating rate; low pre-reduction level with a slow heating rate and a high pre-reduction level with a fast heating rate (Table 39).

The gas pressure drop-temperature curves and the reduction-temperature curves for the three tests are shown in Figures 87 and 88. It was impossible to determine the reduction level in each material separately, hence the reduction level is an average calculated from the total original oxygen content of the sample bed. The 3% contraction temperatures were 1010°C, 1025°C and 1050°C for cases A, B and C respectively.

After the high temperature test at the 200°C.hr<sup>-1</sup> heating rate a small droplet was found adhered to a piece of coke in the bottom of the crucible. X-ray analysis of the crushed droplet showed it to contain FeS (Table 40).

#### 4.6 Photographic Plates

In the course of the experimental studies numerous samples were examined microscopically and this section, with one exception (Plate 1) identifies the plates which are representative of the structures observed. In addition several EDAX spectra are indexed.

##### 4.6.1 High Temperature Apparatus

Plate 1: View of the experimental apparatus.

##### 4.6.2 Acid Pellets

Plate 2: Microstructure of the pellets in the fully oxidised state.

##### 4.6.2.1 Initial Slag Formation Tests with Acid Pellets

Plates 3, 4 and 5: Structures observed after heating pre-reduced pellets in accordance with the procedure described in Section 3.3.

Plate 6: Structure of partially reduced pellets manufactured from ferric oxide and silica sand after reduction at 950°C (test number S5).

Plate 7: Structure of semi-reduced synthetic pellets manufactured from MalMBERGET concentrate and silica sand after reduction at 950°C (test number S8).

Plates 8 and 9: Structure of synthetic pellets manufactured from MalMBERGET concentrate and bentonite in the fully oxidised and semi-reduced state after reduction at 950°C respectively (test number S9).

#### 4.6.2.2 Structure after the High Temperature Test

Plate 10: Comparison of an almost fully reduced pellet bed (low gas pressure drop situation- test number 2) and a semi-reduced pellet bed (high gas pressure drop situation- test number 4).

Plate 11: Structure of the bed of pellets that were pre-reduced at 600°C (test number 13).

#### 4.6.2.3 Dropped Material

Plate 12: Icicles which dripped from a bed of acid pellets during commissioning of the high temperature apparatus.

Plates 13, 14, 15 and 16: Microstructure of the icicles.

Plate 17: Material which dripped from the sample bed of a high temperature test incorporating sulphur in the gas (test number 17).

Plates 18 and 19: Microstructure of the dropped material from a sulphur test (test number 17).

#### 4.6.2.4 Microstructure of the Sample Bed after the High Temperature Test

This section indexes the microstructures observed in three distinct cases, i.e. no additive to the reducing gas; sulphur in the reducing gas and finally alkali vapour in the reducing gas.

##### (i) No Additive

Plates 20, 21, 22, 23 and 24: Structure of pellets that were virtually fully reduced during the high temperature test (test number 2).

Plates 25, 26, 27, 28, 29 and 30: Structure of pellets that were only partially reduced during the high temperature test (test number 3 is the source of plate 27; test number 7 is the source of plate 28 and test number 4 is the source of the remaining plates).

Plates 31 and 32: Microstructure of the pellets that were initially pre-reduced at 600°C (test number 13).

##### (ii) Sulphur Addition

Plates 33 and 34: Influence of sulphur upon the microstructure (test numbers 15 and 17 are the sources of these two plates respectively).

(iii) Alkali Vapour Addition

Plates 35(a) and (b): Nature of the metallic iron grains of the pellets with and without alkali vapour addition (test numbers 20 and 4 are the sources of these two plates respectively).

Plates 36 and 37: Influence of alkali vapour upon the microstructure of the pellets (test numbers 21 and 20 are the sources of three two plates respectively).

4.6.3 Sinters

4.6.3.1 Initial Slag Formation Tests

Plate 38: Structure of partially reduced 1.8 CaO/SiO<sub>2</sub> (superfluxed) sinter after heating to 1100°C.

Plate 39: Structure of partially reduced 1.4 CaO/SiO<sub>2</sub> (self-fluxing) sinter after heating to 1100°C.

4.6.3.2 Structure After the High Temperature Test

Plate 40: Microstructure of a sinter which exhibited a high gas pressure drop (test number 24).

4.6.4 Sinter/Pellet Mixtures

These plates show the microstructure of the bed after the high temperature test using the test conditions of a low level of pre-reduction and a heating rate of 400°C.hr<sup>-1</sup> (test number 41).

Plate 41: Microstructure of a pellet in the bed.

Plate 42: Liquid slag from the pellets advancing into a particle of sinter.

#### 4.6.5 EDAX Spectra

##### 4.6.5.1 Acid Pellets in the Oxidised State

Plate 43: Slag phase in fully oxidised pellets.

##### 4.6.5.2 Acid Pellets in the Softened State

Plate 44: Main slag phase (sample from the initial melting tests after heating to 980°C).

Plate 45: Minor slag phase (same sample as that of Plate 44).

##### 4.6.5.3 Icicles

Plate 46: Olivine crystals.

Plate 47: Slag phase surrounding the olivine crystals.

##### 4.6.5.4 Acid Pellets After the High Temperature Tests with Alkali Vapour in the Reducing Gas

Plate 48: Thin needles precipitated in the slag phase (test number 20).

Plate 49: Olivine crystals precipitated in the slag phase (test number 20).

DISCUSSION

The aim of the experimental studies was to determine the influence of burden composition upon the physical and chemical processes occurring in the softening-melting zone of the blast furnace, within which the molten metal and slag phases form. Evaluation of the data obtained from the experimental studies and published literature, in particular the Japanese dissection studies, has led to the formation of a theory describing the softening and melting process within the blast furnace. The bulk of the experimental study was undertaken using acid pellets and the theories and concepts describing the softening-melting process were developed from evaluation of the experimental data obtained with acid pellets. Sinters were studied to a much lesser degree, but the theories and concepts developed with acid pellets were found to be equally applicable to sinters thus reinforcing the conceptual ideas.

5.1 The Softening and Melting Process - Stage I

The start of the softening and melting process in the high temperature studies was taken as the temperature at which 3% contraction of the sample bed occurred. Acid pellets tested at a heating rate of  $200^{\circ}\text{C}\cdot\text{hr}^{-1}$  exhibited 3% contraction temperatures of  $1010^{\circ}\text{C}$  and  $985^{\circ}\text{C}$  for the 32% and 52% pre-reduced samples respectively (Figure 58). At a heating rate of  $400^{\circ}\text{C}\cdot\text{hr}^{-1}$  identical temperatures were also obtained with different pre-reduction levels (Figure 61). This indicates that within the range of pre-reduction levels studied the temperature at which softening and melting starts is independent of the degree of reduction. Tests using nitrogen only produced similar 3% contraction temperatures (Figure 68), one exception to this was

the 26% reduced sample, but this will be discussed later. The situation found to exist with sinters was that the 3% contraction temperature was approximately 1100°C in every case (Table 37) which corresponds extremely well to the temperature at which the researchers undertaking the Japanese dissection studies found the cohesive zone to start at for furnaces operating on 80% sinter burdens (Tables 4 and 5, Figures 23 and 28).

Microscopic examination of acid pellets (44% reduced) after being subjected to the Initial Slag Formation tests (Section 3.3) revealed the existence of two new slag phases, the quantity of each increasing as the holding temperature rose. At 950°C these new phases were difficult to detect, only occurring in isolated areas, but in contrast the situation at a holding temperature of 980°C (roughly the 3% contraction temperature) and above was very clear, in that these new slag phases were present in many locations throughout the pellets - their volume increasing with the holding temperature. Confirmation that this was not a freak phenomenon was provided by repeating the tests using pellets having a higher degree of reduction and the two new slag phases were again observed. Plate 3 shows the start of the melting process with the two slag phases in view, a light shaded and a dark shaded one. Microprobe examination of these two slags showed that the lighter shaded slag was composed of iron, silicon and calcium (Plate 44), whilst the darker shaded slag was comprised of iron, silicon, calcium and potassium (Plate 45); only iron was detected in the surrounding wustite grains. In many areas the metallic iron present was acting as a barrier between the wustite grains and the slag, i.e. preventing the dissolution of the wustite by the liquid slag (Plate 4). At a holding temperature of 1075°C, the slag formation reaction was visible in many regions of the sample. Plate 5 shows the slag phase attacking a grain of wustite; again two slags are evident, the composition of each being as previously described. Note in this case the protective effect of the metal is far more noticeable than that shown in Plate 4.

The presence of calcium, silicon and potassium in the new slag phase effectively eliminates the possibility of a reaction between wustite and quartz grains, especially at temperatures as low as 980°C. In the FeO-SiO<sub>2</sub> system the solidus is 1177°C (Figure 89)<sup>81</sup>, a considerably higher temperature than 980°C ! Microprobe examination of the small quantities of slag phase present in the fully oxidised pellets showed that it consisted of calcium, iron, silicon plus traces of potassium, aluminium and magnesium (Plate 43), i.e. identical components to that found in the new slags. It is of interest to note that Russian workers<sup>12</sup> found the slag phase in acid pellets to be quantitatively composed of ~25 wt.% CaO, ~25% SiO<sub>2</sub> and ~50% Fe<sub>2</sub>O<sub>3</sub>. As identical elements are present in the new slags in the semi-reduced pellets after heat treatment and the slag in the fully oxidised pellets, the initial slag formation process must be via a reaction between the wustite grains and the slag from the fully oxidised pellets (termed residual slag). The protective barrier effect of the metallic iron strengthens the evidence for a residual slag/wustite reaction. It was impossible to detect whether the Fe<sub>2</sub>O<sub>3</sub> present in the residual slag was reduced during the reduction procedure because only qualitative microprobe data was available. Also the reaction with wustite would contribute a high proportion of ferrous ions anyway. The hypothesis of a residual slag/wustite reaction is made even more plausible by the presence of potassium, which even in small quantities lowers the melting point of slag by a considerable degree as shown in Figure 90<sup>82</sup>. (The CaO-SiO<sub>2</sub>-FeO system has a eutectic at 1105°C - Figure 91<sup>83</sup>).

Acid pellets are relatively homogeneous in structure and the initial liquid slag formation reaction is confined to a two phase system. Sinters on the other hand are heterogeneous and the quantity of phases present are greater, e.g. hematite, magnetite, various ferrites and slag phases. Nevertheless, the 3% contraction temperature, which has been shown to be a good guide to the start of

the melting process, was approximately 1100°C for each sinter (Table 37). Evaluation of the melting process occurring in sinters was undertaken using the same technique as for acid pellets, but with a holding temperature of 1100°C and proved that two distinct liquid slag formation reactions were taking place.

- (i) A reaction between grains of wustite which originated from hematite or magnetite and the slag phase that surrounded the iron oxide in the as-received state. This type of reaction is identical in nature to that occurring in acid pellets. Plate 39 shows the reaction in a region that is deficient in lime. Electron probe analysis of the new slag phase showed that it was essentially a calcium-iron-silicon melt which has a eutectic at 1105°C (assuming the iron to be ferrous iron - thus the melt is CaO-SiO<sub>2</sub>-FeO). This reaction was prevalent in the 1.2, 1.4 and the lime deficient regions of the 1.6 CaO/SiO<sub>2</sub> sinter, i.e. sinters or regions of sinter that were originally hematite or magnetite grains surrounded by a slag.
  
- (ii) The second mechanism observed was one in which melting occurred within partially reduced ferrites (Plate 38). Semi-reduced ferrites are essentially FeO-CaO or FeO CaO and SiO<sub>2</sub>. Consequently it is possible for melting to take place within the partially reduced ferrites at 1105°C (the eutectic temperature of the CaO-FeO-SiO<sub>2</sub> system) or 1100°C (the eutectic temperature of the CaO-FeO system) Figure 92<sup>84</sup>. Verification of the possibility of such a reaction was via electron probe microscopy which showed that the new slag phase was composed essentially of calcium and iron with a trace of silicon in some instances. Naturally this mechanism

is restricted to ferrite rich regions of the 1.6, 1.8, 2.1 and 2.4 CaO/SiO<sub>2</sub> sinters. In the case of the 1.6 CaO/SiO<sub>2</sub> sinter, in particular, both types of reaction mechanisms were observed depending whether the region was lime rich or lime deficient. As the basicity increased the ferrite proportion of the sinters rose (Table 18) and reaction (ii) became the dominant mechanism.

The bulk of the experimental studies was devoted to acid pellets and it was deemed essential to verify that the initial liquid slag formation reaction was via an interaction between wustite and the residual slag. Verification was undertaken by examining a series of synthetic acid pellets.

#### 5.1.1 Melting Behaviour of Synthetic Acid Pellets

In order to verify the hypothesis that the initial slag formation process is via a wustite/residual slag reaction it was necessary to manufacture some acid pellets without creating a slag phase in the oxidised state. The manufacture of these pellets is described in Section 3.3.1.

All the synthetic pellets manufactured from reagent grade ferric oxide and any form of silica which were fired at 1300°C formed a fayalite slag during reduction (Table 25). This was thought to be caused by the firing temperature being sufficiently high to cause some slag to be created from the silica and the ferric oxide. Pellets manufactured using a lower firing temperature of 1100°C still produced fayalite during reduction, irrespective of the form of the silica. The conclusion drawn from this was that the fine nature of the ferric oxide made it so reactive, that production of fayalite by solid state reaction between the ferrous oxide and the silica could occur. Plate 6 shows that the

structure of a pellet manufactured from ferric oxide and silica sand after reduction was one of wustite and fayalite. The latter formed by a solid state reaction. Similar findings were made by El-Geassy<sup>85</sup>.

The problem of fayalite production caused by the over-reactive ferric oxide was solved by replacing it with MalMBERGET iron ore concentrate, which is an extremely pure iron ore. Synthetic pellets manufactured from MalMBERGET and silica sand with a firing temperature of 1300°C did not show a significant proportion of slag phase in the fully oxidised state. Reduction and subsequent heat treatment of these pellets merely resulted in producing a structure of wustite and quartz (Plate 7). Introduction of a slag phase into the fully oxidised structure was accomplished by adding 2 wt.% of bentonite to the MalMBERGET concentrate and firing the pellets at 1300°C. Bentonite is a complex silicate clay and thus is of a suitable form for participating in a reaction with hematite grains. Some indication of the quantity of slag present in the fully oxidised pellets can be obtained by examination of Plate 8. Following reduction at 950°C extensive new slag formation was evident throughout the regions where the wustite/residual slag reaction had taken place. It is interesting to observe that two slags are present, as was the situation with the acid pellets (Plate 9). Examination of the slag phase in the oxidised pellets, manufactured from MalMBERGET and bentonite, with the electron probe showed that the slag consisted qualitatively of iron, calcium, potassium, silicon, aluminium and sodium. The lighter coloured slag in the reduced sample was composed of iron, silicon plus traces of aluminium, potassium and calcium; the darker coloured slag phase consisted of iron, calcium, silicon, potassium and a trace of aluminium. That is, the same elements are present in the slag phase in the fully oxidised pellets and the slags in the reduced pellets, verifying the theory of a wustite/residual slag reaction mechanism for the initial slag formation process.

The two slag phases observed after reduction of the acid pellets and the synthetic pellets, manufactured from the MalMBERGET and bentonite, are believed to be formed by precipitation of solid during cooling, i.e. the molten slag during cooling precipitates a solid phase whilst the liquid composition moves towards the eutectic composition where it finally solidifies. Enrichment of potassium in the darker slag phase verifies this hypothesis as potassium would be rejected by the precipitating phase.

#### 5.1.2 Quantity of Wustite/Residual Slag Reaction Sites

The existence of a wustite/residual slag reaction leads to the conclusion that the maximum number of reaction sites will occur when the iron oxide is converted completely to wustite. The presence of metallic iron limits the quantity of reaction sites by forming a barrier between the wustite grains and the residual slag as shown in Plates 4 and 5. Pre-reduction of all the samples was carried out using a carbon monoxide/nitrogen gas mixture of high reduction potential and consequently capable of reducing iron oxide to metallic iron. Naturally topochemical reduction occurs producing some wustite surrounded by a layer of metallic iron, which shields the wustite from the residual slag and therefore prevents the formation of any liquid slag. Additionally, the metallic iron prevents further reaction between the wustite grains and any liquid slag that may have been formed by the residual slag/wustite reaction. As a result, the presence of metallic iron significantly reduces the number of reaction sites available for liquid slag formation.

As stated, the maximum number of reaction sites must occur when the iron oxide is all converted to wustite, which would correspond to a uniform reduction of 30%. However, at low levels

of reduction in a carbon monoxide/nitrogen gas mixture, the pellet core can still be hematite or magnetite at a time when the surface of the iron oxide grains near the pellet periphery will already have been reduced to metallic iron. Intermediate locations along the pellet radius will possess a wustite structure which can react with the residual slag. As reduction proceeds the core approaches the wustite composition and the thickness of the metallic iron shell increases. This increase in wustite towards the core tends to create more reaction sites, but they can become increasingly shielded by the growing proportion of metallic iron. The overall effect is that the maximum number of reaction sites does not occur at 30% reduction, but at the higher levels of 40 - 50% (Figure 93). Workers at CRM<sup>69</sup> found that the minimum softening temperature of sinters occurred at reduction levels of 40 - 50%. An additional point is that metallic iron acts to strengthen the sample and minimise the total level of contraction, but not the start of contraction to any significant extent.

Attempting to apply this supposition to the softening of pellets as they undergo high temperature reduction is difficult because the reduction state is continuously changing and the time for the reaction between wustite and the residual slag to occur is short. A method of overcoming the problem of an altering reduction level is to examine the data from the nitrogen only tests (Figure 68). The results from this series of tests show that the 3% contraction temperature was a minimum at 44% reduction - very similar to the results obtained at CRM with sinters.

## 5.2 The Softening and Melting Process - Stage II

The development of the softening-melting process after the initial liquid slag reaction has taken place can be considered in two parts, firstly the influence of the ensuing reactions on the

properties of the bed and secondly the actual reactions occurring. The tests with acid pellets at a heating rate of  $200^{\circ}\text{C}.\text{hr}^{-1}$  showed that, although high levels of contraction occurred, the gas pressure drop displayed only a steady rise (Figures 58 and 59). The final degree of reduction for these tests was 95% and 85% for the 52% and 32% pre-reduced samples respectively. Tests with acid pellets at the  $400^{\circ}\text{C}.\text{hr}^{-1}$  heating rate also produced large degrees of bed contraction, but the change in the gas pressure drop showed some remarkable differences to that observed at the slower heating rate (Figures 61 and 62). At the level of 61% pre-reduction the rise in gas pressure drop was similar to that recorded for both tests at a heating rate of  $200^{\circ}\text{C}.\text{hr}^{-1}$ , but the sample having 30% pre-reduction showed a dramatic rise in gas pressure drop at  $\sim 1230^{\circ}\text{C}$ . An intermediate situation was obtained between these two extremes with the 49% pre-reduced sample.

Examination of the reduction-temperature curves for the samples of acid pellets tested at the  $400^{\circ}\text{C}.\text{hr}^{-1}$  heating rate shows that the commencement of direct reduction was detected for both the 49% and the 30% pre-reduced samples (Figure 63). In the case of the 30% pre-reduced sample the total level of reduction was  $\sim 65\%$  and the start of direct reduction is extremely evident by the rapid rise in the rate of reduction. This rapid rise in the reduction rate occurred at  $\sim 1230^{\circ}\text{C}$ , which is the same temperature at which the gas pressure drop rose quickly. Hence one can conclude that iron oxide rich liquid was filling the voids of the bed, causing a rapid rise in the gas pressure drop and the same liquid reacted with the coke layers to produce the acceleration in the rate of reduction, i.e. direct reduction occurred. Evidence of iron oxide rich liquid filling the voids of the bed is shown in Plate 26. Two metallised pellet surfaces can be seen and the void between the pellets contains a slag

phase, within which dendrites of wustite have precipitated during the cooling procedure.

### 5.2.1 Temperature - Reduction - Isobar Diagrams

The data from the gas pressure drop-temperature and reduction-temperature curves for both the  $200^{\circ}\text{C}.\text{hr}^{-1}$  and  $400^{\circ}\text{C}.\text{hr}^{-1}$  reduction tests with acid pellets show that the gas pressure drop is a function of the level of reduction and the temperature. High temperatures and low reduction levels tend to produce high gas pressure drops; equivalent temperatures but with high reduction levels tend to produce low gas pressure drops. This information has been conveniently summarised diagrammatically in Figure 94. This diagram is constructed by plotting the reduction-temperature curves at a heating rate of  $400^{\circ}\text{C}.\text{hr}^{-1}$  and superimposing onto them the increase in gas pressure drop, i.e. the total gas pressure drop at any temperature minus the total gas pressure drop at  $950^{\circ}\text{C}$ . These types of diagrams have been termed 'TRIB' diagrams (Temperature, Reduction, Isobars) and they illustrate 'critical' areas or zones of reduction and temperature where high gas pressure drops are encountered, i.e. a situation where 'melt-down' of the sample bed is occurring. The critical area is where the isobars merge together, i.e. at  $1200 - 1250^{\circ}\text{C}$  and 60 - 65% reduction. The  $200^{\circ}\text{C}.\text{hr}^{-1}$  reduction curve of the 32% pre-reduced sample by-passes the critical region, thus avoiding the production of high gas pressure drops. Naturally in the area below the indicated critical zone, high gas pressure drops will also occur. To obtain data in the lower regions four possible experimental techniques were available:-

- (i) Increasing the heating rate in the reduction tests.

- (ii) Lowering the carbon monoxide content of the reducing gas.
- (iii) Testing samples of different levels of pre-reduction in nitrogen gas.
- (iv) Testing samples with pre-reduction levels less than 30%.

It was experimentally difficult to increase the heating rate, not because of electrical power limitations, but because temperature control was lost at rapid heating rates. Moreover, the rapidity at which reactions could be occurring could cause an experimental reading to be missed. Lowering the carbon monoxide content of the inlet gas was eliminated as a possibility because it would limit the reduction reaction and decrease the level of carbon dioxide in the outlet gas, conceivably to a level insufficient for accurate determination. (The carbon dioxide levels in the outlet gas for the majority of tests ranged between approximately 5 vol. %, at the start of the test and 0.2 vol. % at the conclusion of the test). These experimental limitations led to the decision to test the acid pellets in nitrogen only together with a reduction test on a sample of pellets in the fully oxidised state (i.e. without any pre-reduction).

#### 5.2.1.1 Nitrogen Only Tests

The results of the gas pressure drop-temperature curves shown in Figure 69 have been superimposed onto the TRIB diagram. Three constant reduction levels are shown, 26%, 47% and 65% (Figure 95). Although the gas pressure drops for the nitrogen only tests do not correspond exactly with the values from the reduction tests, the point of rapid rise in gas pressure drop does.

Compare the 65% pre-reduction-nitrogen-only-test with the 60 - 65%; 1200 - 1250°C critical zone. At lower levels of reduction the melt-down temperature is depressed - at 26% reduction melt-down occurred at approximately 1180°C. The reason for the inconsistency between the gas pressure drops for the nitrogen only tests and the reduction tests in areas outside the critical zone most likely lies in the fact that the surface area of the wustite available for reaction, with the residual and newly created liquid slag, is continuously altering in reduction tests. Thus the gas pressure drop at any point on the reduction-temperature curve will depend upon the reactions taking place at that point and upon the extent of the reactions that have occurred prior to that point. In conclusion the nitrogen-only-tests have established the approximate location of the high gas pressure drop (melt-down) region at lower levels of reduction.

#### 5.2.1.2 Reduction Test with Fully Oxidised Pellets

This test is far from typical of the type of reaction that would occur in the blast furnace process in that reduction would not suddenly start at 950°C. However, it gives some useful information at the lower reduction levels. The contraction-temperature curve shows that the 3% contraction level occurred at 1095°C, after which further extensive contraction of the bed followed rapidly (Figure 64). This is in sharp contrast to the 985 - 1010°C range of 3% contraction temperatures found with pre-reduced samples. The discrepancy is caused by the pellets swelling during reduction and acting against the pressure of the ram which naturally delays contraction of the bed until higher temperatures are reached. With pre-reduced samples the majority of the swelling reaction occurred during the isothermal pre-reduction stage and any subsequent swelling in the high temperature test was negligible. During commissioning tests

with the high temperature apparatus, which were basically intended to overcome equipment faults, the sample bed actually expanded with some samples of acid pellets tested in the fully oxidised state. (Note, those particular pellets were not those used in this study).

Returning now to the gas pressure drop-temperature curve for the pellets, it is apparent that melt-down commenced at approximately 1125°C (Figure 64). The final level of reduction attained in this particular test was only 42% (Figure 65). Examination of the microstructure of the sample after the high temperature test shows the presence of metallic iron, but perhaps more interesting is the presence of grains of metallic iron which are not quite fully developed (Plate 27).

#### 5.2.1.3 Gas Pressure Drop - Contraction Relationship

Plotting the total gas pressure drop against the contraction of the bed, for the results obtained from the high temperature reduction tests with pre-reduced samples of acid pellets at a heating rate of 400°C.hr<sup>-1</sup>, shows that the two are related up to a contraction level of approximately 30%, irrespective of the extent of pre-reduction (Figure 96). An identical state of affairs exists for the reduction tests carried out at a heating rate of 200°C.hr<sup>-1</sup>, although the magnitude of the gas pressure drops at the conclusion of the tests was lower than those obtained with the heating rate of 400°C.hr<sup>-1</sup>. The temperature at which 30% contraction occurred in the reduction tests was approximately 1140°C in all cases regardless of heating rate. An exception to this observation was the 61% pre-reduced sample at a heating rate of 400°C.hr<sup>-1</sup> which attained a contraction level of 30% at approximately 1160°C which, however, cannot be reasonably termed as a significant difference.

Wide deviations in the relationships for different samples between the gas pressure drop and the contraction of the bed, at temperatures in excess of  $1140^{\circ}\text{C}$ , are caused by differences in the amount of liquid slag present in the sample and by variations in the balance between the effect that this slag has on the porosity of the individual pellets and on the porosity of the bed as a whole. If the slag only reduces the pellet porosity, it is acting on a micro scale, but if the slag has sufficient volume and fluidity to enter the voids of the bed, it is acting on a macro scale. Micro changes in porosity within pellets would have a relatively small effect on the gas pressure drops. Macro changes on the other hand cause large gas pressure drops, e.g. the dramatic change in the gas pressure drop of the 30% pre-reduced sample at a heating rate of  $400^{\circ}\text{C}\cdot\text{hr}^{-1}$ .

Reconsidering the TRIB diagram (Figure 94) the 'kink' in the diagram caused by the 49% pre-reduced sample exhibiting higher gas pressure drops than the 30% and 61% pre-reduced samples up to  $\sim 1150^{\circ}\text{C}$  can now be explained in terms of the gas pressure drop - contraction relationship. The contraction-temperature curves illustrated in Figure 61 show that between  $1050^{\circ}\text{C}$  and  $\sim 1100^{\circ}\text{C}$  the 49% pre-reduced sample contracted more than the other two samples and as the gas pressure drop is related to the contraction level it follows that the gas pressure drop must be higher. A reason for the increased contraction level of 49% pre-reduced sample could be connected with the extent of slag formation, i.e. the amount of molten slag may have been greater than the quantities present in the other two samples in this temperature range. This would of course be related to the number of the wustite/residual slag and wustite/molten slag reaction sites. It has been demonstrated that the number of the former is a maximum at 40 - 50% reduction. In an athermal reduction test however the microstructure is continuously changing, making detailed interpretation of minor changes in contraction, gas pressure drop, etc. difficult.

The disappearance of the kink in the TRIB diagram is also connected with the amounts of liquid slag and metallic iron present in the sample. At temperatures in excess of  $\sim 1100^{\circ}\text{C}$  the 30% pre-reduced sample started to contract more than the 49% pre-reduced sample, due to the greater liquid slag volume and the smaller quantity of metallic iron. This increased slag volume affects the micro porosity and eventually the macro porosity of the sample bed. These porosity changes increase the gas pressure drop first on a small scale, then finally on a dramatic scale. This results in small temperature changes producing large gas pressure drop changes. Applying this to the TRIB diagram (Figure 94); the 30% pre-reduced sample eventually contains a greater slag quantity than the 49% pre-reduced sample, although at lower temperatures the reverse would appear to be true. Hence the 30% pre-reduced sample 'caught up' and surpassed the 49% pre-reduced sample, ironing out the kink.

The concept of TRIB diagrams conveniently connects the permeability (related to the gas pressure drop) of acid pellets to the degree of reduction and the pertaining temperature of the pellets. Sinters were found to comply with the TRIB diagram concept, with each sinter having its own characteristic diagram. Two examples of TRIB diagrams are shown in Figures 97 and 98 for the 1.4 and 1.8 CaO/SiO<sub>2</sub> sinters respectively. In the case of the 1.4 CaO/SiO<sub>2</sub> sinter both the as-received and the 29% pre-reduced samples entered the zone of rapid build-up of gas pressure. This is the melt-down situation which is analogous to that found with acid pellets. Only the 46% pre-reduced sample avoided the critical zone by attaining a higher reduction level. With the 1.8 CaO/SiO<sub>2</sub> sinter the situation of a similar rapid build-up of gas pressure was not obtained with the 30% pre-reduced sample, illustrating that the 1.8 CaO/SiO<sub>2</sub> sinter possesses a higher melt-down temperature, however, the as-received sample did show signs of melt-down. Micro-examination of sinter samples

that underwent melt-down during the high temperature test showed solidified slag in surface layers of the sinter particles (Plate 40) which is identical to the situation found with acid pellets which underwent melt-down.

Comparison of the TRIB diagrams for each individual sinter showed that a zone of reduction and temperature existed within which the critical zone of each of the individual sinters lay (Figure 99). Consequently this zone is a region that must be avoided by all the sinters, irrespective of chemical composition, if high gas pressure drops and melt-down conditions are to be minimised until greater temperatures are attained. The ability of a particular sinter to avoid this zone during reduction is thus a measure of its high temperature properties.

#### 5.2.2 The Mechanism of the Softening and Melting Process in Burden Materials

Using the information collected from the initial melting tests and from the high temperature tests it was possible to establish a theory outlining the reactions occurring and their influence upon the high temperature properties of burden materials during athermal reduction with a carbon monoxide/nitrogen gas mixture. The basis of this theory was established from the study of acid pellets but it is equally applicable in general terms to other burden materials.

It has been established that the melting process in acid pellets is started by reaction between residual slag and wustite, at about  $980^{\circ}\text{C}$ . Regions of sinter that are deficient in lime exhibit a similar reaction, between wustite and the surrounding Ca-Si-Fe slag, at  $\sim 1100^{\circ}\text{C}$ . Lime rich regions of sinter also start to melt at  $\sim 1100^{\circ}\text{C}$ , but in this case by internal melting of the partially reduced ferrites to form a CaO-FeO melt or a

CaO-FeO-SiO<sub>2</sub> melt depending on the ferrite type. Once a molten slag has been created it proceeds to devour the surrounding wustite and slag (or partially reduced ferrites in the case of high basicity sinters), assisted by the rise in temperature. The reduction process acts in opposition because it decreases the quantity of wustite available for reaction (provided the reduction level is in excess of the optimum reduction level illustrated in Figure 93), and because it forms metallic iron which provides a physical barrier between the wustite grains and the interacting slag phase. A balance thus exists between slag formation and reduction. If slag formation reactions dominate, the large volumes of liquid slag formed will inhibit the transport of reactant and product gas to and from iron oxide rich grains, and will thus impede the reduction reaction. Should the reduction reactions dominate then the extent of liquid slag formation is limited as outlined above. A low rate of temperature rise favours gaseous reduction, whilst a rapid heating rate encourages slag formation.

The effect of the balance between slag formation and reduction with acid pellets is shown by the differences between the gas pressure drop and reduction curves for the 32% pre-reduced sample at a heating rate of 200°C.hr<sup>-1</sup> and the 30% pre-reduced sample at a heating rate of 400°C.hr<sup>-1</sup> (Figures 59, 60, 62 and 63).

The topochemical nature of the reduction reaction results in the surface of the pellets or sinter being reduced to metallic iron whilst the core is reduced to wustite or partially reduced ferrites. Hence the liquid slag formation reactions occur at the core of the burden material. As an example, topochemical reduction of acid pellets creates a surface consisting of metallic iron and quartz grains, whilst the centre is composed of wustite which participates with the residual slag to form the liquid slag.

The situation existing at the surface is shown in Plate 20 - note the unreacted quartz grain. At the core of the burden material the liquid slag, until it is saturated, will attack and devour the remaining wustite, quartz (in the case of pellets), solid slag phases and particles of lime and partially reduced ferrites (in the case of sinters). Intermediate positions between the surface and the centre will of course exhibit structures inbetween the two extremes.

The liquid slag inhibits any further gaseous reduction and as the temperature rises it migrates towards the surface of the burden material by surface tension. Evidence of this migration is provided by the porosity at the pellet core (Plate 25). During its journey to the surface the liquid slag dissolves any slag, lime and quartz in its path. Plates 28 and 23 show, respectively, the slag front advancing to the surface of a pellet and slag attacking a grain of quartz. Whether or not the liquid slag can escape from the burden material depends upon the thickness of the metallic iron shell, the quantity of slag and its viscosity. A thick shell strengthens the material, minimising the squeezing action, which can assist the flow of slag to the surface, and also offers a greater physical resistance to liquid flow. In contrast, a thin shell cannot support the applied load and offers little resistance to liquid flow. Escape of the liquid slag from acid pellets has already been shown in Plate 26 and recognised as the cause of high gas pressure drop.

It is interesting to contrast the two distinct situations provided by a highly reduced bed and by a bed having a low degree of reduction. At the core of a highly reduced pellet the quantity of liquid slag is insufficient to dissolve the quartz completely, resulting in a silicate phase rather than a fully assimilated slag phase (Plate 21). The surface layers of such a sample show little sign of a liquid slag phase (Plate 22). An indication of

the physical appearance of beds of acid pellets that cause high gas pressure drops and low gas pressure drops can be gained from Plate 10.

A schematic representation of the reaction mechanism described above is presented in Figures 100 and 101 for acid pellets. Sinters behave in a similar manner except that their heterogeneous nature complicates the basic reaction; e.g. instead of the liquid slag dissolving quartz as occurs with pellets, the reaction in sinters involve lime, quartz, slag phases, etc.

#### 5.2.2.1 Changes in Slag Composition During the High Temperature Reduction of Acid Pellets

Elucidation of the changes occurring in the composition of liquid slag in sinters is extremely difficult because of their heterogeneous nature. Even with the much simpler nature of acid pellets it is impossible to determine the exact changes occurring within the slag phase during reduction because examination of the pellet microstructure takes place at room temperature. Consequently the structure that is being observed has undergone some alterations during cooling and none of these changes occur under equilibrium conditions. Nevertheless, an approximate summary can be provided.

The basis of the slag system is the CaO-FeO-SiO<sub>2</sub> phase diagram, which is illustrated in Figure 91. The first slag to form corresponds to the eutectic composition at the olivine/wollastonite/tridymite phase boundary; the presence of alumina, magnesia and in particular alkalis lowers the melting point of the slag to approximately 980°C. As the temperature increases the slag dissolves wustite and moves towards the FeO corner of the phase system. To simplify consideration of this system, the

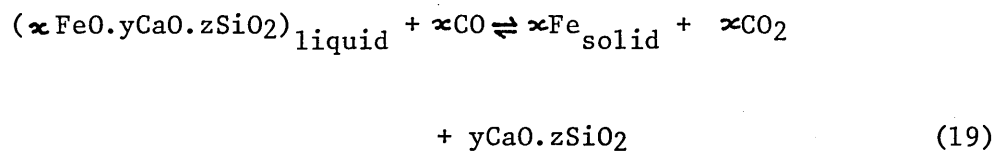
liquidus surface between the eutectic composition and the FeO corner has been constructed and is shown in Figure 102. The dissolution of wustite in the slag lowers the concentrations of alkali, calcium and other trace elements, so that the basic system increasingly becomes the FeO-SiO<sub>2</sub> system. Dissolution of quartz in the slag increases the silica content and could tend to move the slag composition towards the SiO<sub>2</sub> corner of the phase diagram. However, the wustite grains are in far greater abundance than quartz and the change in composition is probably not large so that the slag will tend to remain in the olivine or wustite regions of the phase diagram; the actual region depending upon the temperature and upon the extent of the reaction with the wustite.

Cooling the slag reverses the process leading to precipitation of wustite in dendritic form, as shown in Plates 26 and 32. Further cooling results in the formation of the slag phase which is recognised as the major slag phase when observed at room temperature and to the formation of a liquid corresponding approximately to the eutectic composition enriched by alkali (the darker slag phase present in small quantities in Plates 26 and 32).

A further source of information concerning the changes in slag composition that can occur arose from the incident during the commissioning of the high temperature apparatus when icicles were formed (previously documented in Section 4.3.3.10). These icicles were formed by molten slag rich in iron oxide running out of the crucible and encountering the reducing gas. A rapid reaction then occurred quickly reducing the surface of the liquid to metallic iron (Plate 13). At the interior of the icicles olivine crystals were formed, either during cooling or at the time of reduction, within the slag matrix (Plate 14). Electron probe analysis of the olivine crystals showed them to be essentially

iron silicate with the presence of some calcium and traces of aluminium, titanium and manganese (Plate 46). The surrounding slag was an iron-calcium silicate (Plate 47). As olivine is present at the interior of the icicles, but not in the slag within a bed of acid pellets after the high temperature test, it is feasible that the rapid reduction of the liquid iron oxide in the former could enrich the slag in silica and enhance the rate of formation of olivine from the melt. Evidence of such enrichment, certainly at the surface of the icicles, is provided by the existence of a relatively complex calcium aluminosilicate feathery like precipitate and silica grains near the walls of the icicles (Plates 13 and 15 respectively). Further evidence is provided by the x-ray analysis of the material abraded off the surface of the icicles which revealed the presence of tri-calcium silicate (Table 33).

Hence the basic reduction reaction at the surface of the icicles can be treated viz:



where,  $y \text{CaO} \cdot z \text{SiO}_2$  represents an effective enrichment of the liquid slag to a level sufficient to cause precipitation of a calcium silicate or even silica alone during the cooling process.

#### 5.2.2.2 Reduction Characteristics of Burden Materials

The major factor determining whether burden materials have a high or a low gas pressure drop at elevated temperatures is the extent of reduction that has occurred by the time the slag

starts to form. The greater the degree of reduction the higher the melt-down temperature, so that with acid pellets, for example, the influence of heating rate upon the degree of gaseous reduction is important, i.e. the slower the heating rate the greater the degree of gaseous reduction that is attained before slag starts to form. Sinters, in comparison, are more complicated because other factors such as type and quantity of the phases present must be considered. It has been established that the presence of ferrites in sinters increases their reducibility<sup>23,38</sup>, provided dicalcium ferrite is not present (Table 3). Increasing the basicity of sinters raises the proportion of ferrites in their structure in the as-received state (Table 18). No attempt to distinguish between the different types of ferrites was made because of the conflict that exists concerning the recognition of the numerous members of the ferrite family<sup>86</sup>. Attempts to relate the phases present in sinters to the reducibility is fairly straightforward provided the reduction temperature is below that at which molten slags appear. For example, Mazanek<sup>38</sup> demonstrated the interdependence of the ferrite and ferrous oxide contents of sinters on their reducibility. The presence of liquid slag introduces a new dimension into the study and complicates the issue considerably. Measurement of the reducibility of the sinters using the ISO reducibility test showed that a steady increase occurred as the basicity rose, reaching a maximum at 2.1 CaO/SiO<sub>2</sub>, then dropping slightly as the basicity reached 2.4 CaO/SiO<sub>2</sub> (Table 19). The peak at 2.1 CaO/SiO<sub>2</sub> is almost certainly due to the increase in the proportions of ferrites and hematite (Table 18). It is not unreasonable to assume that a considerable proportion of dicalcium ferrite must be present at 2.4 CaO/SiO<sub>2</sub> lowering reducibility.

The reduction curves obtained from the high temperature studies were analysed using McKewan's<sup>24</sup> rate equation as follows.

### 5.2.2.3 Reduction-Time-Temperature Considerations

The change in the reduction level of the sample bed with time, during the high temperature tests with acid pellets was treated on the basis of McKewan's rate equation (Equation 7, Section 2.2.2.2). McKewan<sup>24</sup> and Hills<sup>26</sup> have different explanations as to the rate controlling step of the reduction mechanism. It is not the intention to enter into this sphere of debate, but merely use McKewan's equation as a tool irrespective of the rate controlling mechanism. Assuming that  $d_0$  and  $r_0$  remain constant in the pellet bed then equation 7 simplifies to:-

$$1 - (1-R)^{\frac{1}{3}} = K_2 t \quad \text{-----} \quad (20)$$

where  $K_2$  is a constant:

The linearity of the reduction-time curves allows the determination of the apparent rate constant,  $K_2$  (Figure 103).

The main feature of these plots is that the reduction procedure is athermal, yet the gradient of the curve shows little change. This would be unexpected if  $K_2$  were regarded as a true chemical rate constant but, since gas phase transport phenomena play a major role in determining the reaction rate, their relative insensitivity to changes in temperature explains why the reduction curves are so similar until approximately 35 minutes reduction time at both heating rates. After this time the 30% pre-reduced sample tested at the heating rate of  $400^\circ\text{C}\cdot\text{hr}^{-1}$  started to melt, impeding further gaseous reduction.

During the high temperature tests, irrespective of the heating rate, the apparent reduction rate constant,  $K_2$ , of all the samples of acid pellets that had been pre-reduced at  $950^\circ\text{C}$  were virtually identical,  $0.0046 \text{ min}^{-1}$ , until melt-down of the

bed was encountered. This is because the small increase in gaseous diffusion rates produced by the rise in temperature is compensated by the decrease in the partial pressure driving forces for diffusion. The net effect is a reasonably constant reaction rate. The partial pressure driving forces decrease because the wustite/iron equilibrium line with carbon dioxide and carbon monoxide approaches the inlet gas composition of  $\text{CO}/(\text{CO} + \text{CO}_2) = 1.0$  as the temperature increases (Figure 104).

Examination of the reduction data arising from the studies with sinters using McKewan's rate equation provided a reduction rate constant for each sinter (Table 41). (As a comparison the rate constants calculated from the ISO reducibility tests are also given). An example of the plots is shown in Figure 105 for the 2.1 CaO/SiO<sub>2</sub> sinter. It is interesting to observe that the maximum reduction rate, in the high temperature test, occurred at 1.8 CaO/SiO<sub>2</sub> as opposed to 2.1 CaO/SiO<sub>2</sub> in the ISO reducibility test. The amount of liquid slag, ferrites and hematite will influence (or determine) the reaction rate in the high temperature test. As stated in an earlier section, large quantities of liquid will restrict the gaseous reduction reaction and increased quantities of hematite and ferrites (not dicalcium ferrite) will accelerate the gaseous reduction rate. It is the balance between these parameters that produce a maximum reduction rate at 1.8 CaO/SiO<sub>2</sub>. To pinpoint the interactions in detail from this study is difficult because of the broad approach used, i.e. the study of several sinters, rather than an in depth study of a selected few. Bearing this in mind, it is possible to make tentative suggestions as to the interactions between the various parameters. The general trend is that the 3% contraction temperature falls as the basicity increases and the amount of liquid would be expected to rise accordingly (Table 37). The rise in the quantity of liquid would decrease the gaseous reduction rate except that the increased proportion of readily reduced hematite and ferrites would tend to increase the reduction

rate. This appears to be true except for the 2.4 CaO/SiO<sub>2</sub> sinter which has a lower reducibility probably caused by the presence of dicalcium ferrite. Pre-reduction of the samples converts the hematite to magnetite, but this magnetite is fairly porous and readily reduced, unlike the magnetite originally present.

In a previous section it was stated that it was the ability of a material to avoid the critical area of reduction and temperature that determined the gas pressure drop. Figure 83 shows that all the sinters in the as-received state entered this critical area or the underlying region. Consequently they all underwent melt-down (Figure 82). After 30% pre-reduction the 1.8, 2.1 and 1.6 CaO/SiO<sub>2</sub> sinter avoided the critical area, whilst the rest still entered into the critical area or the underlying region (Figure 85). The 1.8 CaO/SiO<sub>2</sub> sinter has a large margin between its reduction path and the critical area, the 1.6 CaO/SiO<sub>2</sub> sinter a small margin and 2.1 CaO/SiO<sub>2</sub> is in between the two. Figure 84 shows that melt-down of the 1.2, 1.4 and 2.4 CaO/SiO<sub>2</sub> sinters occurred whilst the 1.8 CaO/SiO<sub>2</sub> sinter showed no sign of melt-down. The 1.6 CaO/SiO<sub>2</sub> sinter showed some sign of melt-down and the 2.1 CaO/SiO<sub>2</sub> sinter was in between the two; exactly the same trend as depicted in Figure 85.

At 45% pre-reduction all the samples by-passed the critical area and consequently melt-down did not occur (Figure 86).

### 5.3 Comparison of the Proposed Softening and Melting Mechanism with the Japanese Dissection Studies

A good correlation between the Japanese dissection studies and the concepts derived from the experimental studies is essential if the latter is to be thought of as the answer to the question:- What are the reactions occurring in the iron bearing materials within the softening-melting zone and what are the consequences of such reactions upon the burden behaviour ?

It has been demonstrated that material near the apex of the cohesive zone in a centre working blast furnace undergoes an extremely rapid rate of heating through the cohesive zone. Material in the base of the cone (near the walls) on the other hand is exposed to a relatively slow heating rate. The majority of the burden material near the centre regions of the furnace, e.g. Layer G-5 (Figure 29) - is only slightly reduced prior to entering the cohesive zone because of the short transit time from the stockline to the start of the cohesive zone, i.e. the lumpy portion D in Figure 29 and Table 6. (It must be remembered that some oxidation of the materials may have occurred during the water quenching operation). An exception to the low level of reduction is portion C, whose volume is relatively small in comparison to portion D and of lesser significance. A boundary exists between the lumpy and the softening portions where the physical state of the burden materials changes from the non-softened to the softened state. This boundary is marked X-X in Figure 29. One can look upon the boundary as being equivalent to the 3% contraction temperature reported in the experimental tests, i.e. the temperature where the materials are starting to soften. The Japanese data indicates that this boundary is approximately at  $1100^{\circ}\text{C}$  for furnaces operating with about 80% sinter in the burden<sup>45</sup>. The experimental work with sinters showed 3% contraction temperatures of approximately  $1100^{\circ}\text{C}$ , which is in extremely good agreement with the Japanese observations. The acid pellets examined, on the other hand, have a 3% contraction temperature of approximately  $980^{\circ}\text{C}$  and it would be expected that the boundary between the granular and softening portions in a blast furnace burden consisting of these pellets only would be at this temperature.

The degree of reduction in the large softening portion, B, is much higher than in the lumpy portion; degrees of reduction of 60 - 80% are in evidence. These significantly higher levels of reduction can be attributed to the kinetics of the gaseous

reduction reaction being favoured by the higher temperature and by the increased reduction potential of the gas issuing from the central coke core (carbon dioxide is absent in this gas). Identical rapid reaction rates were obtained with both the acid pellets and the sinters during the experimental tests. If we now consider the half-molten portion, portion A, we can see that, due to its semi-molten state, all gaseous reduction can be assumed to have effectively stopped. Molten material then starts to drip out from this portion. (This material was frozen during the quenching operation to form icicles). Molten material originating from the commissioning of the high temperature apparatus using acid pellets produced identical icicles from a bed having a reduction degree of about 60% and at a temperature in the region of 1225°C.

The reactions within the cohesive zone under fast heating rates can be summed up as follows. Material entering the cohesive zone possesses a low level of reduction, due to the rapid transit time between the stockline and the start of the cohesive zone. Once into the cohesive zone rapid gaseous reduction occurs and softening of the burden commences. The rate of reduction, although fast, is insufficient to prevent a large amount of liquid slag being produced which effectively stops the process of gaseous reduction. As the temperature rises the iron oxide rich slag runs out of the bed, manifesting itself as icicles in the quenched furnace. Large amounts of direct reduction will occur as the molten slag reacts with the underlying coke bed. The overall reaction is identical to that occurring in the experimental studies with acid pellets, or sinters, having a low level of pre-reduction and at a fast heating rate.

The extent of reduction in the lumpy zone of material which will eventually pass through the cohesive zone at a position near the wall of the blast furnace, e.g. Layer G-19 in Figure 29 and Table 6, is much higher than that in Layer G-5 because it takes

longer for the material to move from the stockline to the start of the cohesive zone. The extent of reduction is not as great as may be expected merely from the transit time because the temperature is lower in this position so that the reduction reaction is not so fast, this being reflected in the degree of reduction obtained. No reduction data is given regarding the levels obtained in portions A, B and A'. However, as the heating rate through the cohesive zone is slow, compared to the central regions of the furnace, it can be surmised that the extent of gaseous reduction is extremely high, reaching virtually 100%, with final melting of the reduced material occurring within the small portion A'. The experimental high temperature tests with acid pellets showed that a slow heating rate allowed gaseous reduction to proceed and limited the quantity of liquid slag formed. The resulting limited slag volume maintains the permeability of the sample bed and increases the melt-down temperature. The experimental tests at the slow heating rate produced melt-down temperatures in excess of 1350°C. The melting process within portion A' is probably only the melting of metallic iron and of the small quantity of slag that would inevitably be present even in virtually 100% reduced material. A relevant result from the experimental work with acid pellets was provided by the test involving pre-reduction at a low temperature. This test showed that, although reduction at 600°C was extremely slow, subsequent reduction at 950°C and above was rapid, far in excess of the corresponding rate of reduction when the samples had been pre-reduced at 950°C. This is the situation that must exist within a centre working blast furnace near the walls, i.e. a low temperature pre-reduction stage followed by a rapid reduction reaction within the cohesive zone to give virtually 100% gaseous reduction and a high melt-down temperature.

The situation existing can be summed up as follows. In both the layers G-5 and G-19 the start of the burden softening process is marked by the boundary X-X, lying at approximately

1100°C for sinters and 980°C for acid pellets. Once in the cohesive zone, the longer time of transit through the cohesive zone of the material within layer G-19 allows a greater degree of gaseous reduction to be achieved than for material in layer G-5. Material within layer G-5 starts to melt in appreciable quantities once past the boundary Y-Y where large gas pressure drops are encountered. Gaseous reduction stops and direct reduction commences caused by the liquid iron oxide rich slag dropping into the underlying coke bed. Melt-down of the material in the layer occurs at temperatures below 1350°C (Figure 28). Nearer the wall, material in layer G-19 is allowed sufficient time to reduce by gaseous means and the permeability of the bed is maintained until higher temperatures are reached. The portion bounded by X-X and Z-Z is in the softened state, but still very permeable. Melt-down occurs in the small portion A' which corresponds to a temperature greater than 1500°C (Figure 28). This is in line with melt-down being associated with the melting of virtually 100% low carbon iron - gaseous carburisation of iron in the experimental tests was shown to be negligible (refer Section 5.5).

It is now possible to split the cohesive zone structure into two distinct zones. The first is the zone between the start of softening and the accumulation of fluid within the pores of the bed. This region is quite permeable and gaseous reduction proceeds readily. The second zone is the one between the build-up of fluid in the voids of the bed and the melting of metallic iron. This zone is not permeable and reduction only proceeds by the process of iron oxide rich liquid dripping onto the underlying coke bed. The relative extent of each zone depends upon the degree of reduction and the pertaining temperature. Low levels of reduction existing at high temperatures give rise to an extensive impermeable zone. High levels of reduction at equivalent temperatures result in a restrained volume of the impermeable zone.

An indication of relative proportions of the two zones has been attempted schematically in Figure 106.

Having verified that the experimental results and the concepts derived from them relate closely to the information obtained from the Japanese dissection studies, it is possible to be confident about the application of the concepts to the analysis of the blast furnace process. Before this can be done however it is wise to ensure that factors such as the temperature of pre-reduction, and the concentration of sulphur and alkali in the reducing gas do not significantly change the basic theory. Further studies were thus carried on these factors, but limited to acid pellets only.

#### 5.4 Effect of Possible Modifying Phenomena on the Proposed Softening and Melting Mechanism

##### 5.4.1 Effect of Applied Load

It was desirable to study the effects of altering the load applied to the sample bed, although in the blast furnace the actual load is difficult to determine accurately. Increasing the load had only a small effect on the contraction-temperature relationship producing the expected trend of a move to higher levels of contraction at an equivalent temperature (Figure 66). The 3% contraction temperature did not vary significantly, still remaining at about 1000°C, so that the melting process started at more or less the same temperature. A better guide to the effect produced by changing the load can be seen from the change in the gas pressure drop with temperature (Figure 66). Increasing the applied load can be seen to move the start of melt-down to significantly lower temperatures, which further demonstrates that contraction of the bed is not necessarily related to gas pressure

drop. The fact that the gas pressure drop rose more slowly with temperature in the 78 and 98 kNm<sup>-2</sup> tests than in the 49 kNm<sup>-2</sup> test (at the lower applied load the rapid rise in gas pressure drop took place over 10 - 20°C compared with 50°C for the other two samples) possibly indicates a lower temperature limit at which the slag viscosity is too high for swift fluid flow. Further evidence of this is obtained from the reduction-temperature curves, since only at 49 kNm<sup>-2</sup> was any direct reduction detected (Figure 67). A higher slag viscosity in the other two tests would corroborate this finding in that it would lengthen the time taken for the liquid slag to drip onto the underlying coke bed. Apart from the direct reduction reaction there was no significant difference between the tests as far as the reduction path was concerned.

Tests without an applied load were not undertaken, but Turkdogan<sup>87</sup> found that slag from the pellet core migrated towards the surfaces of pellets in reduction tests with no applied load if the temperature was high enough. This indicates the importance of slag viscosity in the migratory process.

#### 5.4.2. Effect of Pre-Reduction Temperature

Comparing the contraction and the gas pressure drop curves of the sample pre-reduced at 600°C with the results of the sample that was pre-reduced at 950°C to 30% reduction shows that the former has a much lower contraction level and a higher melt-down temperature (Figures 70, 61 and 62.) Similarly the reduction rate of the sample pre-reduced at 600°C is greater than that of the sample pre-reduced at 950°C to 30% reduction (Figures 71 and 63).

Sectioning the sample bed that was pre-reduced at 600°C showed metallic iron shells of considerable thickness; sufficient

to strengthen the bed and limit the extent of contraction (Plate 11). The interiors of the individual pellets were found to be relatively porous in comparison with pellets pre-reduced at 950°C and subsequently reduced under identical conditions (Plates 25 and 31). Detailed examination of the pellet cores showed a structure consisting practically entirely of wustite grains. Very little slag was found to be present, the majority of the slag having migrated from the core to the surface leaving considerable internal porosity.

The increased melt-down temperature of the sample of pellets pre-reduced at 600°C in comparison to the melt-down temperature of pellets pre-reduced to an equivalent degree at 950°C is probably due to a combination of factors; i.e. the higher degree of gaseous reduction obtained means that the quantity of molten slag is lower and thus would take longer to reach the pellet surface. Secondly, the thicker iron shell provides a greater resistance to the flow of liquid slag to the surface and finally the strength of the iron shells prevents squeezing of the pellet core which would tend to force the liquid slag to the pellet surface.

Undoubtedly the significant increase in reduction rate, compared with the equivalent sample pre-reduced at 950°C, is the key to explaining the thickness of the iron shell. Reduction of iron oxide at low temperatures produces a porous wustite structure, whereas reduction at high temperature produces a denser wustite structure<sup>88</sup>. Creation of porous wustite at a low temperature causes an increased reduction rate at higher temperatures - as found to occur during the high temperature test. Some direct reduction occurred, which can be explained by the fluid slag (fluid due to the high temperature) reacting with the underlying coke bed.

### 5.4.3 Influence of Sulphur in the Reducing Gas

A sulphur level of 0.28 vol.% in the reducing gas had a marginal influence upon the gas pressure drop-temperature curve, but significantly altered the contraction-temperature relationship (Figures 72 and 73) - it is interesting to note that the initial contraction level is less in the presence of sulphur than it was in the test without sulphur, but that at approximately 1050°C the contraction level with sulphur overtakes that without sulphur. The overall result is that the melt-down temperature, as indicated by the gas pressure drop-temperature curve, is not markedly lowered with 0.28 vol.% sulphur in the gas. In the blast furnace the sulphur recirculates and it is feasible that the sulphur level in the cohesive zone is several times that of the level in the bosh gas (Figures 32 and 33). This situation was examined by maintaining the heating rate at 400°C.hr<sup>-1</sup> and by increasing the sulphur level approximately by a factor of three, and this depressed the melt-down temperature by some 150°C and increased the contraction of the bed (Figures 72 and 73). The test at this sulphur level was terminated prematurely by sulphur in the gas stream attacking the inconel sheath of the thermocouples. In both tests with sulphur at the heating rate of 400°C.hr<sup>-1</sup> the start of contraction of the bed (3% level) and thus the start of melting was of the order of 1000°C - 85°C higher than the eutectic temperature in the Fe-O-S system<sup>55,56</sup> (Figure 72). This does not signify that melting did not occur at a lower temperature since a time delay before the melting reactions produce a measurable effect could manifest itself in terms of a higher temperature.

With sulphur in the gas it was impossible to detect which of the possible melting reactions was occurring, i.e. the creation of an Fe-S-O eutectic or the mechanism described in Section 5.1. It is likely that both mechanisms operate initially but, as the

sulphur is continuously supplied in the reduction gas, it is probable that the mechanism involving sulphur becomes the more important as reduction proceeds. It is not possible to explain, however, why the 3% contraction temperature is slightly increased by the presence of sulphur.

In the two tests at a heating rate of  $400^{\circ}\text{C}.\text{hr}^{-1}$  with sulphur in the reducing gas, the reduction rate showed an initial increase before falling to zero (Figure 74). An identical phenomenon was found by Takahashi et al<sup>35</sup>, although they did not attempt to explain it. The production of a Fe-S-O liquid in the pores of the pellet should decrease the rate of gaseous reduction because the presence of the liquid would impede gaseous diffusion. This is indeed found to be the case because reduction actually stops. The increased reduction rate prior to this stage can be tentatively explained by assuming that the kinetics of the gaseous reduction reaction are increased by the oxygen entering into a liquid phase, i.e. a liquid/gas reaction is kinetically preferable to a solid/gas reaction. Evidence of the favourability of such a reaction already exists in the structure of the icicles (Section 5.2.2.1). As the reaction between sulphur, oxygen and iron continues the quantity of liquid will become so large that it effectively seals all the pores in the bed and gaseous reduction effectively stops.

If melting in the presence of sulphur is caused by the formation of an Fe-S-O eutectic, then decreasing the oxygen content of the sample should restrict the quantity of liquid and result in a rise in melt-down temperature. This particular hypothesis was tested by reducing a sample at the  $200^{\circ}\text{C}.\text{hr}^{-1}$  heating rate, whilst maintaining 0.75 vol.% S in the reducing gas. Such a heating rate has been shown to produce high levels of reduction by gaseous means only (Section 5.2). The experimental results show

that even greater contraction of the bed transpired and melt-down started to occur at a lower temperature (Figure 72 and 73). Determination of the reduction rate was impossible because of the large quantity of liquid dripping from the bed (see Plate 17 and section 4.3.3.7). Nevertheless, it is feasible to show from the carbon monoxide content of the outlet gas that a considerable quantity of direct reduction occurred, far in excess of any other sample tested (Figure 75).

Plate 34 shows the slag phase in a void between two pellets after the  $200^{\circ}\text{C}.\text{hr}^{-1}$  heating rate test, whilst the dropped material was found to be a rather complicated structure of various slag phases, iron, iron sulphide and the iron-oxygen-sulphur eutectic (Plates 18 and 19). The Fe-S-O eutectic phase was also fairly abundant in the sample bed from the test with 0.28 vol. % S in the reducing gas (Plate 33 and Table 27). These solidified slag phases were found by examination with the electron probe to be extremely variable in chemical composition. Some areas were basically iron, calcium and silicon whilst some phases were, for example, iron, aluminium and titanium. All one can say is that all the slag forming elements present in the pellet were in this slag, but most important, sulphur was not found in any of these phases. Sulphur was always in the form of iron sulphide, either by itself or in the eutectic. This latter fact may be a clue to the formation of the dropped material because liquid iron sulphide has a low surface tension and it is conceivable that it penetrates into the pellet structure and loosens it so that when the liquid iron sulphide drips out it carries with it quantities of wustite, molten slag and metallic iron. The sulphur level in the dropped material is 8 wt.% (Table 35) and this concentration is insufficient to form two immiscible liquids in accordance with the Fe-S-O phase diagram (Figure 46). (Although the chemical analysis of the dropped material does not include iron it is reasonable to assume that the vast majority of the 92% balance is metallic iron and wustite).

At first sight the  $200^{\circ}\text{C}.\text{hr}^{-1}$  heating rate test has produced data that apparently destroys the hypothesis set up, but one overriding factor that must be considered is the mass effect of sulphur. At a heating rate of  $200^{\circ}\text{C}.\text{hr}^{-1}$  the quantity of sulphur available for reaction within a given temperature span is twice that available at a heating rate of  $400^{\circ}\text{C}.\text{hr}^{-1}$  provided the concentration of sulphur in the inlet gas remains constant. This mass effect more than compensates for any decrease in oxygen content of the system due to the longer reduction time. Determination of the proportions of sulphur phases, wustite, metallic iron and slag present in the samples after the high temperature test shows that this mass effect is definitely occurring (Tables 27 and 28). The results also show that the level of reduction is higher in the sample with 0.28 vol. % S in the gas, as was verified from gas analysis and weight loss data. The chemical and phase analyses also provide some indication of the reduction level in the sample that was subjected to the slow heating rate. It appears from the relative proportions of metallic iron and wustite that the slow heating rate has allowed extra time for reduction, as was postulated, remembering that the actual degree of reduction is impossible to determine due to the extent of dripping from the bed. An additional point is that, at the slower heating rate, reactions will be closer to equilibrium and hence melting will have occurred to a greater extent at any given temperature, but without doubt the mass effect is the dominant factor.

In the blast furnace appreciable quantities of sulphur and alkali are available for possible participation in the melting reactions. It has been experimentally shown that the presence of sulphur in the reducing gas severely limits the quantity of gaseous reduction and depresses the melt-down temperature by an appreciable amount. The main problem with the sulphur tests was that the sulphur concentration in the inlet gas was maintained at a constant level throughout the test. It is known that in the

blast furnace considerable absorption of sulphur occurs in the metal portion, 'filtering out' the sulphur and lowering the concentration in the gas phase before it enters the next increment of bed layer<sup>53</sup> (Figure 33). Such a filtering process would provide a steady increase of sulphur level in the reducing gas as the burden layers descended and would allow gaseous reduction of the iron oxides to occur to an appreciable extent before the sulphur level reached a concentration sufficiently high to cause premature melt-down. A point in favour of this suggestion is provided by the Japanese dissection studies which showed melt-down temperatures in excess of 1500°C near the base of the cohesive zone (Figure 28). Even in the central region of the cohesive zone the melt-down temperature is not as low as would be expected were considerable quantities of sulphur to be present in the gas. Consequently, judging from the experimental studies, it appears improbable that sulphur is a major factor in the melting process within the blast furnace, especially when one considers that the sulphur levels found in the Japanese dissection studies are not as great as those found in the experimental samples that displayed a considerable reduction in melt-down temperature (Tables 11, 28, 35 and Figures 30, 31 and 32). However, the experimental studies have validated Hills' theory of melting due to the creation of an Fe-S-O eutectic<sup>54</sup>. It may be thought that the small droplet of FeS found in one of the tests with sinters (Table 40) can be used as evidence of Hills' theory, but this was an isolated incident and the source of sulphur in this case may well have been from some massive impurity in the coke or the sinter.

#### 5.4.4 Influence of Alkali Vapour in the Reducing Gas

The inclusion of alkali vapour in the reducing gas affected the mode of reduction of the iron oxide grains. Instead of the topochemical reduction behaviour usually observed, the

reduction mode changed to non-topochemical (Plate 36). In addition the final degree of reduction was higher with alkali vapour in the gas stream (Figure 78) which Bleifuss has attributed to the non-topochemical reduction mode allowing a greater surface area of reaction<sup>22</sup>.

Although it was difficult to make quantitative measurements, the presence of alkali vapour in the reducing gas refined the grain size of the iron shell on the pellets (Plates 35(a) and (b)). As a result, the iron shell was stronger and thus reduced the extent to which the bed contracted, (Figure 76) as well as lessening the squeezing effect on the particles in the bed and raising the resistance to liquid slag flow through the iron shell. The nett result was to increase the melt-down temperature (Figure 77).

Chemical analyses of sections cut from the sample bed confirmed that the alkali vapour was absorbed by the pellets (Table 30) although x-ray analysis was unable to detect any change in pellet mineralogy (Table 31). Optical and electron probe micro-examination of the samples showed that the slag phase contained two precipitated phases. The long thin needles (Plate 37) were found to consist of silicon, iron, calcium, potassium, plus some aluminium (Plate 48). The other crystals (Plate 35(a)) which had the appearance of an olivine phase, were composed of iron and silicon with a trace of calcium and magnesium, (Plate 49). Analysis of the slag phase itself showed it to contain a high concentration of potassium along with iron, silicon and aluminium - the potassium level was such that both the  $K\alpha$  and  $K\beta$  lines could be distinguished (Plate 50). The crystals shown in Plates (35(a) and 37) were not detected in every test with alkali vapour but, as the alkali level increased, the morphology of the pellets gradually changed culminating, at the highest alkali level, in the precipitation of the two indicated phases.

Alkali vapour was not absorbed to any great extent during the interrupted test (Table 30), even though the alkali loading was 15 g  $K_2CO_3$ . In fact only half the quantity of carbonate evaporated and entered the gas stream. Nevertheless, the quantity of alkali passed through the bed was in excess of that evaporated in the test using 5 g  $K_2CO_3$ , and yet the alkali concentration in the bed was higher after the latter test. The absence of an applied load in the interrupted test could well have had a significant influence since the absence of a physical load ensures that bed permeability is maintained, thus allowing ample opportunity for gaseous reduction throughout the bed. Absence of an applied load would also decrease the rate of the liquid slag forming reactions because the reacting phases would not be brought into increased contact by the consolidation resulting from the load. The resulting decrease in the quantity of liquid slag would further benefit the gaseous reduction reaction. Another important factor limiting the take up of alkali from the vapour is the small volume of slag. Although the initial liquid slag formation reaction is known to occur at  $980^\circ C$  it is probably not until  $\sim 1100^\circ C$  that significant quantities of liquid slag are present. This supposition is borne out by the contraction curves which show a rapid rate of contraction at  $\sim 1100^\circ C$  (Figure 76). As the alkali is absorbed by the slag phase, the lessened amount of slag would account for the low concentration of alkali in the bed.

Examination of the results shows the concentrations of alkali absorbed by the pellets to be in reasonable agreement with the potassium levels found by the Japanese researchers, although water quenching may have removed some alkalis (Tables 8, 11 and 30 and Figure 48). As the experimental studies revealed no detrimental influence upon the softening-melting behaviour it seems reasonable to assume that in the blast furnace similar levels of alkali should not prove detrimental.

Although alkali was assimilated into the slag phases present in the pellets used in the experimental studies, the amount absorbed was insufficient to lower the melting point of the initial slag significantly. The residual slag in the pellets already contains alkali, of course, which plays a major role in lowering to about 980°C the melting point of the initial slag formed when the residual slag reacts with the wustite. It would require substantial further pick-up of alkali to lower the melting point by a further amount sufficient to hinder gaseous reduction. Further absorption of alkali into the liquid slag is also unlikely to reduce the viscosity significantly because iron silicate slags saturated with iron oxide are very fluid, not to drastically increase the slag volume.

Thus it appears that the role of alkalis in the softening-melting process is limited basically to the alkali present in the residual slag. If the alkali concentration in the residual slag is high it is to be expected that the initial liquid slag would form at a lower temperature, which in turn would lead to a decrease in the extent of gaseous reduction due to the greater quantity of liquid slag.

#### 5.4.5 Influence of Both Sulphur and Alkali Vapour

It is interesting to contrast the influence of sulphur and alkali vapours in the reducing gas upon the softening-melting behaviour of acid pellets. Alkali is beneficial due to the promotion of the gaseous reduction reaction and the formation of a fine grained iron shell. Absorption of the alkali vapour into the slag phase appears to be insufficient to either lower the temperature at which the initial liquid slag formation reaction occurs or to increase the slag volume. Sulphur on the other hand is detrimental because of the formation of a low melting point

Fe-S-O eutectic phase which also enlarges the slag volume, thus severely limiting gaseous reduction. Unlike alkali vapour, sulphur does not show a continuous promoting influence upon the gaseous reduction reaction.

The experimental study with both sulphur and alkali vapour in the reducing gas showed that the contraction-temperature and gas pressure drop-temperature curves were inbetween the two extremes of sulphur alone and alkali alone, but very much biased towards the sulphur only test which indicates the overpowering deleterious influence of sulphur (Figures 79 and 80). Judging from the reduction data it does appear that the alkali vapour was having some influence upon the reduction reaction in the early stages of the test (Figure 81). As expected, considerable absorption of sulphur by the sample bed occurred (Table 32) and in conclusion one can state that, under the test conditions used, sulphur was the dominant species.

## 5.5 Iron Carburisation

Micro-examination of the etched (etched in 2% nital) iron phase in samples after the high temperature test showed the extent to which carburisation had transpired and the types of carburising reactions occurring. In a sample of pellets that was almost fully reduced (the 52% pre-reduced sample at a heating rate of  $200^{\circ}\text{C}\cdot\text{hr}^{-1}$ ) the iron showed no sign of carburisation whatsoever - the only phase present was iron nitride<sup>89</sup> (Plate 24). Whether or not the nitrides form in the course of the reduction process or during the lengthy cooling procedure could not be determined. The possibility of decarburisation of the iron by iron oxide rich molten slag can be ruled out, in this instance, because the quantity of slag in the pellet was negligible. No sign of carburisation of the iron in the icicles was noticeable, again only iron nitride could be seen (Plate 16). However, it

is feasible, in this case, that the iron oxide rich slag could have decarburised the iron and, moreover, the iron was created by reduction of the liquid slag by the carbon monoxide. The contact time between the newly created iron and the carbon monoxide was extremely limited in the test due to its termination shortly after the dropping of the molten material.

In samples where iron was in contact with coke it was generally found that a thin highly carburised layer was formed which possessed a structure of cementite and pearlite, i.e. the classical white cast iron structure found in low silicon cast iron or cast iron that has been quickly cooled. (Plates 29 and 30). Iron of this carbon content has a solidus of  $1135^{\circ}\text{C}^{90}$  and following some of the high temperature tests small droplets of solidified iron, approximately 2 mm in diameter, were found in the bottom of the graphite crucible. These droplets had a flake graphite and pearlite structure typical of a cast iron that has been slowly cooled (grey cast iron structure). A difference in cooling rate between the high carbon iron in the sample bed and the iron droplets is most probably the reason for these differences in structure. Formation of the former carbide in the iron structure is promoted by rapid cooling and/or a low silicon content, and the latter by slow cooling and/or a high silicon content. No silicon was detected in either form of iron using the electron probe microanalyser.

Two distinct modes of carbon pick-up by the iron are possible. The first involves carburisation of the solid iron at point contacts with the coke followed by diffusion of carbon into the iron. Eventually the carbon content will become sufficiently high for the iron to melt, increasing the dissolution rate - this reaction requires the temperature to be in excess of  $1135^{\circ}\text{C}$  (the Fe-C eutectic temperature). The second mechanism involves reaction between molten iron oxide rich slag and the coke to produce metallic iron which carburises in the manner just

described. In this case the area of contact between the coke and the metal will be greater than that of solid iron/coke interface, favouring more rapid carburisation rates. The presence of molten iron oxide slag in this case may also act to decarburise the iron and simultaneously create more iron, gradually increasing the quantity of iron. A carburising reaction between iron and solid carbon can occur with graphite or coke, but in the high temperature tests, carburisation was generally noted in areas where coke was present, i.e. coke appears to be more reactive than graphite. It is interesting to recall that M Sasaki<sup>48</sup> considered that metal separated by two distinct mechanisms within the cohesive zone: mixtures of metallic iron granules and molten slag dropped out in a relatively low temperature region whilst forming icicles, or mixtures of iron granules and molten slag approach 1500°C when the metallic iron is carburised by contact with coke and then abruptly melts.

Information concerning the extent of carburisation in the cohesive zone of the blast furnace is not widely available. Table 10 shows the situation found by the dissection studies in several layers of burden. Care must be taken in considering these results because it may be that the carbon levels reported are an average across the layer; high carbon levels and low carbon levels may well exist within the layer. It is interesting to note that the carbon level is higher in the lower side than in the upper surface. This could be due to iron oxide rich liquids dripping out onto the underlying coke and subsequently being carburised as described above, or to the long contact time between coke and metallic iron allowing carburisation to proceed.

## 5.6 Combinations of Sinter and Pellets

A sinter and pellet burden is common practice in blast furnace operation and the study of a superfluxed sinter with an

acid pellet is of particular interest in terms of blast furnace operation. The high temperature tests with samples having high pre-reduction levels employing a fast heating rate or with samples having a low pre-reduction level using a slow heating rate showed no sign of melt-down because high levels of reduction could be achieved before the melt-down temperature range was reached (Figures 87 and 88). Reduction of a sample having a low level of pre-reduction at the fast heating rate produced melt-down of the bed and the commencement of direct reduction. These findings are analogous to the reactions occurring with acid pellets. The melt-down temperature is inbetween those of the pellets and of sinter alone, indicating that a bed of sinter is weakened by the inclusion of acid pellets or, conversely, that a bed of pellets is strengthened by the incorporation of sinter. Further proof of the weakening effect that pellets have on a sinter bed is to be found in the decrease of the 3% contraction temperature from 1065°C for sinter alone to 1010°C for the mixed bed. Examination of the sample bed after the test showed that molten slag from the pellets was advancing into the sinter particles (Plates 41 and 42).

### 5.7 Application to the Blast Furnace Process

The experimental work has shown that the two factors that maintain bed permeability and maximise the melt-down temperature, which is related to the quantity of gaseous reduction, are the reducibility of the material and the heating rate. Slow heating rates produce the maximum amount of gaseous reduction and lead to high melt-down temperatures. All the materials examined behaved extremely well under these conditions and the general conclusion is that differences in the reducibility of materials do not present problems at slow heating rates. Fast heating rates provide a severe test for burden materials and, as a result, differences in high temperature reducibility manifest themselves

under these conditions in terms of the melt-down temperature.

### 5.7.1 Sinter Burdens

Considering sinters alone the experimental work showed that an overall critical zone on a TRIB diagram could be established, in which all the critical zones of individual sinters lay. The ability of a material to avoid this zone is a measure of its high temperature properties. All the sinters examined at a heating rate of  $400^{\circ}\text{C}\cdot\text{hr}^{-1}$  in their as-received state underwent melt-down because their reduction paths led into or beneath the critical zone (Figures 82 and 83). At a pre-reduction level of 30% the 1.2, 1.4 and 2.4 CaO/SiO<sub>2</sub> sinters underwent melt-down because of entry into the critical zone. The 1.8 CaO/SiO<sub>2</sub> sinter showed no signs of melt-down because its reduction path by-passed the critical zone, whereas the 2.1 and 1.6 CaO/SiO<sub>2</sub> sinter only just avoided entering the critical zone and consequently they were nearer to a melted-down condition at the end of the test. This is especially true for the 1.6 CaO/SiO<sub>2</sub> which was nearest to the critical zone. (Figures 84 and 85). All the sinters with a 45% pre-reduction level showed no sign of melt-down because the reduction path by-passed the critical zone (Figure 86).

A possible direct application of the results of the tests on the sinters would be in the selection of basicities to provide maximum resistance to melt-down. Placing the basicities of the sinters in order of their decreasing resistance, as derived from the 30% pre-reduced tests with a heating rate of  $400^{\circ}\text{C}\cdot\text{hr}^{-1}$  gives  $1.8 > 2.1 > 1.6 > 1.4 > 1.2 > 2.4$ . Consequently, if no other restrictions are placed on the choice of sinter basicity a CaO/SiO<sub>2</sub> ratio of 1.8 is the optimum. In practice other factors come into operation, e.g. the control of slag chemistry, the proportion of other constituents in the burden, etc.

These other factors are often a major consideration and may override the attraction of maximising the melt-down temperature. It is interesting to observe that in isolated areas of the surface of the 2.4 CaO/SiO<sub>2</sub> sinter a white powdery deposit, consisting mainly of dicalcium silicate, was found (Table 38). The melting point of dicalcium silicate is in excess of 2000°C (Figure 10) and one may speculate that it may not dissolve completely in the molten slag when complete melt-down occurs. Such action may lead to viscous slag formation in the melting zone of the furnace, which may hinder furnace production<sup>91</sup>.

It is possible to use the derived reduction rate constant to estimate the heating rate at which problems may arise due to entry into the critical zone. This concept is schematically illustrated in Figure 107 for a material with a reducibility constant of 0.0075 min.<sup>-1</sup> (K<sub>2</sub>): the value for 2.1 CaO/SiO<sub>2</sub> sinter. Assuming that the material is 30% reduced prior to entry to the cohesive zone, it can be seen that even at a heating rate of 400°C.hr<sup>-1</sup> the reduction path does not enter the critical zone, and this fact was verified experimentally. Even in the hypothetical situation of unreduced sinter entering the cohesive zone it can be seen that only the 400°C.hr<sup>-1</sup> heating rate leads to the critical zone. Again, this was verified in the experimental work. Diagrams similar to Figure 107 can be constructed for other materials possessing different rate constants. These would allow an estimation to be made of reduction behaviour at various locations within the cohesive zone. As an example of how the rate constant alters the proximity of the reduction path to the critical zone, consider three sinters having rate constants of 0.0075, 0.0067 and 0.0058 min.<sup>-1</sup> (equivalent to the 2.1, 1.6 and 1.4 CaO/SiO<sub>2</sub> sinters respectively) at a pre-reduction level of 30% and a heating rate of 400°C.hr<sup>-1</sup> (Figure 108). It is apparent that the

material having the highest rate constant by-passes the critical zone; the material having the lowest rate constant enters it, whilst the intermediate material just touches it. Such circumstances should lead to the materials having no apparent melt-down; a definite melt-down and an intermediate situation. Verification of this concept is provided by the experimental tests (Figure 84).

### 5.7.2 Acid Pellet Burdens

Using the extensive data collected from the experimental work it is possible to demonstrate the relative differences in permeability between pellets at the centre and pellets at the walls of a hypothetical centre working furnace operating on a 100% acid pellet burden by applying the relationship<sup>92</sup>:-

$$Q = \frac{K.A.P}{L} \quad \text{_____} \quad (21)$$

where,

- Q = Volume of gas flowing through the bed, m<sup>3</sup>.sec.<sup>-1</sup>
- K = Bed permeability, m<sup>4</sup>.N<sup>-1</sup>.sec.<sup>-1</sup>
- A = Cross sectional area of the bed, m<sup>2</sup>
- L = Depth of the bed, m
- P = Gas Pressure drop across the bed, N.m<sup>-2</sup>

The use of the data collected from the experimental tests prohibits the calculation of a true value of K because the gas pressure drop measured in the test was from the base of the graphite crucible to the top of the crucible, i.e. it

included the coke layers, the Triton Kaowool, etc. However, any change in gas pressure drop during the high temperature test was caused by (a) the bed of iron bearing material softening and melting - the coke beds and the Kaowool were unaffected during the test and (b) by the change in the gas volume flowing per second as the temperature rose, but if one is comparing one situation with another then, provided the temperatures are equal, this effect is eliminated. Consequently comparison of gas pressure drop curves is perfectly valid to show differences between materials, but the curves cannot be used to determine the absolute values of permeability - however, relative permeability can be calculated as follows:-

Transposing equation (21):-

$$K = \frac{Q \cdot L}{A \cdot P} \quad \text{_____} \quad (22)$$

and in the high temperature test procedure

$$Q = 10^{-3} \text{ m} \cdot \text{sec}^{-1} \text{ at } 15^{\circ}\text{C and } 760 \text{ mm Hg absolute pressure}$$

$$A = \frac{\pi}{4} \left( \frac{90}{10^3} \right)^2 \text{ m}^2$$

$$P = 9.80665 \cdot \left( P_{\text{mmH}_2\text{O}} \right) \text{ Nm}^{-2}$$

$$L = \left[ 1 - \frac{\% \text{ contraction}}{100} \right] \cdot \frac{66}{10^3} \text{ m}$$

$$K = 10^{-3} \cdot \frac{(T+273)}{288} \cdot \left[ \frac{1-\% \text{ cont.}}{100} \right] \cdot \frac{66 \cdot 10^{-3} \cdot 10^6 \cdot 4}{\pi (90)^2 \cdot 9.80665 \cdot P_{\text{H}_2\text{O}}} \quad \text{_____} \quad (23)$$

$$K = \frac{(T+273)}{P_{\text{H}_2\text{O}}} \cdot \left[ \frac{1-\% \text{ cont.}}{100} \right] \cdot 3.6733 \times 10^{-6} \text{ m}^4 \cdot \text{N}^{-1} \cdot \text{sec}^{-1} \quad \text{_____} \quad (24)$$

Taking the data from the experimental tests carried out with pellets, which were 30% pre-reduced, at the heating rate of  $200^{\circ}\text{C}\cdot\text{hr}^{-1}$  and  $400^{\circ}\text{C}\cdot\text{hr}^{-1}$  as an example and substituting the values of P, % contraction and temperature into equation (24) the values of K can be calculated for equivalent temperatures at both heating rates. As stated, these values of K are not absolute but they can be converted into relative values, which are comparable, using the following expression:-

$$K'_{T^{\circ}\text{C}} = \frac{1000}{K_{950^{\circ}\text{C}}} \cdot K_{T^{\circ}\text{C}} \quad (25)$$

where,

$K'_{T^{\circ}\text{C}}$  = Relative value of K at a temperature  $T^{\circ}\text{C}$

$K_{950^{\circ}\text{C}}$  = Value of K at  $950^{\circ}\text{C}$  calculated from equation (24)

$K_{T^{\circ}\text{C}}$  = Value of K at temperature  $T^{\circ}\text{C}$  calculated from equation (24)

Consequently by definition  $K'_{950^{\circ}\text{C}}$  is equivalent to 1000.

The values of  $K'$  for both the tests used as an example have been 'graphically' displayed in Figure 109 along with the corresponding temperatures and reduction levels. (It has been assumed, for the purpose of construction of this diagram, that the time between charging of the burden layers is ten minutes). It is apparent that the pellets towards the centre of this hypothetical centre working furnace melt-down at a relatively low temperature and attain a fairly low degree of gaseous reduction.

Although it is realised that the applied load in the cohesive zone is unknown, variations of the magnitude of the load simply repositions the cohesive zone within the furnace, i.e. a higher load will move the impermeable zone to lower temperatures and vice versa.

### 5.7.3 Acid Pellets and Superfluxed Sinter Burdens

The use of combined sinter and pellet burdens in the blast furnace is an established practice, the proportions of the two components depending upon the composition balance that can be established between them; the use of superfluxed sinter and acid pellets being common. These experimental studies have shown that large differences in melt-down temperatures exist between sinters and acid pellets under conditions of rapid heating rate. Consequently the charging of the burden components should be examined in the light of the experimental work in order to improve the operational efficiency of the blast furnace process. In a centre working furnace to alleviate the problem of high gas pressure drops occurring at relatively low temperatures coupled with a rise in the quantity of direct reduction; the material with the least resistance to softening and melting should be charged towards the walls of the furnace. This allows the material (acid pellets in this situation) to be subjected to a slow heating rate giving ample time for reduction to proceed, i.e. the critical zone of the TRIB diagram is by-passed. The more resistant material (the sinter) should be charged towards the centre of the furnace because it is capable of withstanding the rapid heating rate. (In a wall working furnace this situation would obviously be reversed). Using this philosophy the gas pressure drop in the cohesive zone should decrease along with the coke rate, because the quantity of gaseous reduction of the pellets would increase. This concept has been demonstrated, in the same

hypothetical centre working furnace used in the previous section, in Figure 110 by processing the data (using equations 24 and 25) from the high temperature test on the 1.8 CaO/SiO<sub>2</sub> sinter with a degree of pre-reduction of 30% at a heating rate of 400°C.hr<sup>-1</sup>. Comparing figures 109 and 110 it is apparent that the burden layers towards the centre in Figure 110 are more permeable; have achieved a greater level of gaseous reduction and persist to higher temperatures. The nature of the burden layers towards the wall naturally remain the same. Thus, in this conjectural furnace, the amount of gaseous reduction has increased, and the permeability has been maintained until higher temperatures are reached, by the preferential charging of the burden components.

Layering of the components across the furnace should be avoided as the less resistant material (the pellets) under conditions of rapid heating rate will soften and form an impermeable layer which may detrimentally influence gas flow in the adjoining sinter layer. If selected charging of the burden materials cannot be undertaken the best compromise would be to mix the pellets and sinter prior to charging; because it has been demonstrated that mixtures of pellets and sinter have higher melt-down temperatures and achieve greater levels of gaseous reduction than pellets alone under conditions of rapid heating rates.

CONCLUSIONS

By reviewing the literature detailing the findings of the Japanese research on the inside state of quenched blast furnaces, the heating rate and change of reduction of burden materials within the cohesive zone have been estimated. Using the estimated heating rates and reduction levels an experimental laboratory procedure has been developed for the appraisal of the behaviour of burden materials within the cohesive zone. The process of evaluation has resulted in the following conclusions.

1. The start of the melting process in acid pellets is via a reaction between wustite and the slag phase which existed in the fully oxidised state (termed residual slag) to form a calcium-silicon-iron rich slag containing traces of potassium, magnesium, etc. This reaction was found to occur at  $\sim 980^{\circ}\text{C}$ ; the potassium being responsible for the lowering of the melting point of the slag to  $\sim 980^{\circ}\text{C}$ . Some sinters were found to be subject to a similar mechanism, i.e. a reaction between wustite and the surrounding slag phase, which existed in the fully oxidised state, to form a calcium, silicon, iron rich liquid slag having a melting point of  $\sim 1100^{\circ}\text{C}$ . However, this type of reaction only occurred in the low basicity sinters or in regions of sinters that were lime deficient. In high basicity sinters, or regions of sinter which were lime rich, a second melting mechanism occurred caused by the 'internal melting' of semi-reduced calcium ferrites to form a calcium-iron rich slag also having a melting point of  $\sim 1100^{\circ}\text{C}$ .

2.           The important parameter which dictates whether a material has a high gas pressure drop (low permeability) or a low gas pressure drop (high permeability) at elevated temperatures is the degree of gaseous reduction. A high level of gaseous reduction, existing at a high temperature, produces a low gas pressure drop; but a low level of gaseous reduction existing at equivalent temperatures causes a high gas pressure drop and melt-down of the bed of material. The interplay of reduction, temperature and gas pressure drop has been summarised in the form of Temperature-Reduction-Isobar Diagrams which pinpoint critical areas of reduction and temperature within which melt-down occurs.
  
3.           A balance exists, between the rate of gaseous reduction and the speed of the slag forming reactions, which dictates whether a material will exhibit a high or a low gas pressure drop. Dominance by the gaseous reduction reaction produces a low gas pressure drop and a high melt-down temperature, but if the slag forming reaction prevails then high gas pressure drops and a low melt-down temperature result. The heating rate governs whether the slag forming reactions or gaseous reduction predominates, i.e. a slow heating rate favours gaseous reduction whilst a fast heating rate favours the slag forming reaction.
  
4.           Carburisation of the metallic iron is by diffusion in the solid state of carbon from the coke into the iron; the latter formed either by gaseous reduction of the iron oxide or reduction of the liquid iron oxide rich slag by coke. Carburisation by gaseous means would appear to be extremely limited at temperatures up to 1350°C.

5.

A limited study of the influence of rogue elements (potassium and sulphur) upon the softening and melting process occurring within acid pellets showed that gaseous potassium in the reducing gas increased the rate of gaseous reduction and changed the reduction mode from topochemical to non-topochemical. Although the potassium was absorbed into the liquid slag phase in the pellets, the enhanced reduction rate and the changed reduction mode produced a fine grained iron shell on the pellets which constrained the outflow of liquid slag, resulting in a rise in the melt-down temperature. Consequently it would appear unlikely that gaseous alkali would cause a deterioration of the softening and melting properties of pellets within the blast furnace - it is the inherent level of alkali in the pellets which is important, because it affects the melting point of the initial liquid slag.

Sulphur in the reducing gas has been shown to depress melt-down temperature due to the formation of large amounts of an Fe-S-O low melting point eutectic phase. This low melting point eutectic phase has two important influential aspects. First it eventually limits the diffusion of the reducing gas and stops the gaseous reduction reaction. Secondly, the quantity of the liquid Fe-S-O eutectic phase eventually reaches such a high level that the voids of the bed are filled and the gas pressure drop rises rapidly.

Although the experimental technique adopted demonstrated that sulphur had a strong influence upon the softening and melting process in acid pellets, the experimental results are inconsistent with the Japanese dissection studies. Consequently it appears inconceivable from the present studies that sulphur has a strong influence on the melting process within the blast furnace.

6. Application of the experimental studies to the blast furnace process is in several areas. First the work has shown that the cohesive zone is not a completely impermeable zone, but consists of two distinct zones; a permeable zone within which gaseous reduction proceeds readily and an impermeable zone, from which the iron oxide rich slag drips into the underlying coke layer.

Secondly the melt-down temperature and the speed of gaseous reduction was shown to vary with basicity, a CaO/SiO<sub>2</sub> ratio of 1.8 producing the maximum melt-down temperature and reduction rate with sinters.

An important perspective for furnaces operating with a burden of superfluxed sinters and acid pellets is the concept of preferentially charging the burden components to different positions on the stockline in order to take advantage of the softening and melting characteristics of the materials, e.g. in a centre working furnace the sinter should be charged towards the centre, because it can withstand rapid heating rates, and the pellets should be charged towards the walls where they are subjected to a slow heating rate. Using this philosophy the pressure drop in the cohesive zone and the coke rate should both decrease. If selective charging cannot be practiced then the compromise of mixing of the sinter and pellets should be implemented as the incorporation of sinter into a bed of pellets raises the melt-down temperature.

## CHAPTER 7

### SUGGESTIONS FOR FURTHER WORK

The high temperature apparatus has a temperature limit of 1350°C and although melt-down of burden materials can be detected there would be advantages in constructing an apparatus suitable for attaining temperatures sufficient to completely melt the sample bed and capable of collecting the resultant liquids. Such a study would be of most benefit with superfluxed sinters, which show limited signs of melt-down in the present apparatus, and superfluxed sinter/acid pellet mixtures. In the latter case it should be possible to ascertain whether the acid pellets and sinter melt-down together, or whether a two stage process occurs in which the acid pellets melt first followed by the sinter at a higher temperature.

The completed studies have demonstrated that sulphur in the reducing gas can have a strong influence upon the softening and melting characteristics of acid pellets, however, the particular test condition adopted, i.e. a constant level of sulphur in the reducing gas throughout the test procedure, is somewhat unrealistic in terms of blast furnace operation - indeed the experimental results are inconsistent with the Japanese dissection studies in terms of the concentration of sulphur existing within the cohesive zone. Consequently the test procedure should be modified by using a programmed test, within which the sulphur level in the gas gradually increases as the temperature rises. Such a modification would enable the true influence of sulphur upon blast furnace burdens to be determined.

The addition of dolomite to pellets is now being practiced by certain companies because of the claim that magnesia

raises the melting point of the slag, thus making the high temperature properties superior to acid pellets, and in some cases sinters. Hence it would be useful to study the influence of the chemical composition of dolomite fluxed pellets upon their softening and melting properties.

## REFERENCES

1. F A Berezynski - "The Blast Furnace, a Transition"  
Blast Furnace Technology - Science and Practice.  
Proceedings of the C C Furnas Memorial Conference on  
Ironmaking Technology, New York State University,  
Buffalo, October 1970. Edited by J Szekely.
2. K Masubuchi - Iron Age, December 10 1970, 85-89.
3. Y Ishikawa - "Some Considerations on the Operation of  
Large Blast Furnaces". Journees Internationales de  
Siderurgie. Paris, 2-3 October 1975.
4. "The Blast Furnace: More a Phoenix than a Dying Swan".  
The Magazine of Metals Producing, June 1968, 59-80.
5. M Higuchi, K Kuroda and G Nakatani - Iron and Steel Engineer,  
September 1974, 44-50.
6. C Bodsworth - "Physical Chemistry of Iron and Steel  
Manufacture". Longmans Press.
7. S Yamazaki, F Nakatani, T Kano, M Nakagawa and S Kobayashi.  
Trans. ISI Japan, vol. 13, 1973, 229-234.
8. N Nakamura - "Design and Engineering of Large Blast Furnaces  
in Japan". Chairman of Cokemaking Committee. Joint  
Research Soc. ISI Japan.
9. Journal of the Iron and Steel Institute 1881, vol. II,  
625-669.
10. G Heynert and E Legille - "Bell-less Top for High Top  
Pressure Furnaces". ISI Special Report 152, Developments in  
Ironmaking Practice.

11. LKAB News Special Report 1972:2.
12. F M Zhuravlev et al - Metallurgist 21(7-8) March 1978.  
Translation of Metallurg No.8, 8-11.
13. B Phillips and A Muan - J. Amer. Ceram. Soc. 42, 413-423,  
1959.
14. LKAB News Special Report, October 1974.
15. LKAB News, 1973:1.
16. J Craig and J O'Hanlon - "European Blast Furnace Trials  
with Fluxed Pellets", 37th AIME Ironmaking Proceedings,  
Chicago, April 1978.
17. L Bentell and G Mathisson - Scand. Jour. of Metallurgy,  
7(1978),5 230-236.
18. B Phillips and A Muan - J. Amer. Ceram. Soc. 448(1958).
19. B Phillips, S Somiya and A Muan - J. Amer. Ceram. Soc.  
44 [4], 169 (1961).
20. N L Bowen and O Andersen - Amer. J. Sci. [4], 37,  
448 (1914).
21. L S Darken and R W Gurry - J. Amer. Chem. Soc. 1945,  
vol. 67, 1398-1412; 1946, vol. 68, 799.
22. R L Bleifuss - "Single Particle Studies Applied to Direct  
Reduction and Blast Furnace Operation". Blast Furnace  
Science and Practice. Proceed. of the C C Furnas Memorial  
Conf. on Ironmaking Technology, Buffalo, October 1970.

23. L von Bogdandy, H J Engell - "The Reduction of Iron Oxides". Verlag Stahleisen m.b.H. Dusseldorf, Springer - Verlag, Berlin.
24. W M McKewan - "Kinetics of Iron Oxide Reduction". Trans. Met. Soc. AIME, 212, 791 (1958); 218, 2, (1960); 221, 140 (1961); 224, 2, (1962); 224, 387, (1962).
25. J O Edstrom - Journ. of the Iron and Steel Institute, November 1953, 289-304.
26. A W D Hills ed. - "Heat and Mass Transfer in Process Metallurgy", Institute of Mining and Metallurgy, London, 1967, 39-77.
27. K A Shehata and S Y Ezz - "Study of the Final Stages of Reduction of Iron Oxides". Institution of Mining and Metallurgy, March 1973.
28. T S Yun - Trans. Amer. Soc. Metals, 54 (1961) 129-142.
29. B G Baldwin - Jour. of the Iron and Steel Institute, 179 (1955) 30-36.
30. C Borgianni - Ironmaking and Steelmaking, 1978, No.2, 61-66.
31. J Davies, J T Moon and F B Traice - Ironmaking and Steelmaking, 1978, No.4, 151-161.
32. K P Abraham and L I Staffanson - Scand. Jour. of Metallurgy, 4 (1975), 193-204.
33. Z I Nekrasov, et al - Steel in the USSR, Nov. 1976, 587-592.

34. S E Khalafalla and P L Weston Jr. - Trans. Met. Soc. AIME, 239, October 1967, 1494-1499.
35. R Takahashi, Y Omori, Y Takahashi and J Yagi - Ironmaking Proceedings of AIME, Vol. 37, Chicago 1978, 78-92.
36. N H Harbord and D C Goldring - Jour. of the Iron and Steel Inst. 203, April 1965, 349-360.
37. O Nyquist - "The Effects of Lime on Sintering". Agglomeration Meeting, Philadelphia, April 1961, Proceedings Edited by W A Knepper.
38. E Mazanek and S Jasienka - Journ. of the Iron and Steel Inst., November 1968, 1104-1109.
39. J Hancart, V Leroy and A Bragard - CNRM Report No.11, June 1967.
40. B B L Seth and H V Ross - Canad. Metallurgical Quarterly, 2 (1963), 16-30.
41. J Dartnell - Jour. of the Iron and Steel Inst., March 1969, 282-292.
42. T Nakamura et al - Ironmaking Proceedings of AIME, vol. 33, 1974, 416-422.
43. K Sasaki, et al - BISI Transl. 14868, January 1972.
44. Y Omori and Y Takahashi - Agglomeration 77, Vol. I, Proceed. of the 2nd International Symp. on Agglomeration, Atlanta, Ga, March 6-10, 1977, 286-305.
45. K Kanbara, et al - Trans. ISI Japan, Vol. 17, 1977, 371-380.

46. K Sasaki, et al - ibid, 252-261.
47. Y Shimomura, et al - ibid, 381-390.
48. M Sasaki, et al - ibid, 391-400.
49. M Kanbara and A Shigemi - Nippon Steel Technical Report Overseas, No.10, November 1977.
50. I Z Buklan, et al - Stal in English (1970), No.3, March 183.
51. M Sasaki et al - Tetsu-to-Hagane, 1976, 5, 99-109.
52. R Jon, et al - "Study of the Ironmaking Processes in the Bosh and in the Tuyere Region of an Experimental Blast Furnace in Liege", CNRM Report No.15, June 1968, 3-19.
53. J C Lecomte, R Nicolle and F Temoin - "Behaviour of Sulphur in the Shaft of the Blast Furnace. Influence on the Properties of the Agglomerates". Paper presented at a joint BSC-IRSID-MEFOS meeting, September 1977.
54. A W D Hills - "Process of Engineering and Pyrometallurgy". A joint meeting of the Institute of Mining and Metallurgy and the Institute of Chemical Engineers, 1974, 81-93.
55. D C Hilty and W Crafts - Trans. Amer. Inst. of Mining Engrs. 194, 1952, 1307-1312.
56. A J Naldrett - Jour. of Petrology 10, 1964, 171-201.
57. K A Orrebo - "Behaviour of Fuel Sulphur in the Bosh of the Blast Furnace and its Effect on the Burden". Paper presented at a joint BSC-IRSID-MEFOS meeting, September 1977.
58. ISO Standard 3271/1975.

59. Japanese Industrial Standard M8712, 1971.
60. R Linder - Jour. of the Iron and Steel Inst., July 1958, 233-243.
61. R A Oliver and R Wild - Jour. of the Iron and Steel Inst. Vol. 206, November 1968, 1070-1076.
62. R A Oliver - Jour. of the Iron and Steel Inst., November 1967, 1131-1135.
63. L von Bogdandy et al - Journees Internationales de Siderurgie, Luxembourg, October 1962 (BISIT 3033).
64. A Poos and R Linder - ibid (BISIT 3032).
65. ISO/TC/SC3/284E, 1974.
66. B Bjorkvall, L Granse and L Lindahl - LKAB News Special Report February 1971.
67. R Vidal, N Ponghis and A Poos - CNRM Report No.10, March 1967, 3-6.
68. O Burghardt and K Grebe - Stahl und Eisen 89 (1969) 561-573.
69. P Lecomte, R Vidal, A Poos and A Decker - "The Softening of Sintere, Pellets and Iron Ores". CNRM Report No.21, December 1969, 21-28.
70. M Nakamura, Y Seki and S Kondo - Trans. ISI Japan, Vol 11, 1971, 331-338.
71. T Sugiyama, M Onada and I Fugita - Ironmaking Proceedings of AIME, Vol. 37, Chicago 1978, 300-318.

72. K Narita, M. Mackawa, I Shigaki and Y Seki - Trans. ISI Japan, Vol. 18, 1978, 712-720.
73. C E Grip, B Johansson, B Bäcklund and N O Lindfors - Scand. Jour. of Metallurgy, 5, (1976) 229-247.
74. P Barnaba - Ironmaking Proceedings of AIME, Vol. 37, Chicago 1978, 53-68.
75. S Kondo, M Sugata and T Sugiyama - Proceedings of ICSTIS Suppl. Trans. ISI Japan, Vol. 11, 1971, 36-40.
76. M S Bykov, V A Dolinskii and A A Permyakov - Steel in the USSR, October 1976, 539-541.
77. M Sugata - Private communication.
78. M C Udy and C H Lorig - Trans. AIME, 1943, 154, 162-181.
79. O Kubaschewski, E L L Evans and C B Alcock - "Metallurgical Thermochemistry", Pergamon Press.
80. British Oxygen Company Ltd. - "Gas Data and Safety Sheet for Sulphur Dioxide".
81. N J Bowen and J F Schairer - Amer. J. Sci., 5th Series, 24, 200 (1932).
82. F W Roedder - Amer. J. Sci. Bowen Vol. (1952) p445.
83. E F Coburn and A Muan - "Phase Equilibrium Diagrams of Oxide Systems". Published by the Amer. Ceram. Soc.
84. R E Johnson and A Muan - J. Amer. Ceram. Soc. 48 (7) 360, (1965).

85. A A El-Geassy, K A Shehata and S Y Ezz - Iron and Steelmaking International, Oct. 1977, 329-332.
86. K Kojima, K Nagano, T Inazumi and K Shinada - Trans. ISI Japan, vol. 9, 1969, 324-334.
87. E T Turkdogan - Transactions of AIME Met. Trans. B. June 1978, 163-179.
88. J T Moon and R D Walker - Ironmaking and Steelmaking (Quarterly) 1975, No.1, 30-36.
89. R Cochrane - private communication.
90. Metals Handbook - Amer. Soc. of Metals.
91. G Clixby - 36th Ironmaking Proceedings of AIME, April 17-20th 1977, Pittsburgh, 308-325.
92. G H Geiger and D R Poirier - "Transport Phenomena in Metallurgy", Publisher Addison -Wesley.

Test		Unsize	Sized
Wind rate	scfm	41000	46000
Hanging time	hr/day	10	2
Production	NTHM/day	reference	+164
	%	reference	+16.1
Coke rate	lb/NTHM	reference	-30

Table 1 Comparison of Sized to Unsize (100%) Sinter Burden Distribution<sup>4</sup>

Burden	Burden Resistance Index
Unsize sinter	$6.72 \times 10^{-4}$
Sized sinter	$5.69 \times 10^{-4}$
As-received pellets	$4.74 \times 10^{-4}$
Screened pellets	$4.31 \times 10^{-4}$

Table 2 Burden Permeability<sup>4</sup>

	%
Fe <sub>2</sub> O <sub>3</sub>	49.4
CaO.Fe <sub>2</sub> O <sub>3</sub>	49.2
2 CaO.Fe <sub>2</sub> O <sub>3</sub>	25.5
CaO.2 Fe <sub>2</sub> O <sub>3</sub>	58.4
3 CaO.FeO. 7 Fe <sub>2</sub> O <sub>3</sub>	59.6
CaO.Al <sub>2</sub> O <sub>3</sub> .2 Fe <sub>2</sub> O <sub>3</sub>	57.3
4 CaO.Al <sub>2</sub> O <sub>3</sub> .Fe <sub>2</sub> O <sub>3</sub>	23.4

Table 3 Degree of Reduction of Sinter Minerals after Reduction For Forty Minutes in Pure CO at 800°C<sup>23</sup>

Data	Production (t/day)	Blast condition			ore coke	Fuel O.R. F.R. (kg/t-p)	Metal			Slag		Top gas CO <sub>2</sub> CO (%)					
		Volume (m <sup>3</sup> /min)	P/V (%)	Temp. Humid. O <sub>2</sub> (°C) (g/m <sup>3</sup> ) (%)			Top press. (g/cm <sup>2</sup> )	Si (10 <sup>-2</sup> %)	S (10 <sup>-2</sup> %)	Mn (10 <sup>-2</sup> %)	Vol. (kg/t-p)		CaO /SiO <sub>2</sub>				
July 20	2.593	1.84	2.300	0.96	981	30.9	0.96	900	2.99	511	36	547	66	261	1.14	19.0	23.7
21	2.580	1.83	2.300	0.93	954	32.0	0.96	900	3.00	504	37	511	61	287	1.15	19.1	23.6
22	3.289	2.34	2.300	0.90	941	32.0	0.96	900	2.97	471	31	502	62	265	1.12	19.2	23.4

Kukioka No. 4 BF, quenched on May 25, 1971. Charge sequence CGJ OOJ

Data	Production (t/day)	Blast condition			ore coke	Fuel O.R. F.R. (kg/t-p)	Metal			Slag		Top gas CO <sub>2</sub> CO (%)					
		Volume (m <sup>3</sup> /min)	P/V (%)	Temp. Humid. O <sub>2</sub> (°C) (g/m <sup>3</sup> ) (%)			Top press. (g/cm <sup>2</sup> )	Si (10 <sup>-2</sup> %)	S (10 <sup>-2</sup> %)	Mn (10 <sup>-2</sup> %)	Vol. (kg/t-p)		CaO /SiO <sub>2</sub>				
May 22	2.257	1.76	2.046	0.62	980	13.5	1.97	61	3.94	388	78	464	69	266	1.19	18.8	23.3
23	2.262	1.77	2.024	0.62	980	14.5	1.98	60	3.94	388	77	465	71	266	1.19	18.7	23.1
24	2.268	1.77	2.039	0.61	980	16.5	1.99	58	3.94	387	78	465	60	267	1.22	19.0	22.7

Table 4 Operating Results of Hirohata No.1 and Kukioka No.4 Blast Furnaces During the Three Days Prior To Quenching<sup>45</sup>

Hirohata No. 1 BF: Sinter ratio 50.4%, Pellet ratio 15.2%

	kg/charge	T.Fc (%)	SiO <sub>2</sub> (%)	Al <sub>2</sub> O <sub>3</sub> (%)	CaO (%)	MgO (%)	Mn (%)
Sinter	18 900	54.32	5.75	1.80	11.56	0.95	0.60
Hammersley pellet	5 700	63.16	3.11	3.11	0.46	0.08	0.04
Blended lump ore	7 800	65.00	3.00	1.70	0.24	0.06	0.09
(sub total)	37 500	61.80	5.20	1.45	0.85	0.55	0.26
India Mn ore	400	20.50	7.00	4.48	1.30	0.16	33.04
Olivine	660	6.09	37.92	0.88	0.66	36.96	
Lime stone	1 080	0.77	0.36	0.18	54.29	0.12	
Coke	12 500	0.62	6.10	3.20	0.34	0.26	

Kukioka No. 4 BF: Sinter ratio 68.7%, Pellet ratio 11.6%

	kg/charge	T.Fc (%)	SiO <sub>2</sub> (%)	Al <sub>2</sub> O <sub>3</sub> (%)	CaO (%)	MgO (%)	Mn (%)
Sinter (Kukioka DL)	13 000	56.68	5.91	2.20	10.86	0.20	0.33
Sinter (Tobata DL)	6 500	56.31	5.82	1.97	9.59	1.26	0.40
Kowa pellet	3 300	62.19	4.32	0.86	3.65	0.29	0.07
Swaziland lump ore	3 600	64.30	4.00	1.46	0.16	0.06	0.31
Hammersley lump ore	1 000	65.50	2.40	0.08	0.14	0.08	0.06
South Africa mixed lump ore	1 000	67.20	1.88	1.09	0.06	0.03	0.05
(sub-total)	28 400						
MHL scale	300	73.89	9.46	1.03	1.20	0.13	0.56
Africa Mn ore	150	21.02	6.04	6.13	1.18	0.25	31.80
Coke	7 200	0.65	5.00	2.83	0.51	0.18	

Table 5 Burdens of Hirohata No.1 and Kukioka No.4 Blast Furnaces During the Three Days Prior to Quenching<sup>45</sup>

Softening-melting layer	Portion*	Reduction degree (%)		
		Sinter	Lumpy Ore	Pellet
G-5	B	65.6	65.0	79.3
	C	72.8	68.2	81.2
	D	11.5	12.3	14.6
G-19	D	35.4	36.6	41.3
* B: Softening portion C and D: Lumpy portion				

Table 6 Degree of Reduction of the Burden Materials in the Softening-Melting Layers of Hirohata No.1 Blast Furnace <sup>51</sup>

Softening-melting layer	Sampling position (distance from the boundary*) (m)	Mean value of the reduction of the sample pellets (%)
G-3	2.0	12.7
	0.2~0.3	23.1
G-10	1.0	14.1
	0.2~0.3	(55)**
G-12	1.3	13.9
	0.9	14.3
	0.5	14.3
* Between the lumpy and softening portions ** The value of the reduced pellet being not reoxidized		

Table 7 Degree of Reduction of the Pellets in the Lumpy Portion <sup>51</sup>

Sample	Position		Chemical Component (%)								CaO/SiO <sub>2</sub>
			CaO	SiO <sub>2</sub>	Al <sub>2</sub> O <sub>3</sub>	MgO	FeO	K <sub>2</sub> O	Na <sub>2</sub> O		
Icicle	G-8	Centre	40.0	34.85	12.6	2.3	3.53	1.45	1.10	1.15	
		Edge	35.3	30.80	10.2	2.2	2.37	0.68	0.77	1.15	
Drop materials	G-25	Centre	41.2	34.75	14.7	4.8	1.20	0.46	0.67	1.19	
		Edge	40.0	36.60	11.7	6.4	0.57	0.83	0.95	1.09	
Drop materials	G-10~11 G-25~26		39.5	35.15	12.9	3.9	1.70	0.33	0.44	1.12	
			39.3	36.45	11.6	7.0	0.65	0.17	0.47	1.08	

Table 8 Change of Slag Composition in the Dropping Process in Hirohata No.1 Blast Furnace<sup>48</sup>

Sampling level	Iron Ore Granule	Analysed Phase	As oxide (%)*					
			CaO	FeO	Al <sub>2</sub> O <sub>3</sub>	SiO <sub>2</sub>	Sum	
11	Sinter	Dicalcium silicate Glass	60.0 37.0	4.1 12.4	nd 15.0	36.0 27.0	100 91.4	
13	Lumpy ore	Fayalite Glass	0.9 16.4	66.3 33.4	nd 12.0	32.9 31.0	100 92.4	
13	Slag materials in the lower side of the portion	Glass Glass	44.0 36.0	nd 0.4	25.0 18.0	36.0 40.0	105 94.4	

\* Determined by X-ray microanalyser

Table 9 Composition of the Slag Minerals in the Reduced Burden Materials in the Molten Portion of Kukioka No.4 Blast Furnace<sup>48</sup>

Sample	Position		Chemical component (%)	
			Combined C	Alloying Si*
Half-molten portion	G-8	Upper side	0.16	<0.01
		Lower side	0.35	<0.01
	G-25	Upper side	0.22	<0.01
		Lower side	0.57	
"Icicle"	G-2		0.34	
	G-12		0.87	
	G-25		0.67	

\* Obtained by the non-water soluble solution electrolytic extraction method

Table 10 Metal Composition of the Softening-Melting Layers in Hirohata No.1 Blast Furnace<sup>48</sup>

(a) Metal portion										
Sampling		Chemical Component								
Level No.	Position*	Combined C	Alloying Si	S	Mn					
13	(1)	0.13	<0.04	0.026	0.36					
	(2)	0.74	-	0.062	0.43					
	(3)	1.90	0.23	0.115	0.63					
14	(1)	0.33	<0.04	0.036	0.11					
	(2)	1.27	-	0.085	0.66					
	(3)	1.50	Trace	0.070	0.32					
15	(2)	1.53	-	0.057	0.57					
	(3)	2.65	0.24	0.044	0.61					
	(1)	0.64	<0.04	0.057	0.46					
(3)	3.68	3.69	0.041	1.77						
(b) Slag portion										
Sampling		Chemical component (%)								
Level No.	Position*	CaO	SiO2	Al2O3	MgO	FeO	K2O	Na2O	S	CaO/SiO2
13	(2)	28.5	25.6	9.8	3.6	8.3	2.29	1.24	0.57	1.11
	(3)	31.4	27.6	9.5	3.1	8.3	1.39	0.77	0.69	1.14
15	(2)	44.6	30.9	11.4	4.2	1.3	0.47	0.34	0.49	1.44
	(3)	35.0	30.1	12.0	3.6	3.9	0.08	0.04	1.32	1.16
	(3)	36.0	32.3	11.9	3.5	4.6	1.06	0.64	0.91	1.11

\* (1): The lower side of half-molten

(2): Icicle

(3): Drop material in the coke layer

Table 11 Change in Composition of the Metal and Slag Portions in the Dropping Process in Kukioka No.4 Blast Furnace<sup>48</sup>

Ore	Wt.% in Blend
Mount Wright	25
Carol Lake	38
Minercoes Brasileiras Reunidas (M.B.R.)	20
Kiruna B Fines (K.B.F.)	17

Table 12 Iron Ore Blend used in the Manufacture of the Acid Pellets

Total Fe	66.30 wt. %
FeO	-
CaO	0.30
SiO <sub>2</sub>	4.60
Al <sub>2</sub> O <sub>3</sub>	0.40
MgO	0.50
K <sub>2</sub> O	0.10
S	0.03
Loss on ignition	0.08

Table 13 Chemical Analysis of the Acid Pellets

Peak Firing Temperature Holding time at temperature	1340°C 8 minutes
% Open porosity % Closed porosity	26.4 0.6
ISO Tumble Index +6.3 mm -500 μm	98.4 wt. % 1.6 wt. %
Compressive Strength	402 kg

Table 14 Firing Data and Physical Properties of the Acid Pellets

Test	Value
ISO Reducibility Index $\frac{dR}{dt}$ (at 40% reduction)	0.31% min <sup>-1</sup>
Low temperature breakdown test +6.3mm	99.89 wt. %
Free swelling test (maximum % swelling/% reduction)	24%/51%
Burghardt test -	
- pressure drop (at 80% reduction)	4 mm H <sub>2</sub> O
- drop in bed height (at 80% reduction)	0.10%
- reducibility $\frac{dR}{dt}$ (at 40% reduction)	0.44% min <sup>-1</sup>

Table 15 Reduction Tests Indices for the Acid Pellets

Hammersley
Kiruna B
Tazadit siliceous
Tazadit fines
South American Manganese fines
Sinter screenings
Pellet screenings
Mill scale
Dolomite
Limestone
Coke

Table 16 Materials Used in the Manufacture of the Sinters

Sinter CaO/SiO <sub>2</sub>	Wt. %					
	Fe	FeO	CaO	SiO <sub>2</sub>	Al <sub>2</sub> O <sub>3</sub>	MgO
2.4	54.5	8.1	12.6	5.1	1.5	2.5
2.1	56.5	8.2	11.1	5.1	1.8	2.5
1.8	57.4	12.8	9.6	5.3	1.7	1.8
1.6	56.9	16.8	9.6	5.9	2.0	2.9
1.4	57.9	18.7	8.7	6.1	2.0	2.8
1.2	59.7	20.8	7.7	6.3	2.1	3.3

Table 17 Chemical Analyses of the Sinters

Phase	Sinter CaO/SiO <sub>2</sub>					
	2.4	2.1	1.8	1.6	1.4	1.2
Hematite	18.6	20.0	23.8	14.0	5.2	7.6
Magnetite	21.4	22.2	21.6	48.2	59.6	70.8
Slag	6.4	4.4	6.8	11.0	9.6	18.2
Ferrites	45.0	47.2	39.4	23.0	20.8	3.2
Dicalcium silicate	8.6	6.2	8.4	3.8	4.6	-

Table 18 Phase Analyses of the Sinters in Volume %

Sinter CaO/SiO <sub>2</sub>	ISO Reducibility Index $\frac{dR}{dt}$ (at 40% reduction)
2.4	1.15
2.1	1.23
1.8	1.01
1.6	0.89
1.4	0.76
1.2	0.49

Table 19 Variation of ISO Reducibility Index with Sinter CaO/SiO<sub>2</sub> Ratio

Heating rate from 950°C	200 or 400°C.hr <sup>-1</sup>
Gas flow*	60 l.min <sup>-1</sup>
Gas composition	40% CO, 60% N <sub>2</sub>
Applied load	49 KN.m <sup>-2</sup>
Bed diameter	90 mm
Initial bed height	66 mm
Bottom coke layer height	40 mm
Top coke layer depth	15 mm
Particle size range	10 - 12.5 mm

\* Measured at 15°C and 760 mm Hg. absolute pressure

Table 20 Test Conditions Used in the High Temperature Test

Total Fe	CaO	SiO <sub>2</sub>	Al <sub>2</sub> O <sub>3</sub>	MgO	MnO	P <sub>2</sub> O <sub>5</sub>	L.O.I.
61.70	3.30	3.00	0.70	2.80	<0.05	0.18	0.10
ISO Reducibility Index $\frac{dR}{dt}$ (at 40% reduction)=0.90%.min <sup>-1</sup>							

Table 21 Chemical Analysis (wt.%) and ISO Reducibility Index of the Pellets used in the Gas Flow and Reproducibility Tests

Coke rate (dry)	387.4 kg.tonne <sup>-1</sup>
Tuyere injection rate	80 kg.tonne <sup>-1</sup>
Wt.% S in coke	1.10
Wt.% S in injectant	1.00
Total sulphur load	5.06 kg.tonne <sup>-1</sup>
Blowing rate (air)	1049.85 Nm <sup>3</sup> .tonne <sup>-1</sup>
Bosh gas rate	1270.32 Nm <sup>3</sup> .tonne <sup>-1</sup>
Sulphur load in the bosh gas	3.98 g.Nm <sup>-3</sup>
Elemental sulphur concentration in the bosh gas	0.28 vol.%

Table 22 Steps in the Calculation of the Elemental Sulphur Concentration in the Bosh Gas of the Redcar Blast Furnace (Data Taken from Scheduled Operating Parameters for the Furnace)

	Burghardt Test	High Temperature Test
Cold gas velocity in empty tube*, m.sec <sup>-1</sup>	0.119	0.157
Ratio of reducing gas to sample weight, m <sup>3</sup> .kg <sup>-1</sup> .min <sup>-1</sup>	0.069	0.075 <sup>+</sup>
<p>* Gas flow measured at 15<sup>o</sup>C and 760 mm Hg absolute pressure</p> <p>+ Calculated on an 800 g sample weight, but in practice the sample weight was less than this</p>		

Table 23 Comparison of Gas Flow Conditions in the Burghardt Test and the High Temperature Test

Phase	Vol.%
Hematite	70.8
Magnetite	4.4
Slag	15.4
Quartz	9.4

Table 24 Phase Analysis of the Acid Pellets in the Oxidised State

Test No.	System	Firing Temperature ° C	Slag formation in oxidised state	Fayalite formation after partial reduction at 950° C
S1	Ferric oxide/silica sand	1300	Extensive	Yes
S2	Ferric oxide/silica glass	1300	Extensive	Yes
S3	" " "	1100	Extensive	Yes
S4	Ferric oxide/silica glass	1100	Yes	Yes
S5	Ferric oxide/silica sand	1100	Yes	Yes
S6	MAC* only	1100	No	No
S7	MAC/silica sand	1100	No	No
S8	" " "	1300	No	No
S9	MAC/bentonite	1300	Extensive	Yes
* Malmberget iron ore concentrate				

Table 25 Results of the Synthetic Acid Pellet Tests

Test No.	% Pre-Reduction	Heating rate °C.hr <sup>-1</sup>	Additive		Termination temperature °C	Failure Mode*	Remarks
			Sulphur	Alkali			
1	32	200			1330	T	
2	52	200			1316	T	
3	0	400			1178	P	
4	30	400			1245	P	
5	49	400			1308	P	
6	61	400			1272	T	
7	31	400			1178	P	
8	27	400			1170	P	
9	26	400			1195	P	
10	44	400			1227	P	
11	47	400			1221	P	
12	65	400			1240	P	
13	26	400			1294	P	
14	44	400			1125	Interrupted at 1125°C	
15	33	400	0.28vol.%		1221	P	
16	32	400	0.75		1128	T	
17	30	200	0.75		1130	T	
18	32	400		5gK <sub>2</sub> CO <sub>3</sub>	1250	P	
19	31	400		10g	1275	P	
20	29	400		15g	1283	P	
21	30	400		15g	1106	Interrupted at 1106°C	
22	30	400	0.75	15g	1144	P	

\* T = thermocouple failure      P = terminated due to rapid rate of rise of gas pressure drop

Table 26 High Temperature Tests Carried out with Acid Pellets

Phase	Heating rate ( $^{\circ}\text{C}\cdot\text{hr}^{-1}$ )/elemental sulphur concentration in the gas (vol.%)		
	400/0.28	400/0.75	200/0.75
Metallic iron	35.6	15.0	28.2
Slag	27.4	33.8	21.8
Wustite	32.0	42.4	32.0
FeS and FeS eutectic	5.0	8.8	18.0

Table 27 Phase Analyses (vol.%) of the Acid Pellets after the High Temperature Tests Incorporating Sulphur in the Reducing Gas (Test Numbers 15 - 17)

Test No.	Sulphur Level Vol. %	Heating Rate °C. hr <sup>-1</sup>	Chemical Analysis (wt. %)									
			Met. Fe	Tot. Fe	FeO	CaO	SiO <sub>2</sub>	Al <sub>2</sub> O <sub>3</sub>	MgO	Na <sub>2</sub> O	K <sub>2</sub> O	S
15	0.28	400	33.40	75.20	49.90	0.30	5.30	1.00	1.30	0.19	0.10	0.92
16	0.75	400	24.40	74.10	63.80	0.20	5.10	0.90	0.80	0.20	0.07	1.80
17	0.75	200	31.90	76.70	57.80	0.20	4.80	1.00	0.80	0.18	0.08	2.70

Table 28 Chemical Analyses of the Pellets after the High Temperature Test with Sulphur in the Reducing Gas

Test No.	Sulphur Level Vol. %	Heating Rate °C. hr <sup>-1</sup>	Phase						
			Fayalite	αFe	FeO	Fe <sub>3</sub> O <sub>4</sub>	Troilite	FeO <sub>SS</sub>	Amorphous material
15	0.28	400	W	MM	MM	Tr	VVW	-	Present
16	0.75	400	W	MM	MM	Tr	W	-	Present
17	0.75	200	VW	MM	VVW	Tr	W	Tr	Present

Troilite - FeS

Table 29 X-Ray Analyses of Pellets after the High Temperature Test with Sulphur in the  
Reducing Gas

Test No.	Alkali Loading g K <sub>2</sub> CO <sub>3</sub>	Heating rate °C.hr <sup>-1</sup>	Chemical Analysis (wt.%)									
			Met. Fe	Tot. Fe	FeO	CaO	SiO <sub>2</sub>	Al <sub>2</sub> O <sub>3</sub>	MgO	Na <sub>2</sub> O	K <sub>2</sub> O	S
18	5	400	40.90	76.90	41.20	0.20	4.90	1.00	0.90	0.17	0.38	0.04
19	10	400	52.30	79.00	28.90	0.20	4.20	1.00	1.10	0.20	0.77	0.03
20	15	400	49.90	78.20	31.60	0.20	5.50	1.20	1.00	0.21	0.70	0.03
21	15	400	N.A.	77.90	95.90*	0.30	6.20	0.60	0.60	0.23	0.11	N.A.

N.A. Not analysed for

\* Includes metallic iron

Table 30 Chemical Analyses of Pellets after the High Temperature Test with Alkali Vapour in the Reducing Gas

Test No.	Alkali Loading g K <sub>2</sub> CO <sub>3</sub>	Heating Rate °C.hr <sup>-1</sup>	Phase						
			Fayalite	αFe	FeO	Fe <sub>3</sub> O <sub>4</sub>	Quartz	Amorphous material	
18	5	400	W	M	MW	-	-	-	Present & unknown material
19	10	400	VVW	MM	VW	-	-	-	Present
20	15	400	W	MM	W	-	-	-	Present
21	15	400	W	M	MW	Tr	Tr	Tr	Present

Table 31 X-Ray Analyses of Pellets after the High Temperature Test with Alkali Vapour in the Reducing Gas

Metallic Fe	25.20 wt. %
Total Fe	75.40
FeO	67.20
Na <sub>2</sub> O	0.19
K <sub>2</sub> O	0.68
S	1.80

Table 32 Partial Chemical Analysis of the Sample Bed  
of the Joint Sulphur/Alkali Test  
(Test Number 22)

Form of Icicle	Phase									
	FeO	Fayalite	$\alpha$ Fe	Alite	MgO	CaO	Ca(OH) <sub>2</sub>	$\beta$ C <sub>2</sub> S	Amorphous material	
Crushed*	WM	MM	Tr	-	-	-	-	-	Present	
Powder abraded off surface	-	-	Present	SM	Tr	Tr	Tr	VW	Present	

Alite - Ca<sub>3</sub>SiO<sub>5</sub> - Note line pattern slightly displaced, possibly caused by impurities in solid solution

$\beta$  C<sub>2</sub>S - Larnite

\* Note: Some metallic iron was removed with a magnet prior to x-ray analysis

Table 33 X-Ray Analyses of Icicles

Total Fe	CaO	SiO <sub>2</sub>	Al <sub>2</sub> O <sub>3</sub>	MgO	K <sub>2</sub> O	Na <sub>2</sub> O
65.10	1.50	16.20	1.90	1.30	0.18	0.29

Table 34 Chemical Analysis (wt.%) of the Icicles  
after the Removal of the Metallic Iron

S	8.10 wt.%
K <sub>2</sub> O	0.14

Note: Metallic iron and FeO unavailable due to analysis errors caused by the high sulphur level

Table 35 Partial Chemical Analysis of the Dropped  
Material from the Sulphur Test (Test No. 17)

Test No.	% Pre-Reduction	Sinter CaO/SiO <sub>2</sub>	Termination Temperature °C	Failure Mode*
23	4	2.4	1267	P
24	30	2.4	1305	P and T
25	45	2.4	1342	T
26	4	2.1	1276	P
27	33	2.1	1320	T
28	45	2.1	1331	T
29	6	1.8	1323	P and T
30	30	1.8	1350	T
31	47	1.8	1286	T
32	8	1.6	1296	P
33	33	1.6	1326	P
34	47	1.6	1334	T
35	8	1.4	1323	P
36	29	1.4	1335	P and T
37	46	1.4	1320	T
38	9	1.2	1298	P
39	32	1.2	1305	P
40	46	1.2	1318	T

\* T = Thermocouple failure

P = Termination due to rapid rate of gas pressure drop

Note: All tests carried out at the 400°C.hr<sup>-1</sup> heating rate

Table 36 High Temperature Tests Carried out with Sinters

Sinter CaO/SiO <sub>2</sub>	3% Bed Contraction Temperature, °C		
	As-Received	30% Pre-Reduced	45% Pre-Reduced
2.4	1025	1065	1085
2.1	1060	1080	1077
1.8	1077	1070	1075
1.6	1077	1086	1070
1.4	1127	1100	1115
1.2	1120	1090	1077

Table 37    3% Bed Contraction Temperatures for the  
Sinters at the Different Levels of  
Pre-Reduction

Phase						
Calcio-Olivine	T-Phase	Calcio-Olivine <sub>SS</sub>	Mellilite	αFe	MgO	Amorphous material
M	VW	W	VW	VW	Tr	Present

Calcio-Olivine- $\gamma$ C<sub>2</sub>S

T-phase-approximates to C<sub>5</sub>MS<sub>3</sub>

Calcio-Olivine<sub>SS</sub>- $\gamma$ C<sub>2</sub>S but impurities causing slight line displacement

Table 38 X-Ray Analysis of White Powder found on the Surface of the 2.4 CaO/SiO<sub>2</sub> Sinters after the High Temperature Test (Sample from Test Number 25)

Test No.	% Pre-Reduction		Average % Pre-Reduction of the Bed	Heating Rate °C.hr <sup>-1</sup>	Termination temp. °C	Failure Mode*
	Sinter	Pellets				
41 (A)	37	30	34	400	1272	P
42 (B)	37	30	34	200	1337	T
43 (C)	61	39	50	400	1325	T

\* T = Thermocouple failure

P = Termination due to rapid rate of rise of gas pressure drop

Table 39 High Temperature Tests Carried out with Sinter/Pellet Mixtures

Phase		
Troilite	$\alpha$ Fe	
W	Tr	+ Amorphous material, possibly carbon

Troilite - FeS

Table 40 X-Ray Analysis of a Small Droplet found in the Bottom of the Crucible after a High Temperature Test with a Sinter/Pellet Mixture (Test Number 42)

Sinter CaO/SiO <sub>2</sub>	ISO Reducibility Test	High Temperature Test
2.4	0.0052 min. <sup>-1</sup>	0.0063 min. <sup>-1</sup>
2.1	0.0058	0.0075
1.8	0.0047	0.0080
1.6	0.0046	0.0067
1.4	0.0035	0.0058
1.2	0.0020	0.0045

Table 41 Values of K<sub>2</sub> Determined from the ISO Reducibility Test and the High Temperature Test

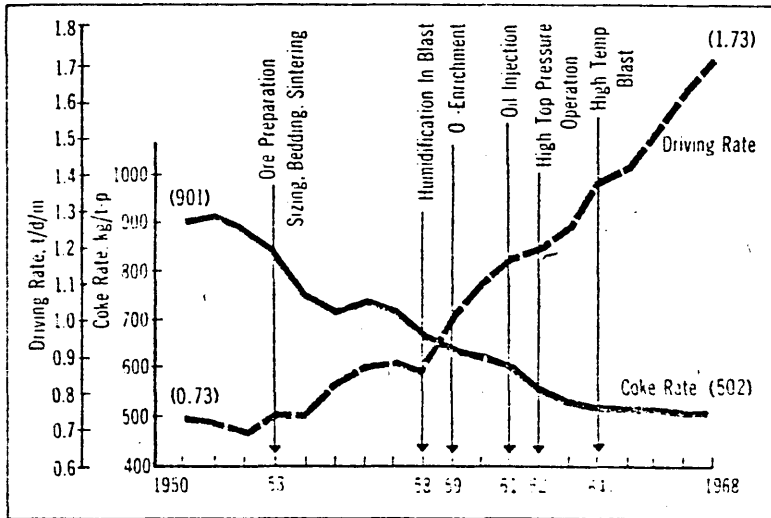
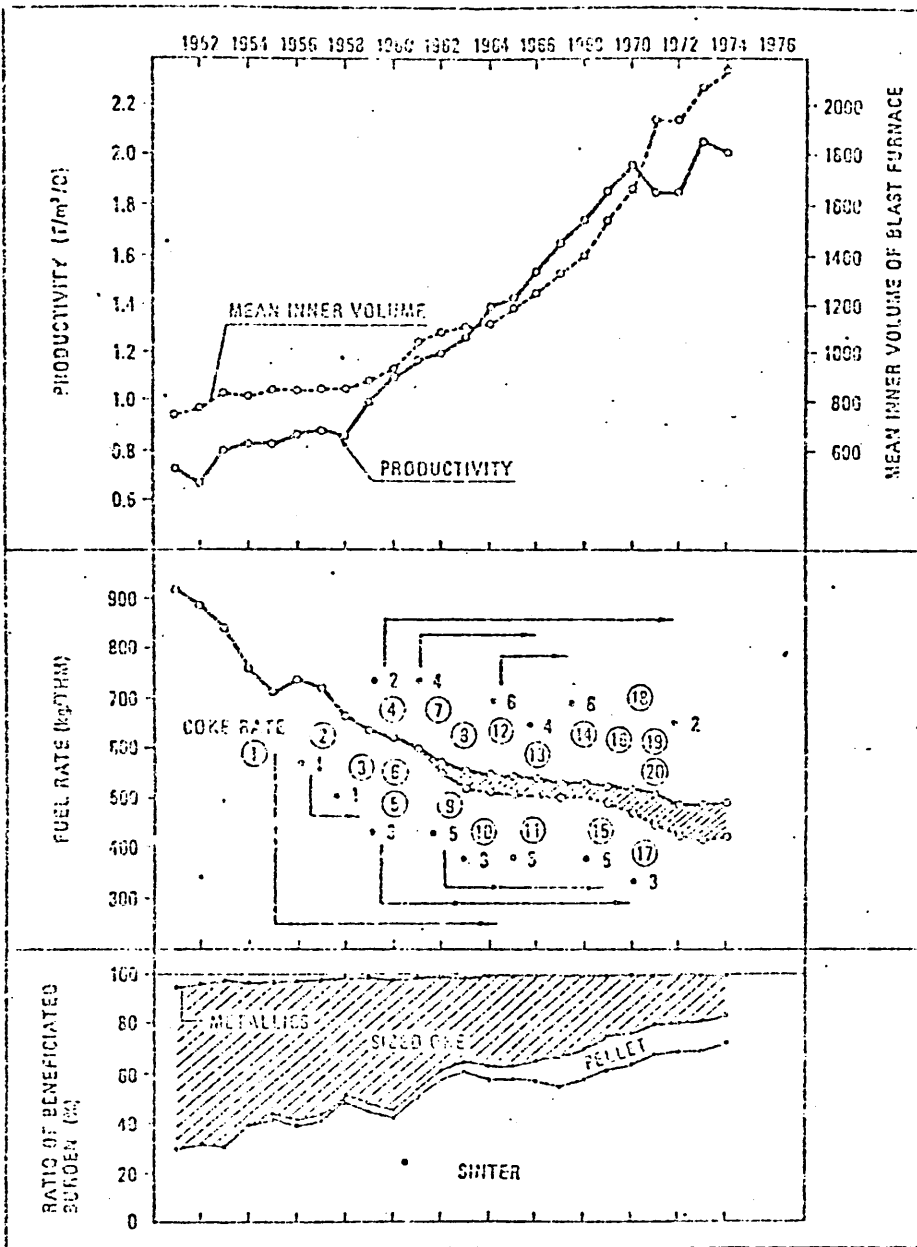


Figure 1 Improvements of Productivity and Fuel Rate<sup>2</sup>



- |  |   |
|--|---|
| ① STRENGTHENING OF ORE SIZING                  | ⑩ SPREAD OF HIGH TOP PRESSURE OPERATION 5                 |
| ② DEVELOPMENT OF SELF-FLUXING SINTER 1         | ⑪ USE OF IMPORTED PELLET 5                                |
| ③ CHANGE TO SELF-FLUXING SINTER 1              | ⑫ APPLICATION OF HIGH-BLAST TEMPERATURE HOT STONE 4       |
| ④ CONSTRUCTION OF LARGE-BLAST FURNACE 2        | ⑬ INCREASE OF PELLET RATIO 5                              |
| ⑤ APPLICATION OF FUEL INJECTION AT TUYERE 3    | ⑭ CONSTRUCTION OF SUPER-HIGH TOP PRESSURE BLAST FURNACE 5 |
| ⑥ APPLICATION OF COPILED BLAST                 | ⑮ SPREAD OF OXYGEN-ENRICHED BLAST OPERATION               |
| ⑦ INCREASE OF BLAST TEMPERATURE 4              | ⑯ EXTREME INCREASE OF OIL INJECTION 5                     |
| ⑧ WIDE USE OF OXYGEN CONVERTER                 | ⑰ APPLICATION OF ON-LINE COMPUTER CONTROL OPERATION 7     |
| ⑨ APPLICATION OF HIGH TOP PRESSURE OPERATION 5 | ⑱ CONSTRUCTION OF 10-COUPLED BLAST FURNACE 2              |
| ⑲ INCREASE OF FUEL INJECTION 3                 | ⑳ APPLICATION OF COAL BRACKET BLEND COOKING PROCESS       |

**Figure 2 Trends in Technical Development and their Influence on Blast Furnace Operation in Japan<sup>3</sup>**

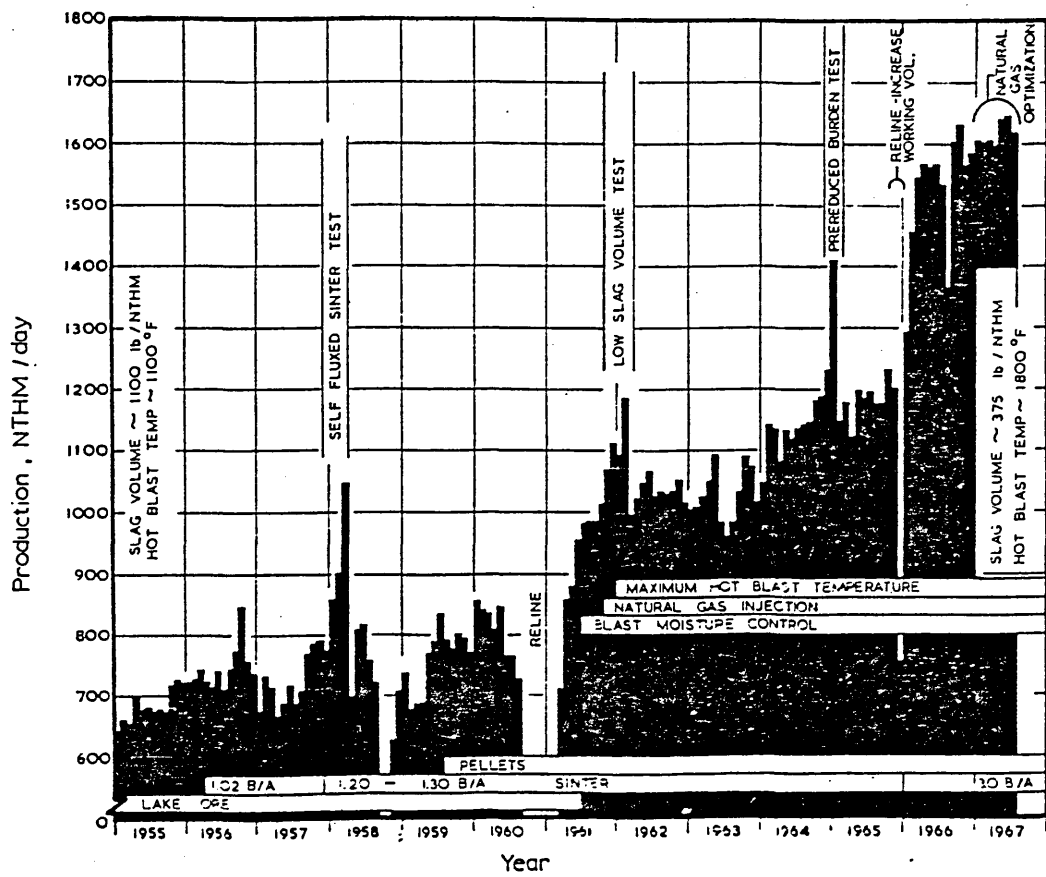


Figure 3 Improvement in Production of 'B' Blast Furnace<sup>4</sup>

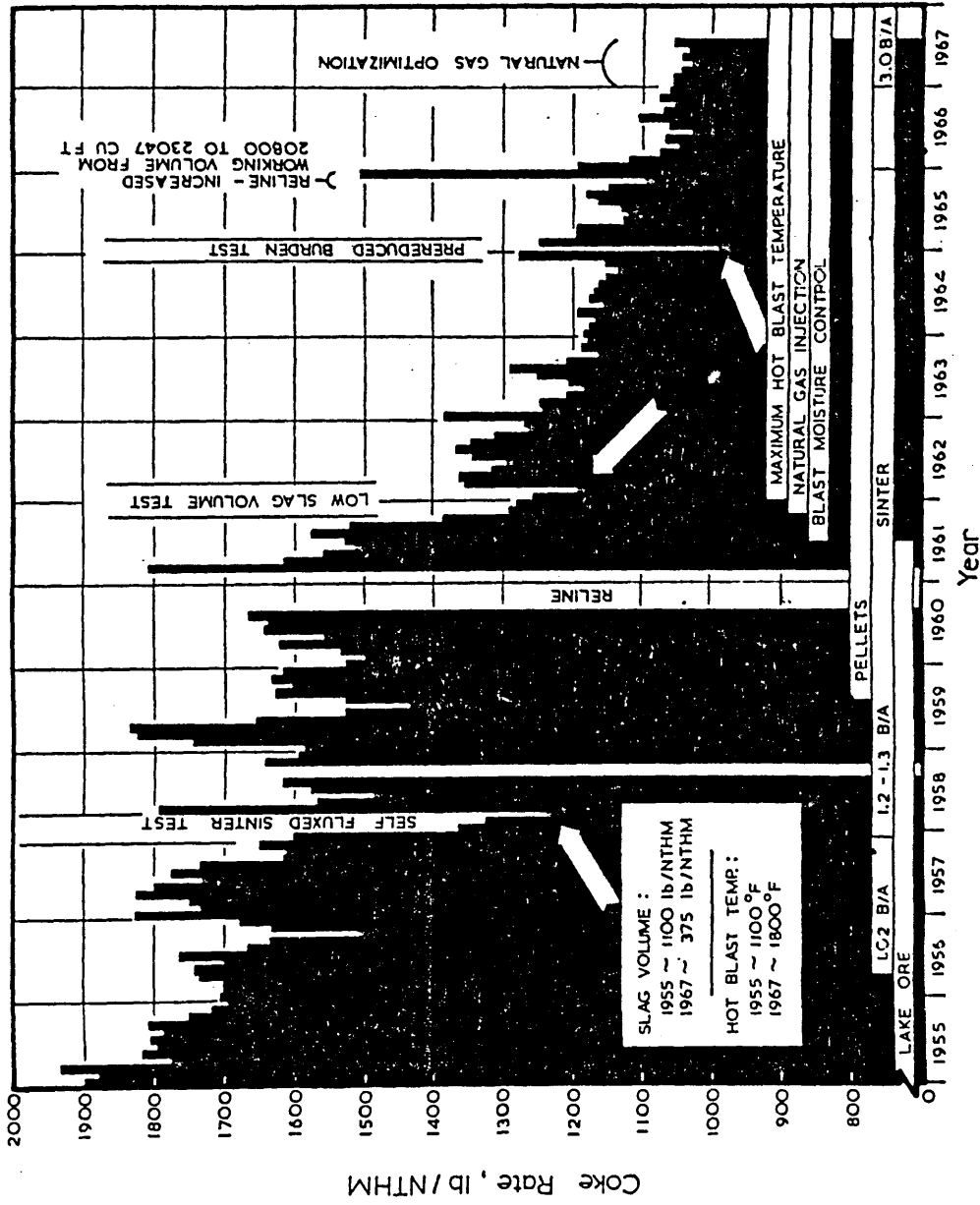


Figure 4 Improvement in Coke Rate of 'B' Blast Furnace<sup>4</sup>

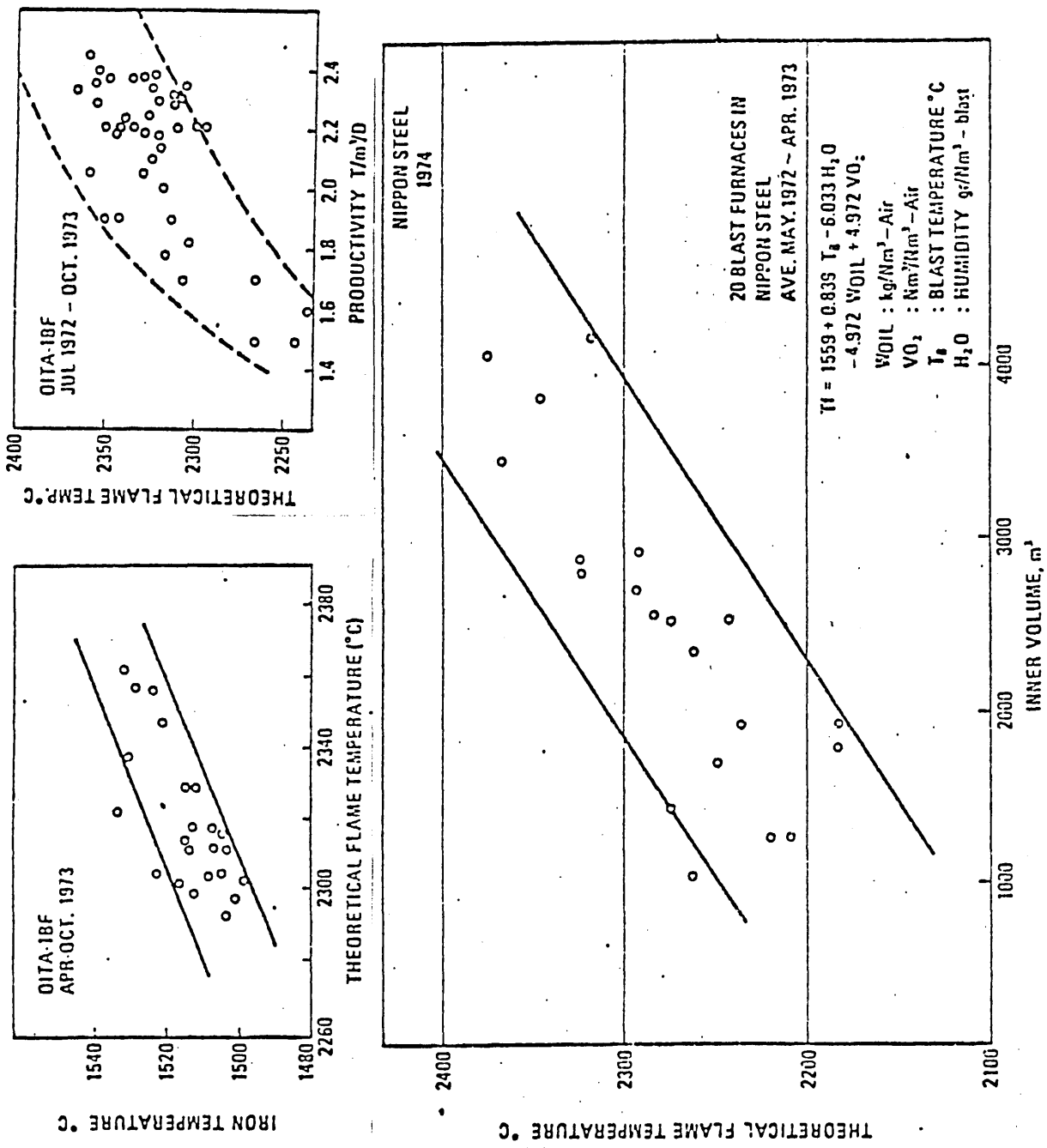


Figure 5 Interrelationship of Flame Temperature, Iron Temperature and Inner Volume<sup>3</sup>

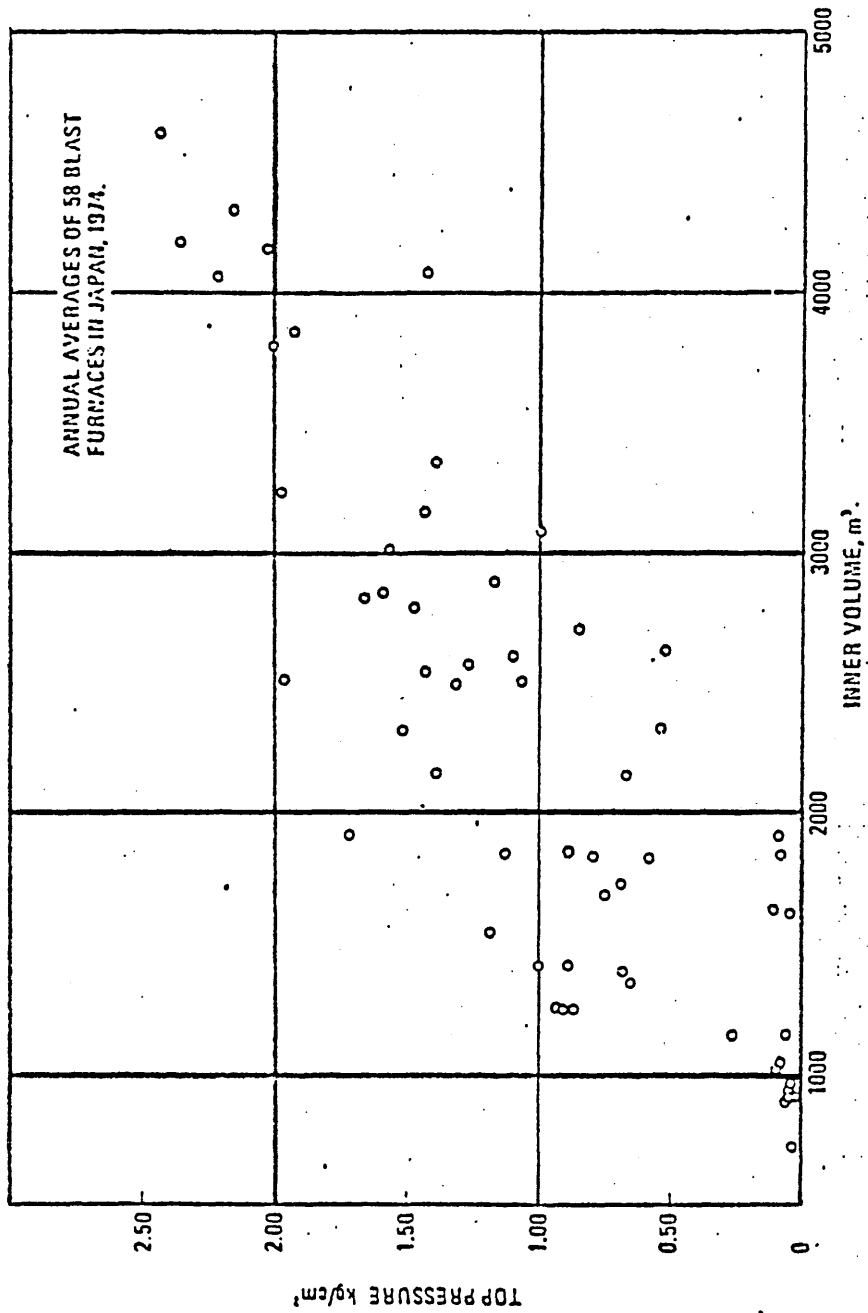


Figure 6 Relationship of Top Pressure and Inner Volume of Blast Furnaces in Japan<sup>3</sup>

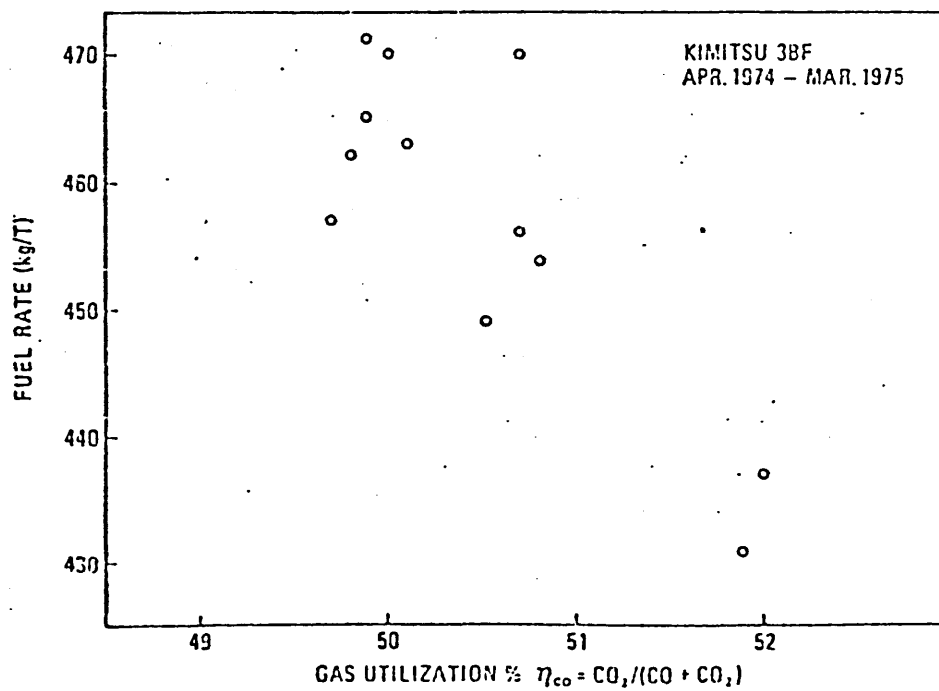


Figure 7 Influence of Gas Utilisation on Fuel Rate<sup>3</sup>

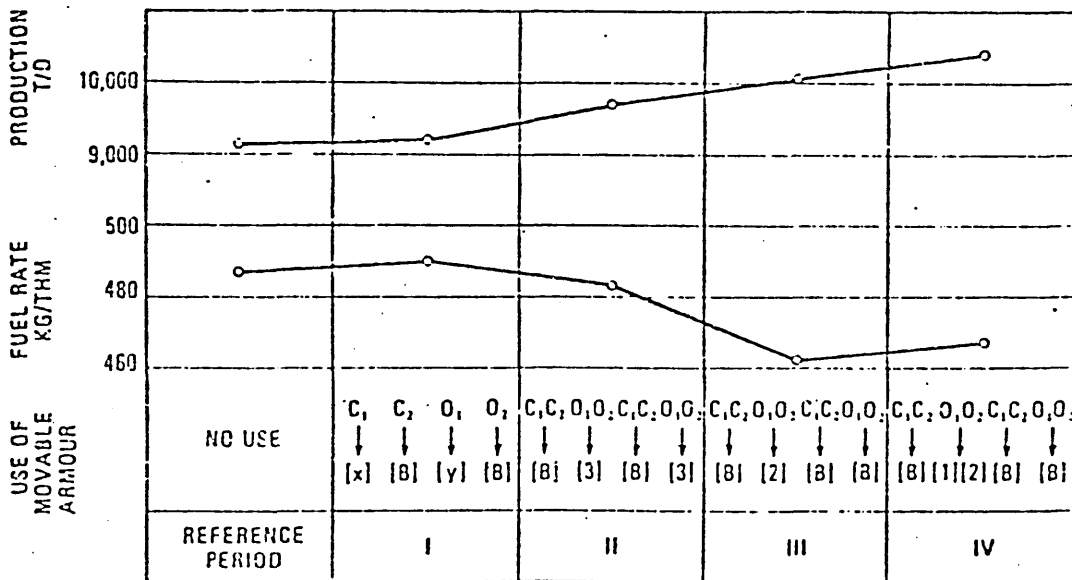


Figure 8 Influence of Movable Armour on Fuel Rate of Fukuyama No.5 Blast Furnace<sup>3</sup>

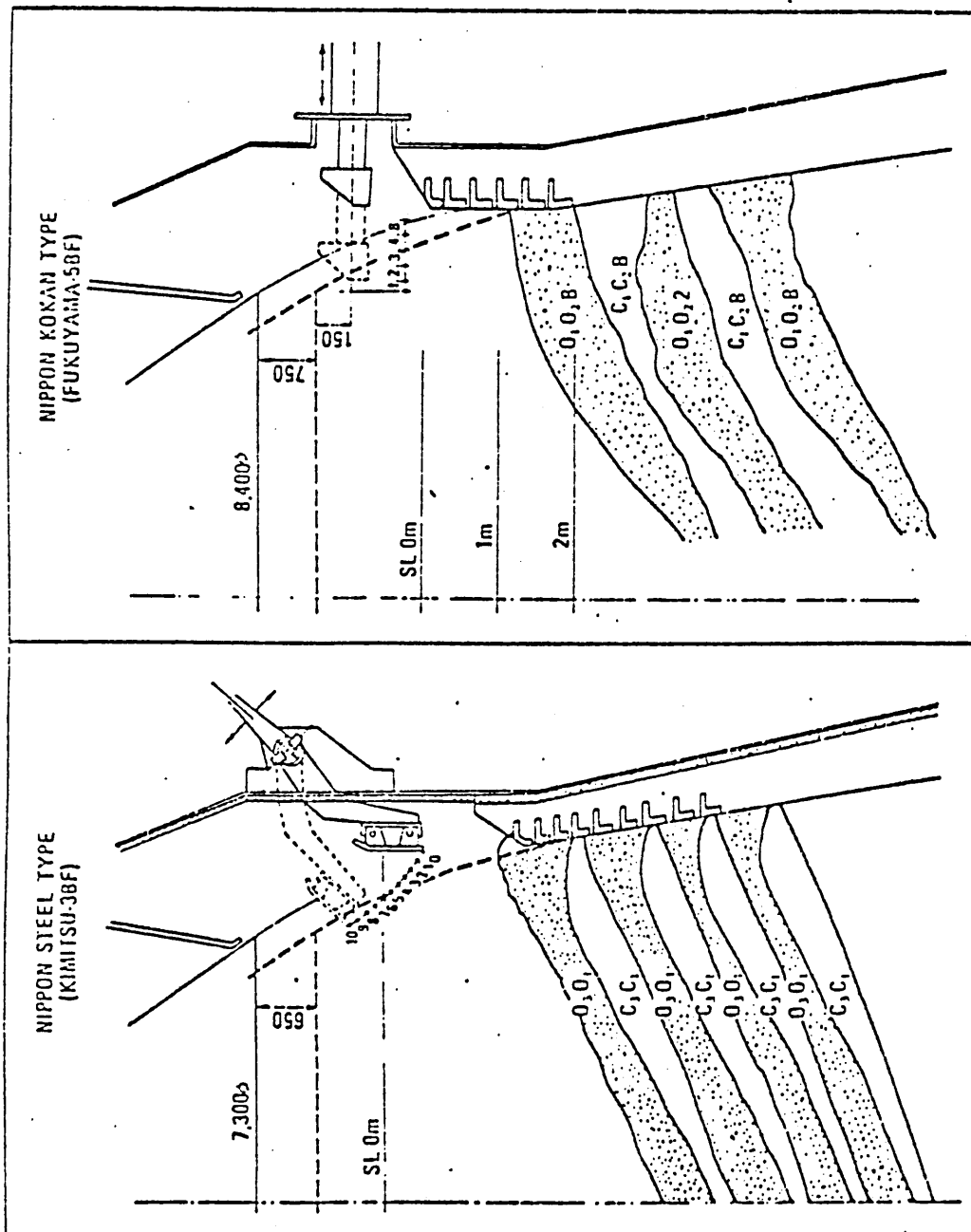


Figure 9 Design of Movable Armours and their effect on the Burden Distribution<sup>3</sup>

Phase relations in the system  $\text{CaO}-\text{Fe}_2\text{O}_3-\text{SiO}_2$  in air, after Phillips and Muan. The crosshatched areas defined by the  $1300^\circ\text{C}$  liquidus isotherm comprises compositions of mixtures which are all liquid at  $1300^\circ\text{C}$ .

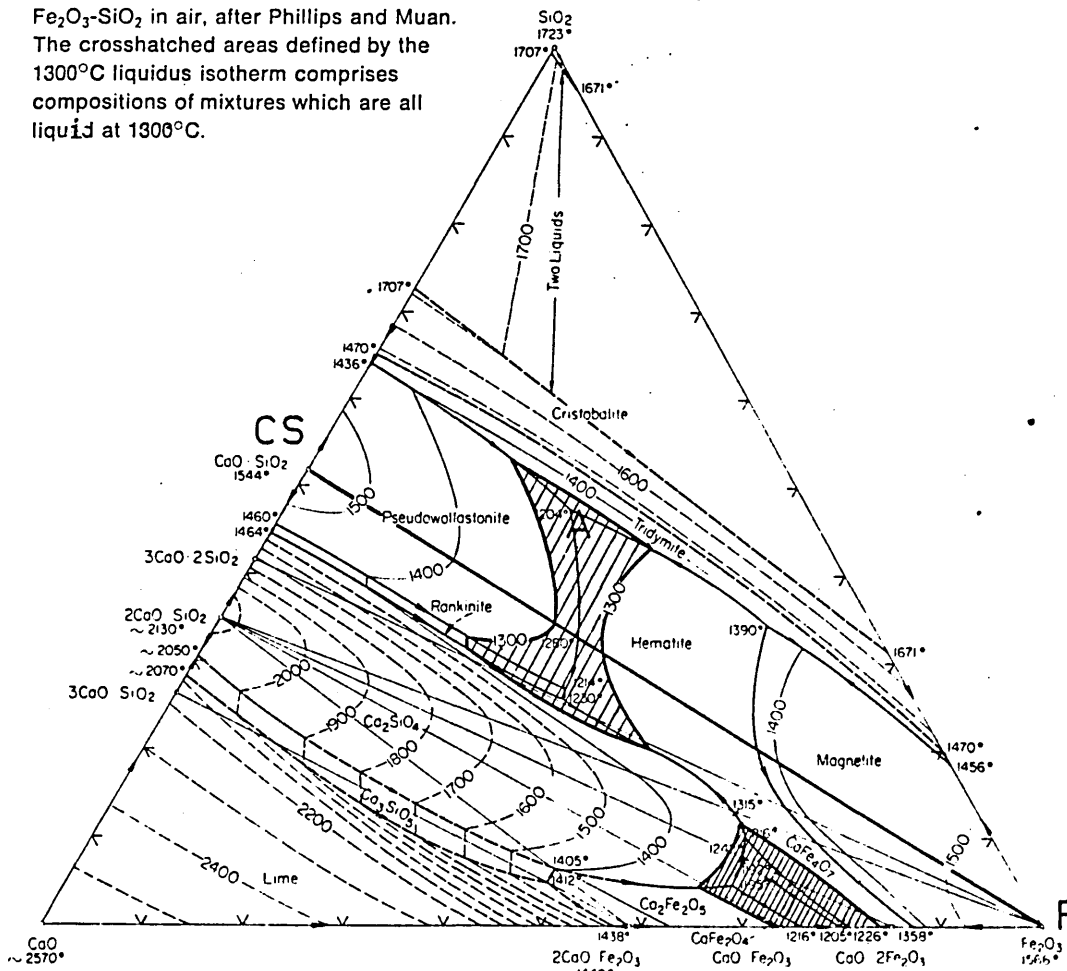


Figure 10 Liquidus Surface of the  $\text{CaO}-\text{Fe}_2\text{O}_3-\text{SiO}_2$  Phase Diagram<sup>13</sup>

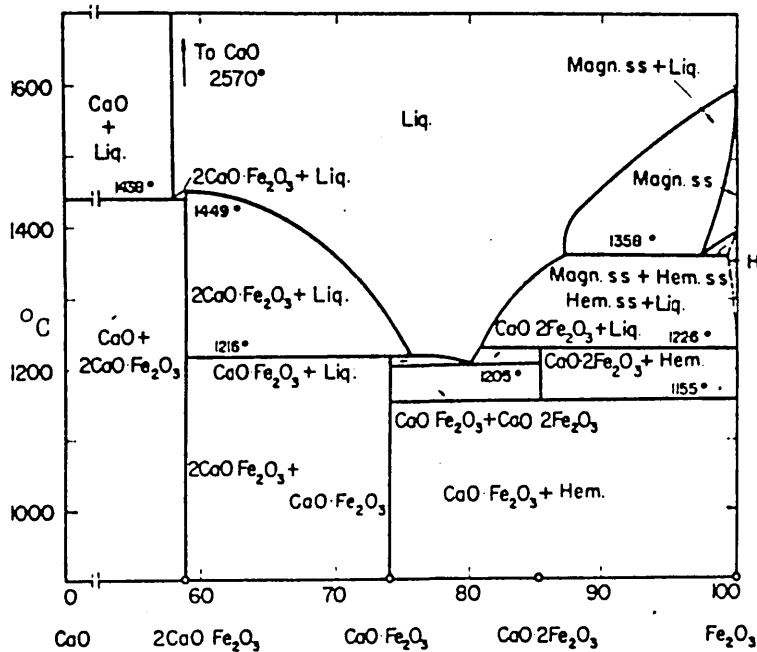


Figure 11 The  $\text{CaO}-\text{Fe}_2\text{O}_3$  Phase Diagram<sup>18</sup>

Phase relations in the system MgO—FeO·Fe<sub>2</sub>O<sub>3</sub> in air after Phillips, Sômiya and Muan.

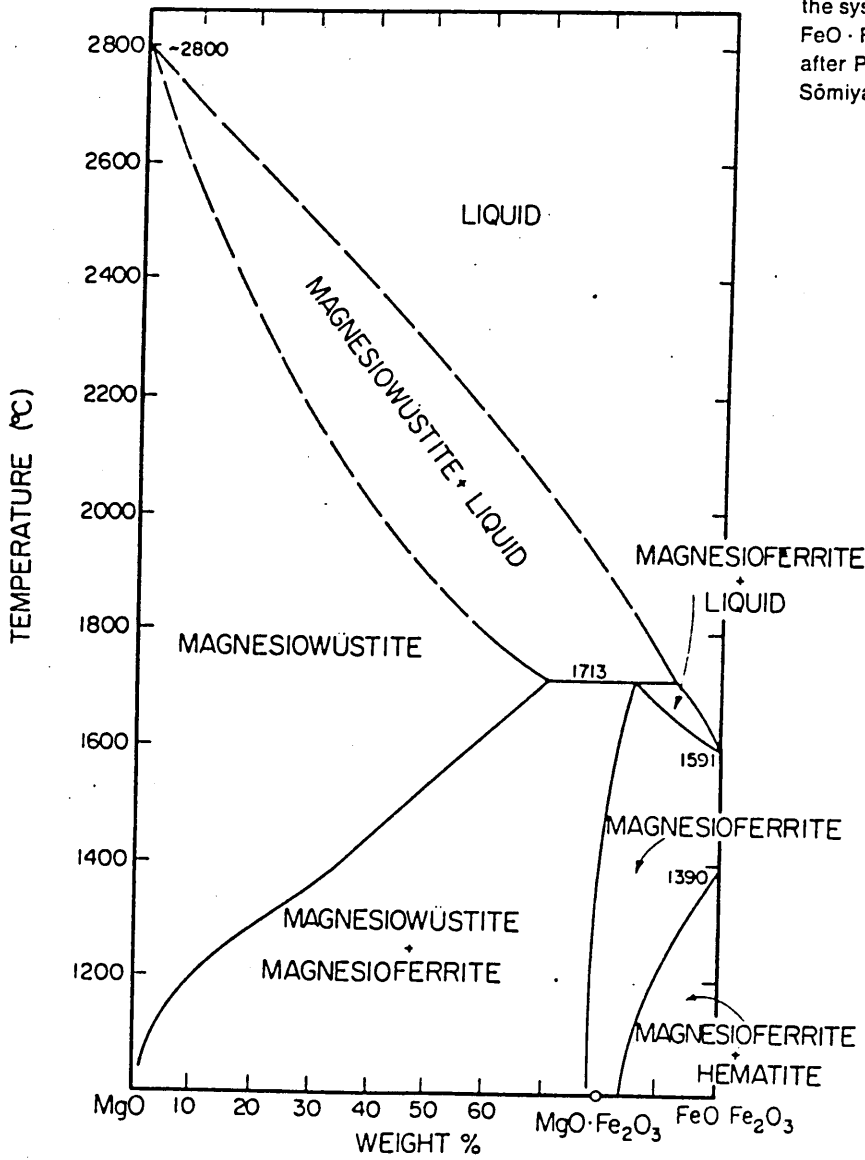


Figure 12 MgO-FeO·Fe<sub>2</sub>O<sub>3</sub> Phase Diagram<sup>19</sup>

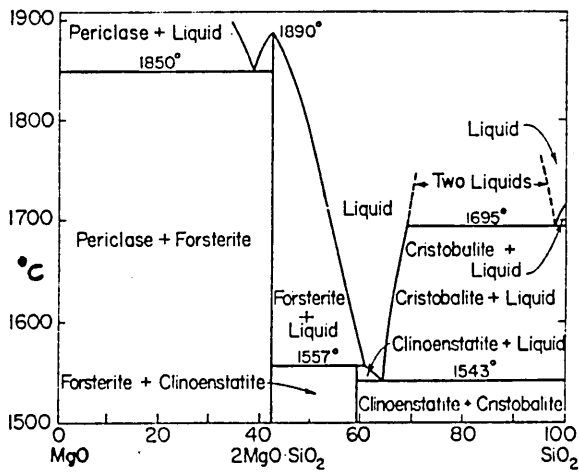
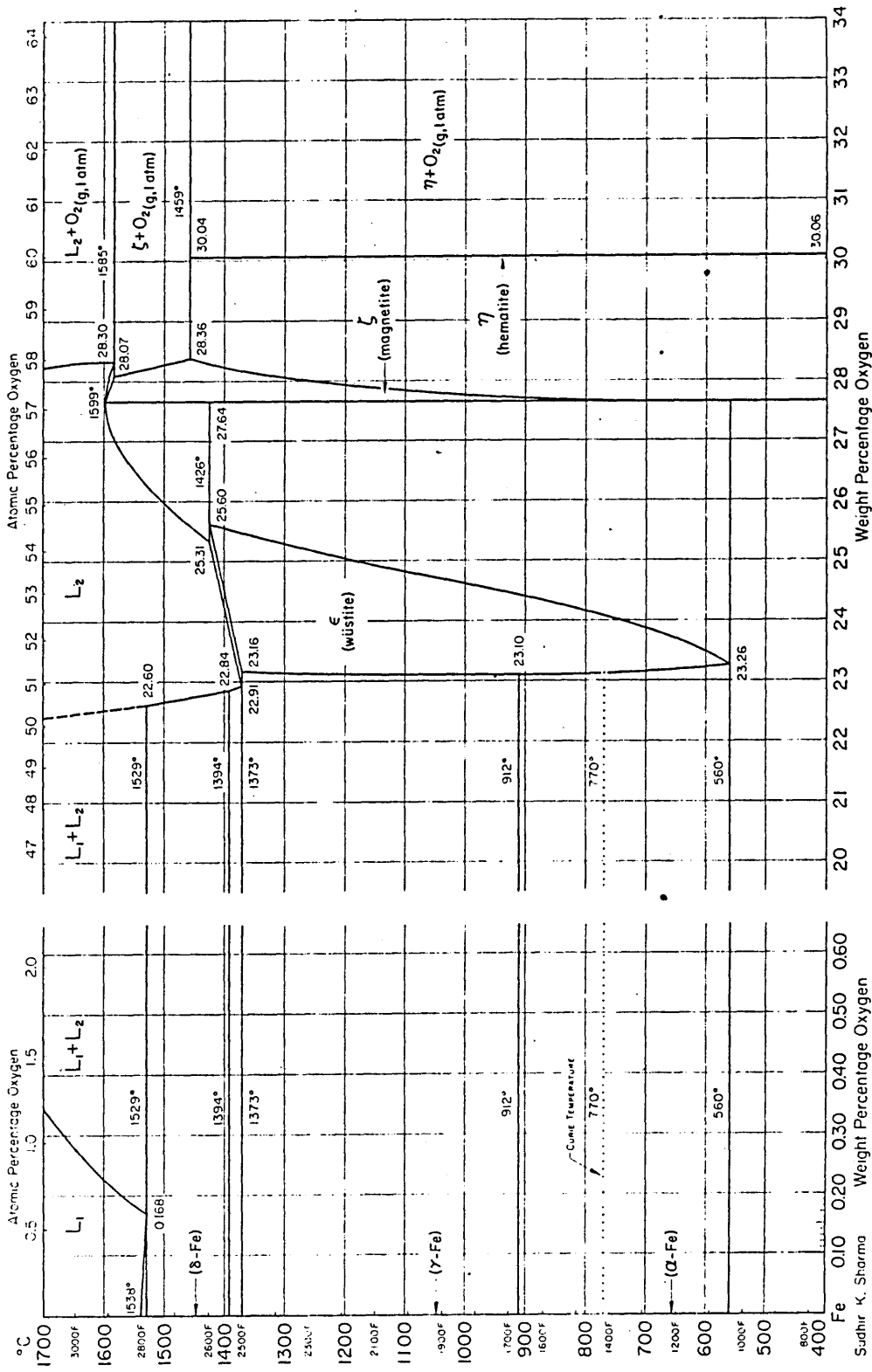


Figure 13 The MgO-SiO<sub>2</sub> Phase Diagram<sup>20</sup>



Sudhir K. Sharma

Figure 14 The Fe -Fe<sub>2</sub>O<sub>3</sub> Phase Diagram <sup>21</sup>

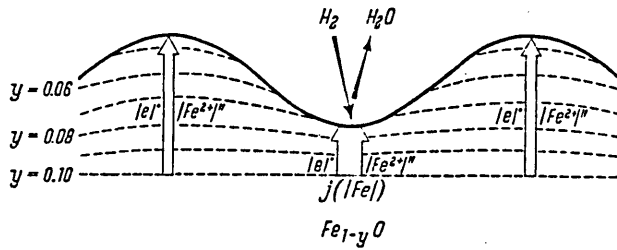


Figure 15 Diagrammatic Representation of the Flow of Material and the Formation of Surface Roughness in the Reduction of Wustite<sup>23</sup>

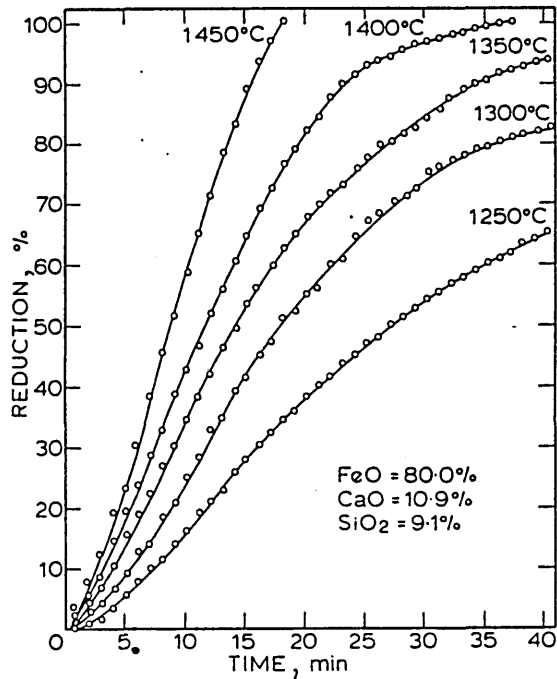
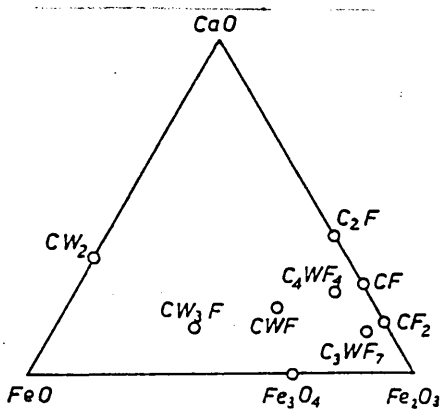


Figure 16 Influence of Temperature on the Reduction Rate of Molten Slag<sup>30</sup>



Notations:  $C_2F = 2CaO \cdot Fe_2O_3$ .  
 $CF = CaO \cdot Fe_2O_3$ .  $CF_2 = CaO \cdot 2Fe_2O_3$ .  
 $C_4WF_4 = 4CaO \cdot FeO \cdot 4Fe_2O_3$ .  
 $C_3WF_7 = 3CaO \cdot FeO \cdot 7Fe_3O_4$ .  
 $CWF = CaO \cdot FeO \cdot Fe_2O_3$ .  
 $CW_3F = CaO \cdot 3FeO \cdot Fe_2O_3$ .

Figure 17 Phases in CaO-FeO-Fe<sub>2</sub>O<sub>3</sub> System<sup>37</sup>

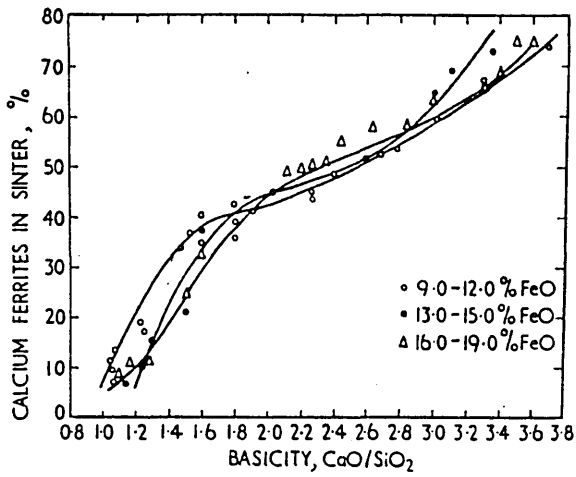


Figure 18 Influence of Sinter Basicity on the Quantity of Calcium Ferrites<sup>38</sup>

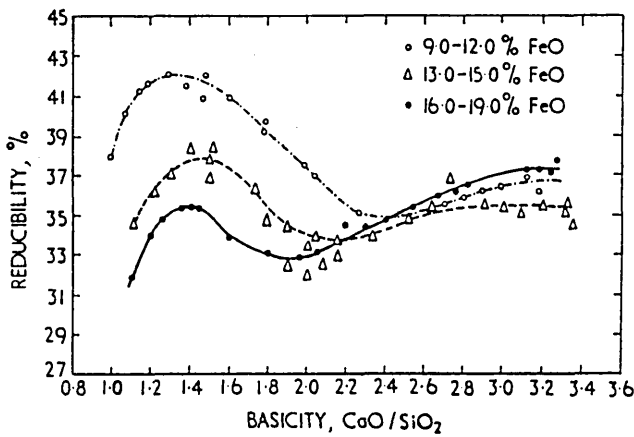
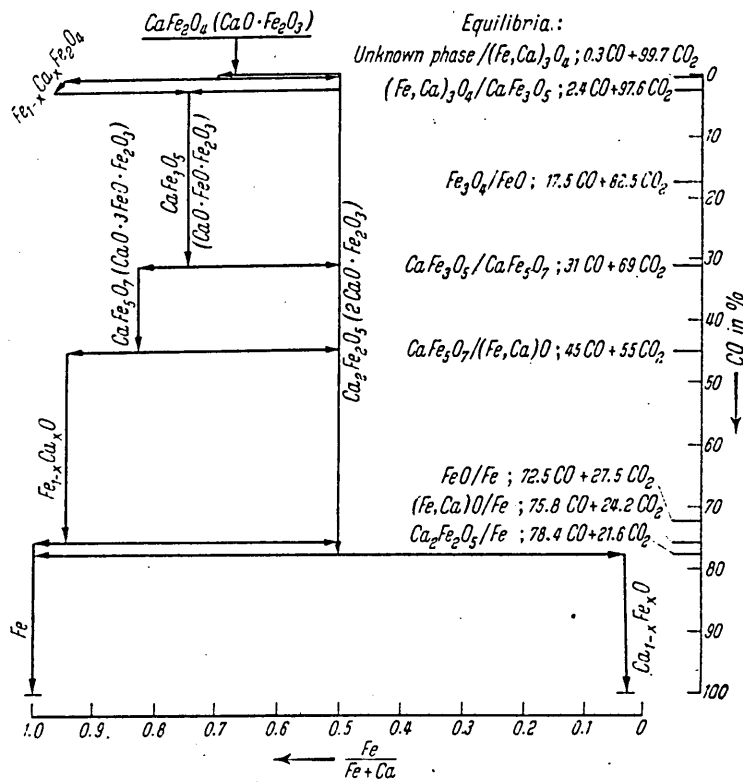
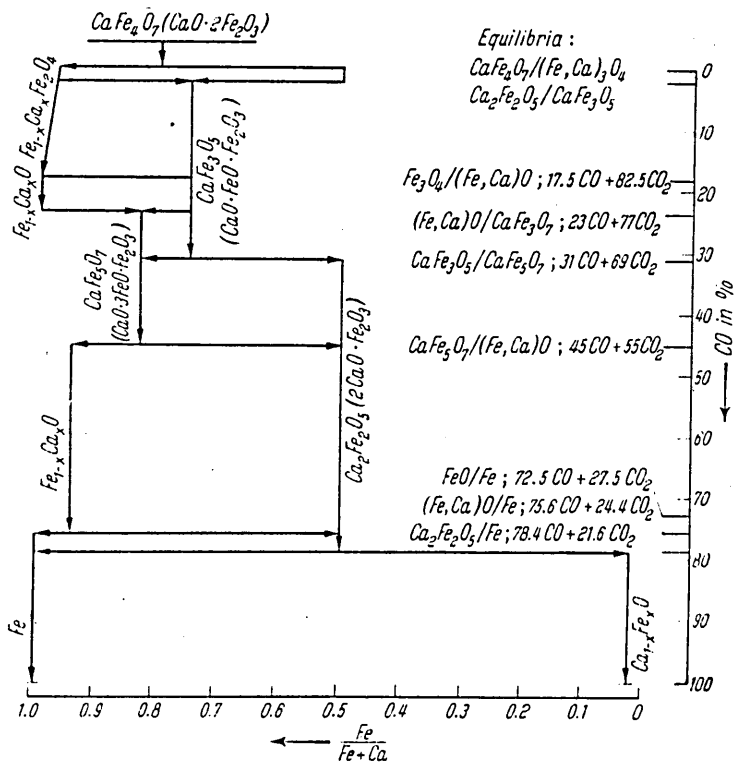


Figure 19 Influence of Sinter Basicity on the Reducibility<sup>38</sup>



**Figure 20** Phase Equilibria and Reduction Path During the Reduction of Calcium Ferrite at 1000°C by Carbon Monoxide<sup>23</sup>



**Figure 21** Phase Equilibria and Reduction Path During the Reduction of Calcium Diferrite at 1000°C by Carbon Monoxide<sup>23</sup>

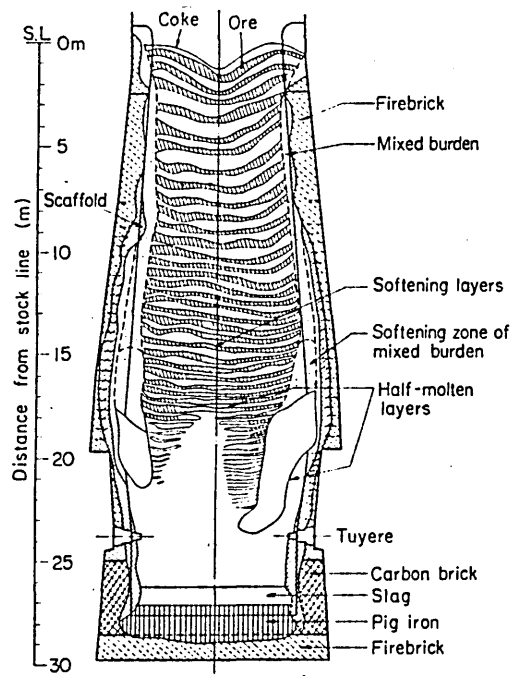


Figure 22 Internal Structure of Kukioka No.4 Blast Furnace<sup>49</sup>

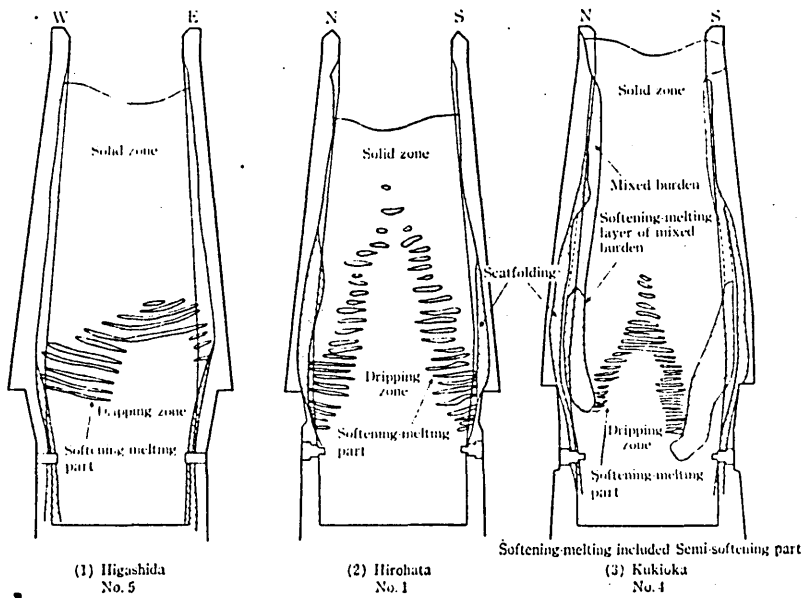


Figure 23 Distribution of the Softening and Melting Layers<sup>49</sup>

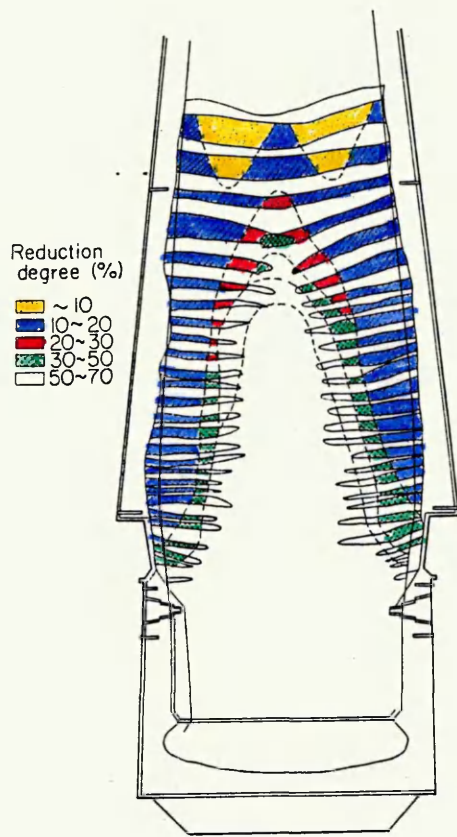


Figure 24 Distribution of the Reduction Degree in Hirohata No.1 Blast Furnace<sup>47</sup>

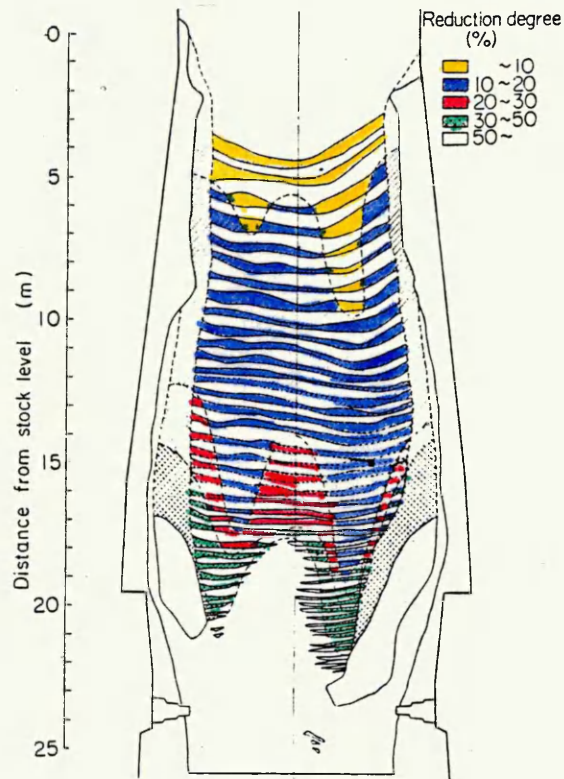


Figure 25 Distribution of the Reduction Degree in Kukioka No.4 Blast Furnace<sup>47</sup>

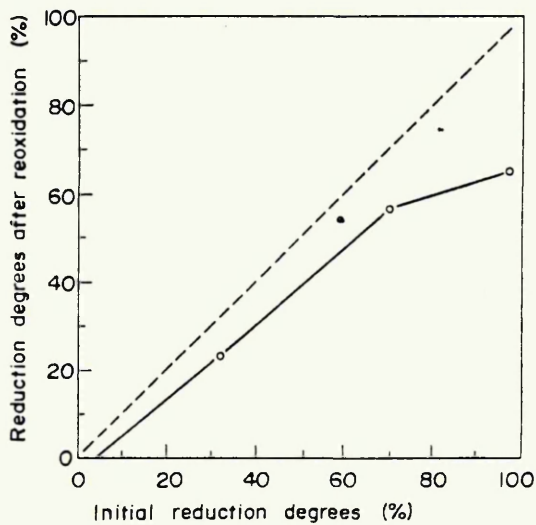


Figure 26 Relationship Between the Initial Reduction Degree and the Reduction Degree after Reoxidation<sup>46</sup>

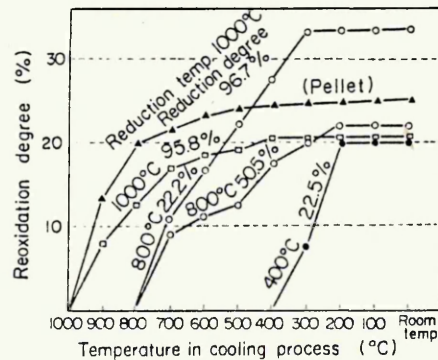


Figure 27 Results of the Reoxidation Tests on Reduced Sinter<sup>47</sup>



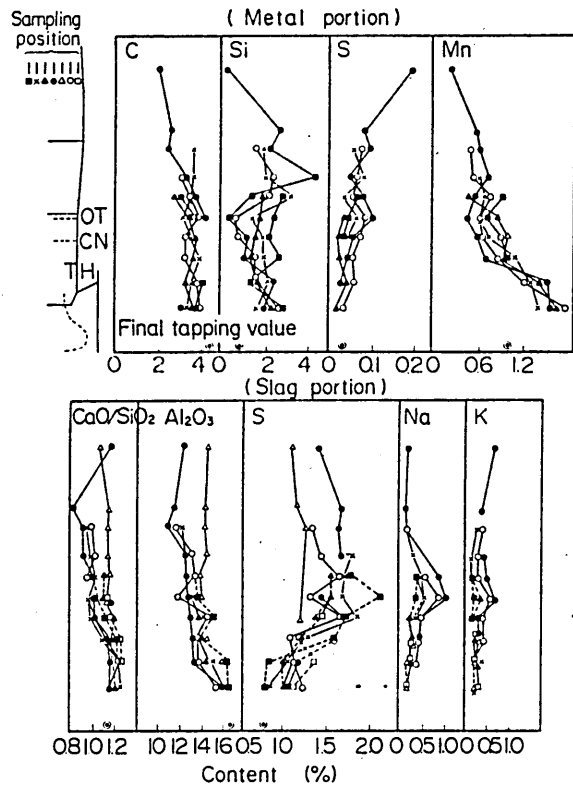


Figure 30 Change in Composition of the Drop Materials in Hirohata No.1 Blast Furnace<sup>48</sup>

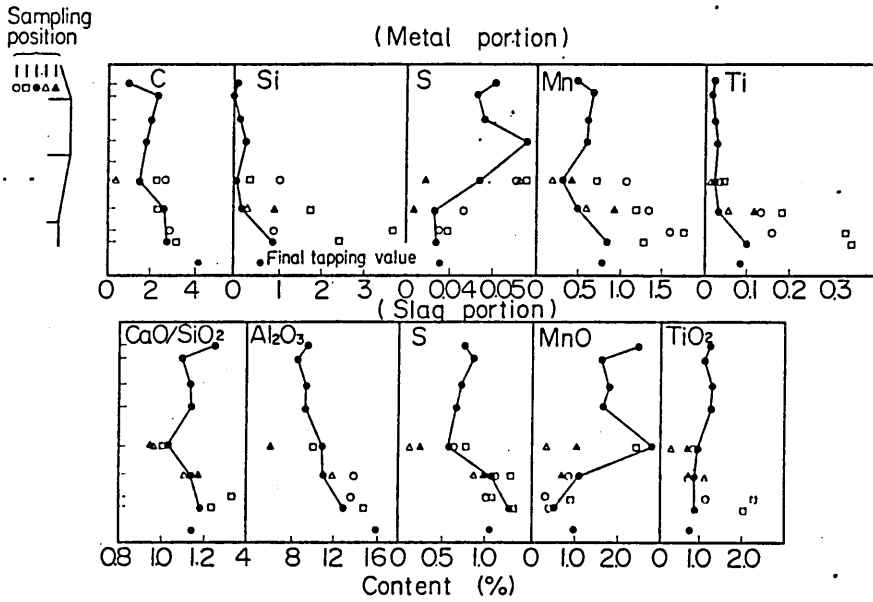


Figure 31 Change in Composition of the Drop Materials in Kukioka No.4 Blast Furnace<sup>48</sup>

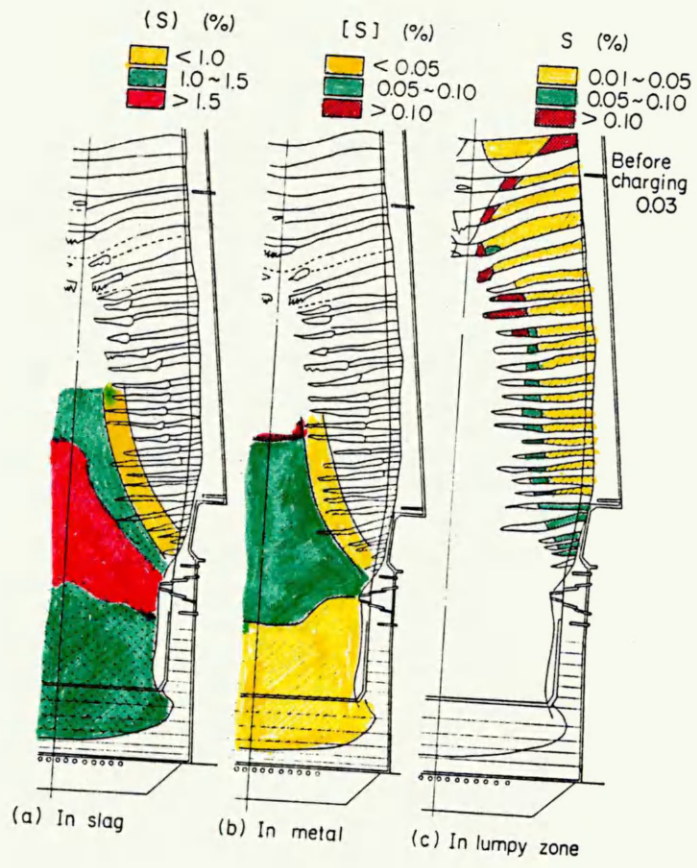


Figure 32 Distribution of Sulphur within Hirohata No.1 Blast Furnace<sup>47</sup>

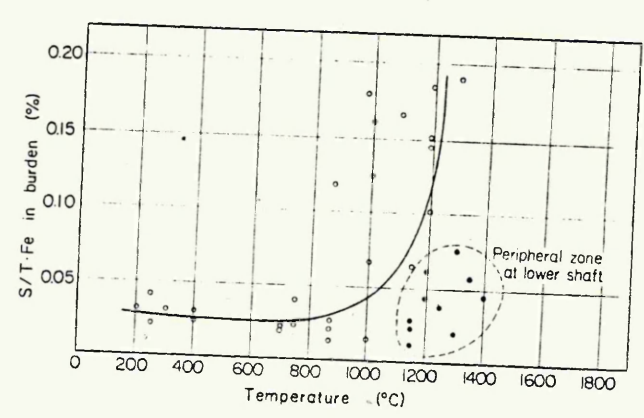


Figure 33 Relationship of Temperature and Absorption of Sulphur in the Lumpy Zone of Hirohata No.1 Blast Furnace<sup>47</sup>

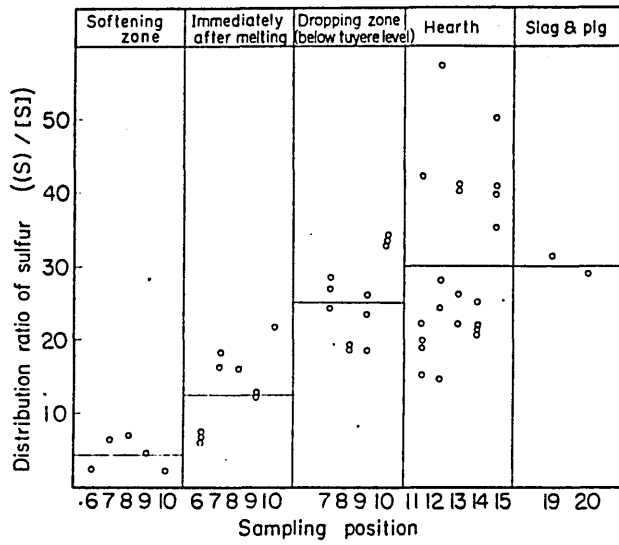


Figure 34 Desulphurisation Process in the Blast Furnace<sup>47</sup>

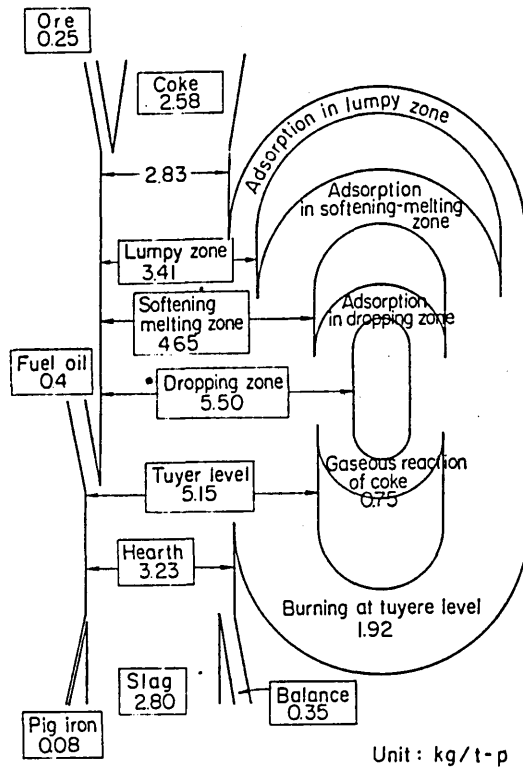


Figure 35 Circulation of Sulphur within Hirohata No.1 Blast Furnace<sup>47</sup>

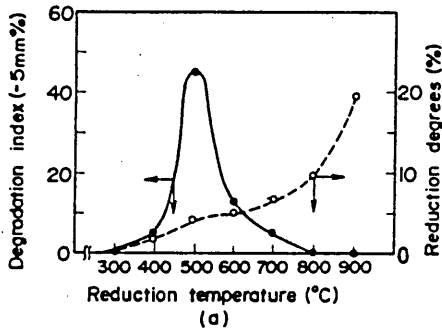


Figure 36 Relationship of Reduction Temperature and the Degradation Index<sup>46</sup>

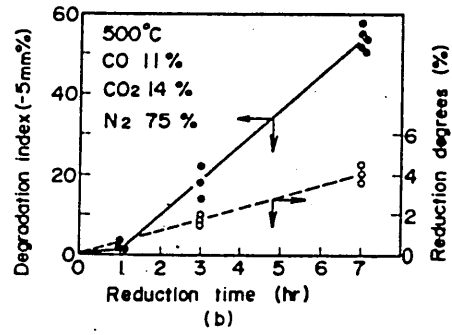


Figure 37 Relationship between Reduction Time and the Degradation Index<sup>46</sup>

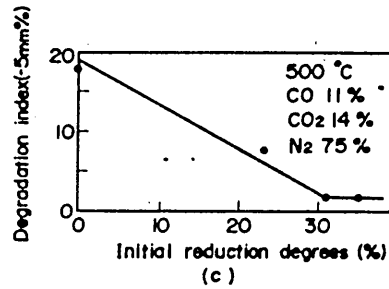


Figure 38 Relationship between Initial Reduction Degree and the Degradation Index<sup>46</sup>

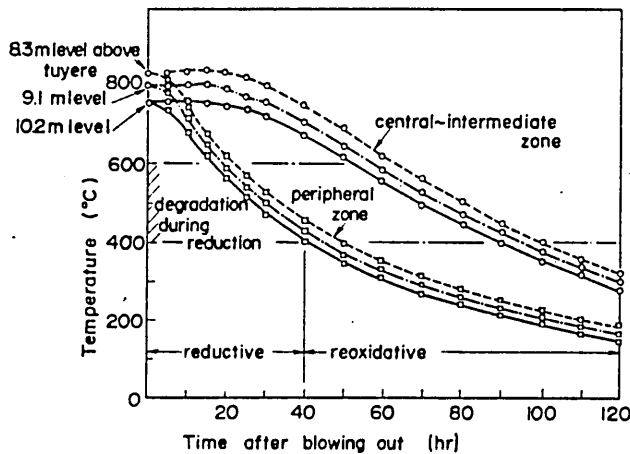


Figure 39 Relationship between the Reductive, or Reoxidative, Period and the Cooling Pattern<sup>46</sup>

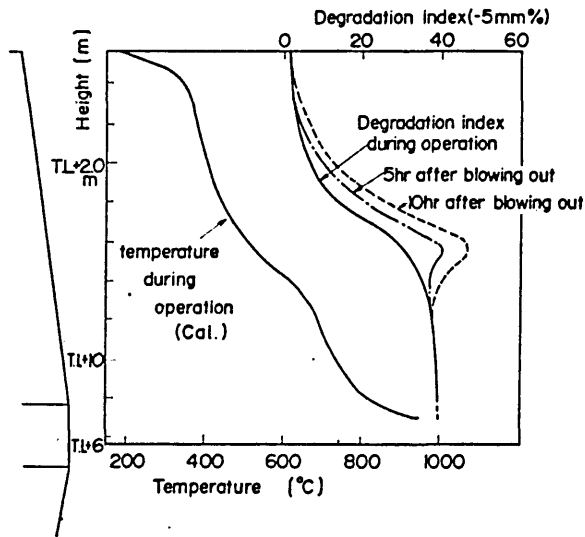


Figure 40 Calculated Estimation of the Distribution of the Degradation Index after Blowing Out<sup>46</sup>

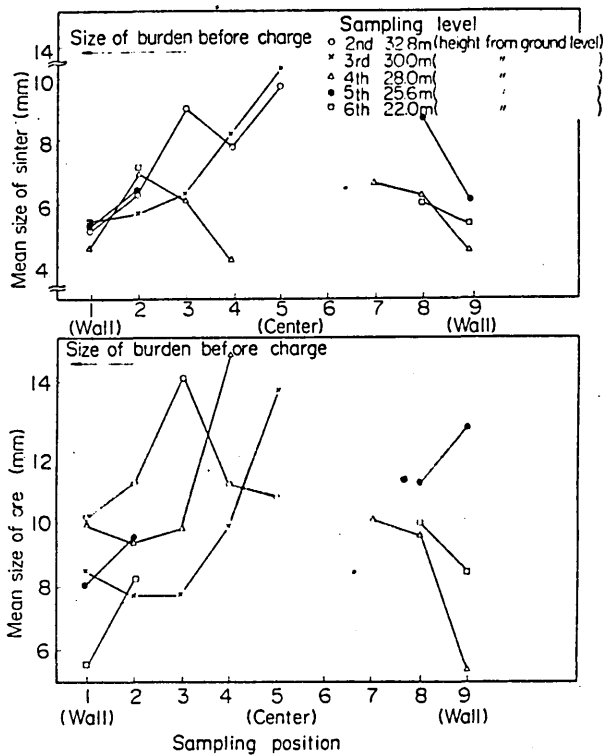


Figure 41 Change of Burden Size in the Lumpy Zone of Hirohata No.1 Blast Furnace<sup>47</sup>

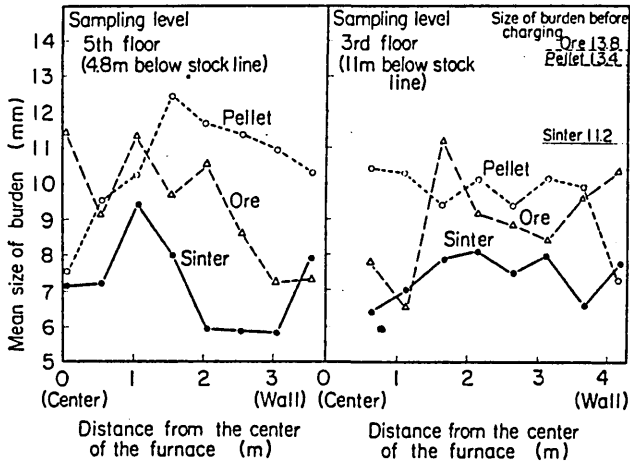


Figure 42 Change of Burden Size in the Lumpy Zone of Kukioka No.4 Blast Furnace<sup>47</sup>

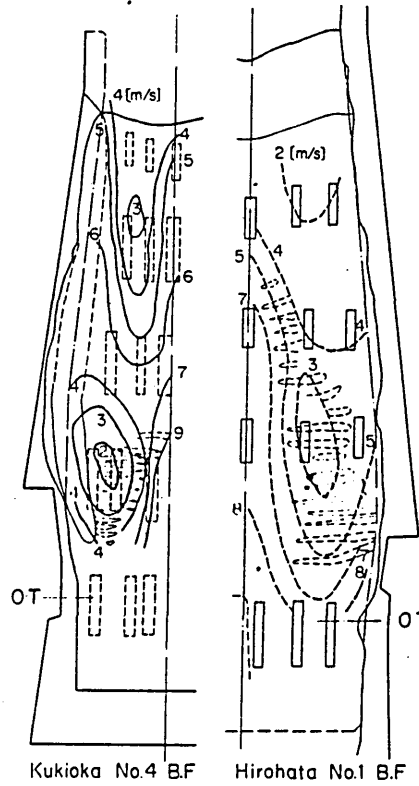


Figure 43 Calculated Gas Velocity Distribution in Kukioka No.4 and Hirohata No.1 Blast Furnace<sup>45</sup>

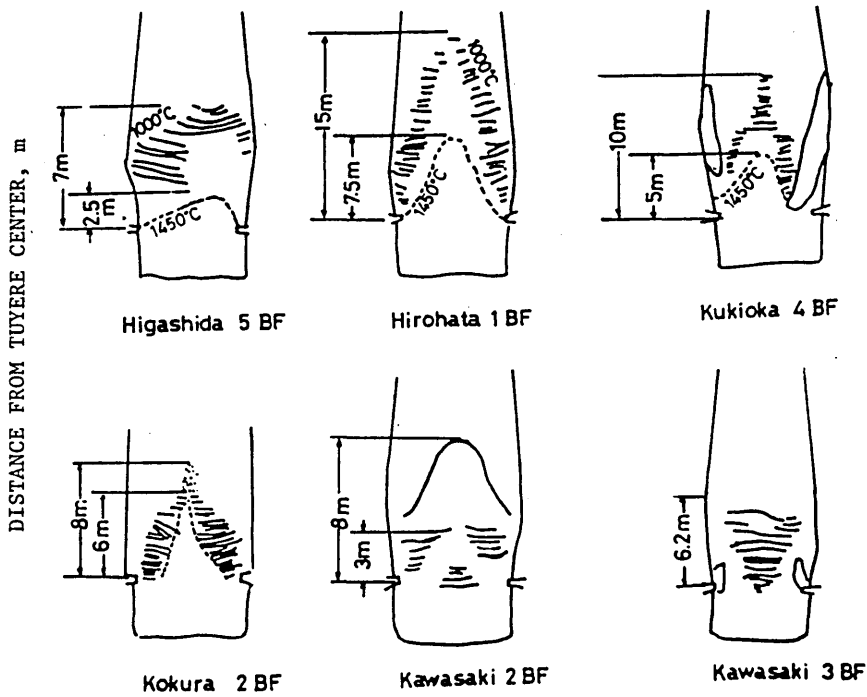


Figure 44 Schematic Profiles of Softening-Melting Zones Within Six Dissected Blast Furnaces<sup>44</sup>

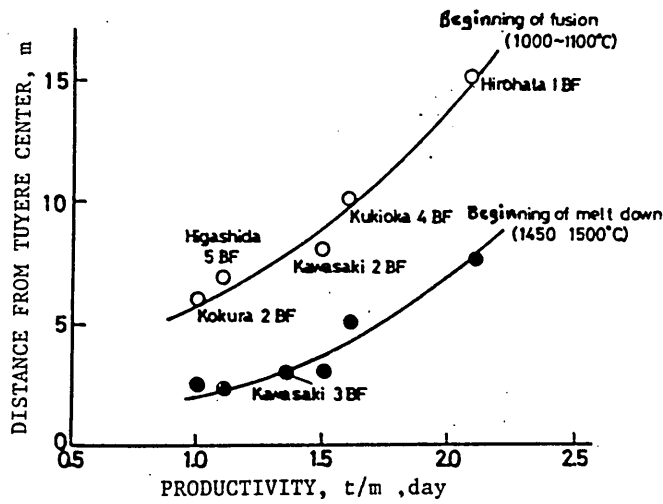


Figure 45 Relationship between Blast Furnace Productivity and the Height of the Melt-Down Zone<sup>44</sup>

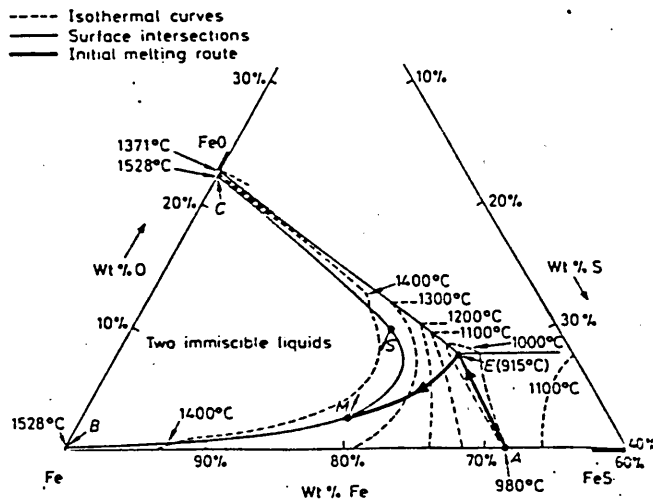


Figure 46 Liquidus Surface of a Section of the Fe-S-O Phase Diagram<sup>55,56</sup>

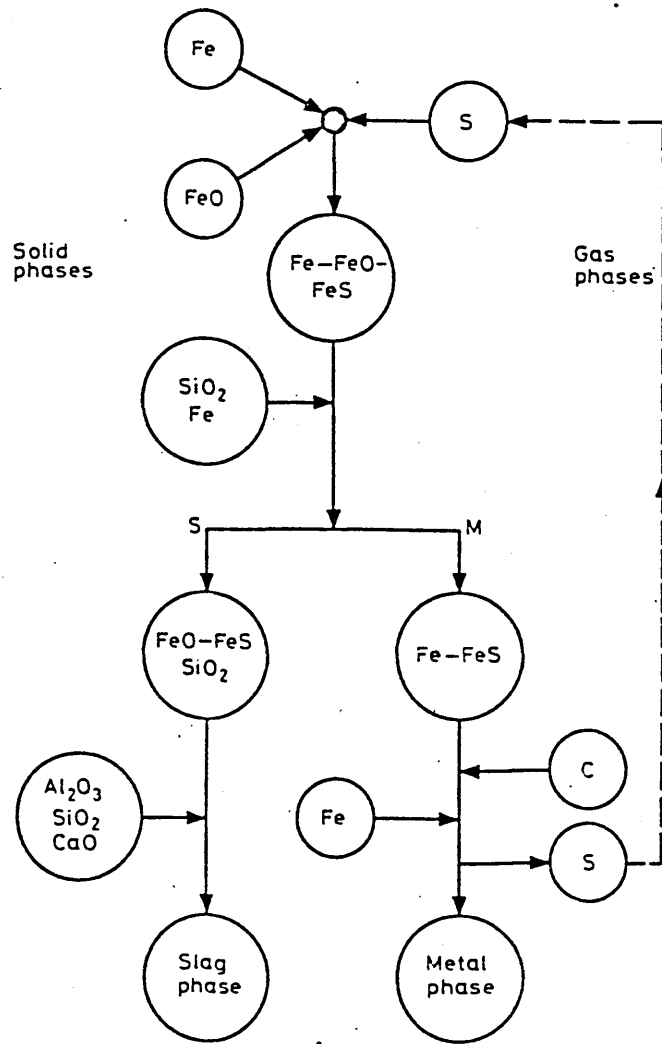


Figure 47 Schematic Diagram Showing the Proposed Melting Mechanism Involving Sulphur<sup>54</sup>

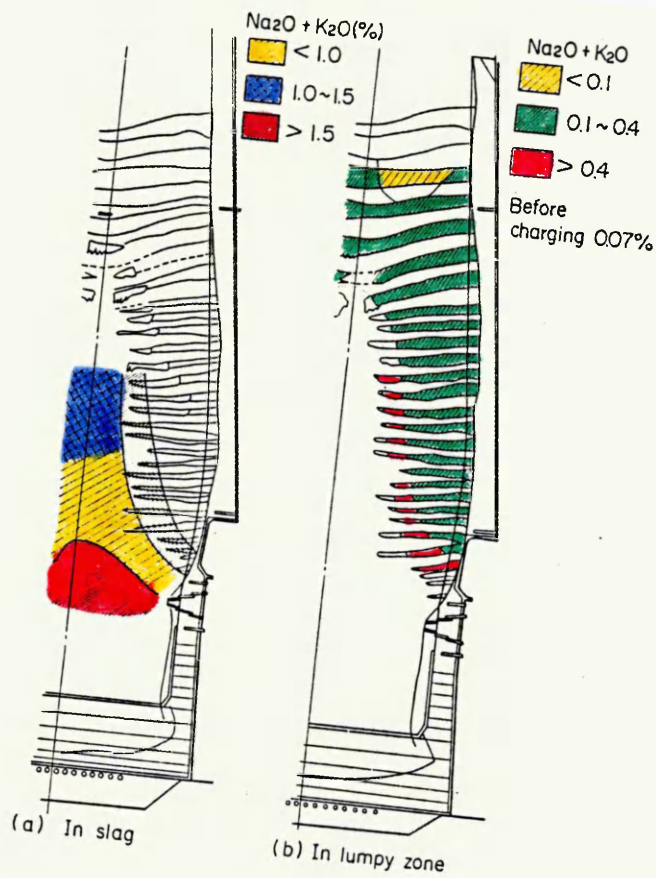


Figure 48 Distribution of Alkalis within Hirohata No.1 Blast Furnace<sup>47</sup>

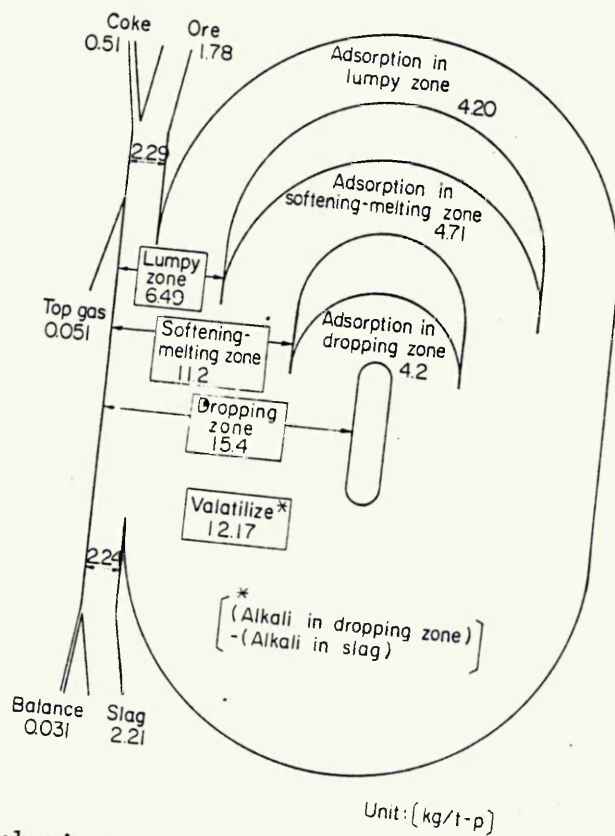


Figure 49 Circulation of Alkalis ( $\text{Na}_2\text{O}+\text{K}_2\text{O}$ ) within Hirohata No.1 Blast Furnace<sup>47</sup>

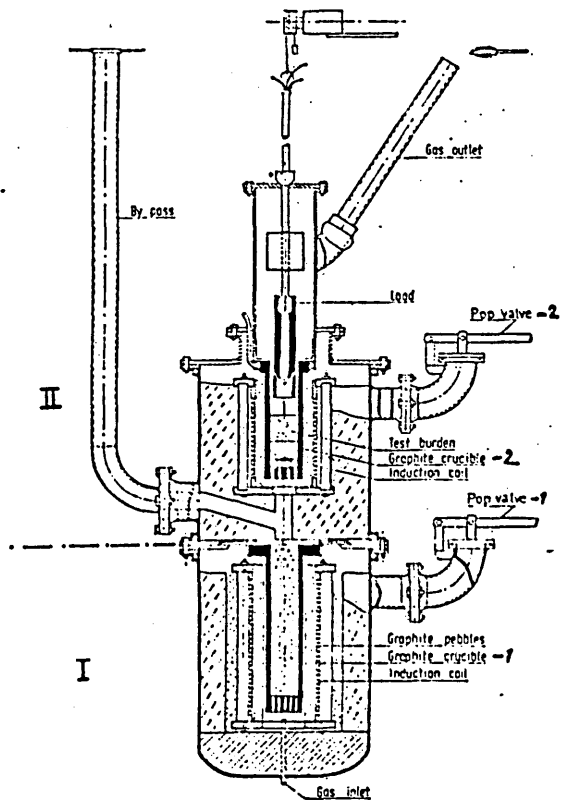


Figure 50 Apparatus used for Softening and Melting Studies  
at MEFOS<sup>13</sup>

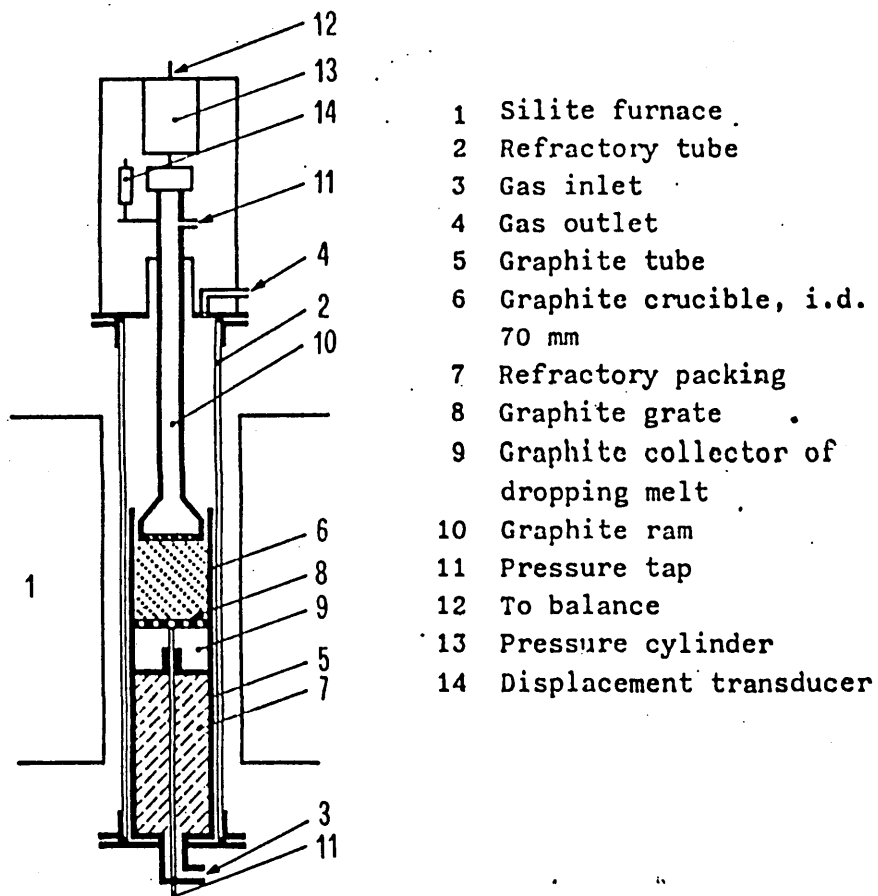


Figure 51 Apparatus used for Softening and Melting Studies at CSM<sup>74</sup>

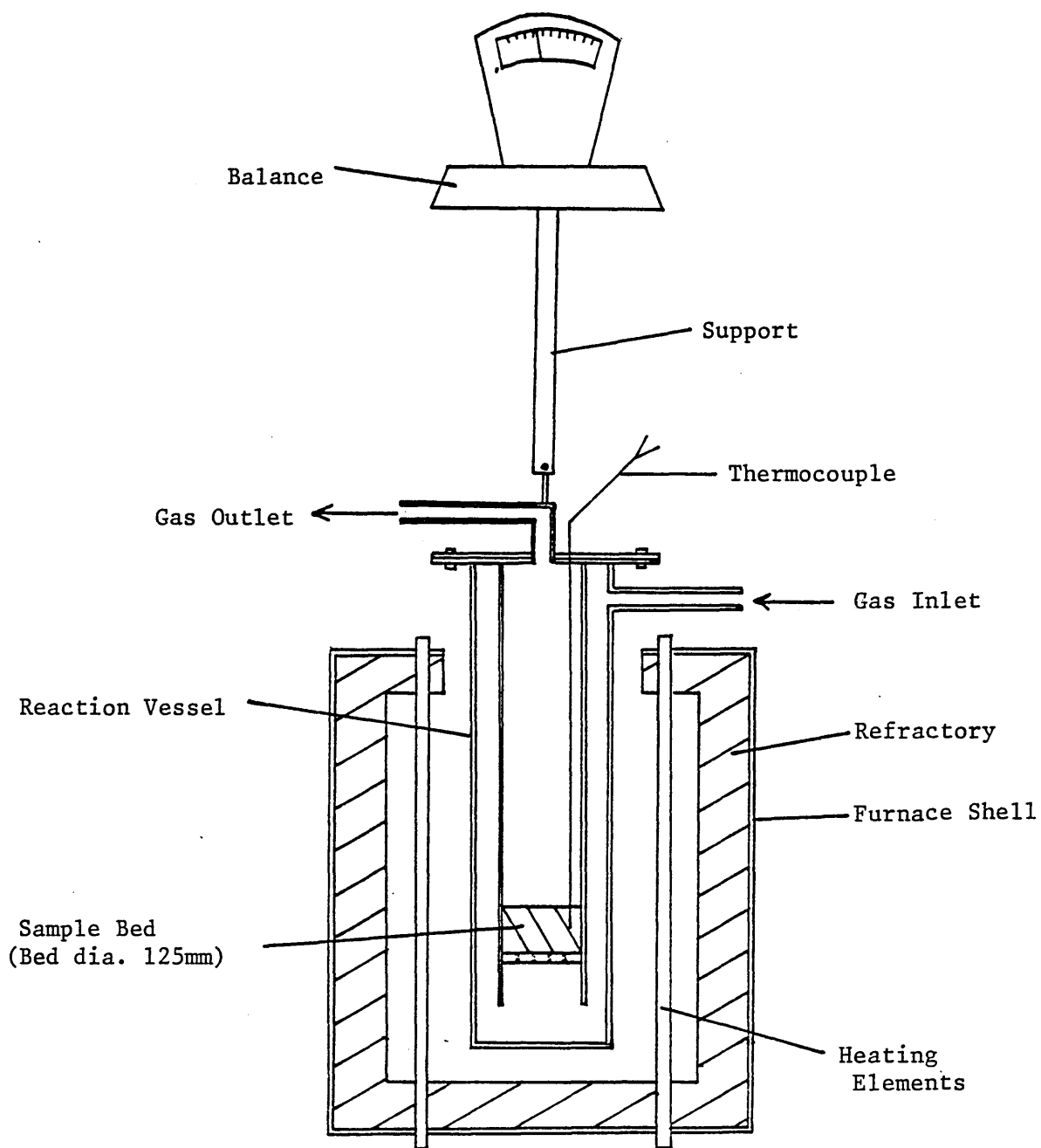


Figure 52    The Pre-Reduction Apparatus

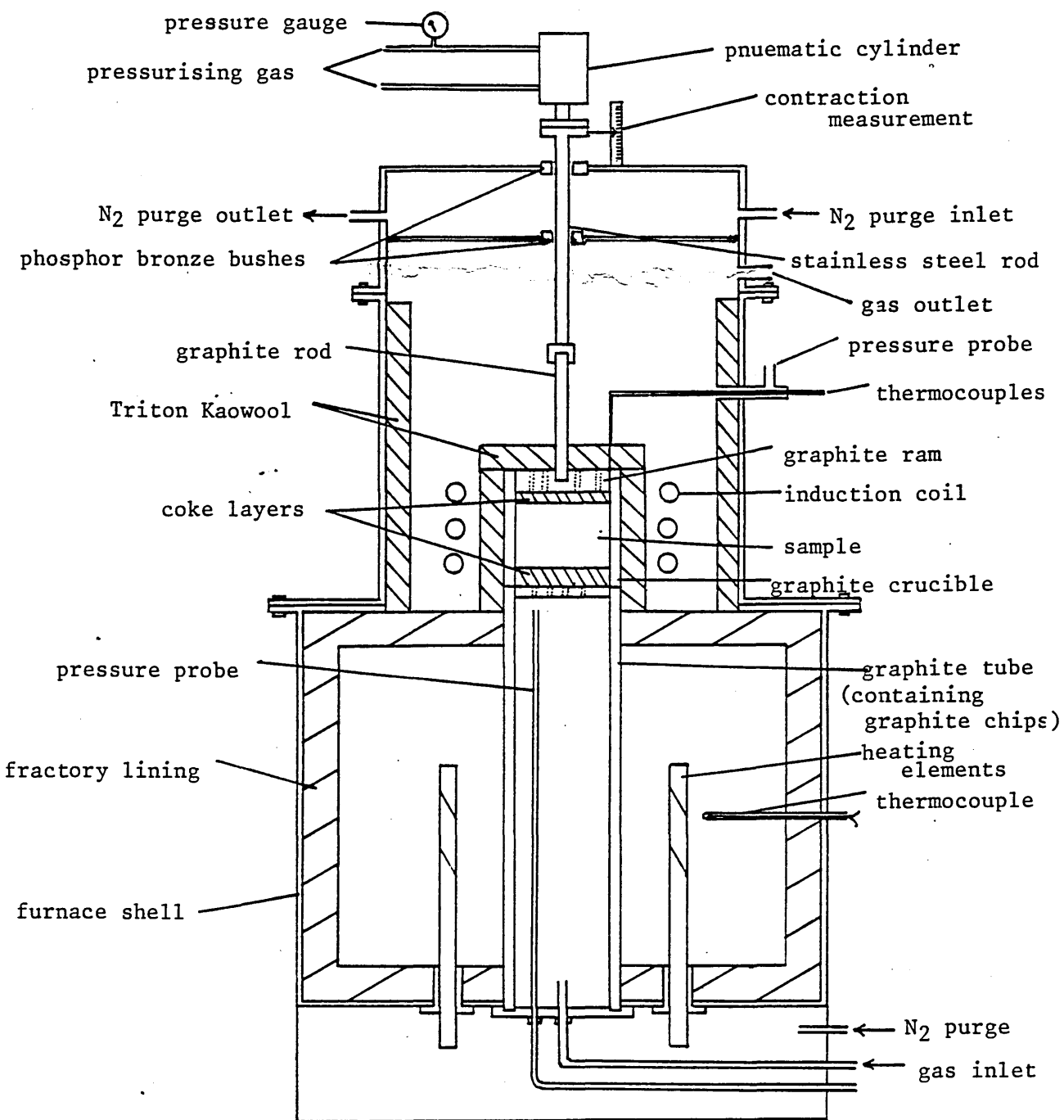


Figure 53    The High Temperature Apparatus

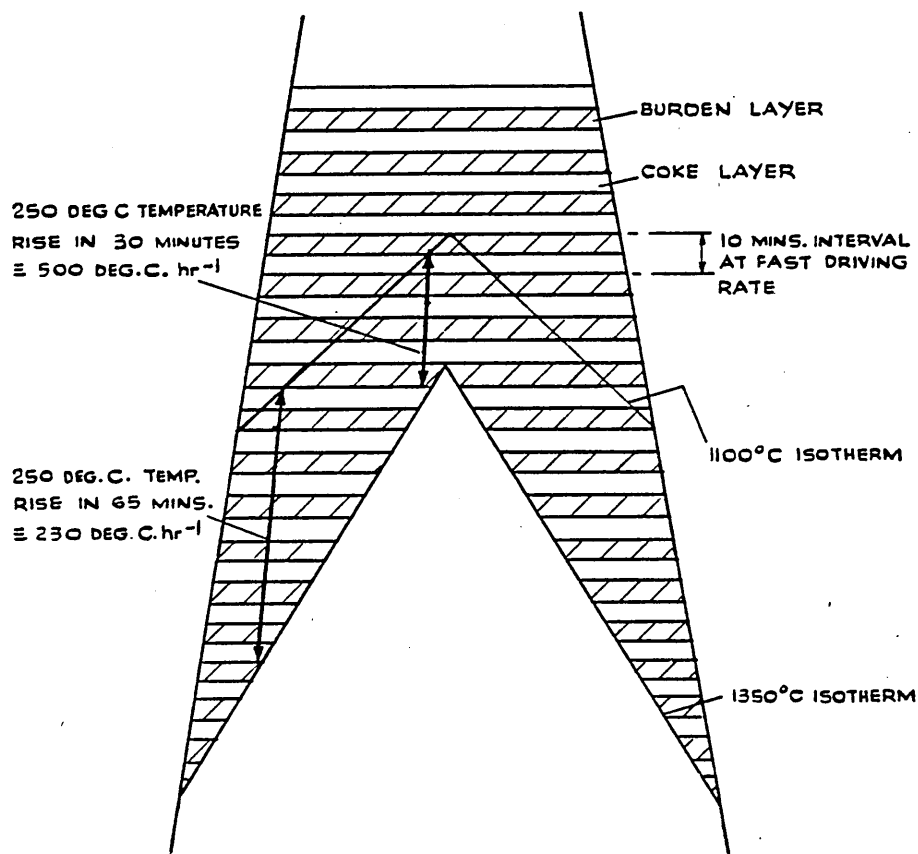


Figure 54 Example of the Method of Calculation of the Heating Rate

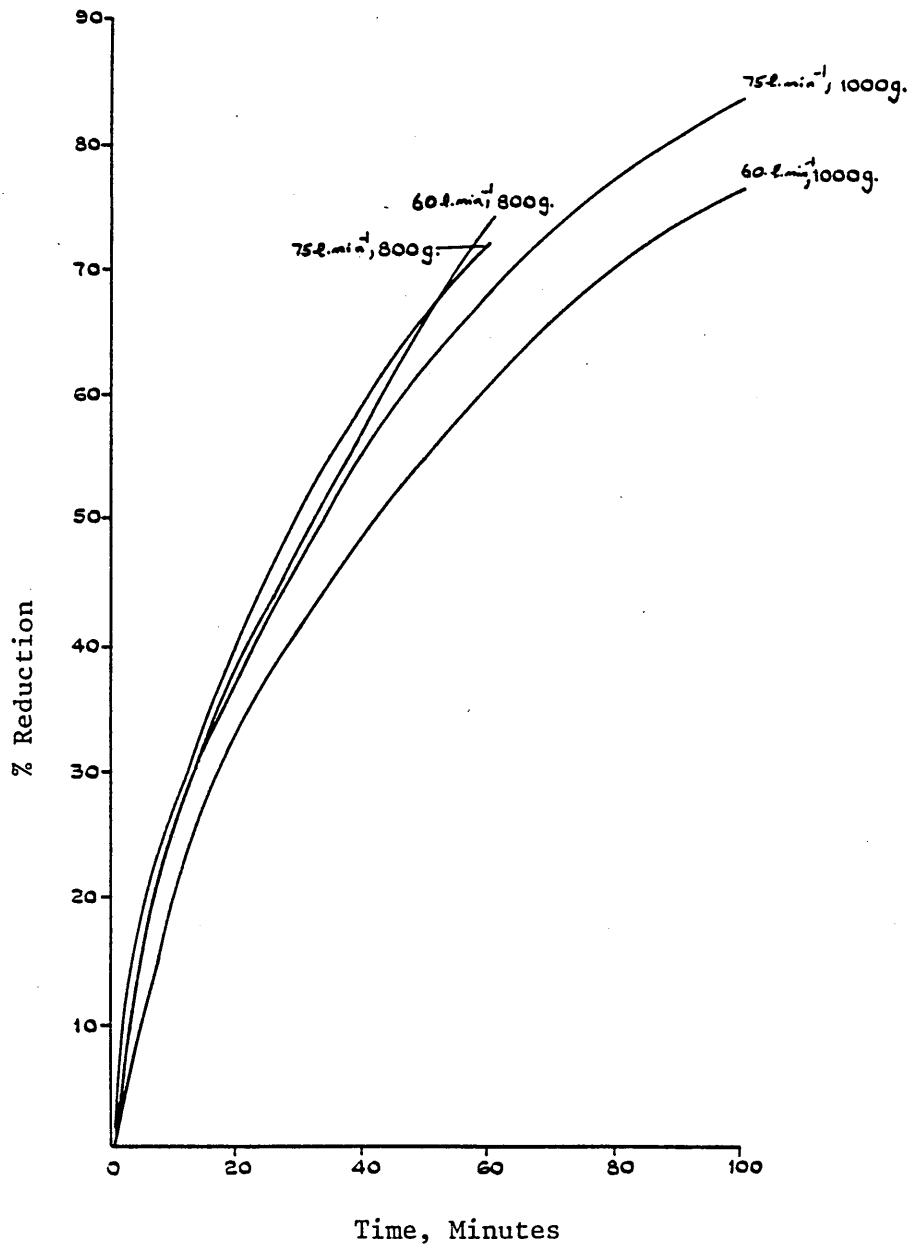


Figure 55 Reduction Curves for the Critical Gas Flow Tests

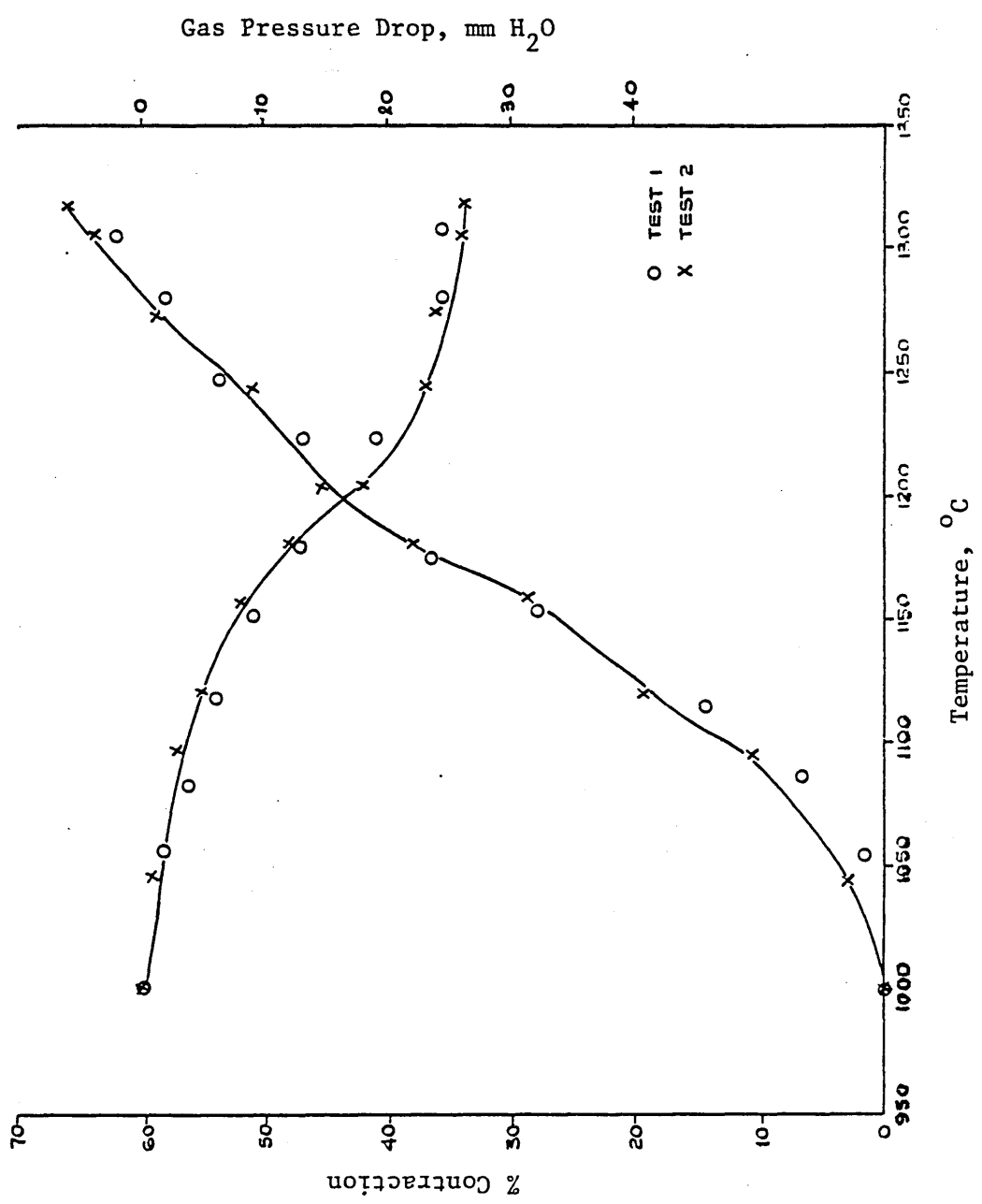


Figure 56 Reproducibility Tests: Gas Pressure Drop and Contraction Curves

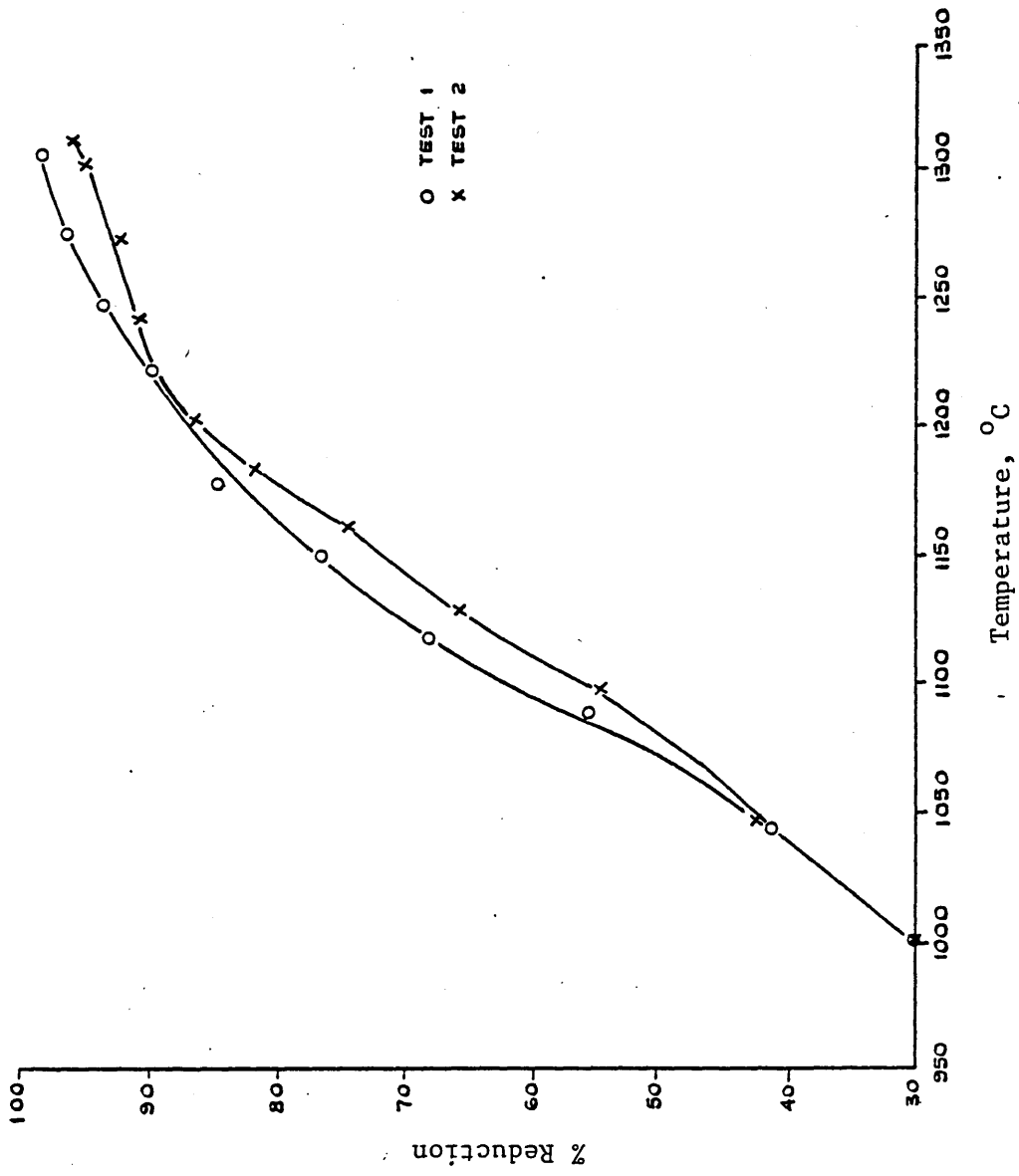


Figure 57 Reproducibility Tests: Reduction Curves

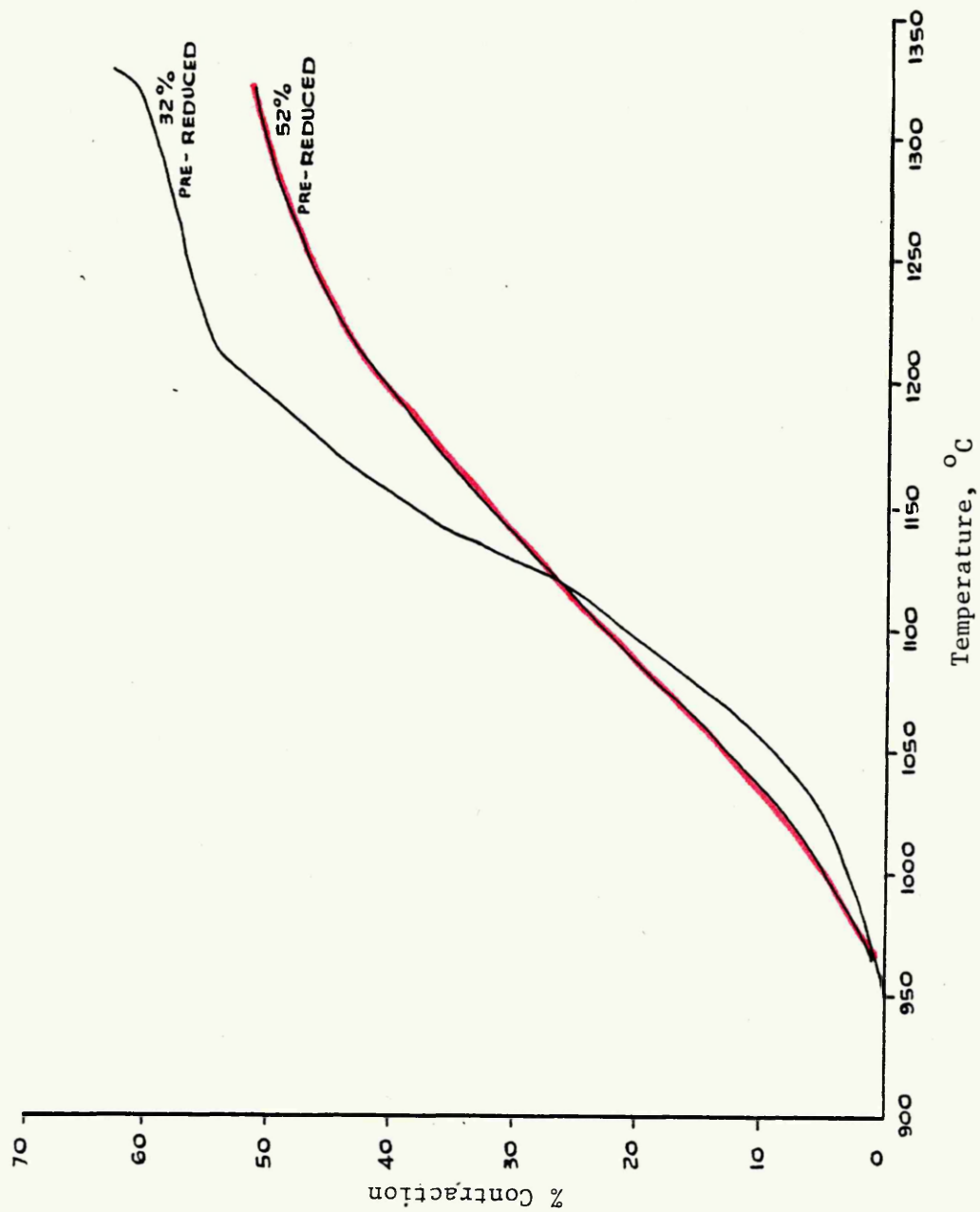


Figure 58 Contraction-Temperature Curves for Pellets at a Heating Rate of 200°C.hr<sup>-1</sup>

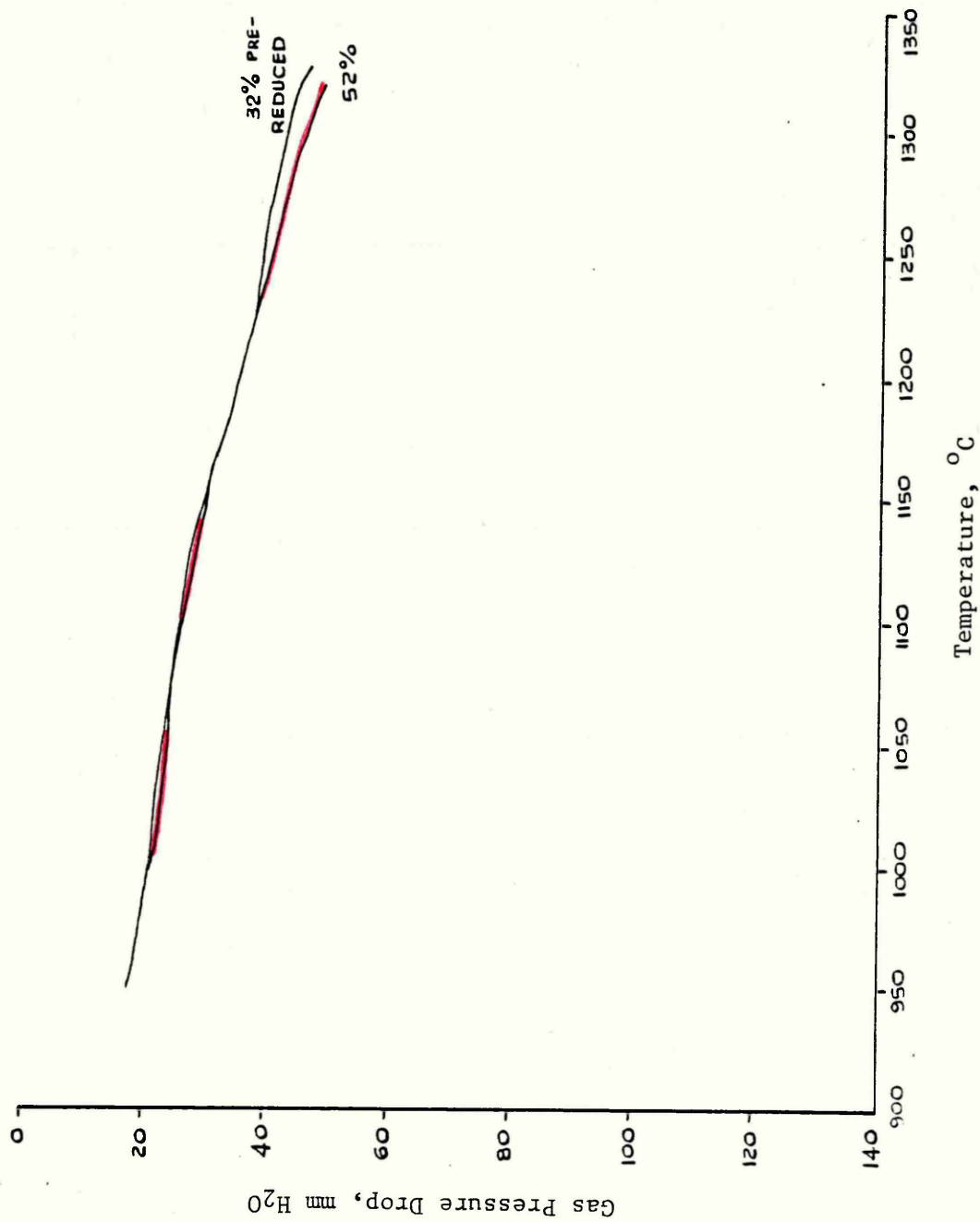


Figure 59

Gas Pressure Drop Temperature Curves for Pellets  
at a Heating Rate of 200° C.hr<sup>-1</sup>

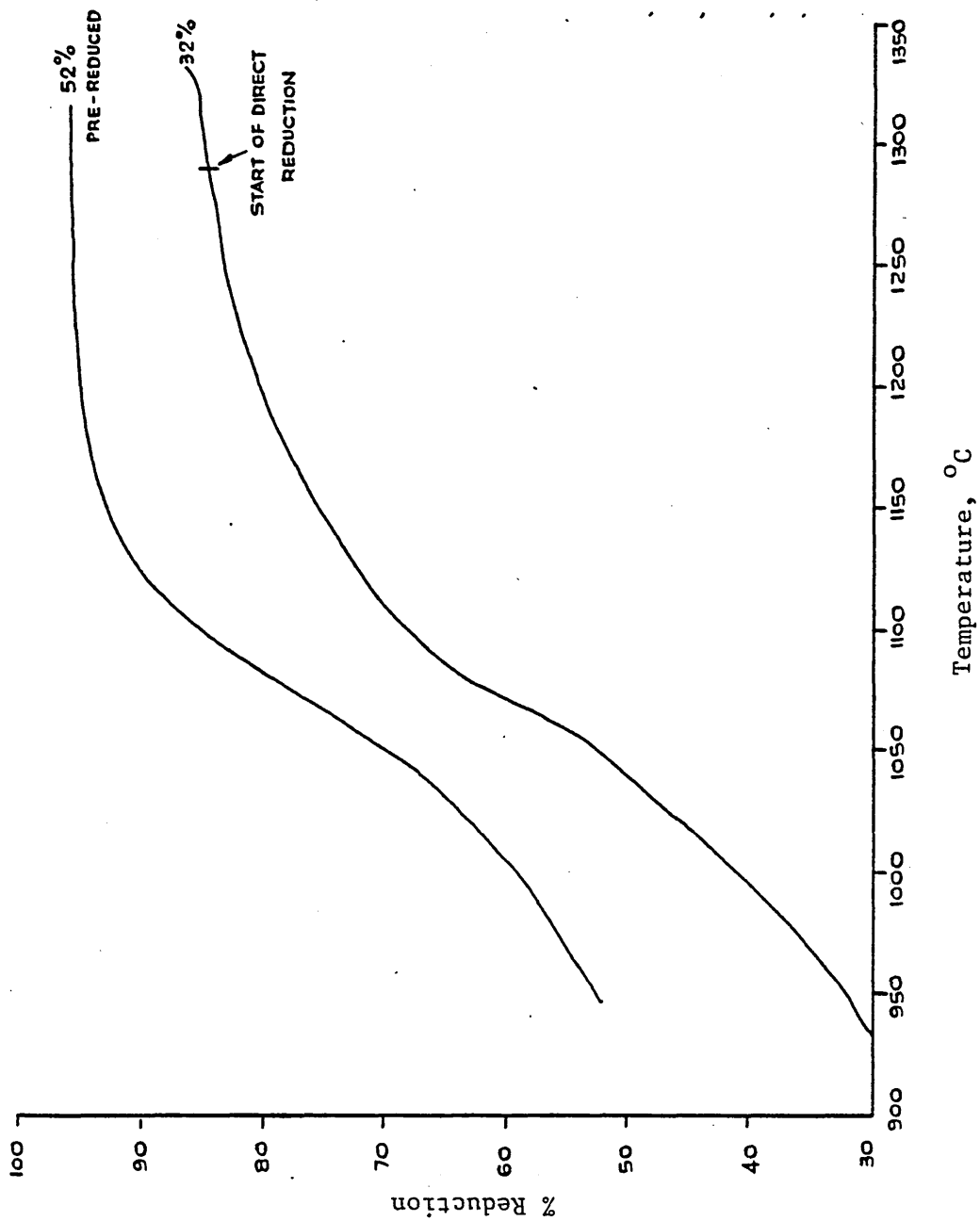


Figure 60 Reduction-Temperature Curves for Pellets at a Heating Rate of 200°C.hr<sup>-1</sup>

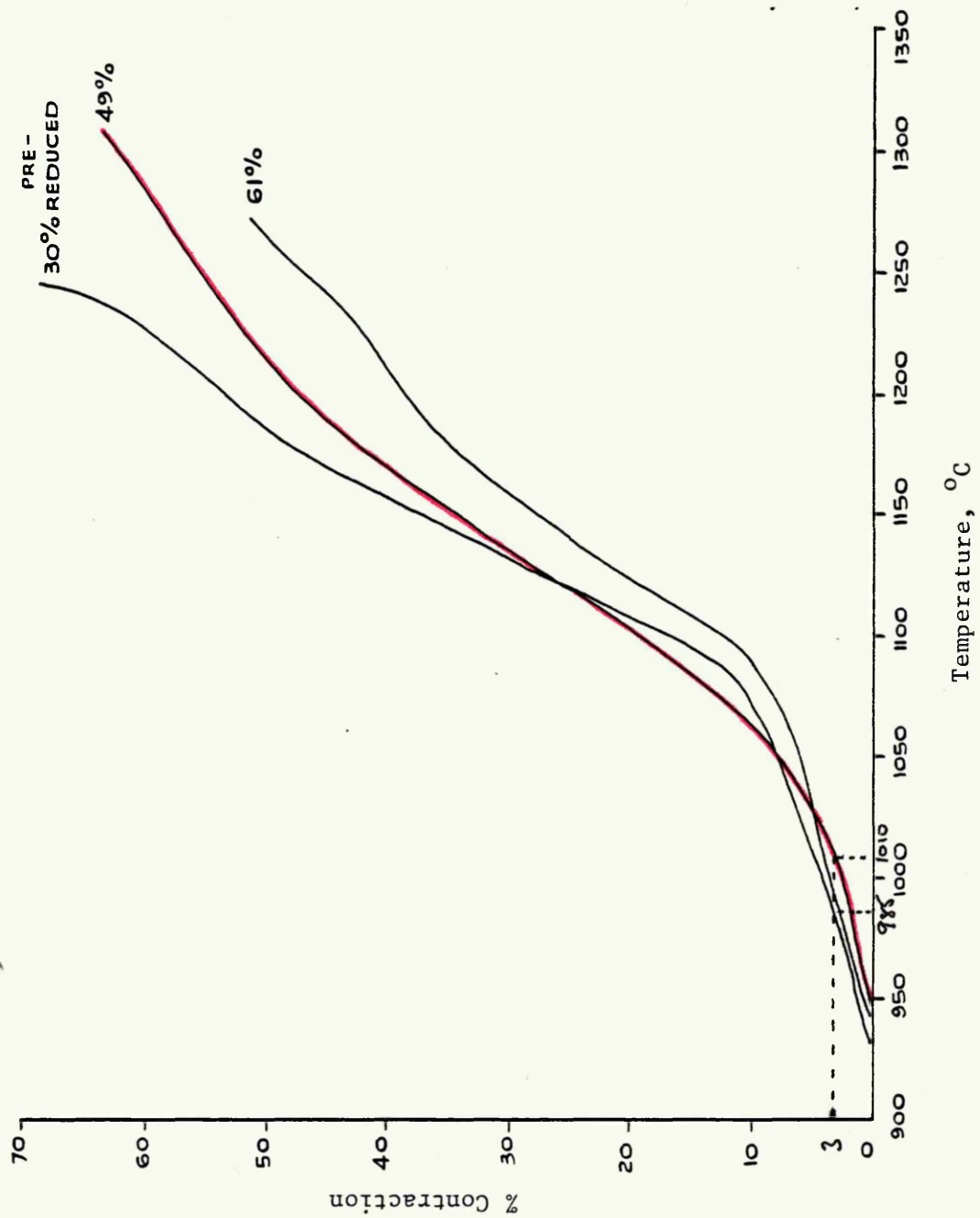


Figure 6k Contraction-Temperature Curves for Pellets at a Heating Rate of 400 °C.hr<sup>-1</sup>

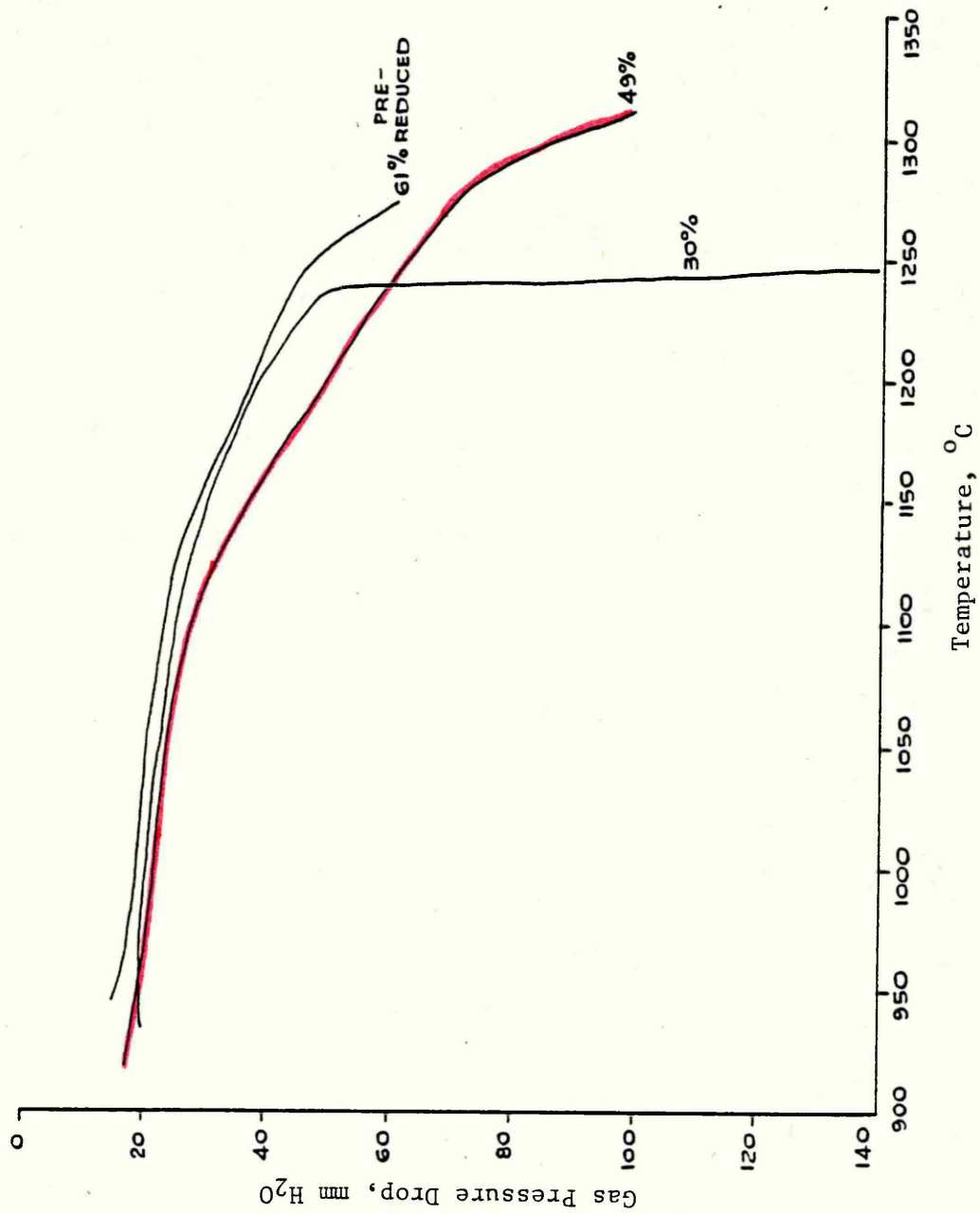


Figure 62 Gas Pressure Drop-Temperature Curves for Pellets  
at a Heating Rate of 400 °C.hr<sup>-1</sup>

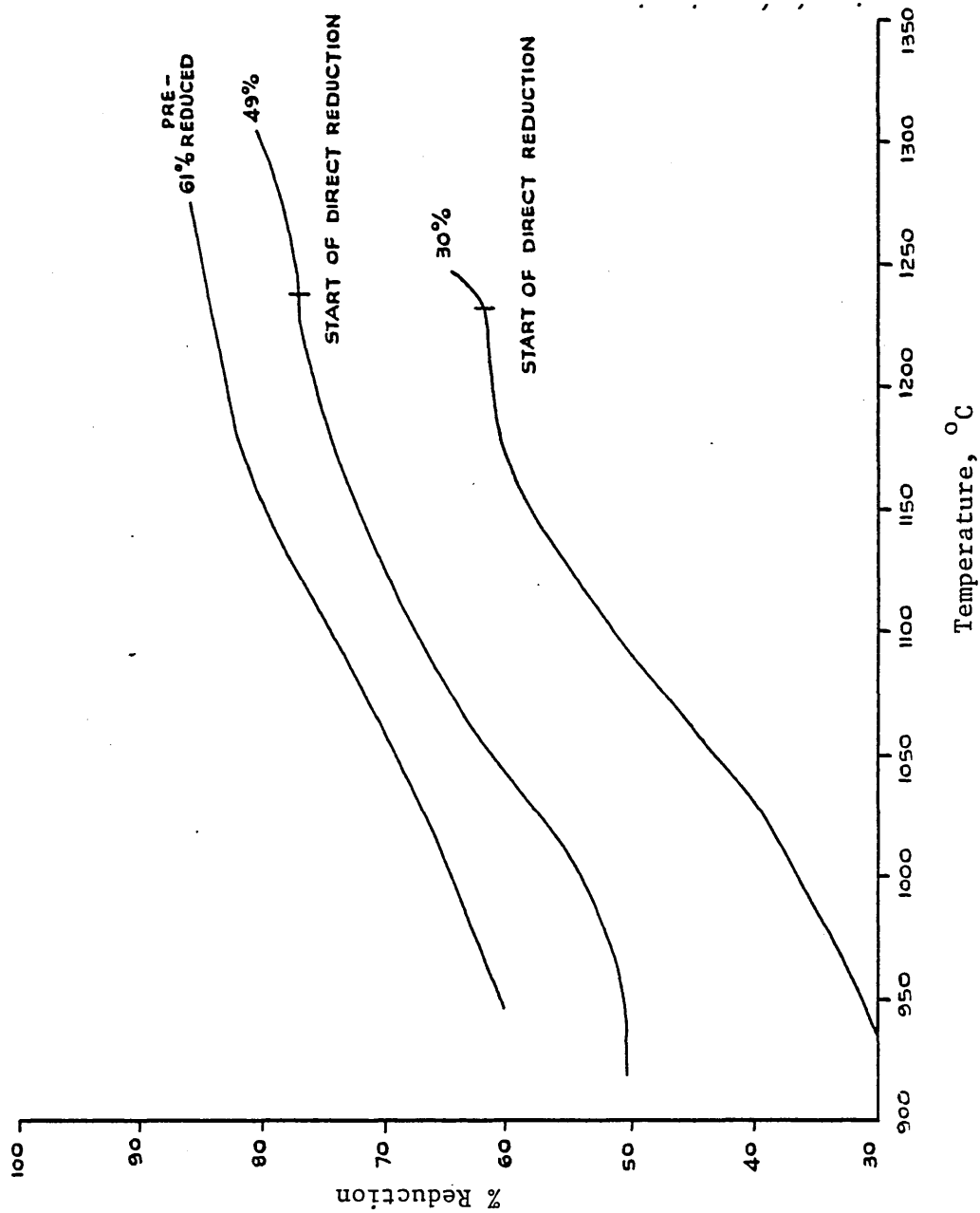


Figure 63 Reduction-Temperature Curves for Pellets at a Heating Rate of 400°C.hr<sup>-1</sup>

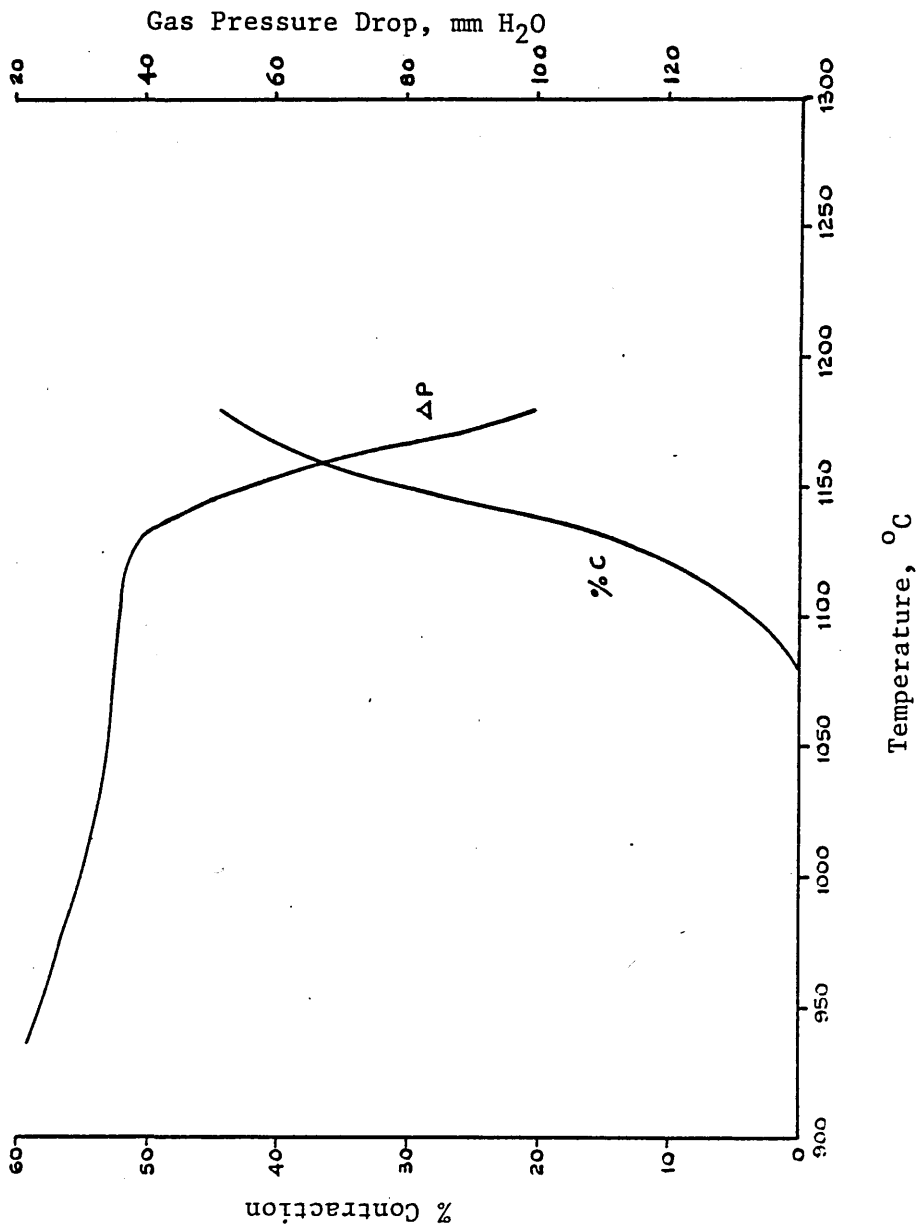


Figure 64 Contraction and Gas Pressure Drop Curves for Pellets with 0% Pre-Reduction at a Heating Rate of 400°C.hr<sup>-1</sup>

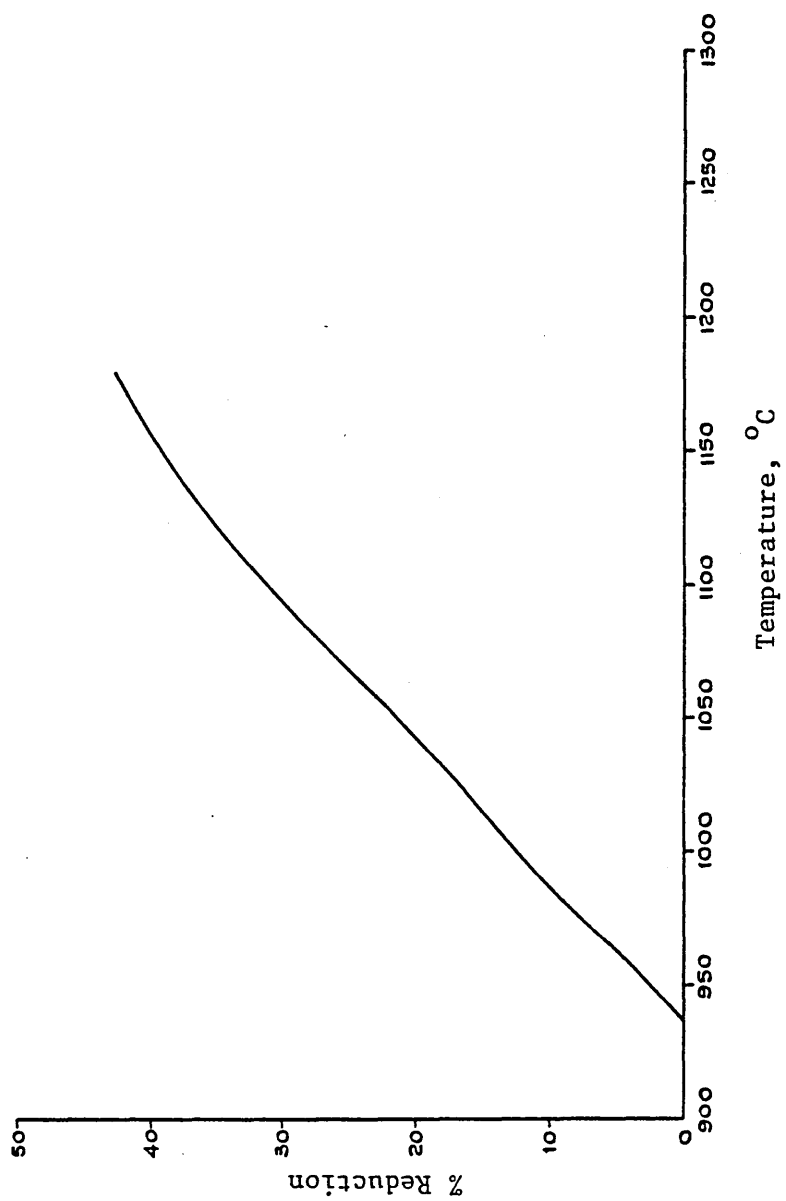


Figure 65 Reduction-Temperature Curve for Pellets with 0% Pre-Reduction at a Heating Rate of 400°C.hr<sup>-1</sup>

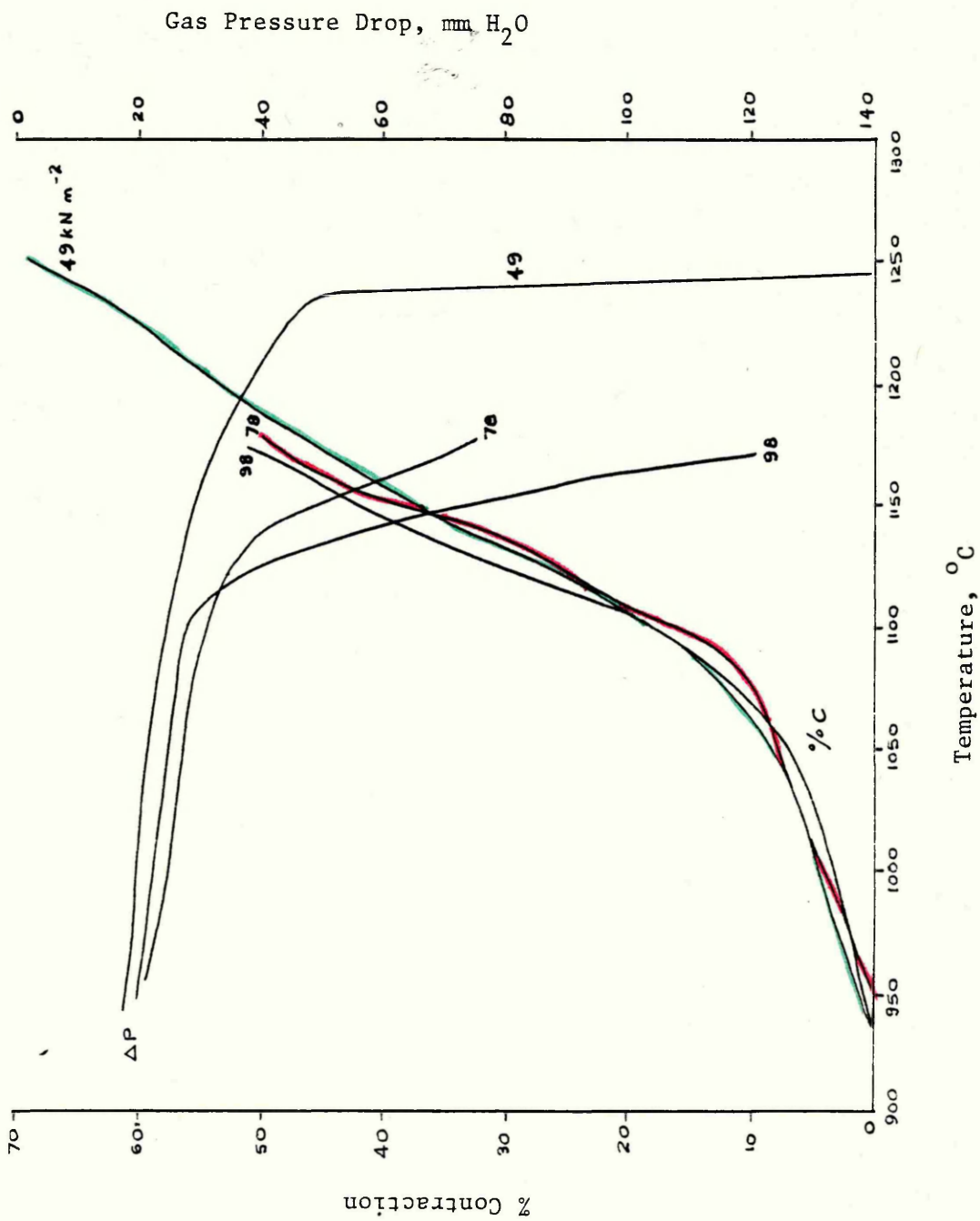


Figure 66 Effect of Variation of the Applied Load on the Contraction and Gas Pressure Drop of Pellets

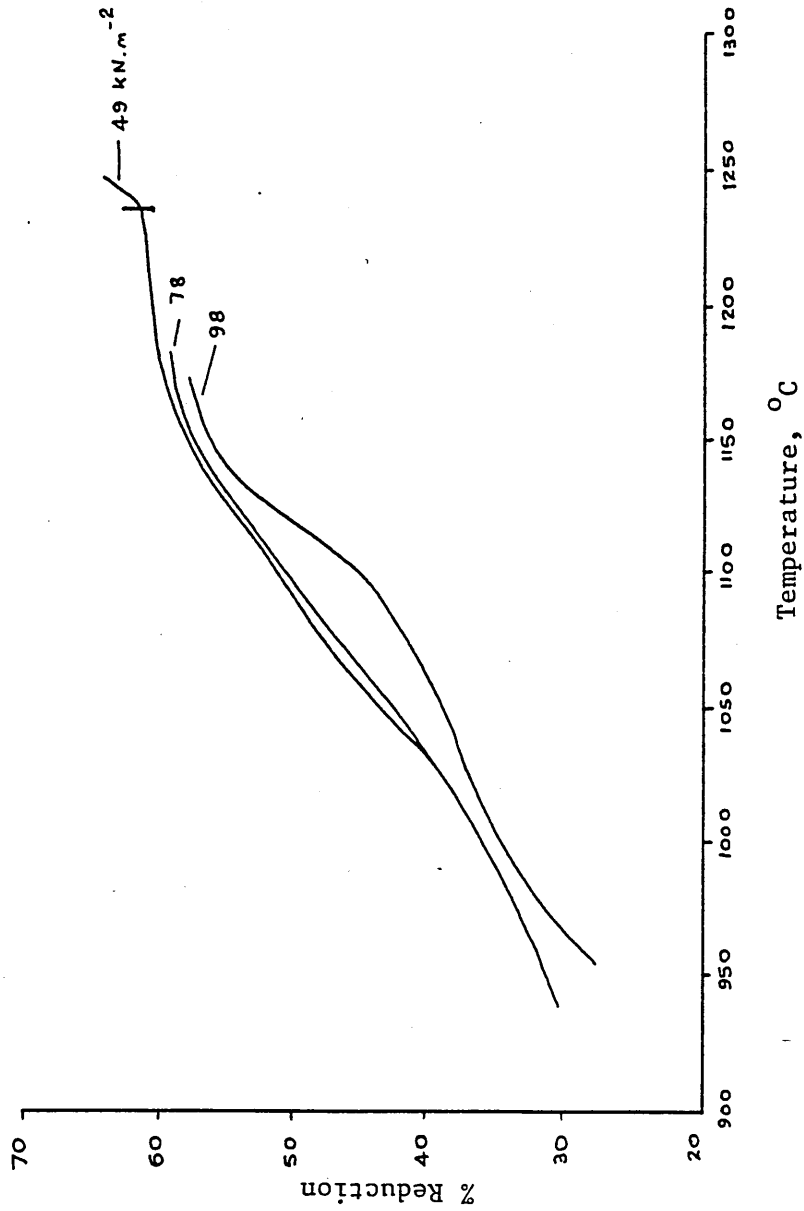


Figure 67 Effect of Variation of the Applied Load on the Reduction of Pellets

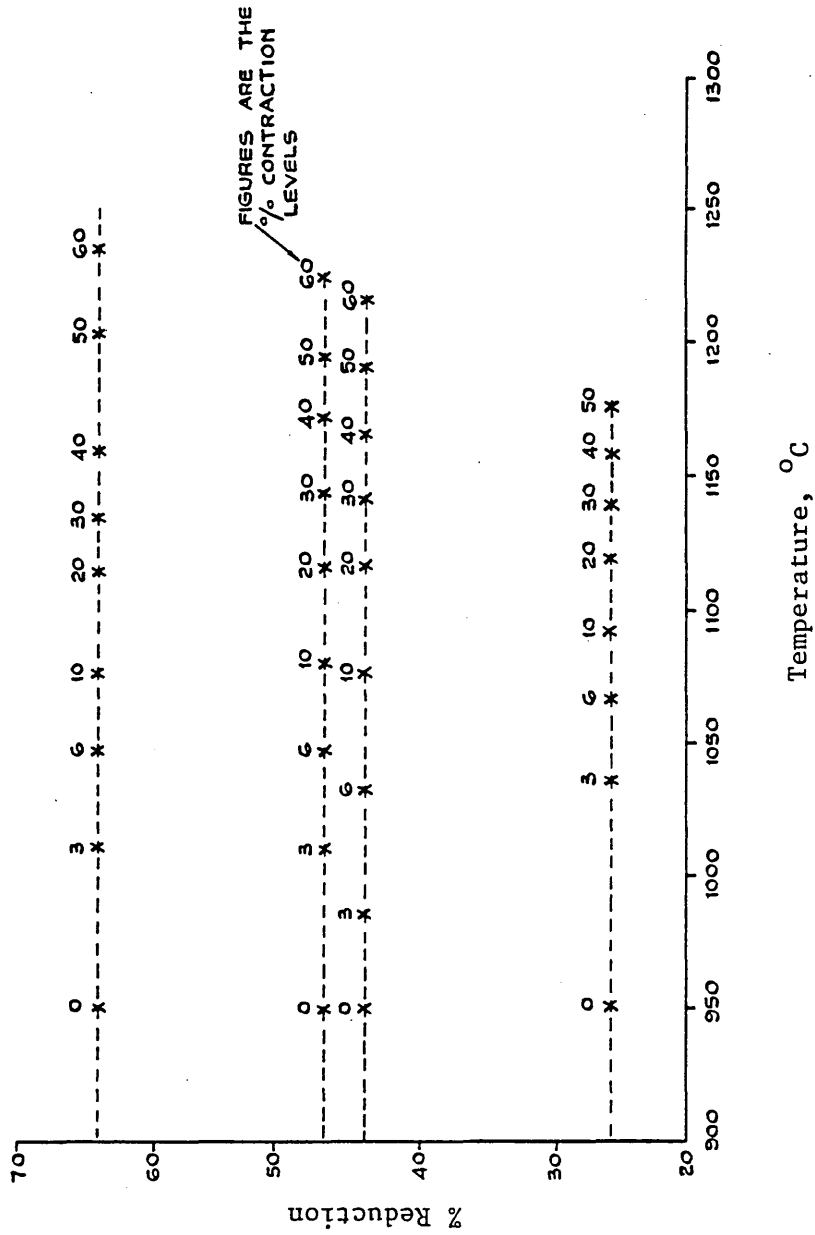


Figure 68 Contraction Values of Semi-Reduced Pellets Tested in Nitrogen Only

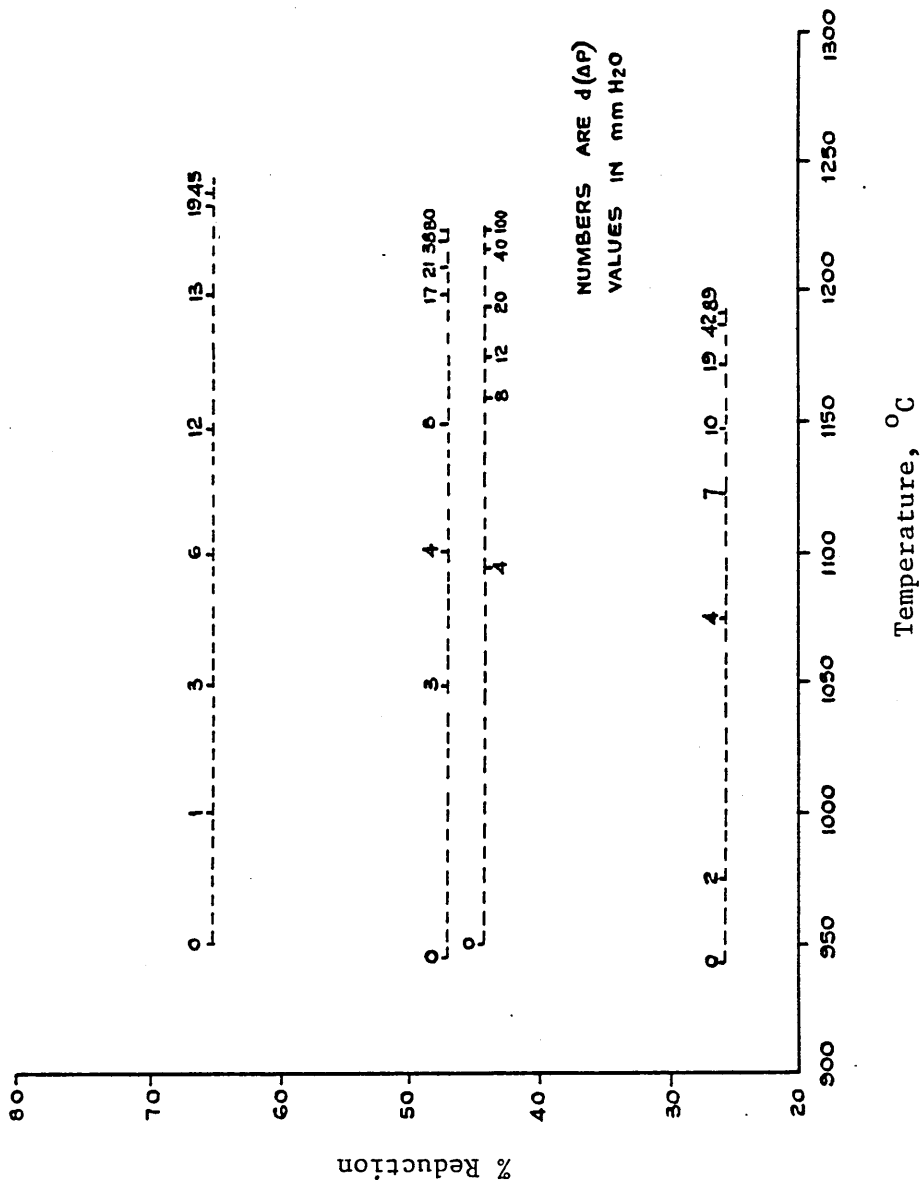


Figure 69 Gas Pressure Drop Values of Semi-Reduced Pellets  
Tested in Nitrogen Only

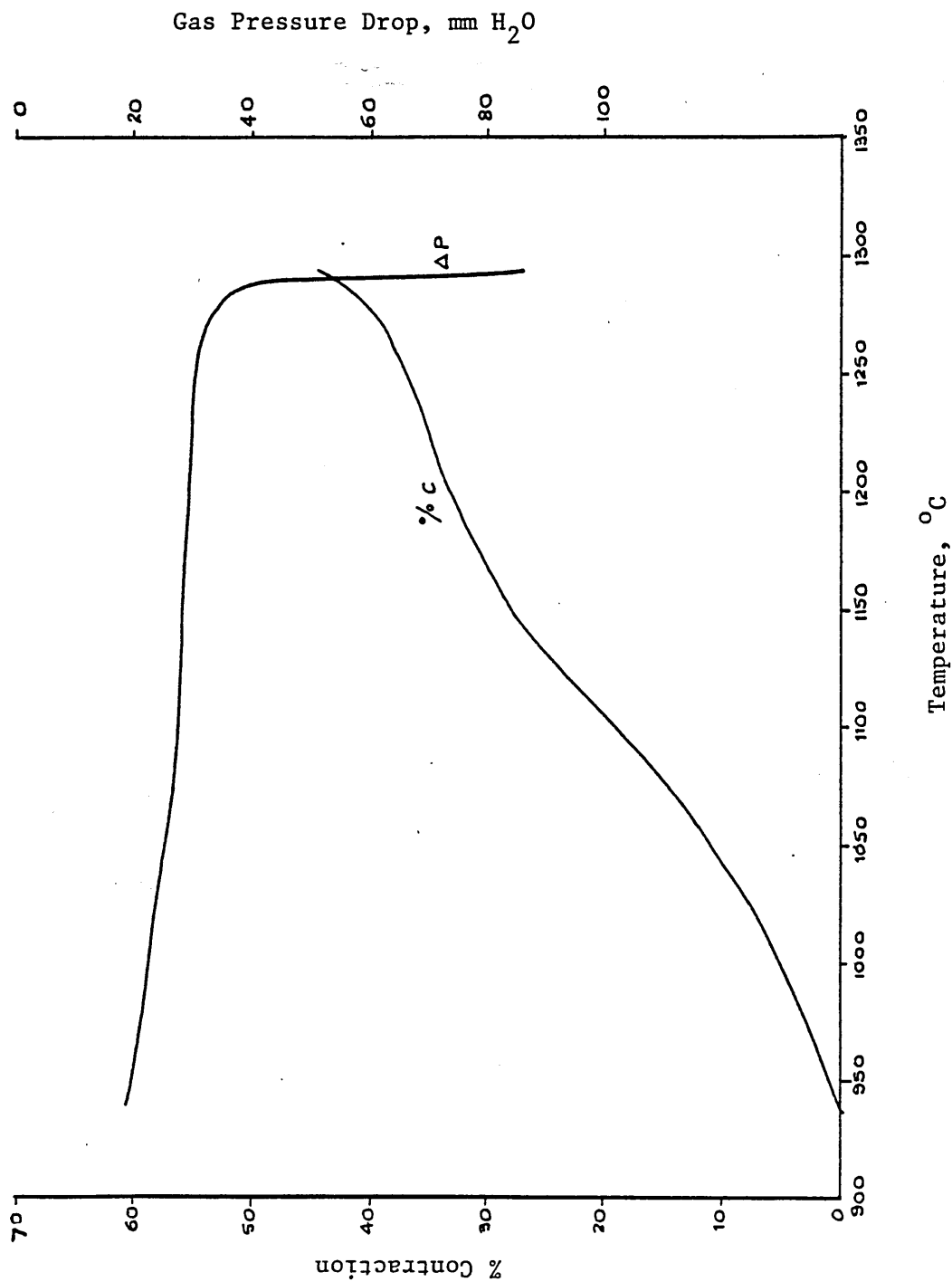


Figure 70 Contraction and Gas Pressure Drop Curves for Pellets Pre-Reduced at 600°C

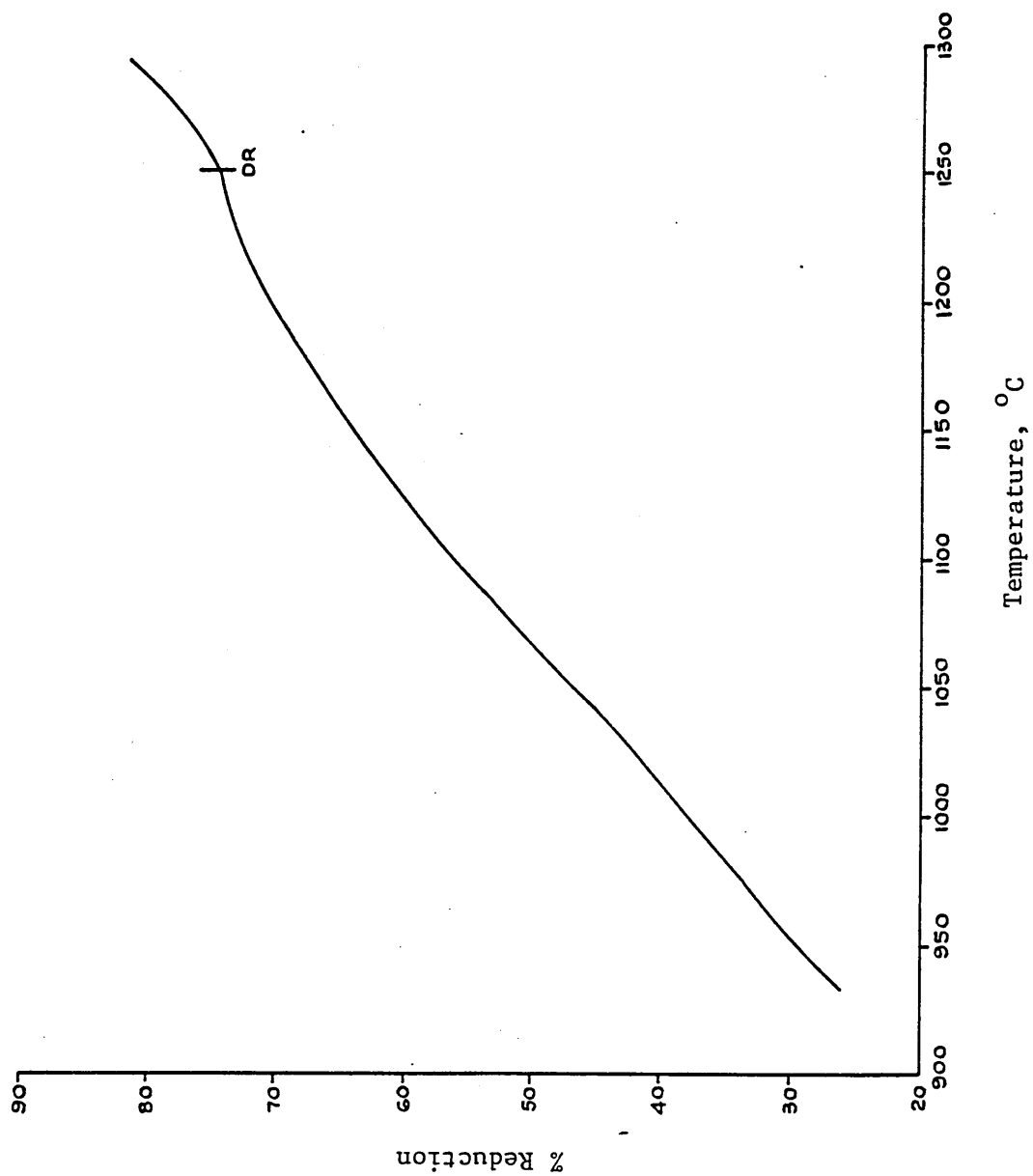


Figure 71 Reduction Curve for Pellets Pre-Reduced at 600°C

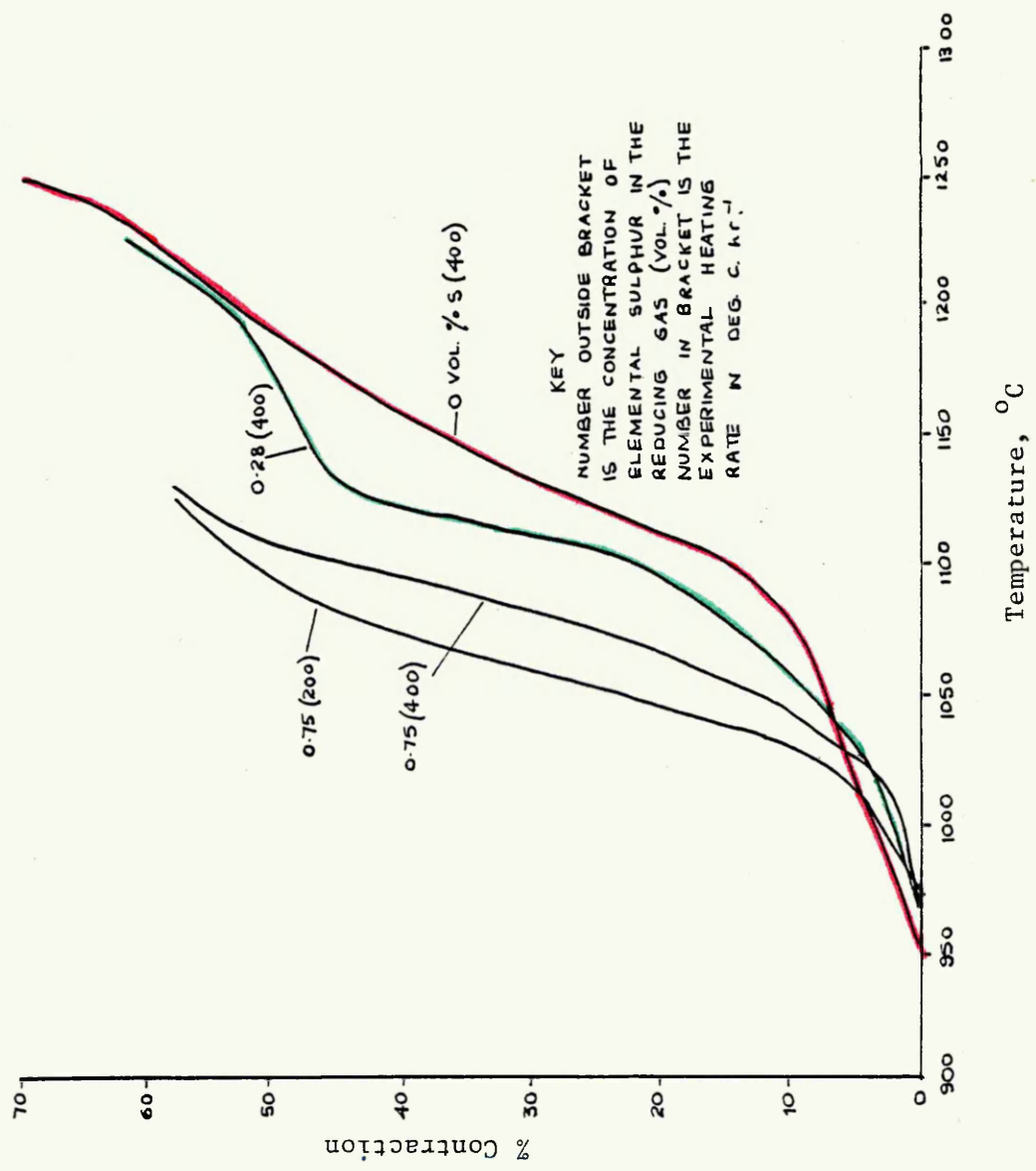


Figure 72 Effect of Sulphur in the Reducing Gas on the Contraction of Pellets

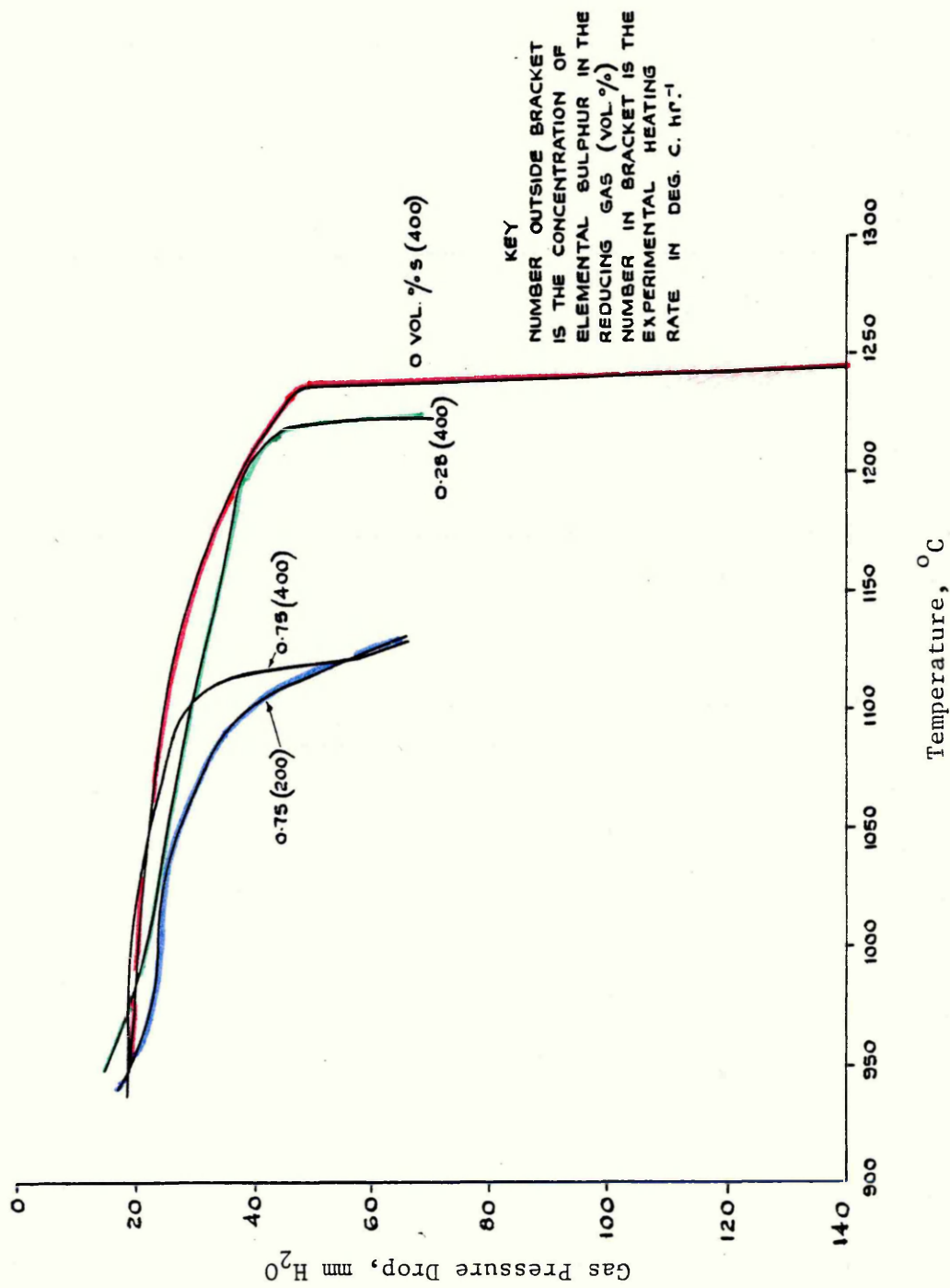


Figure 73 Effect of Sulphur in the Reducing Gas on the Gas Pressure Drop of Pellets

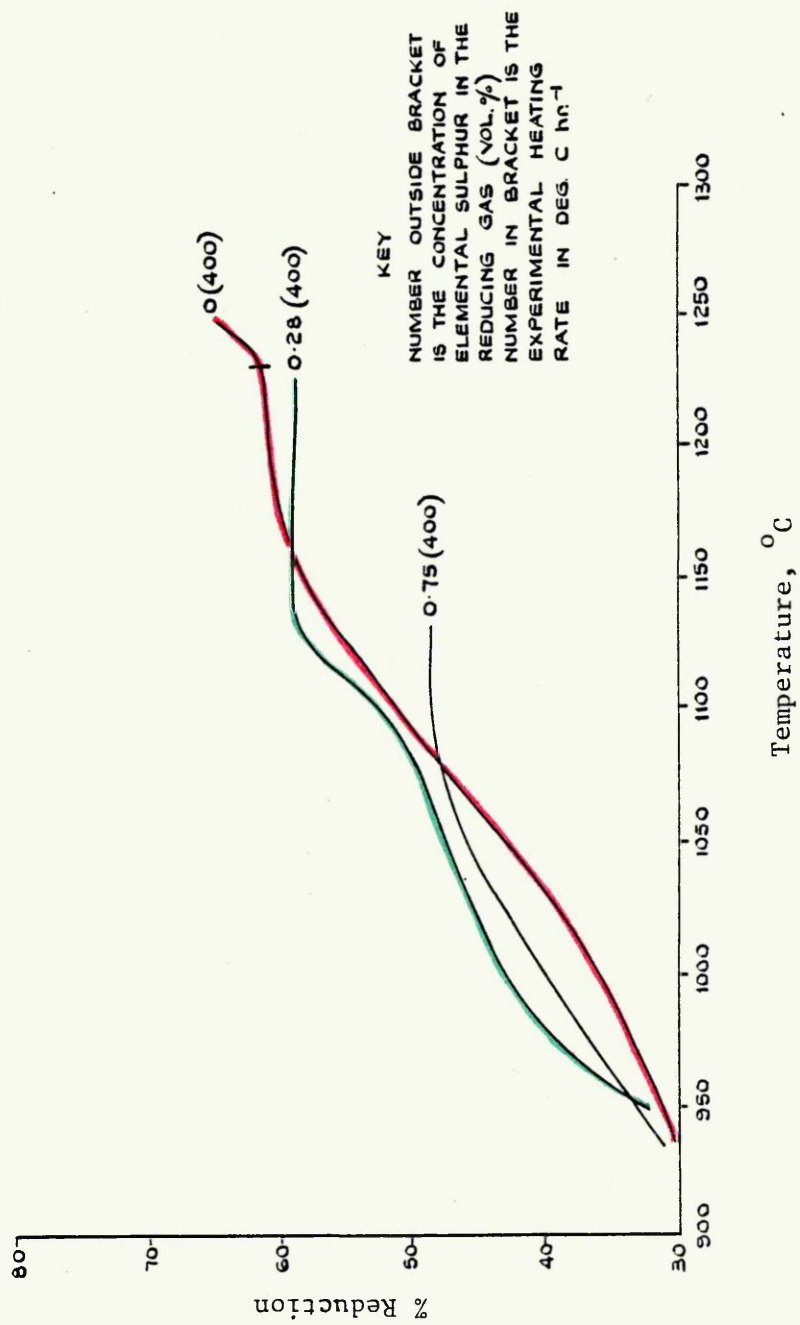


Figure 74 Effect of Sulphur in the Reducing Gas on the Reduction of Pellets

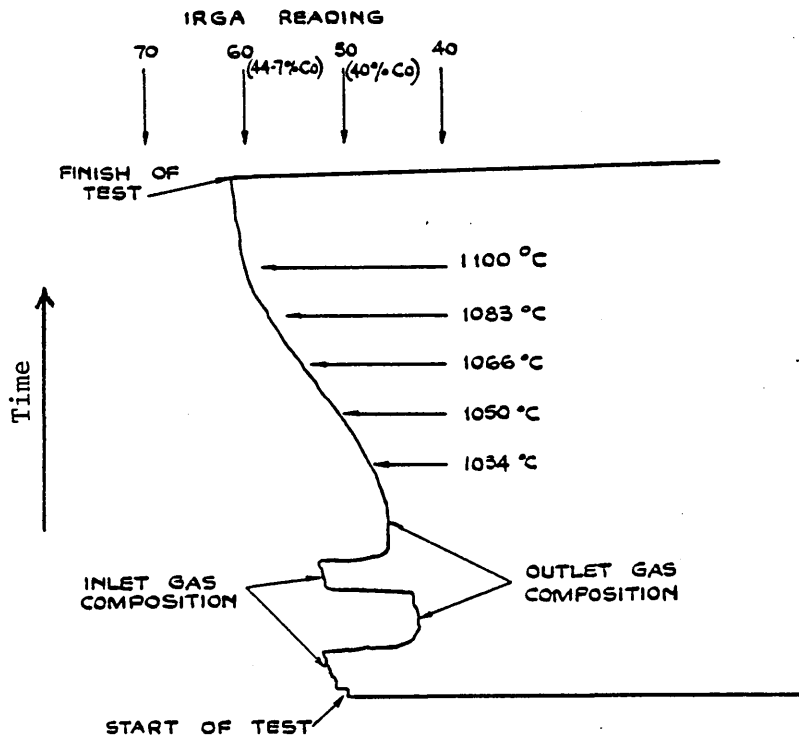


Figure 75 Recorder Trace of the Carbon Monoxide Concentration in the Outlet Gas which emanated from the Test at a Heating Rate of  $200^{\circ}\text{C}\cdot\text{hr}^{-1}$  with a Sulphur Concentration of 0.75 vol.%

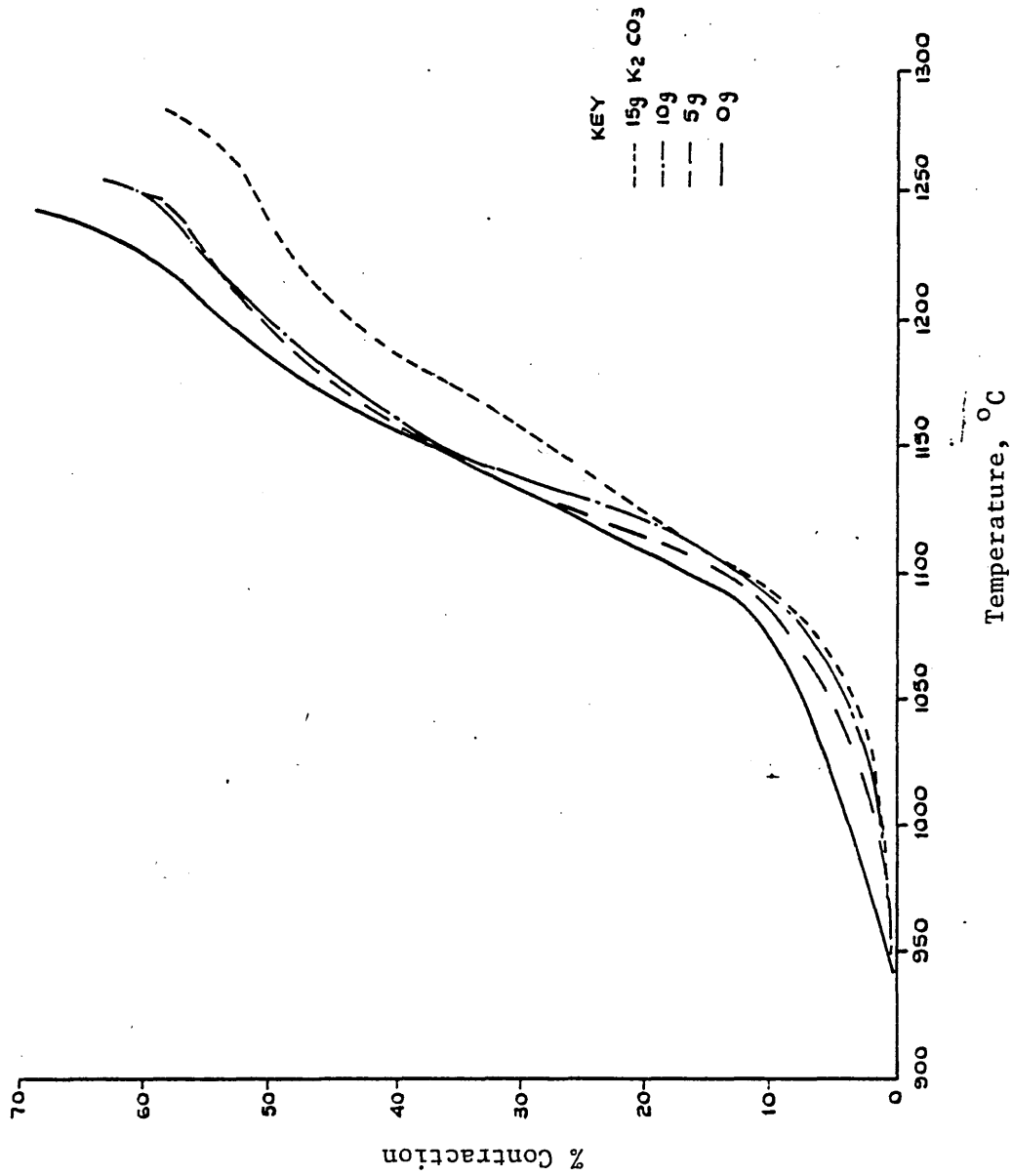


Figure 76 Effect of Alkali Vapour in the Reducing Gas on the Contraction of Pellets

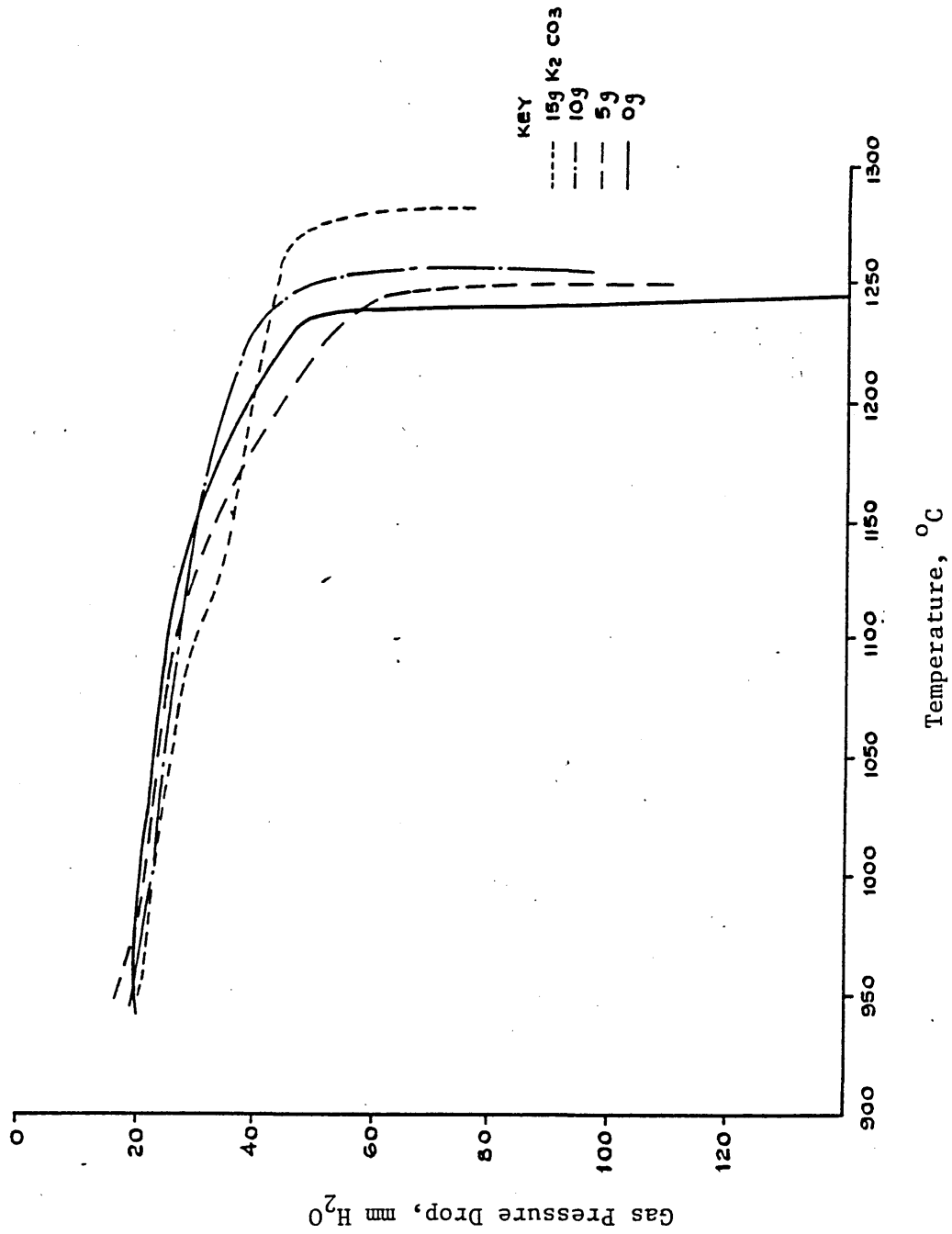


Figure 77 Effect of Alkali Vapour in the Reducing Gas on the Gas Pressure Drop of Pellets

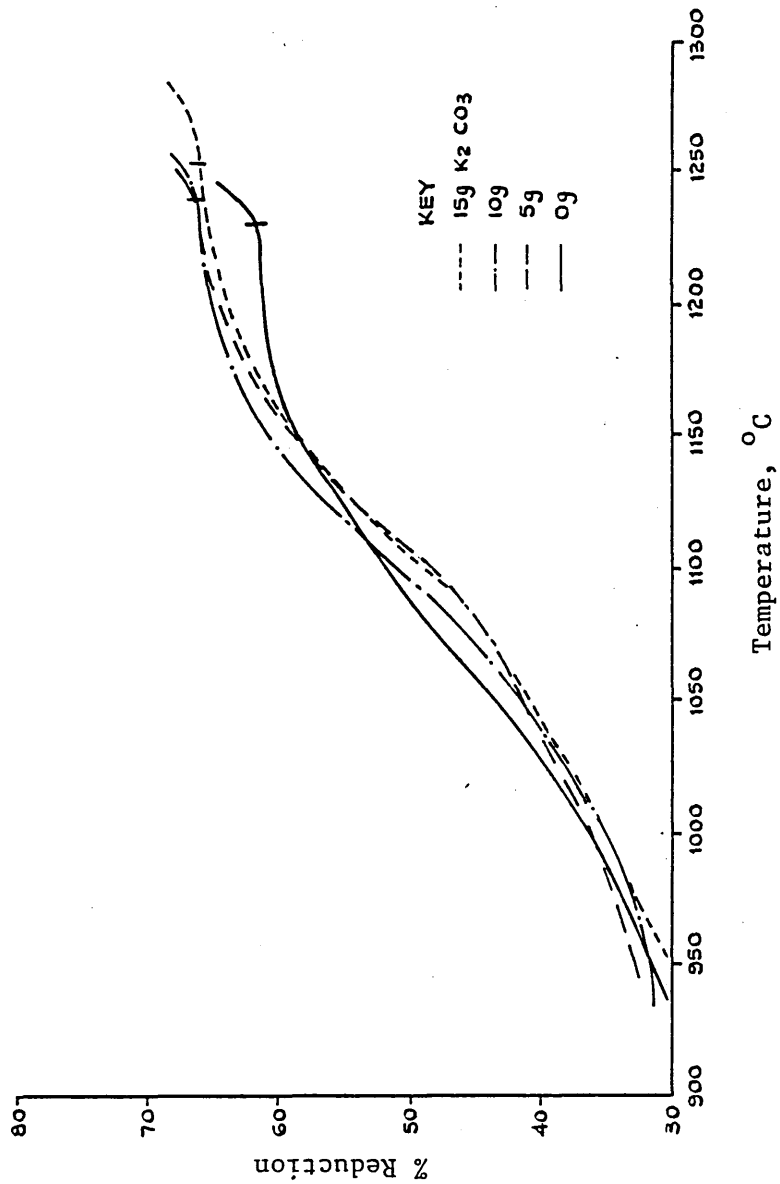


Figure 78 Effect of Alkali Vapour in the Reducing Gas on the Reduction of Pellets

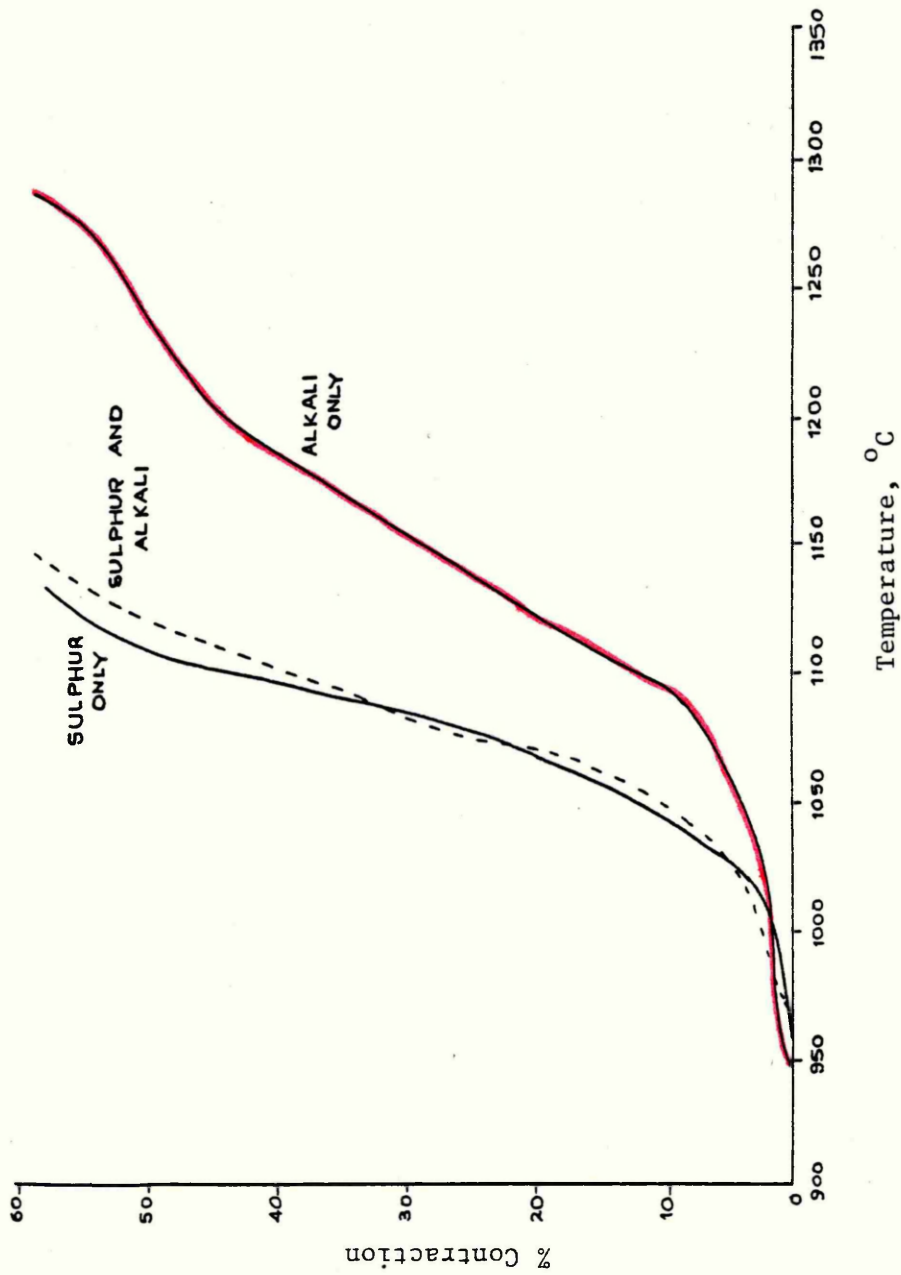


Figure 79 Effect of Sulphur and Alkali Vapour in the Reducing Gas on the Contraction of Pellets

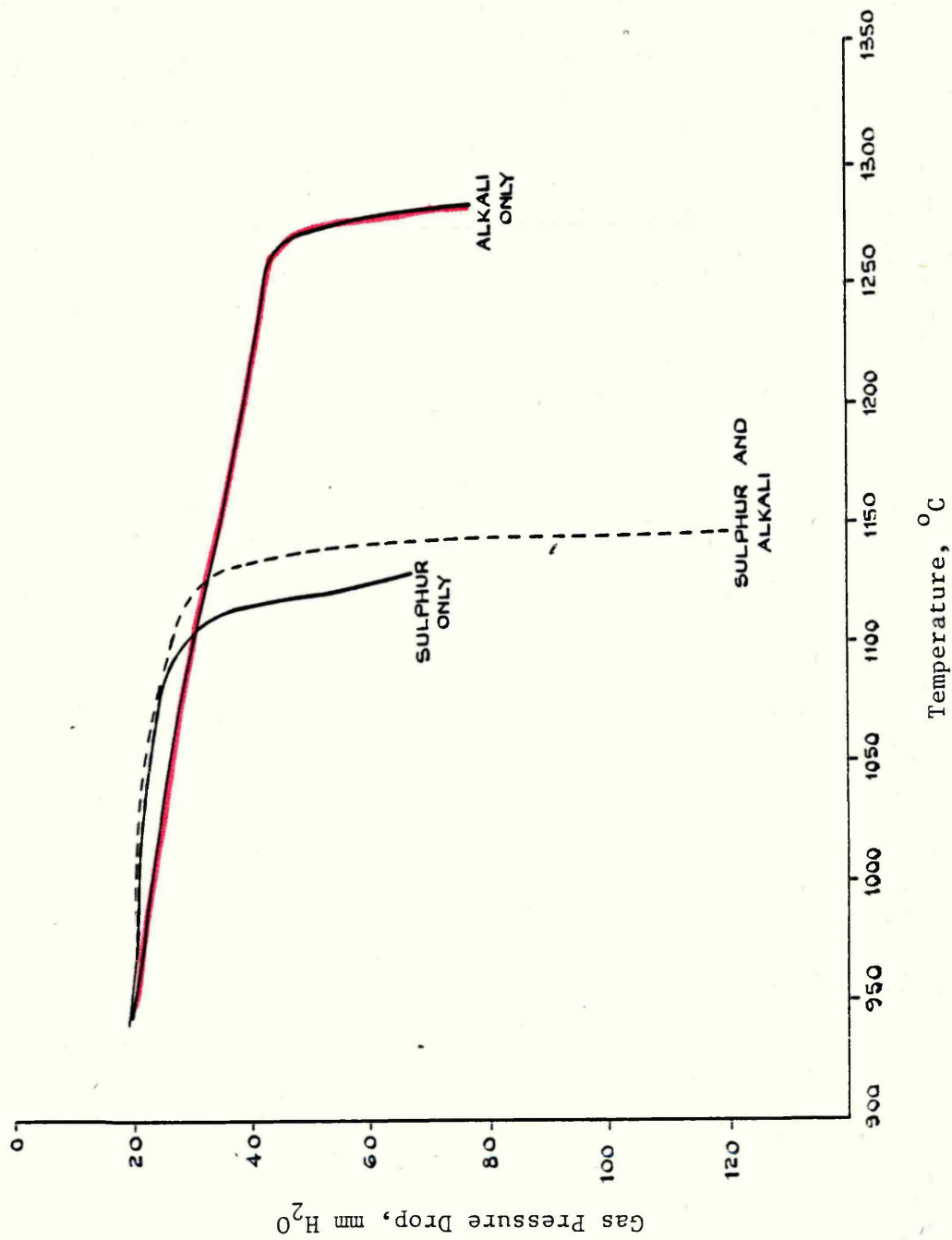


Figure 80 Effect of Sulphur and Alkali Vapour in the Reducing Gas on the Gas Pressure Drop of Pellets

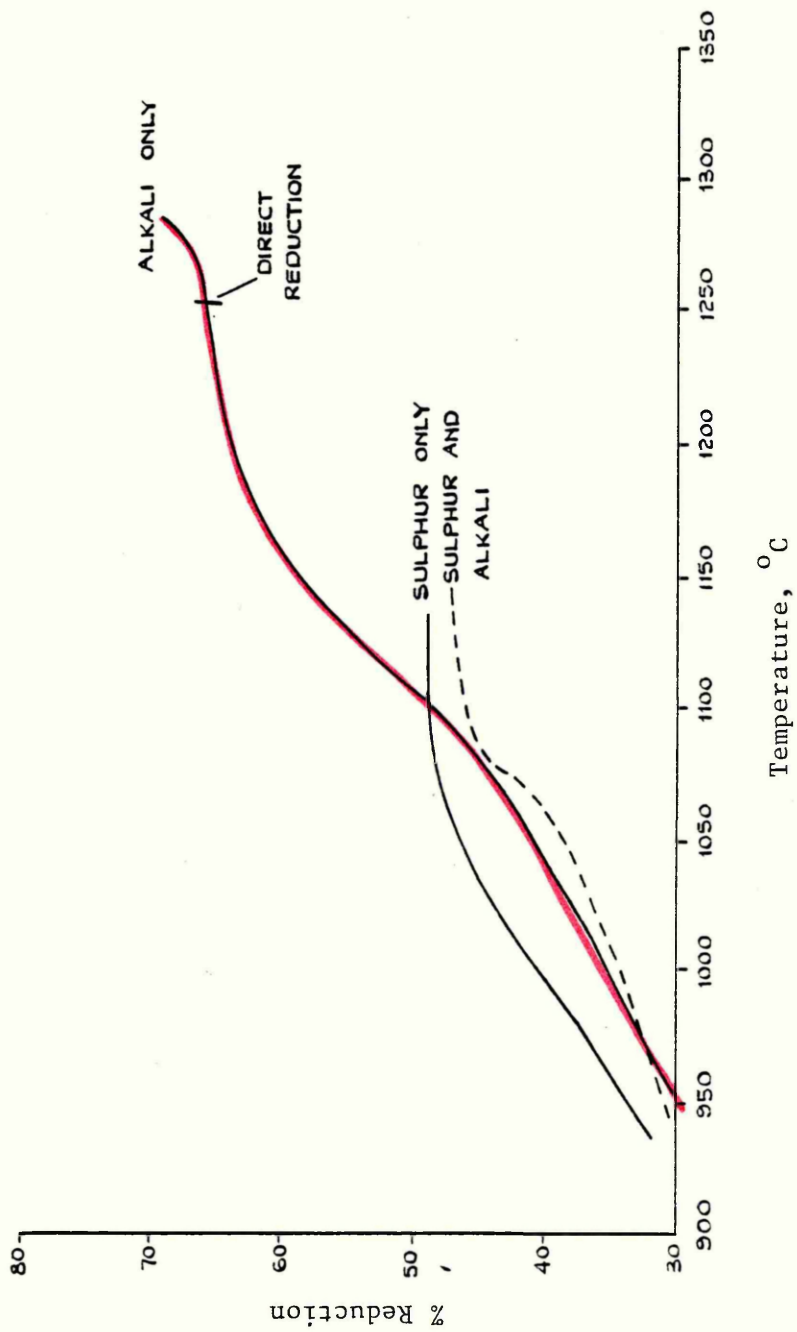


Figure 81 Effect of Sulphur and Alkali Vapour in the Reducing Gas on the Reduction of Pellets

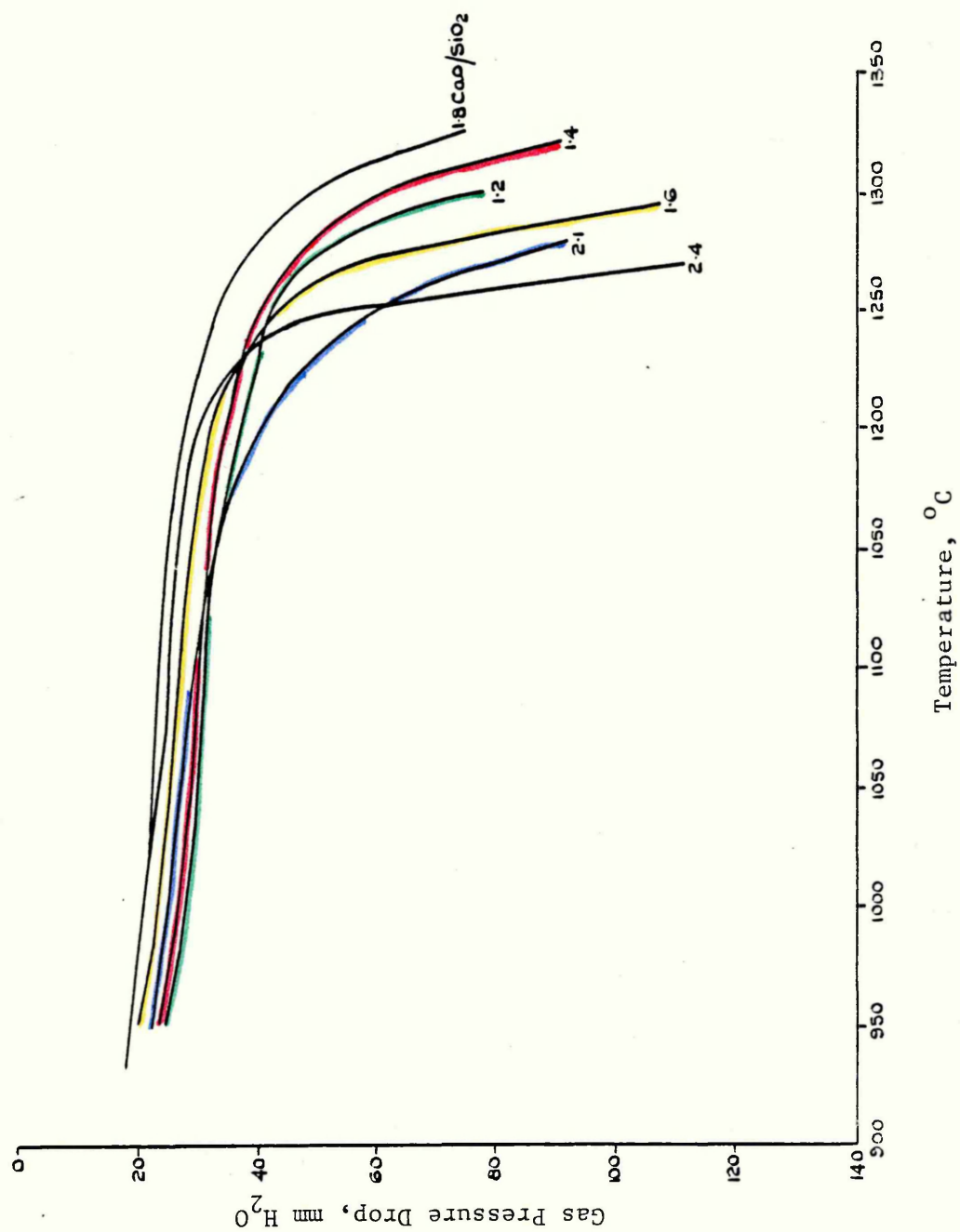


Figure 82 Gas Pressure Drop-Temperature Curves for the Different Sinters, Tested in their As-Received State

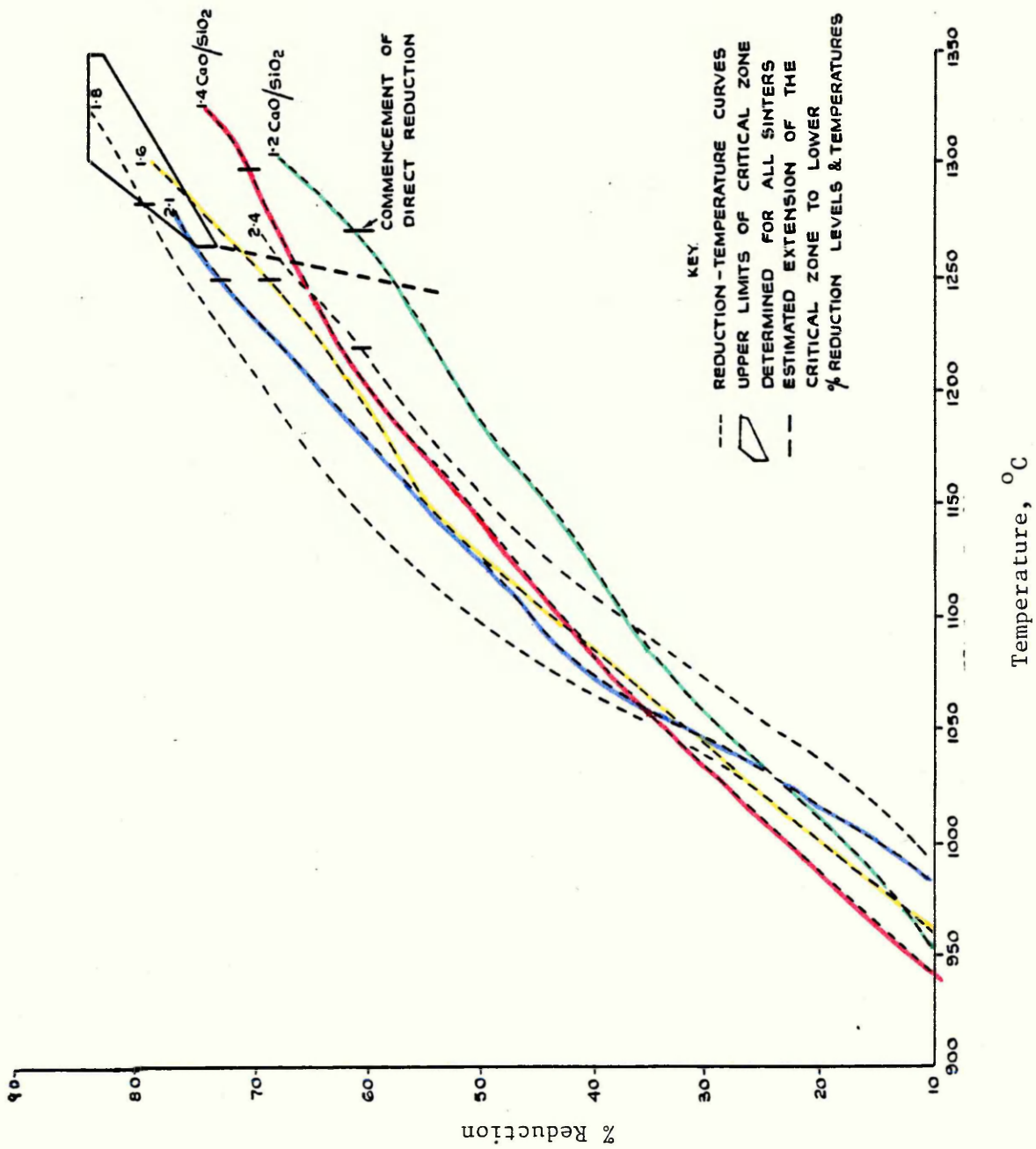


Figure 83 Reduction-Temperature Curves for the Different Sinters Tested in their As-Received State

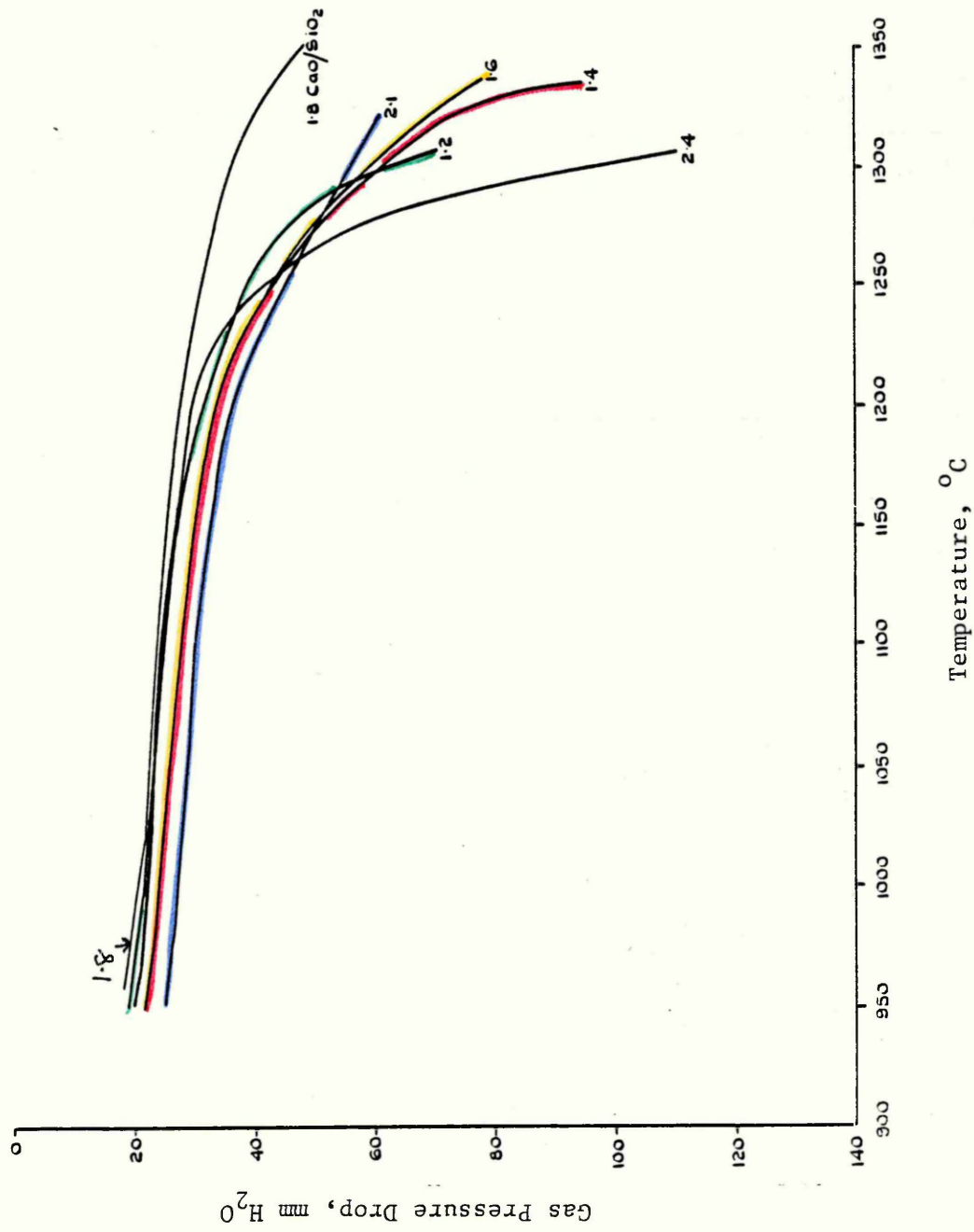


Figure 84 Gas Pressure Drop-Temperature Curves for the Different Sinters Tested after 30% Pre-Reduction

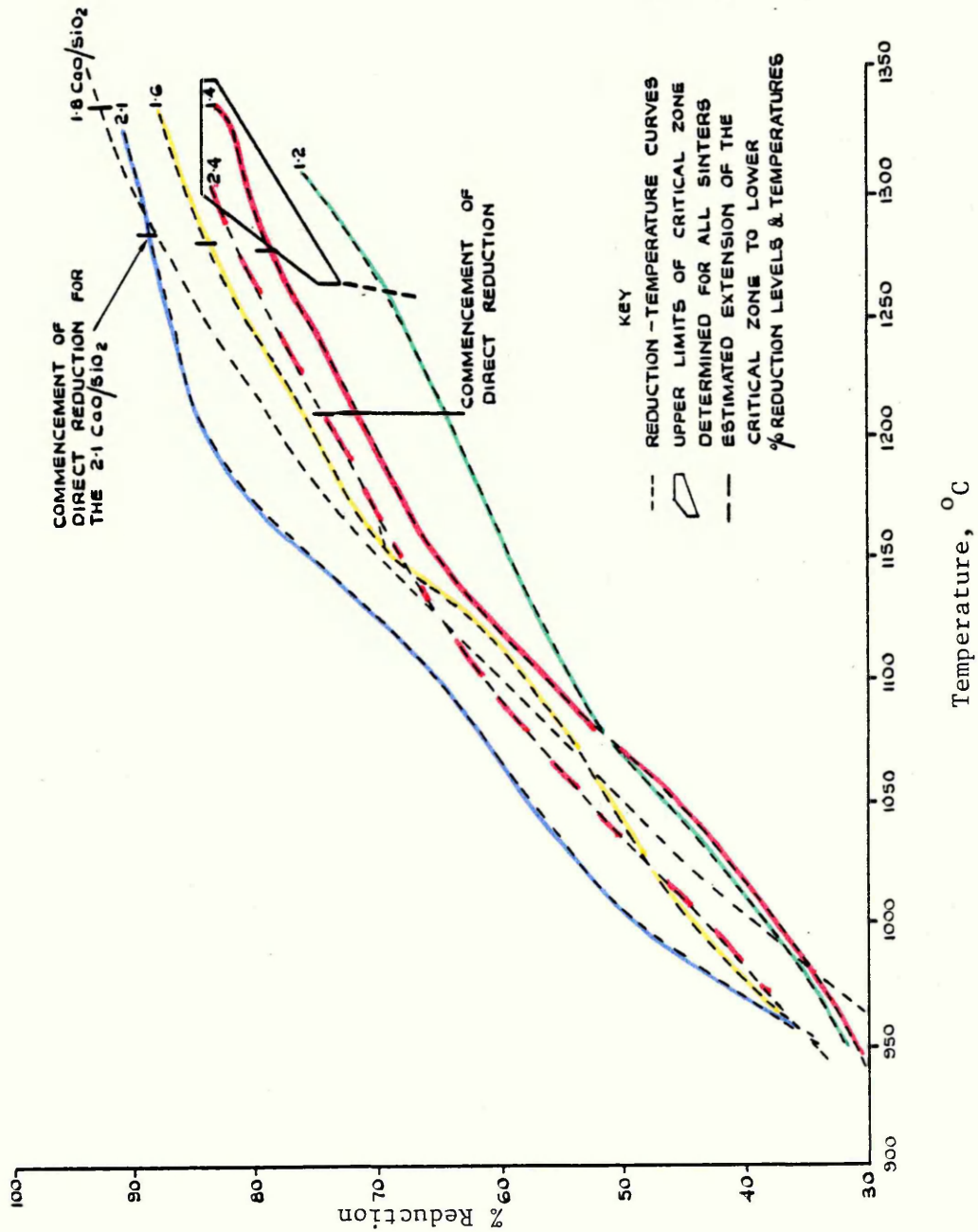


Figure 85 Reduction-Temperature Curves for the Different Sintners Tested after 30% Pre-Reduction

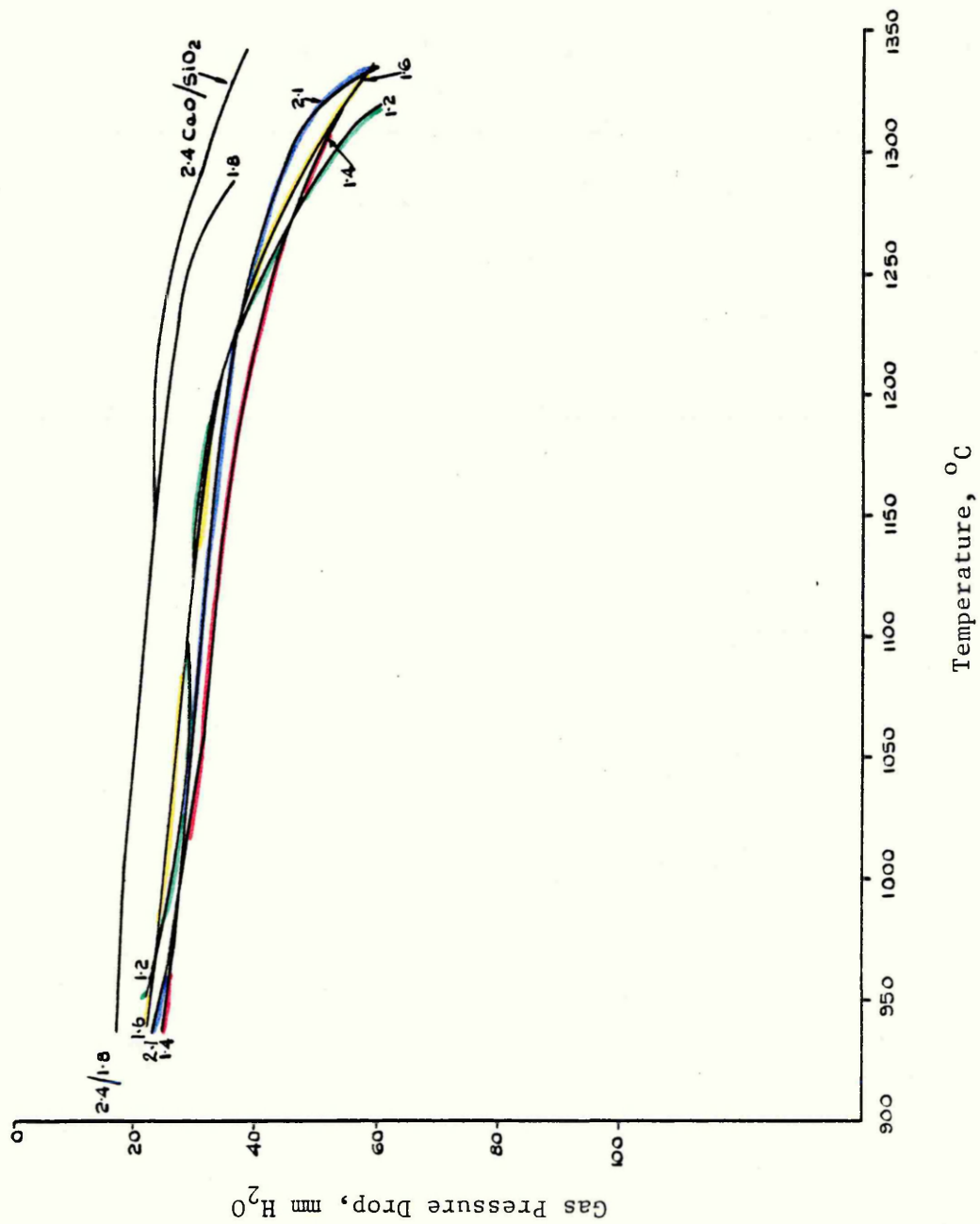


Figure 86 Gas Pressure Drop-Temperature Curves for the Different Sinters Tested after 45% Pre-Reduction

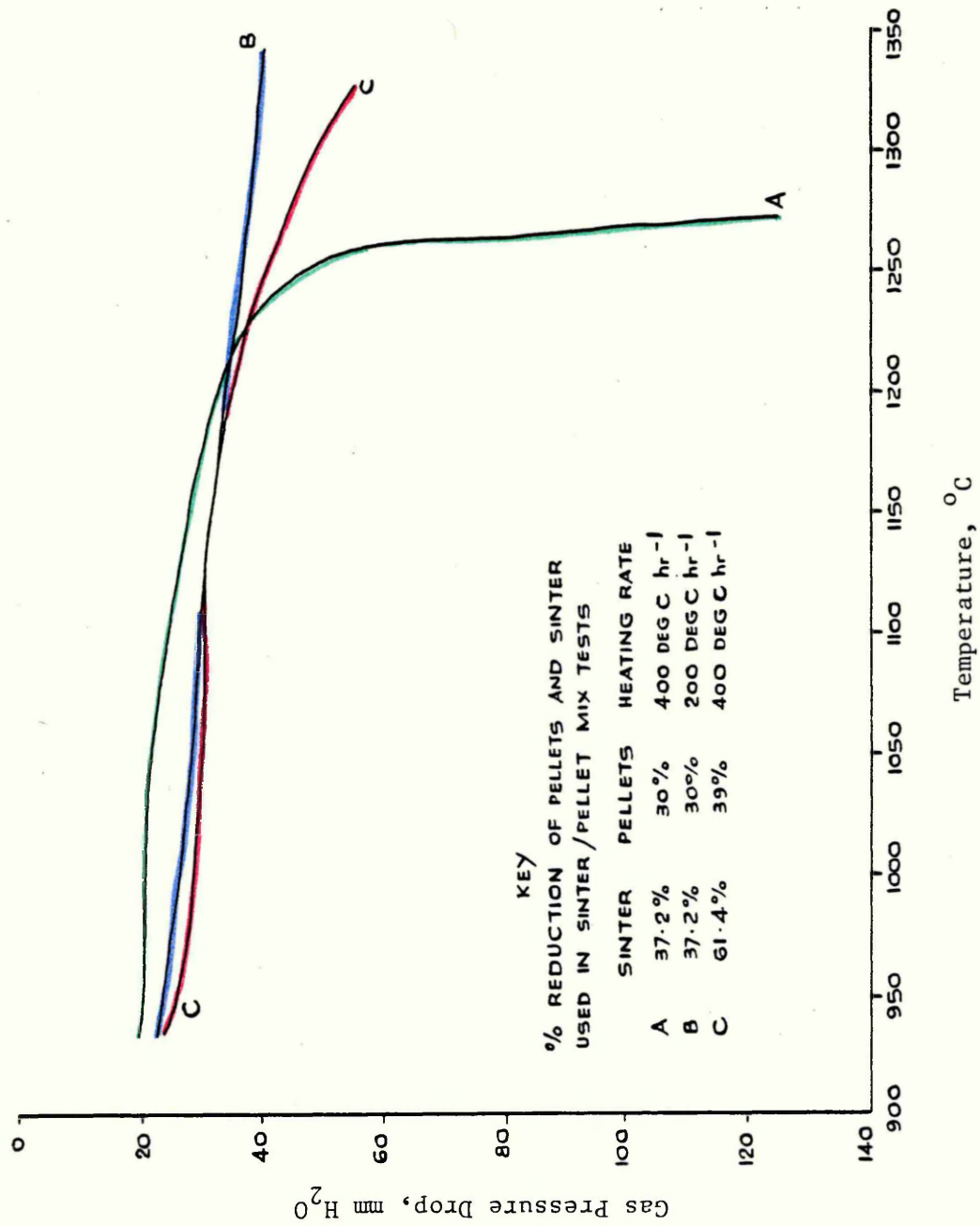


Figure 87 Gas Pressure Drop-Temperature Curves for the Sinter/Pellet Mixtures

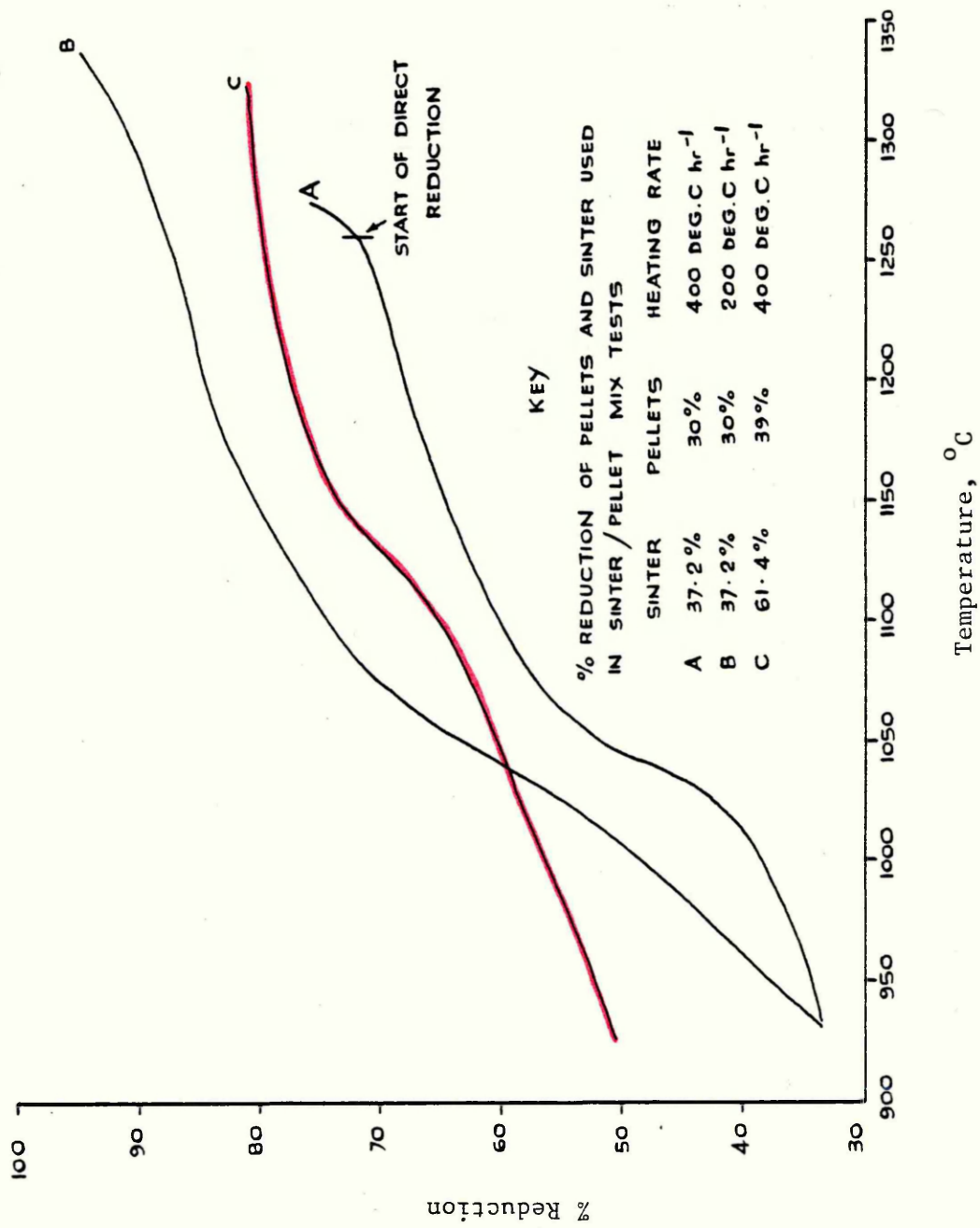


Figure 88 Reduction-Temperature Curves for the Sinter/Pellet Mixtures

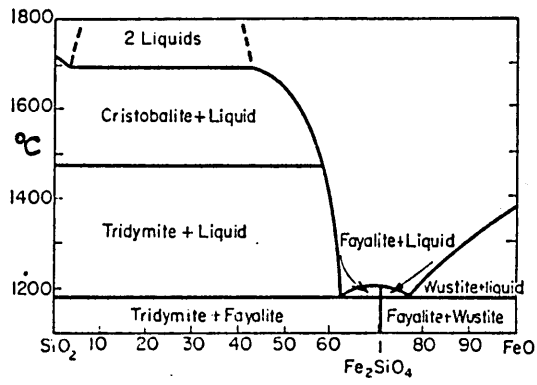


Figure 89 The FeO-SiO<sub>2</sub> Phase Diagram<sup>81</sup>

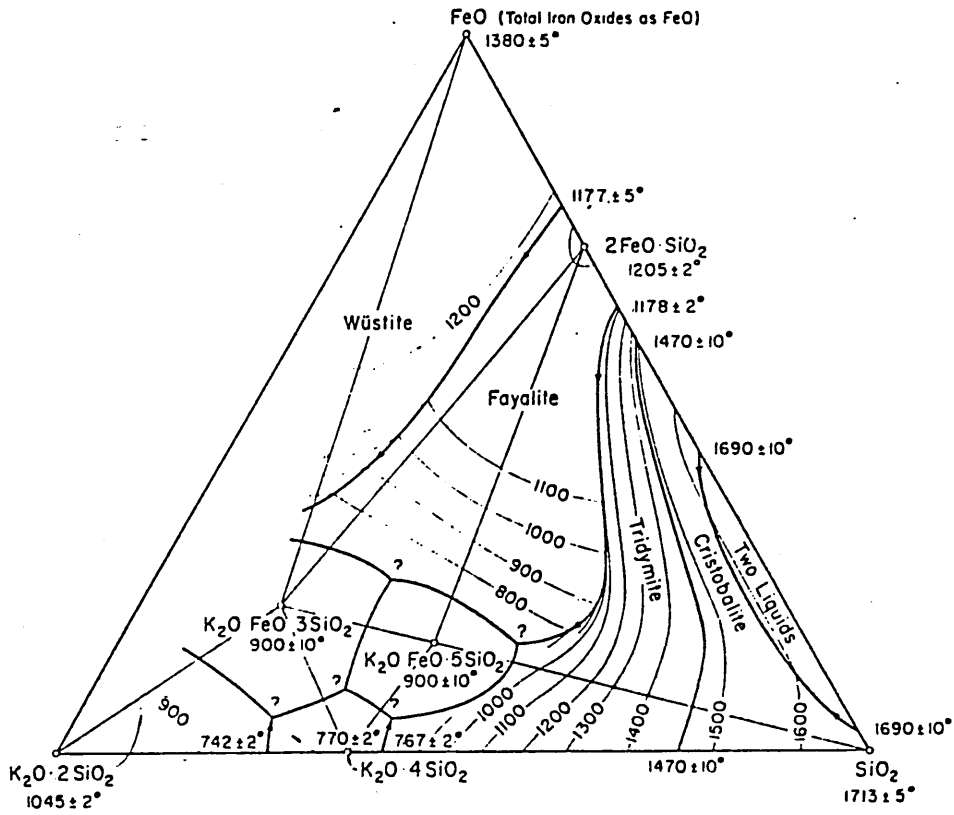


Figure 90 The FeO-SiO<sub>2</sub>-K<sub>2</sub>O.2SiO<sub>2</sub> Phase Diagram<sup>82</sup>



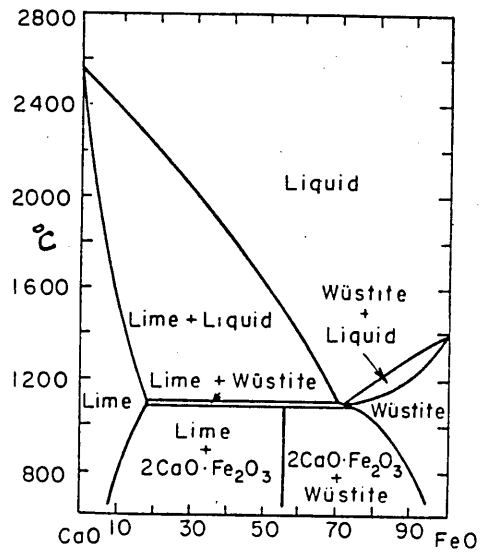


Figure 92 The CaO-FeO Phase Diagram<sup>84</sup>

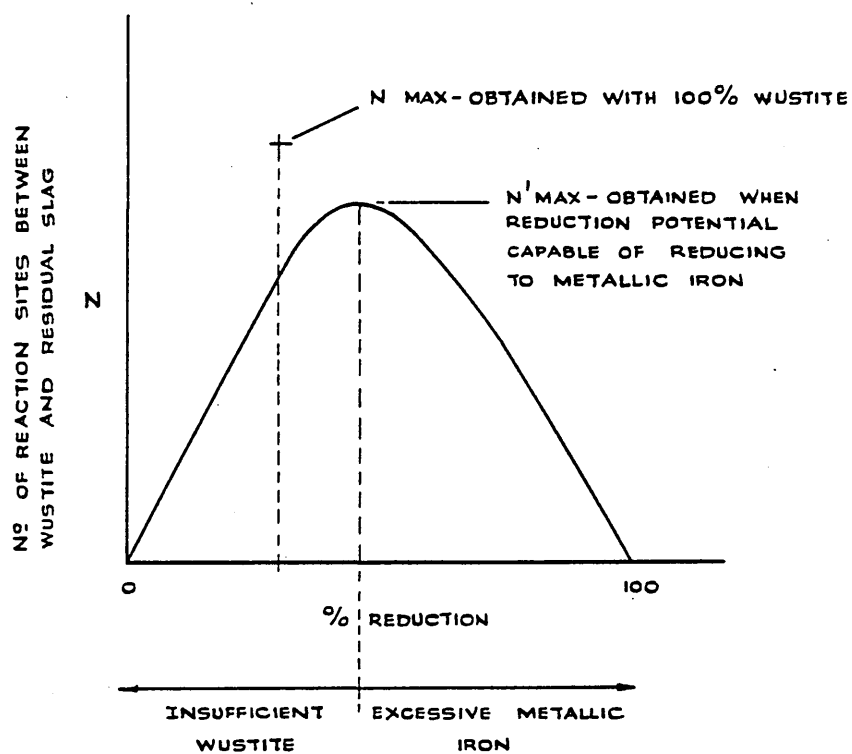


Figure 93 Quantity of Reacting Sites in the Residual Slag/  
Wustite System

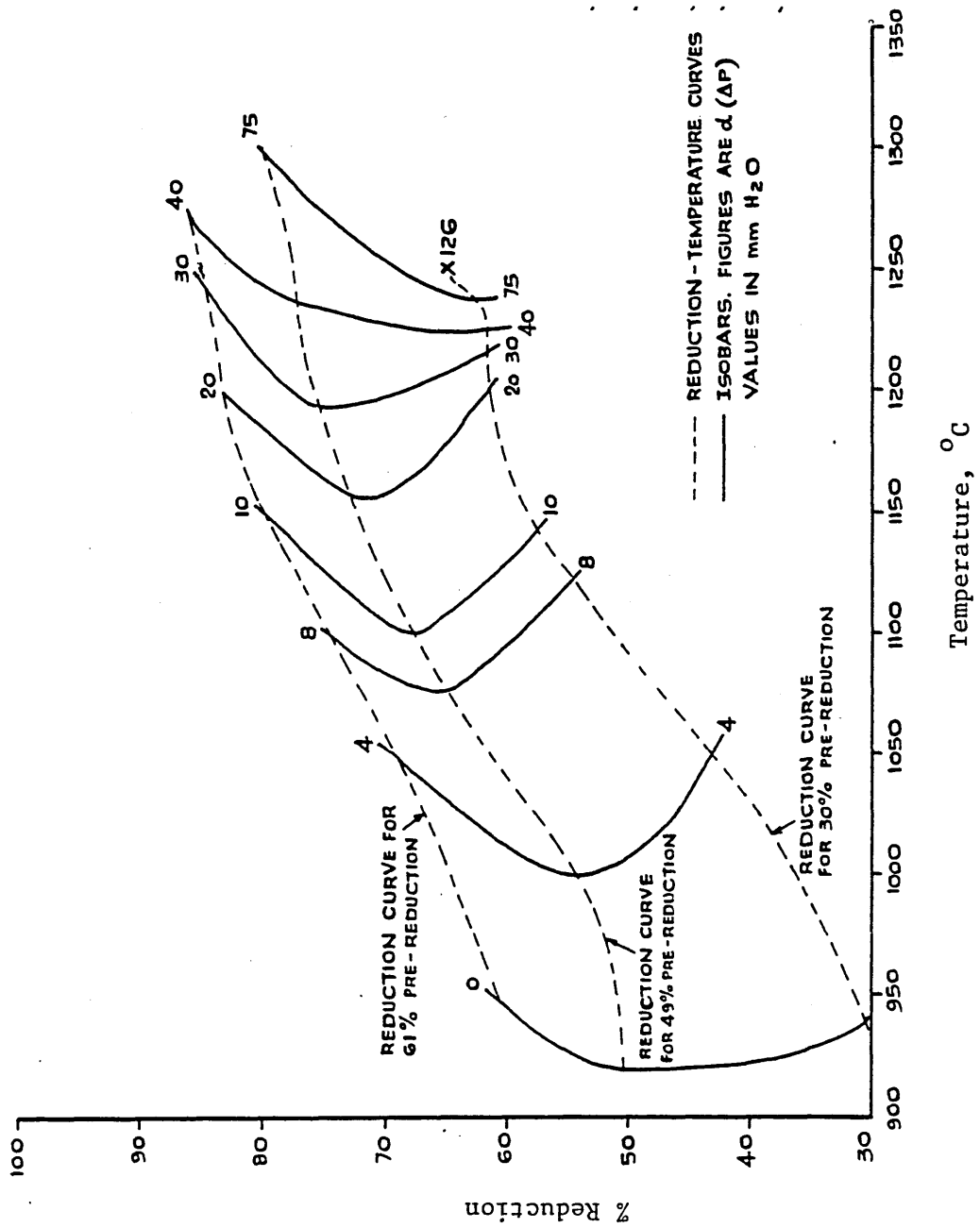


Figure 94 TRIB Diagram for Acid Pellets

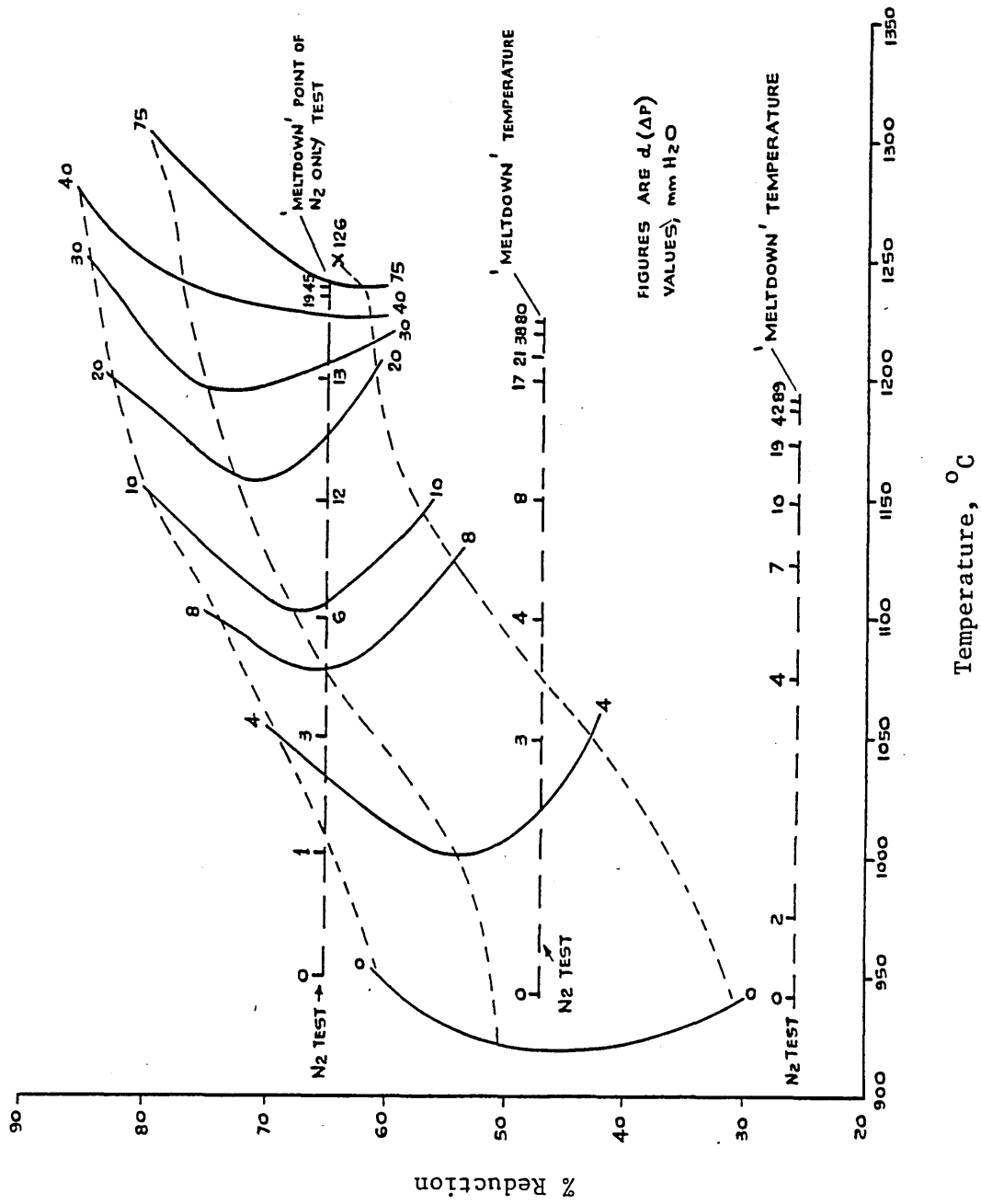


Figure 95 TRIB Diagram for Acid Pellets with the Results of the Nitrogen Only Tests Superimposed

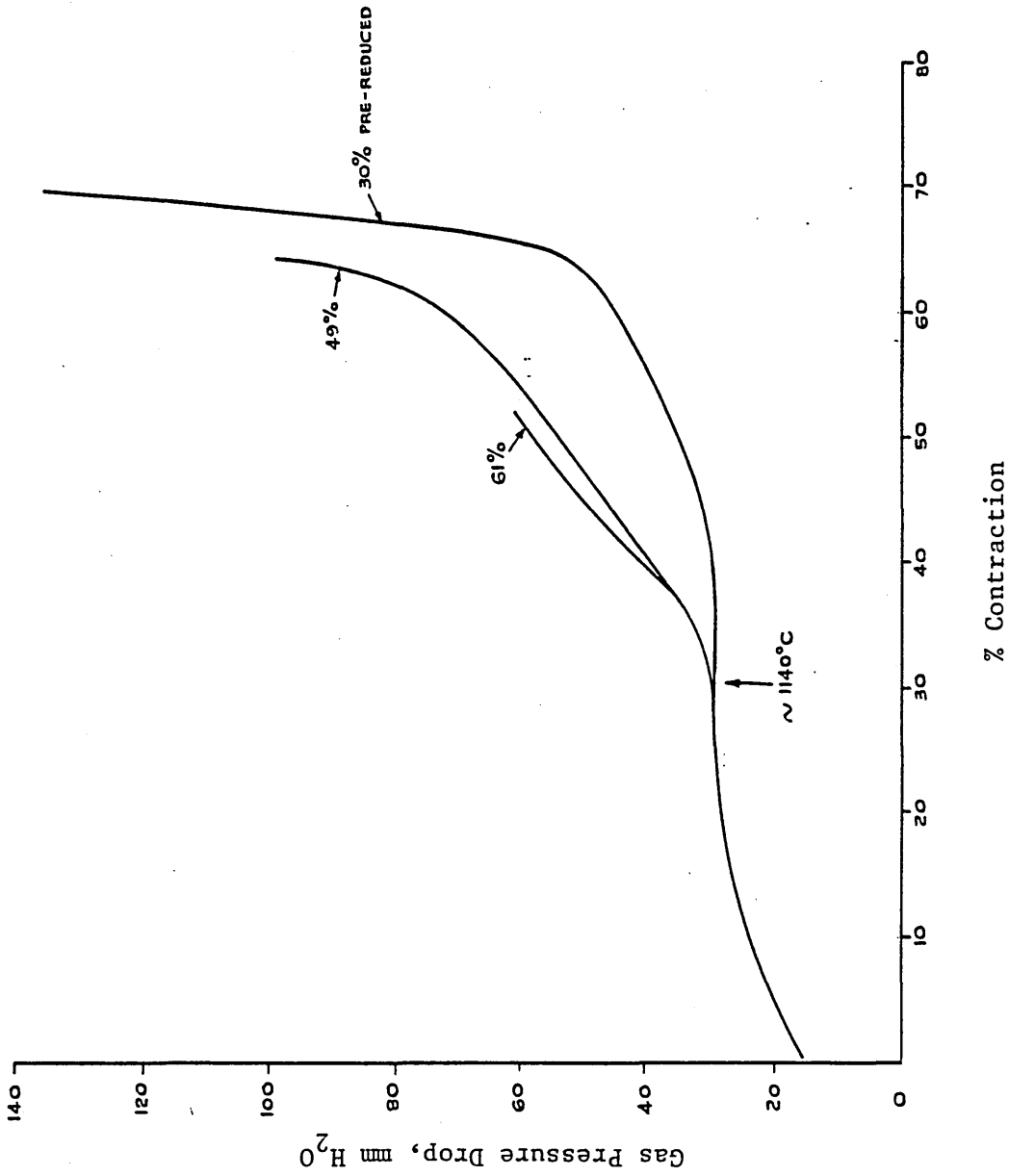


Figure 96 Contraction-Gas Pressure Drop Curves for Pellets at a Heating Rate of 400°C.hr<sup>-1</sup>

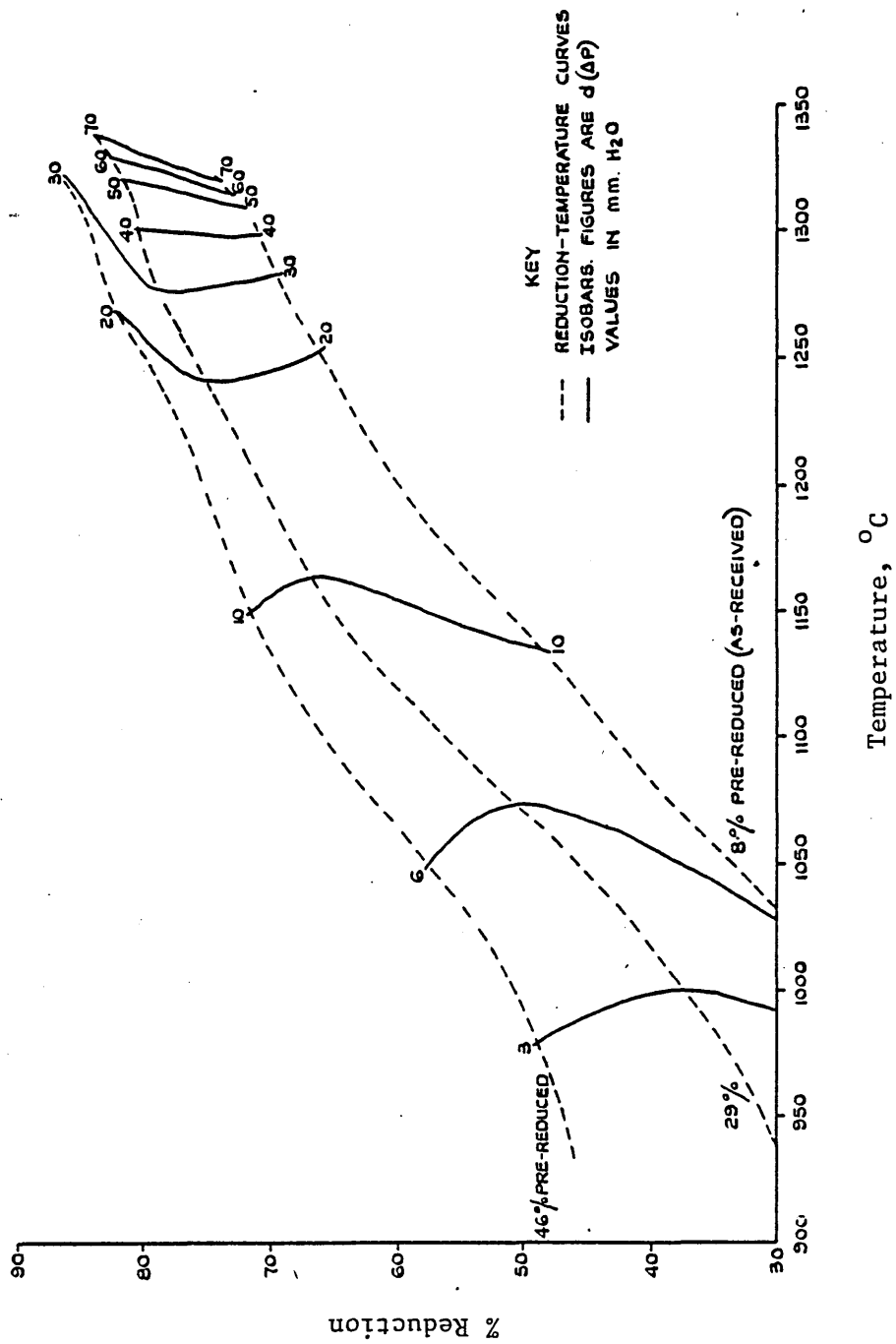


Figure 97 TRIB Diagram for the 1.4 CaO/SiO<sub>2</sub> Sinter

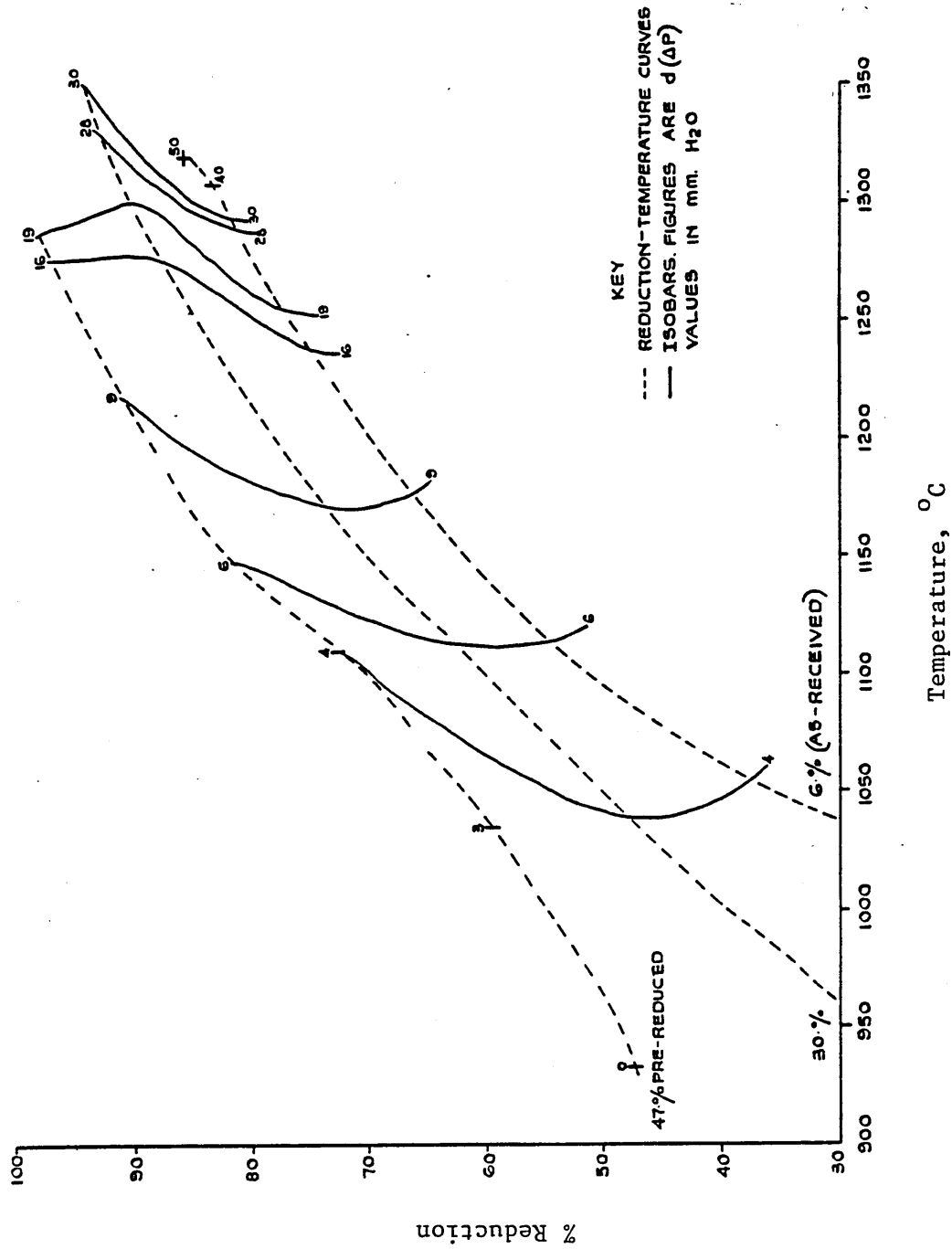


Figure 98 TRIB Diagram for the 1.8 CaO/SiO<sub>2</sub> Sinter

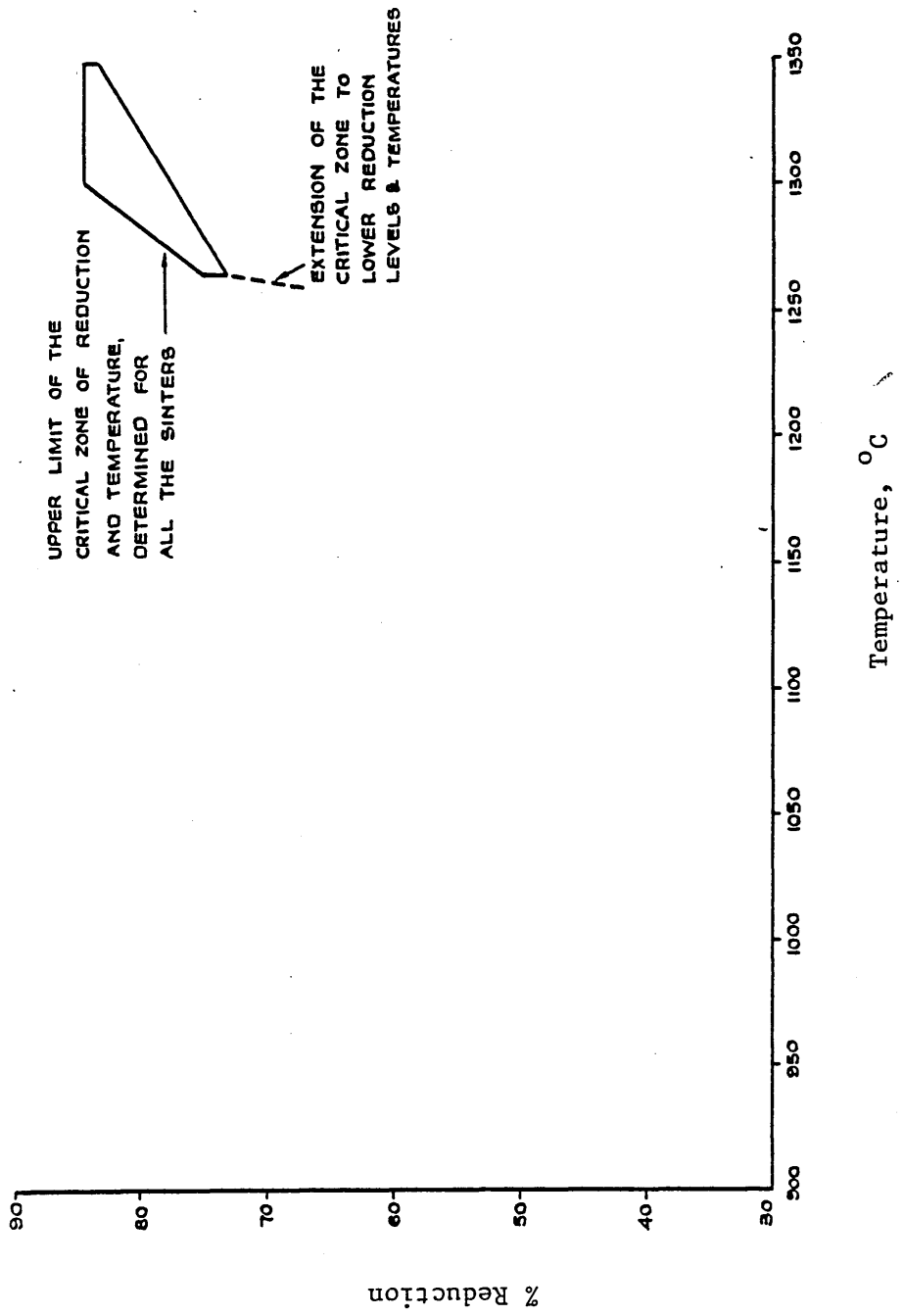


Figure 99 Critical Zone for all Sintors

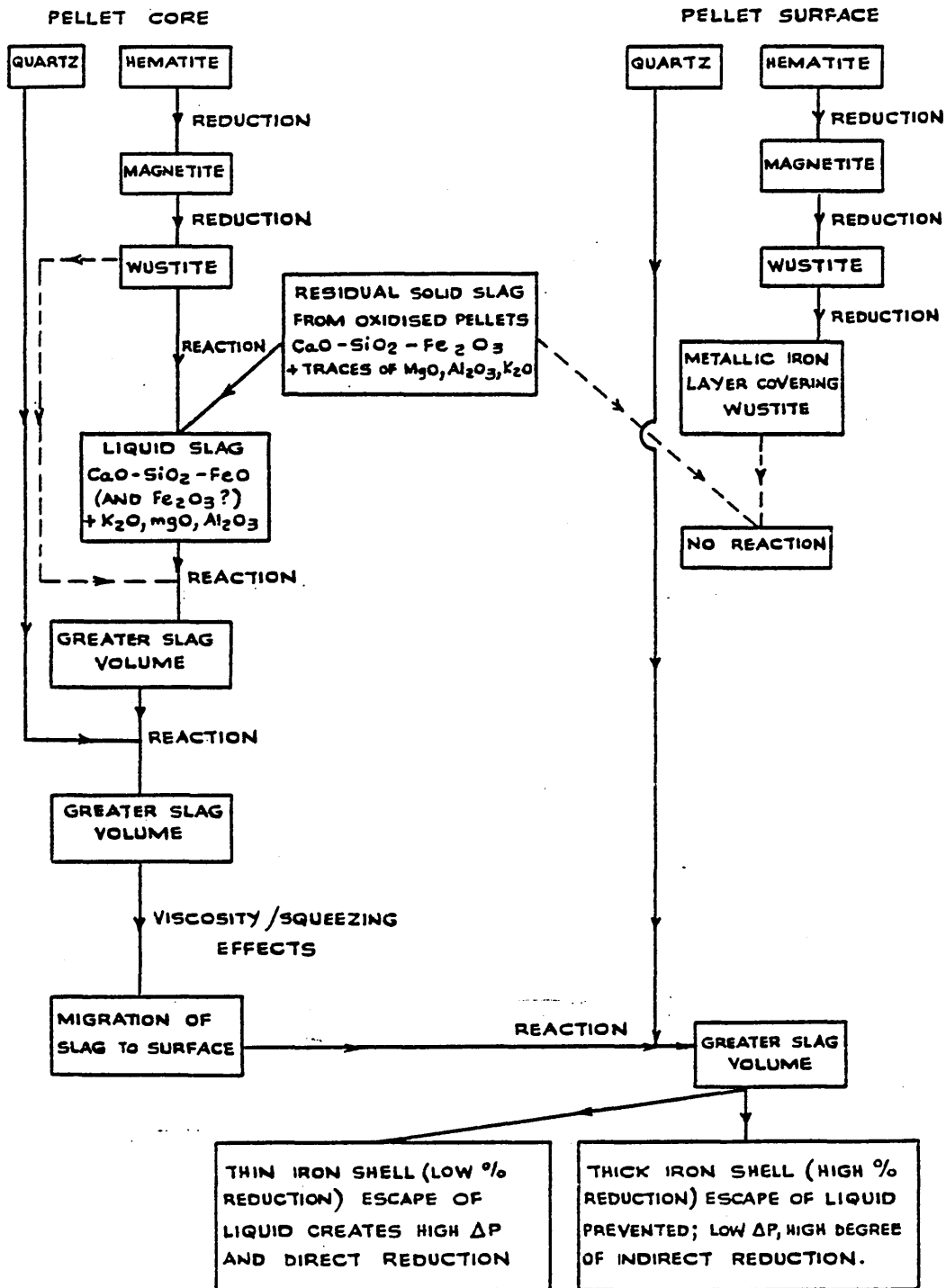
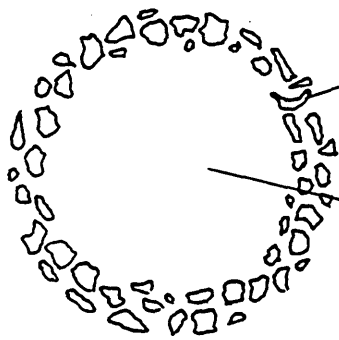


Figure 100 Flow Diagram Outlining the Liquid Slag Forming Reactions in Acid Pellets

Partially Reduced Pellet.  
High Gas Pressure Drop  
Situation.

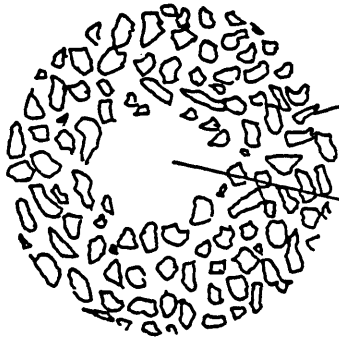


Metallic iron  
grains

Core consists of wustite  
and liquid slag.

The liquid slag can easily  
penetrate the thin iron  
shell and escape from the  
pellet.

Partially Reduced Pellet.  
Low Gas Pressure Drop  
Situation.



Metallic iron  
grains

Core also consists of wustite  
and liquid slag.

The liquid slag is prevented  
from flowing from the pellet  
by the thick iron shell.

Fully Reduced Pellet.  
Low Gas Pressure Drop  
Situation.



Metallic iron  
grains.  
No liquid or  
wustite present.

Figure 101 Schematic Representation of the Structure of Acid Pellets Exhibiting High and Low Gas Pressure Drops

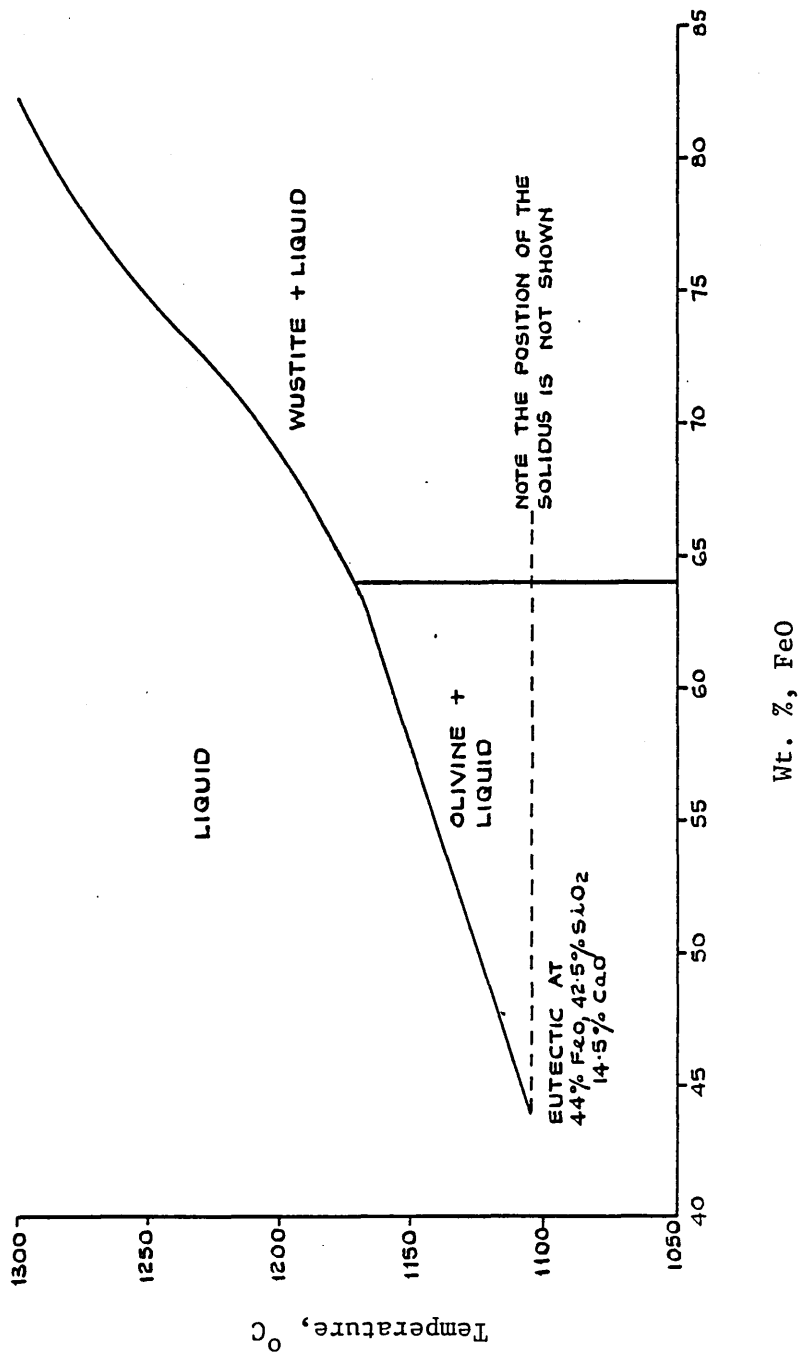


Figure 102 Simplified Section from the CaO-SiO<sub>2</sub>-FeO System

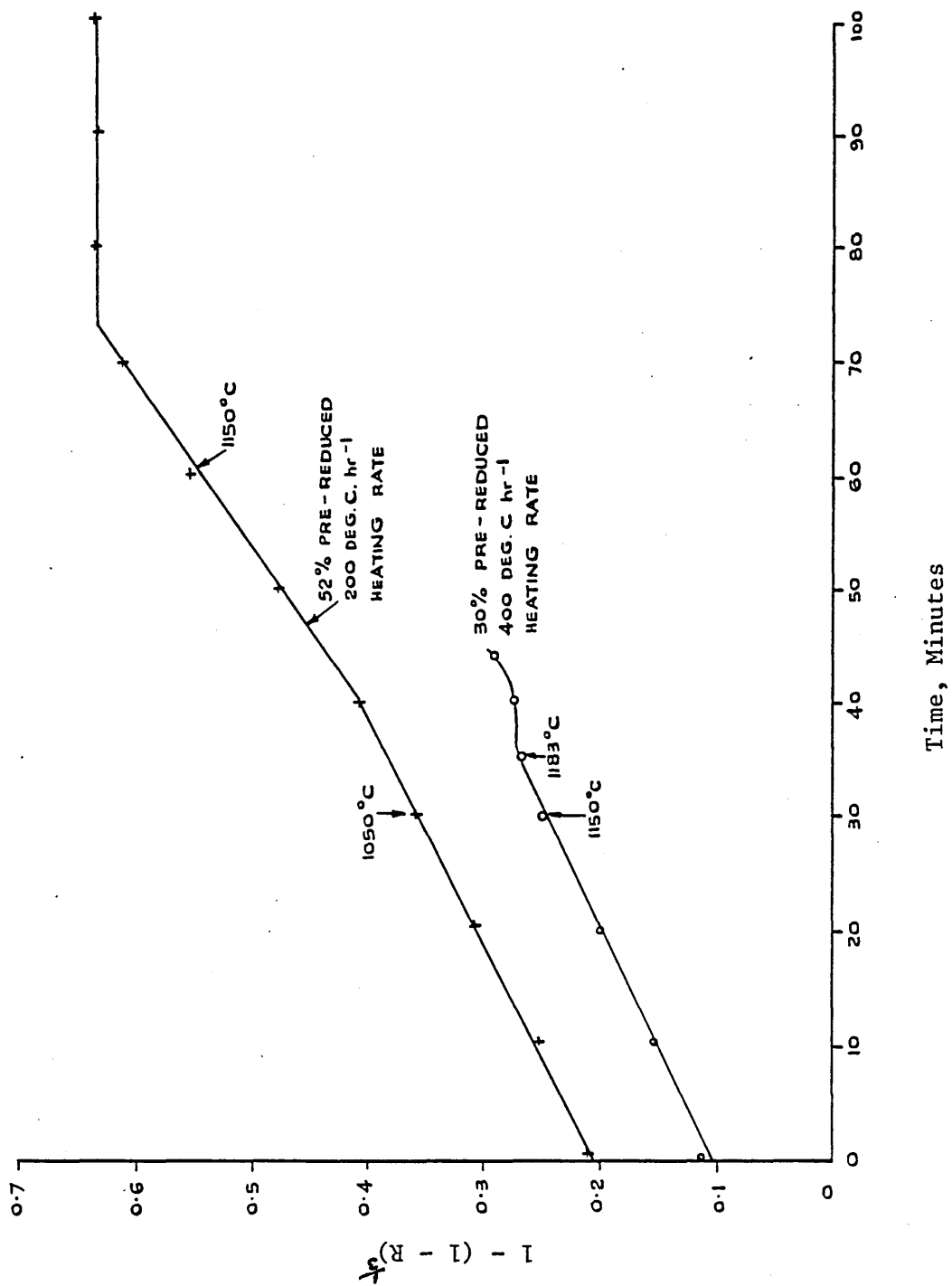


Figure 103 Determination of the Apparent Rate Constant, K<sub>2</sub>, for Acid Pellets

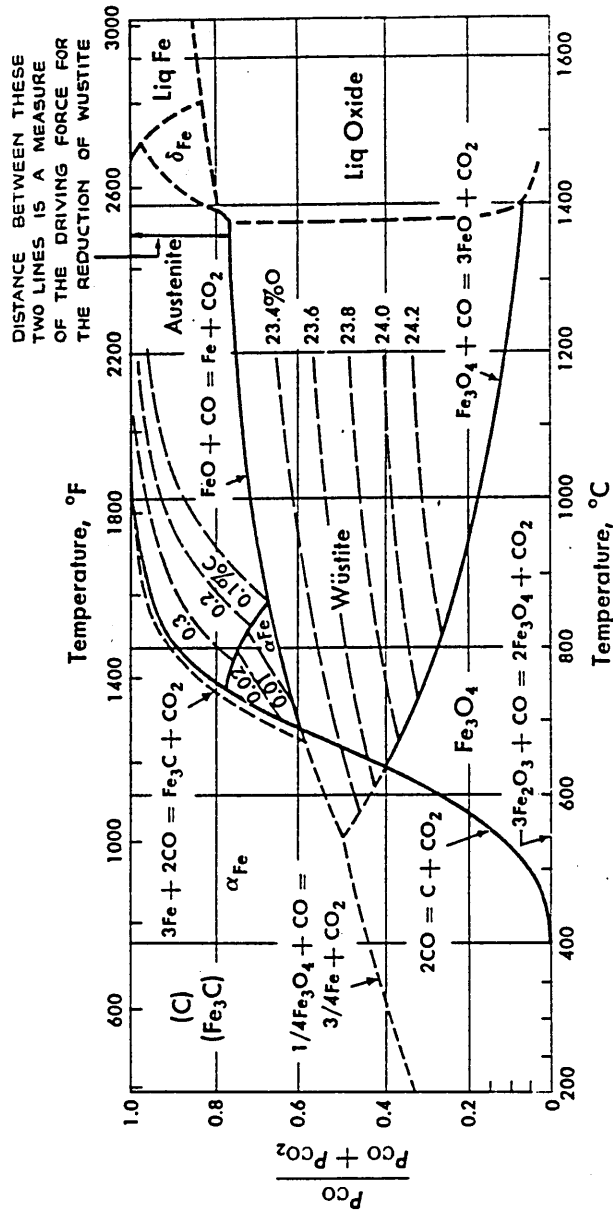


Figure 104 The  $CO/(CO+CO_2)$  - Temperature Equilibrium Diagram for Iron Oxide

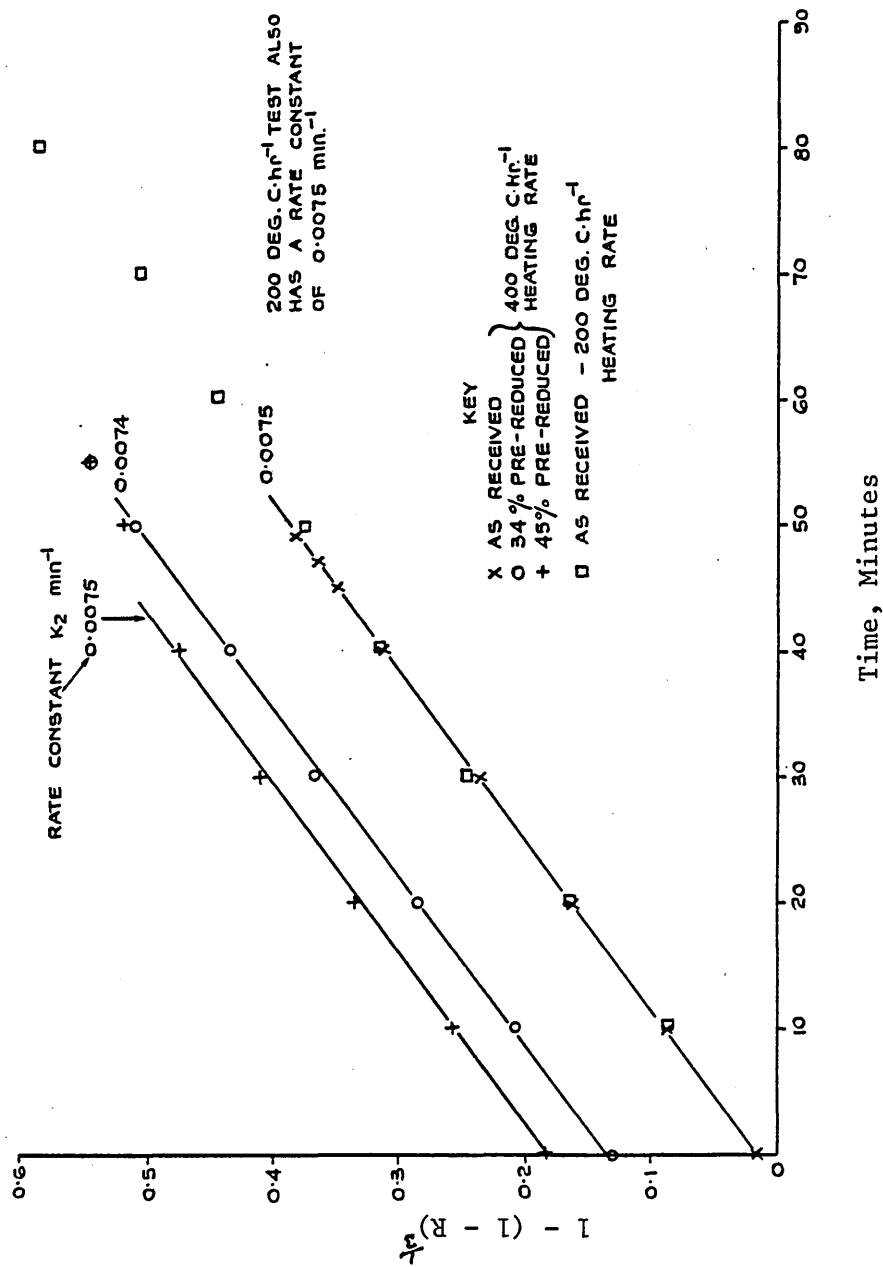


Figure 105 Determination of the Apparent Rate Constant,  $K_2$ ,  
 for the 2.1 CaO/SiO<sub>2</sub> Sinter



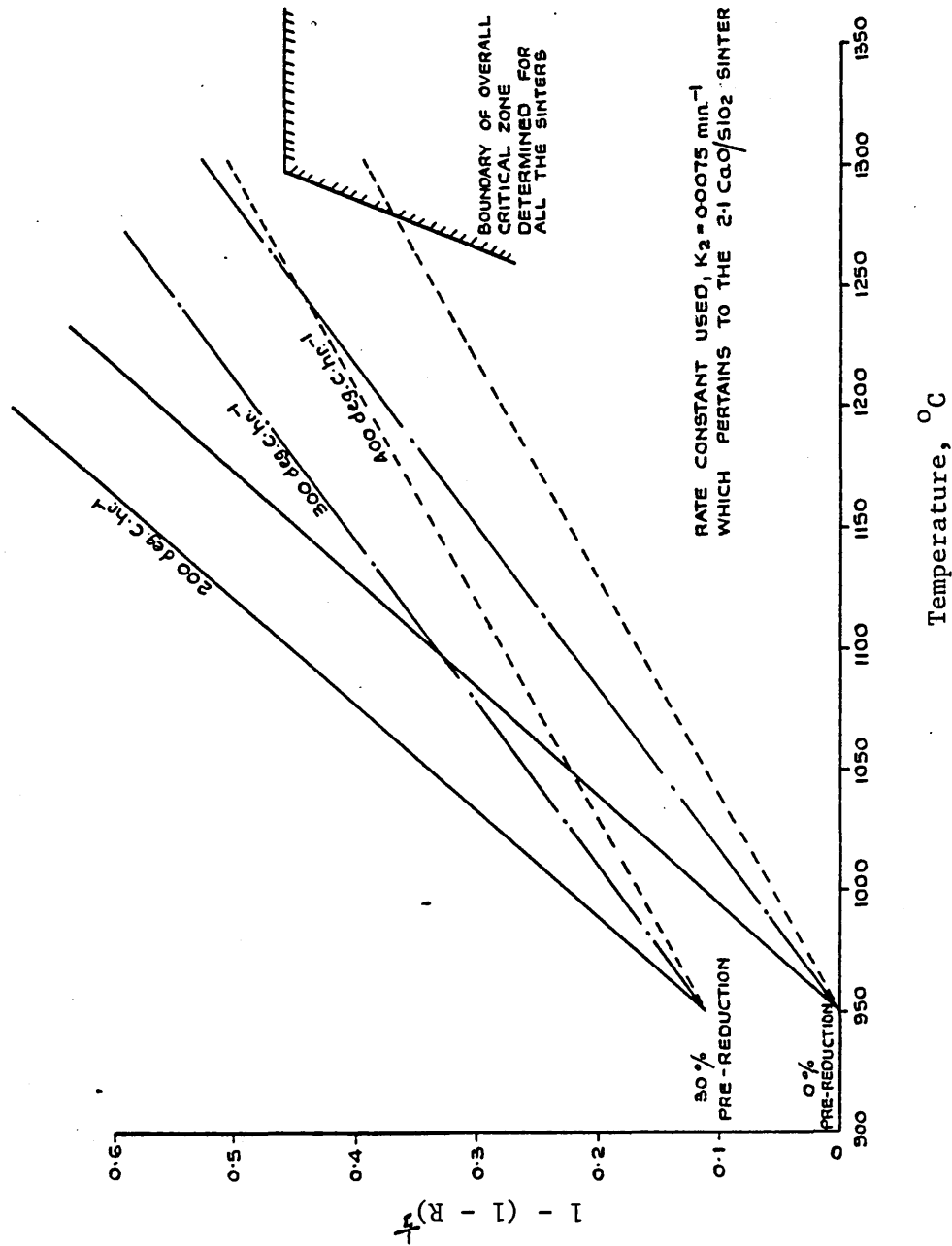


Figure 107 Influence of the Heating Rate upon the Approach to the Critical Zone for the 2.1 CaO/SiO<sub>2</sub> Sinter

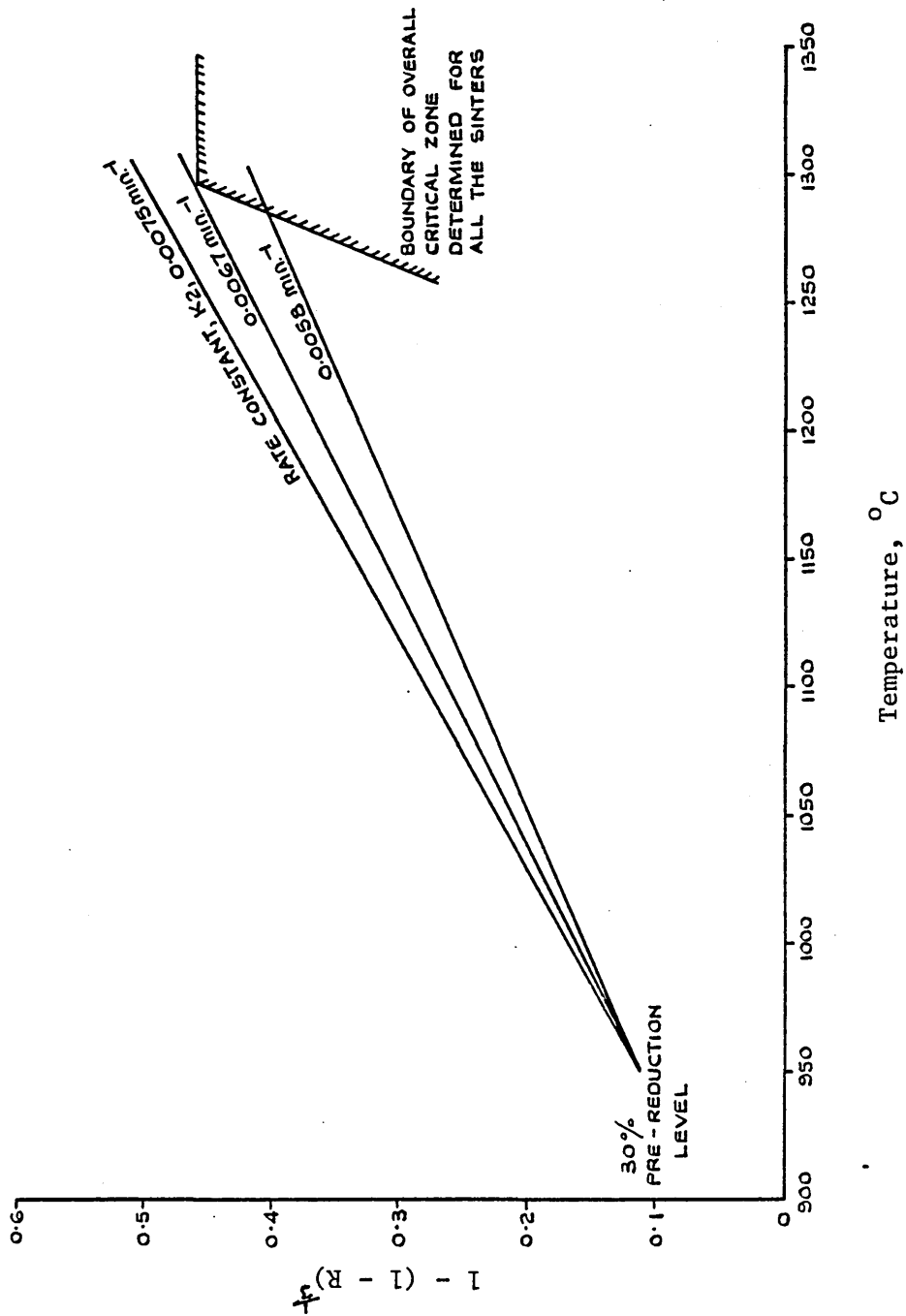


Figure 108 Effect of Different Apparent Rate Constants,  $K_2$ , upon the Approach to the Critical Zone

← Furnace Centre Direction  
Furnace Wall Direction →

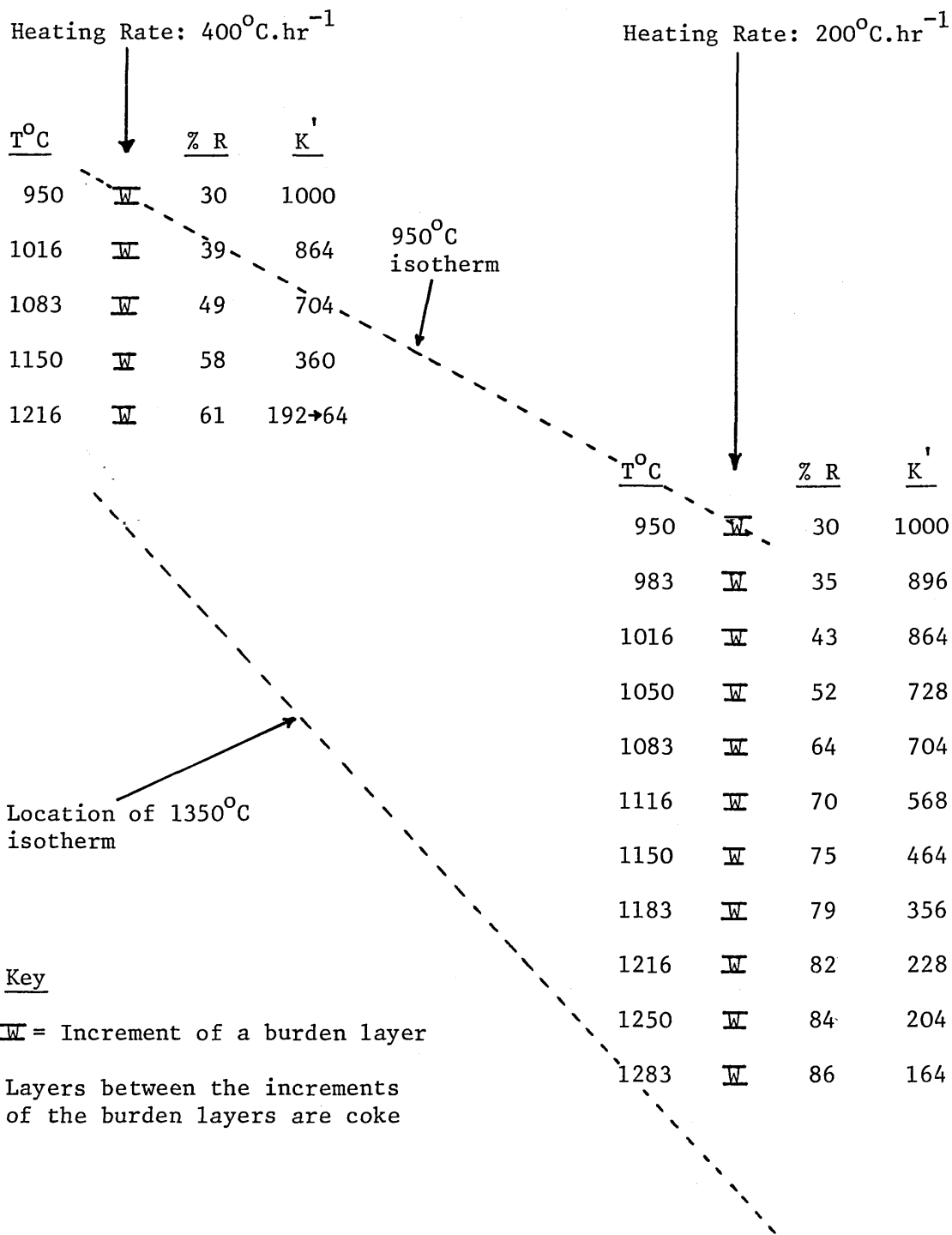


Figure 109 Relative Permeability Data for Acid Pellets within the Cohesive Zone

← Furnace Centre Direction  
Furnace Wall Direction →

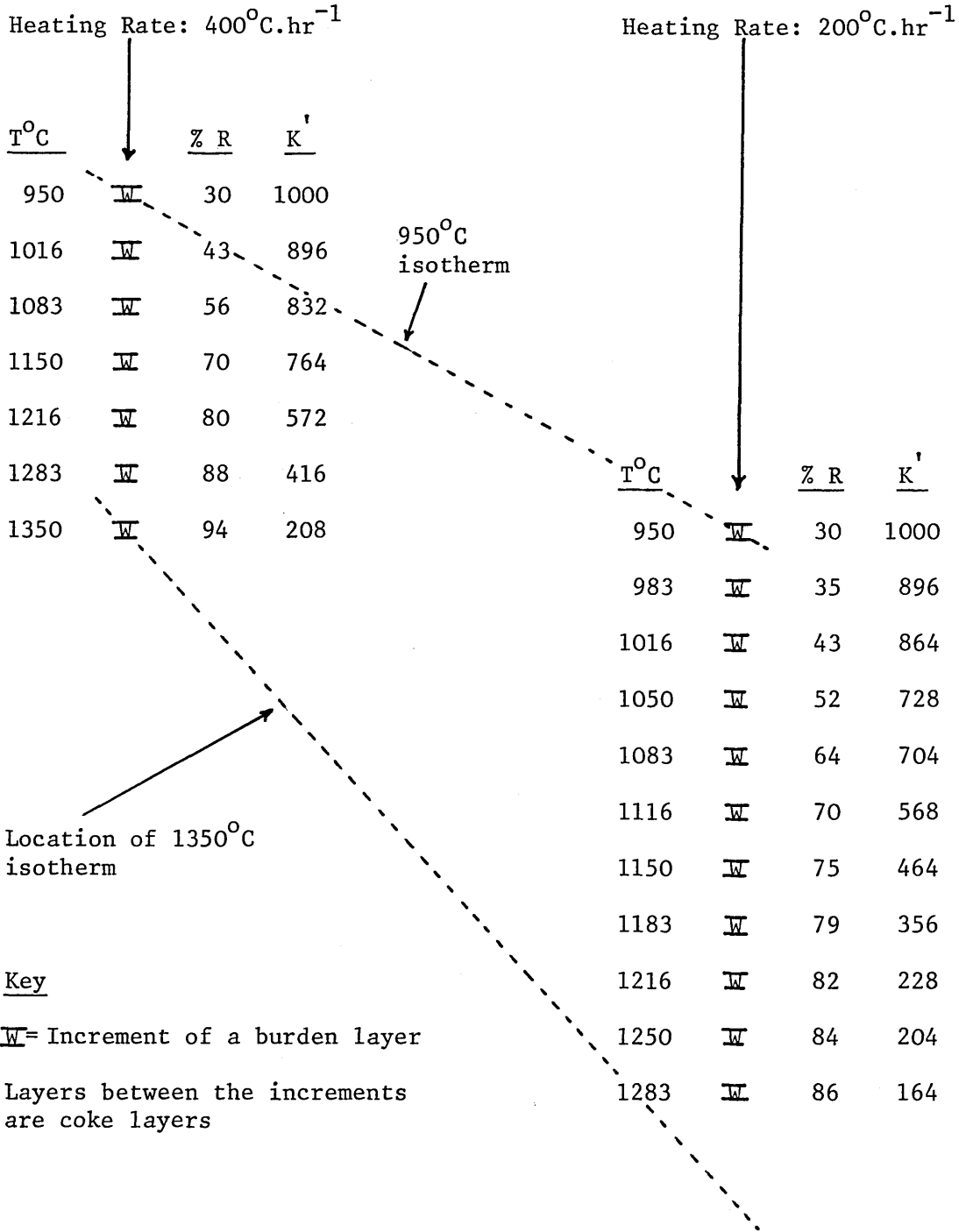


Figure 110 Relative Permeability within the Cohesive Zone Produced by Selective Charging of Sinter and Pellets - Sinter Charged Towards the Centre and Pellets Towards the Walls of the Furnace

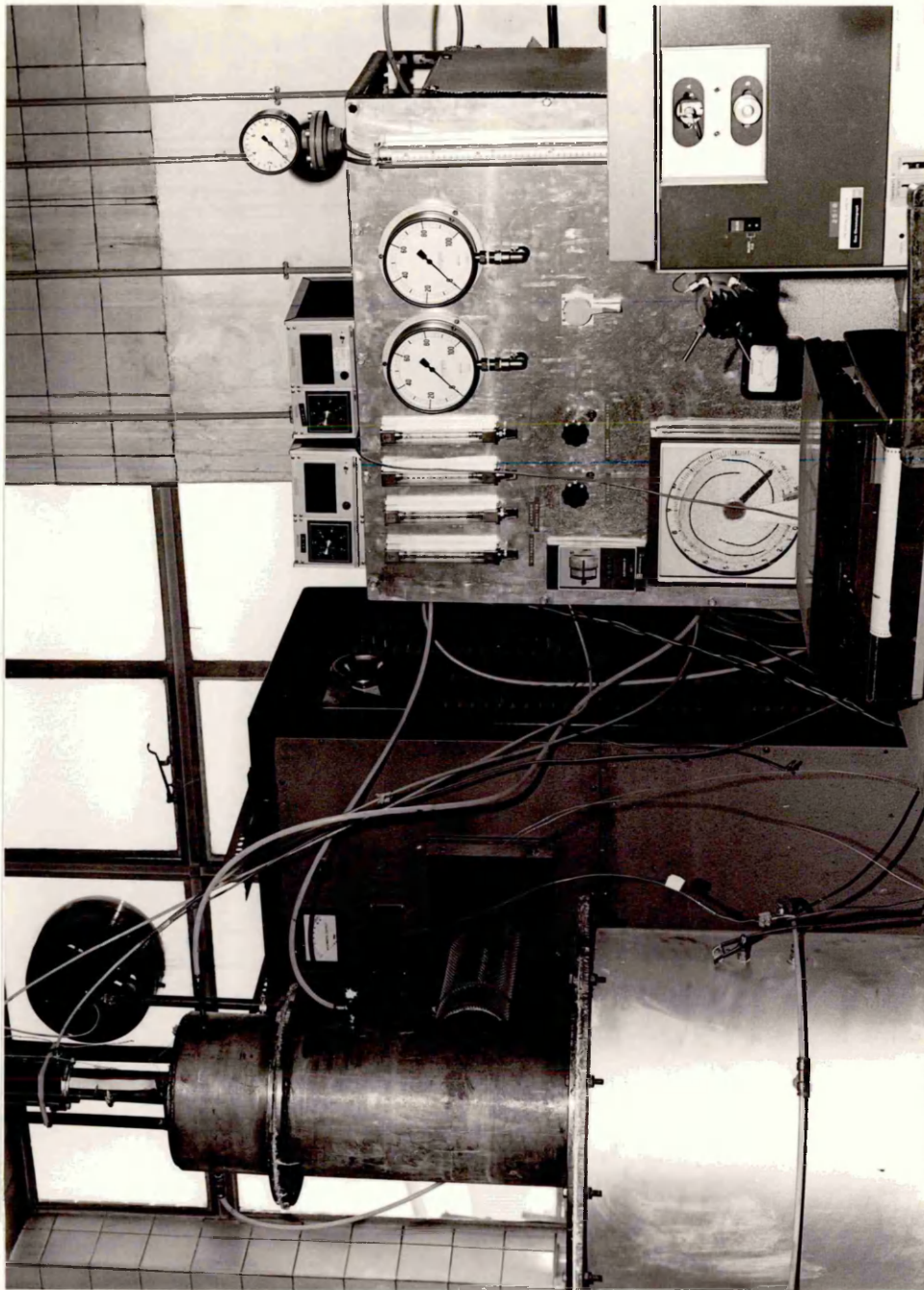


Plate 2 Fully Oxidised Pellet Showing Hematite Grains (H)  
and the Slag Phase (S).  
Magnification x 880.

Plate 3 Partially Reduced Acid Pellet (44 % Reduced)  
Which has been Heated to 1015°C in the Initial  
Melting Test Showing Wustite (W), Iron (I) and  
the Two Slag Phases (S<sub>1</sub> and S<sub>2</sub>).  
Magnification x 880.

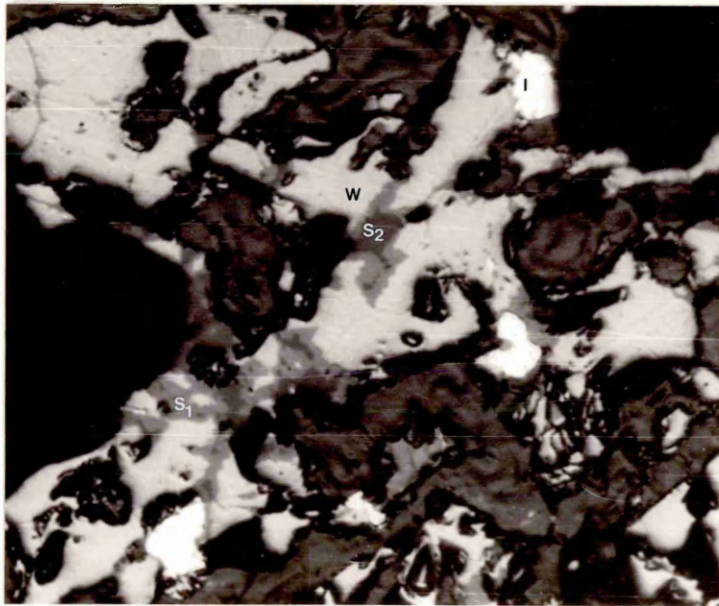
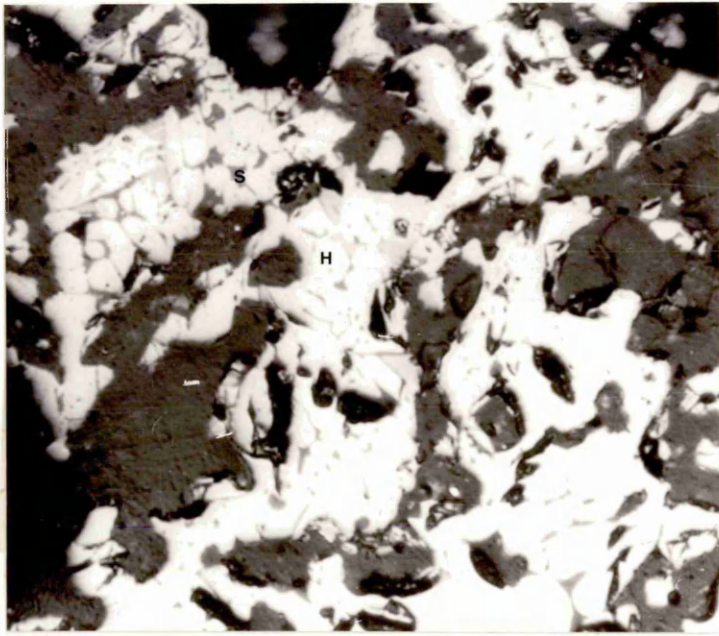


Plate 4

Partially Reduced Acid Pellet (44% Reduced) after Heating to 980°C in the Initial Melting Test, Showing Metallic Iron (I), Wustite (W) and the Slag Phase (S).  
Magnification x 1760

Plate 5

Partially Reduced Acid Pellet (44% Reduced) after Heating to 1075°C in the Initial Melting Test, Showing Metallic Iron (I), Wustite (W) and the Two Slag Phases (S<sub>1</sub> and S<sub>2</sub>).  
Magnification x 880

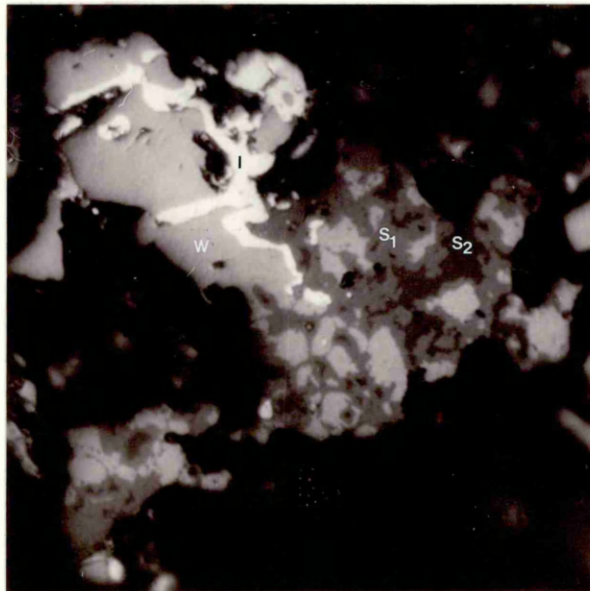
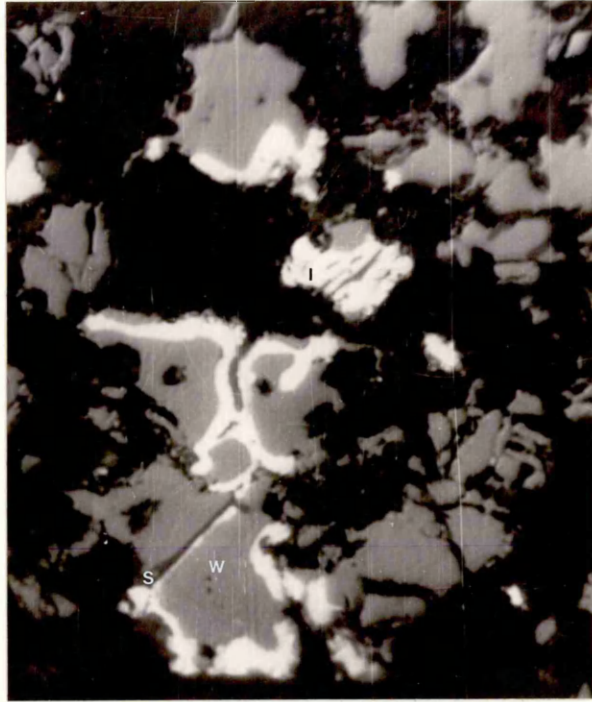


Plate 6     Synthetic Acid Pellets Manufactured from Reagent Grade  
Ferric Oxide and Silica Sand (Test Number S5) after  
Reduction at 950°C. Wustite (W) and Fayalite Slag  
Phase (S).  
Magnification x 880.

Plate 7     Synthetic Acid Pellets Manufactured from Malmberget  
Iron Ore and Silica Sand (Test Number S8) after  
Reduction at 950°C. Wustite (W) and Quartz Grains (Q)  
Magnification x 880.

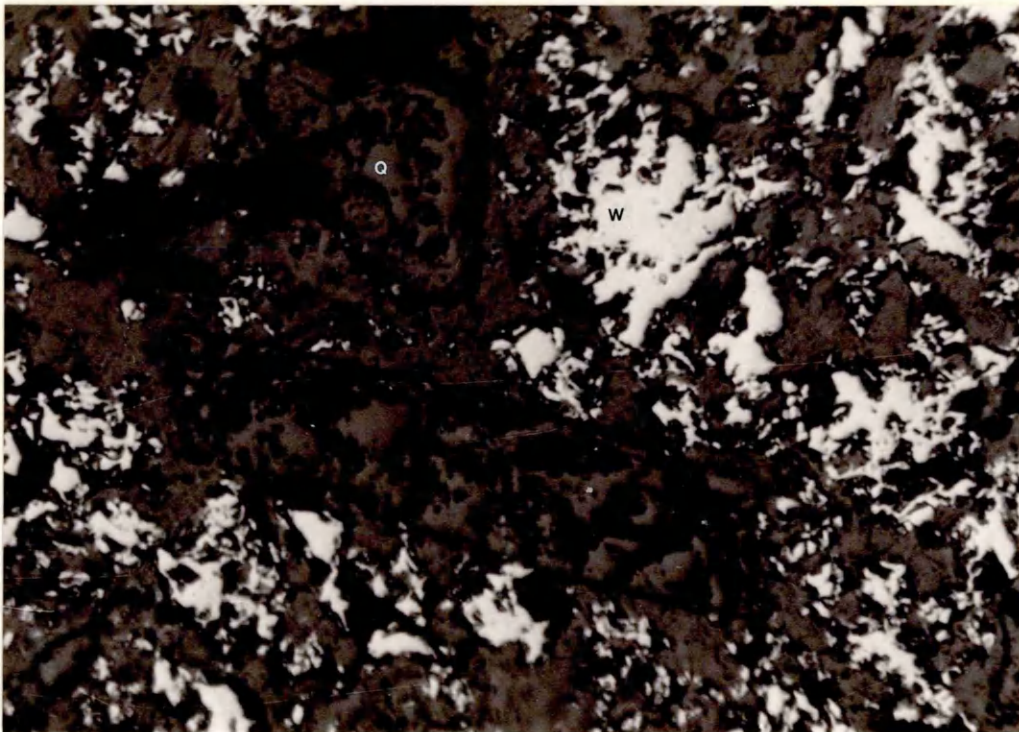
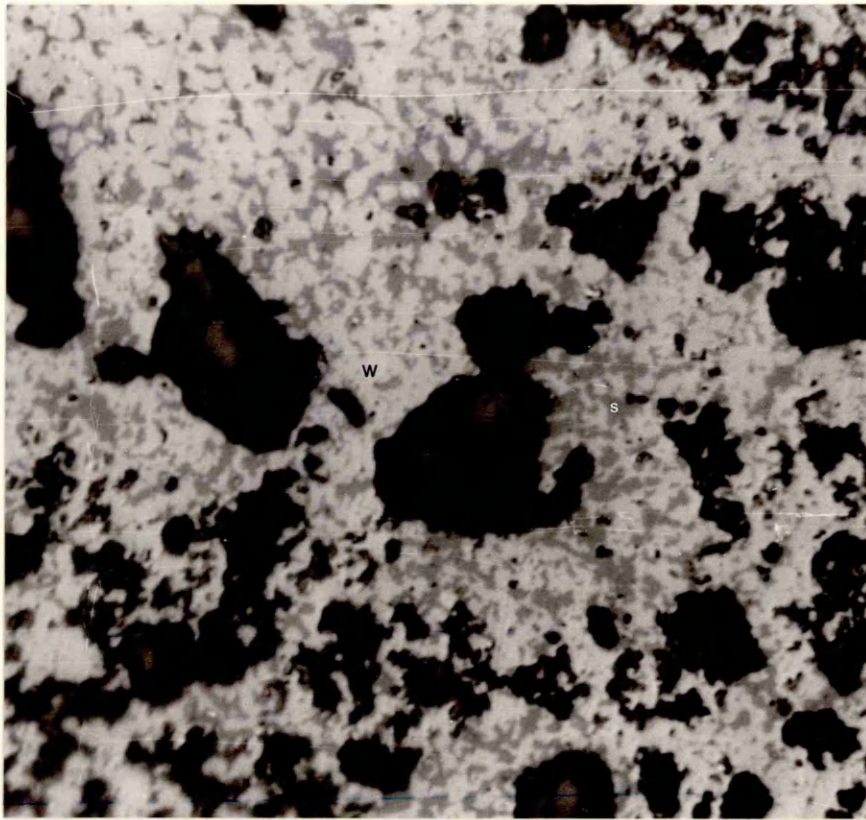


Plate 8     Synthetic Acid Pellets Manufactured from MalMBERGET  
Iron Ore and Bentonite (Test Number S9) in the  
Fully Oxidised State. Hematite (H) and Slag (S).  
Magnification x 880.

Plate 9     Synthetic Acid Pellets Manufactured from MalMBERGET  
Iron Ore and Bentonite (Test Number S9) after  
Reduction at 950°C. Wustite (W) and Slag Phases (S &  $\bar{S}$ )  
Magnification x 1760.

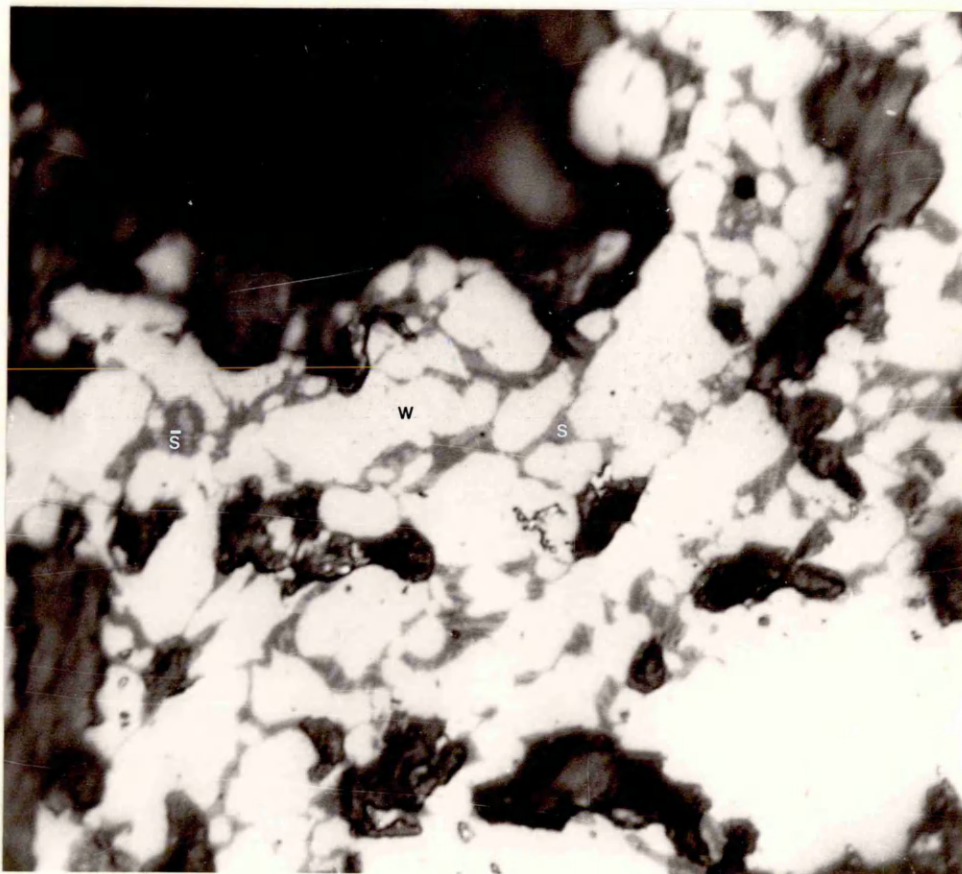
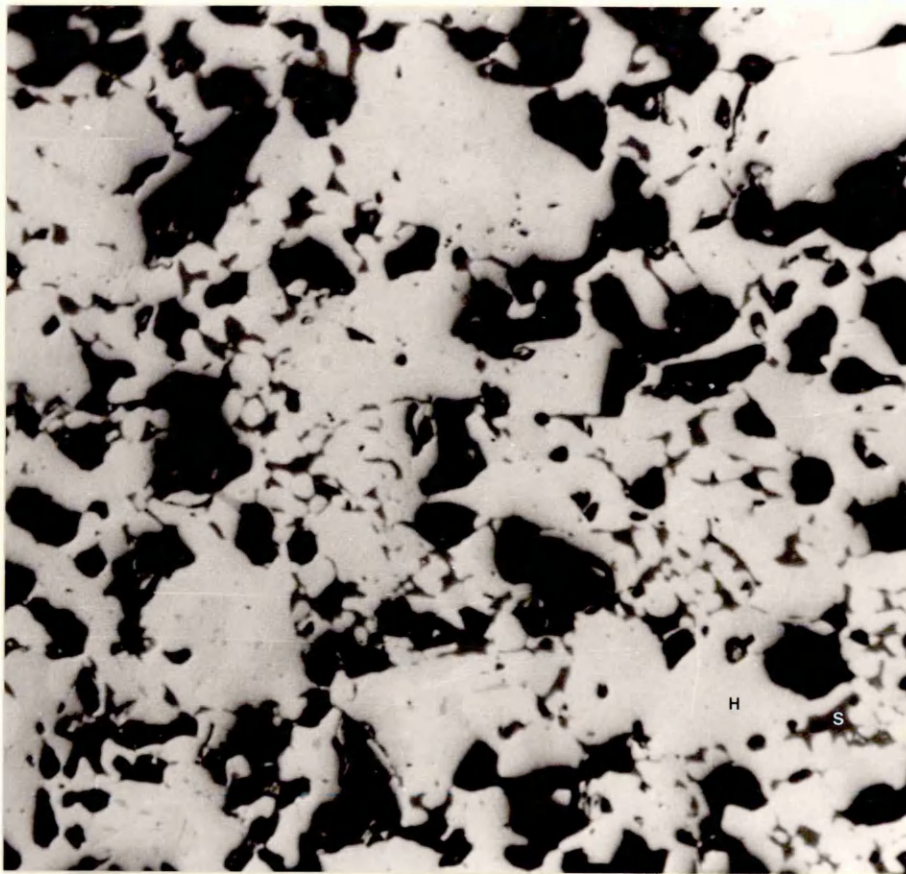


Plate 10 Contrast Between Sections Through the Sample Bed  
After the High Temperature Test. The Top Sample is  
a Semi-Reduced Sample (High Gas Pressure Drop  
Situation - Test Number 4) Whilst the Bottom Sample  
is a Virtually Fully Reduced Sample (Low Gas  
Pressure Drop Case - Test Number 2).

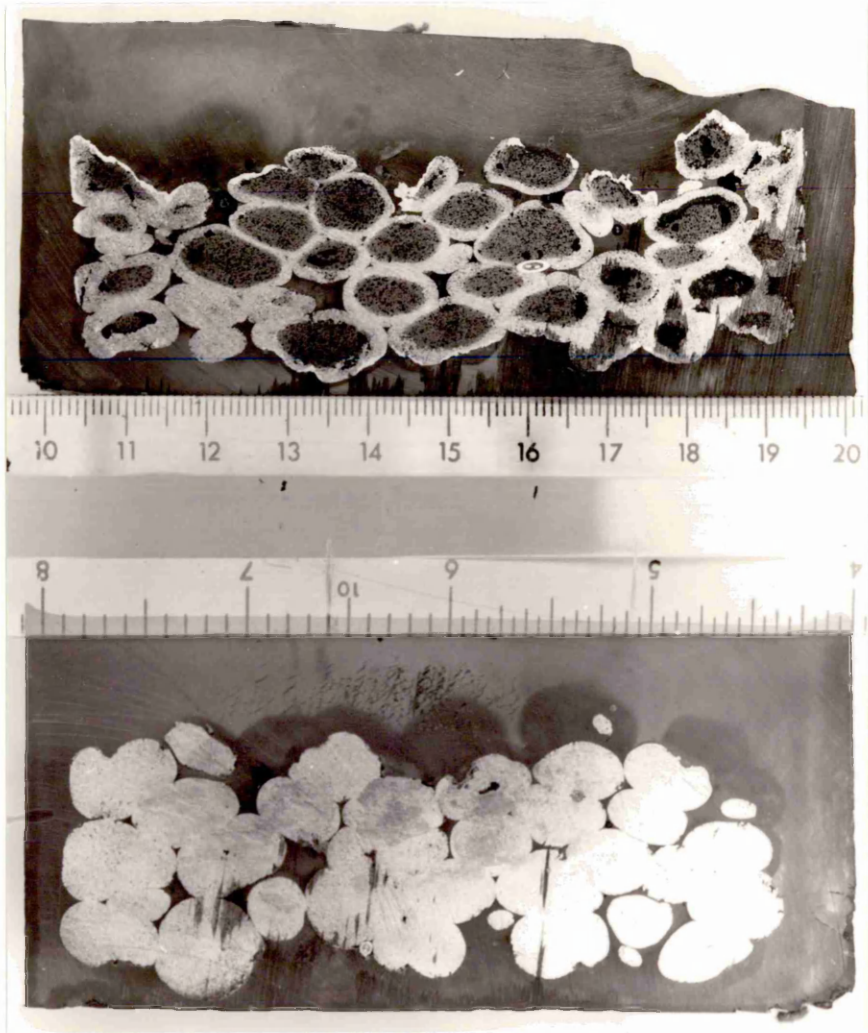


Plate 11 Section Through the Sample Bed after the High Temperature Test Following Pre-Reduction at 600°C (Test Number 13). Note the Dense Metallic Iron Shells. A Centimetre Rule is Included for Scale.

Plate 12 Icicles Which Dripped from a Bed of Acid Pellets During Commissioning Tests. A Centimetre Rule is Included for Scale.



Plate 13    Structure Near the Wall of an Icicle. The Metallic Iron Shell (I) can be Clearly Distinguished on the Left. A Feathery Alumino Silicate Precipitate (F) and Olivine Crystals (O) are Precipitated in the Slag Phase.  
Magnification x 220.

Plate 14    Central Region of an Icicle Showing Olivine Crystals (O) Precipitated Within the Slag Phase. Some Grains of Metallic Iron are also Visible (I).  
Magnification x 220.

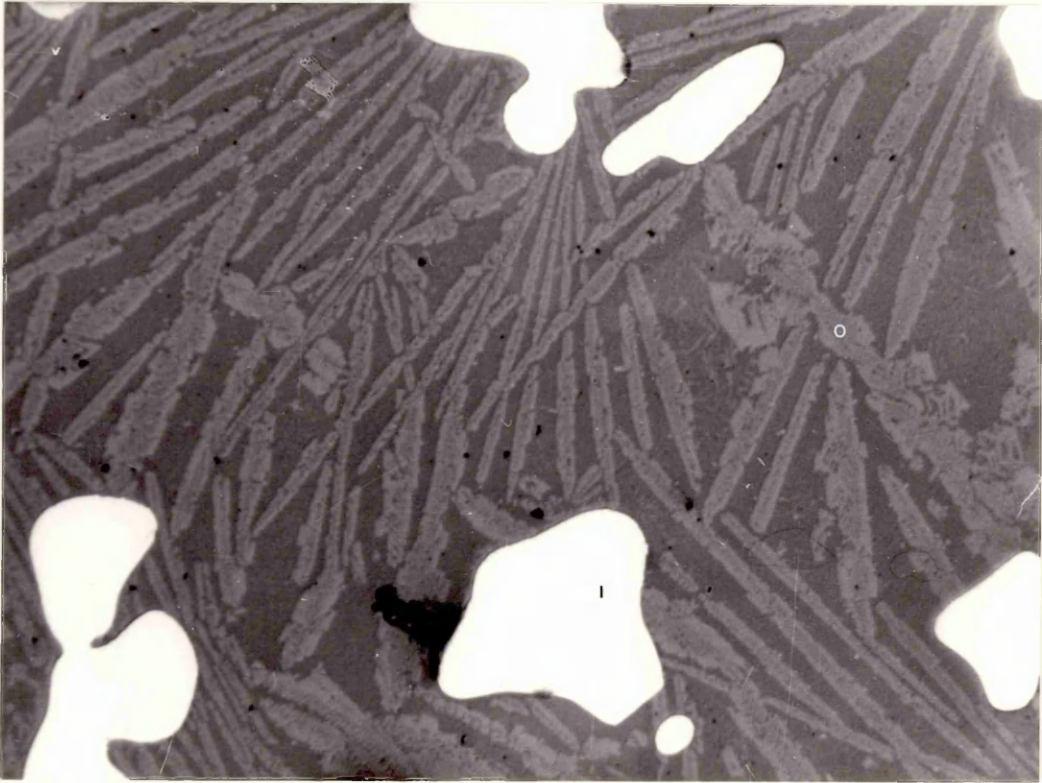
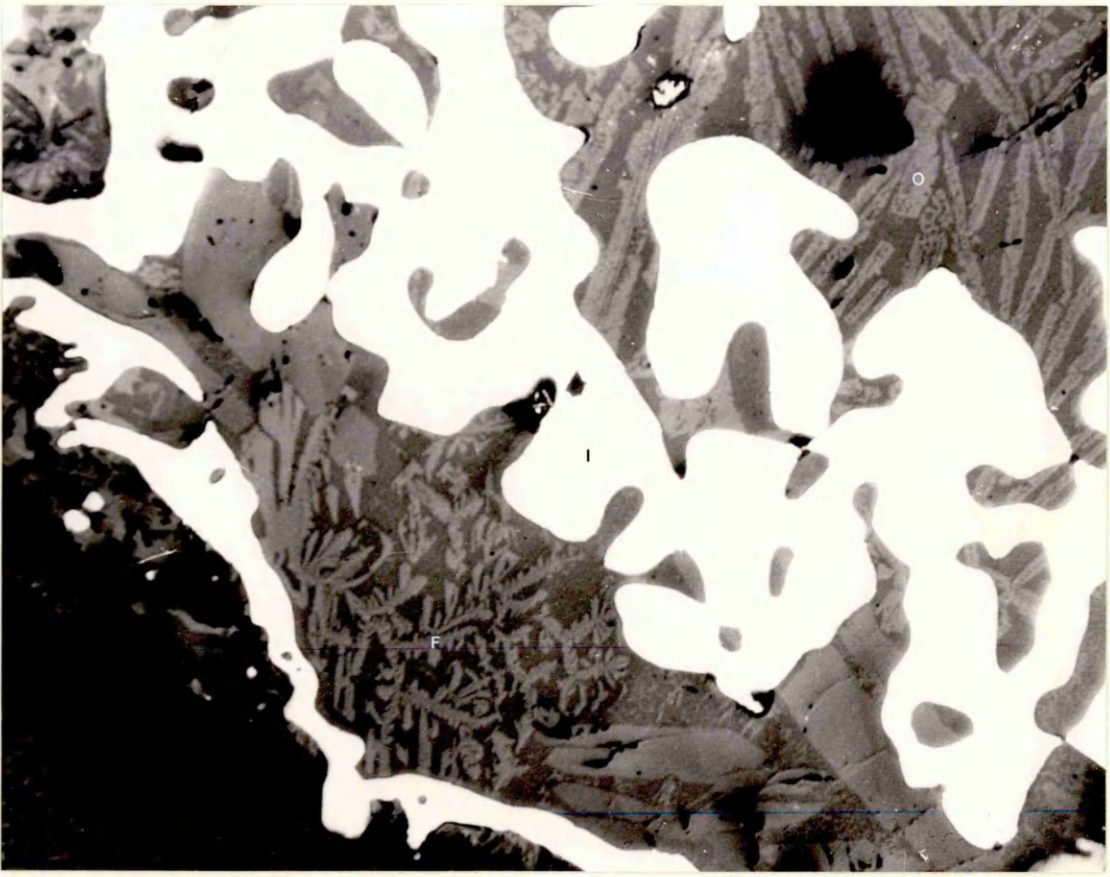


Plate 15    Region Near the Wall of an Icicle Showing Grains of Quartz (G) Precipitated in the Slag Phase and the Iron Shell (J).  
Magnification x 880.

Plate 16    Structure of the Metallic Iron in an Icicle after Etching in 2% Nital Showing Dark Thin Needles of Iron Nitride.  
Magnification x 880.



Plate 17 Dropped Material from One of the Sulphur Tests  
(Test Number 17).  
Magnification x 2.



Plate 18 Dropped Material from One of the Sulphur Tests  
(Test Number 17). Two Slag Phases are Visible  
(R and Y) Along with Grains of Ferrous Sulphide (T).  
Magnification x 880.

Plate 19 Dropped Material from One of the Sulphur Tests  
(Test Number 17). The Fe-S-O Eutectic Phase is  
Clearly Visible, Covering the Majority of the Plate.  
Some Metallic Iron Grains are Prominent in the Bottom  
Right Hand Corner (T).  
Magnification x 880.

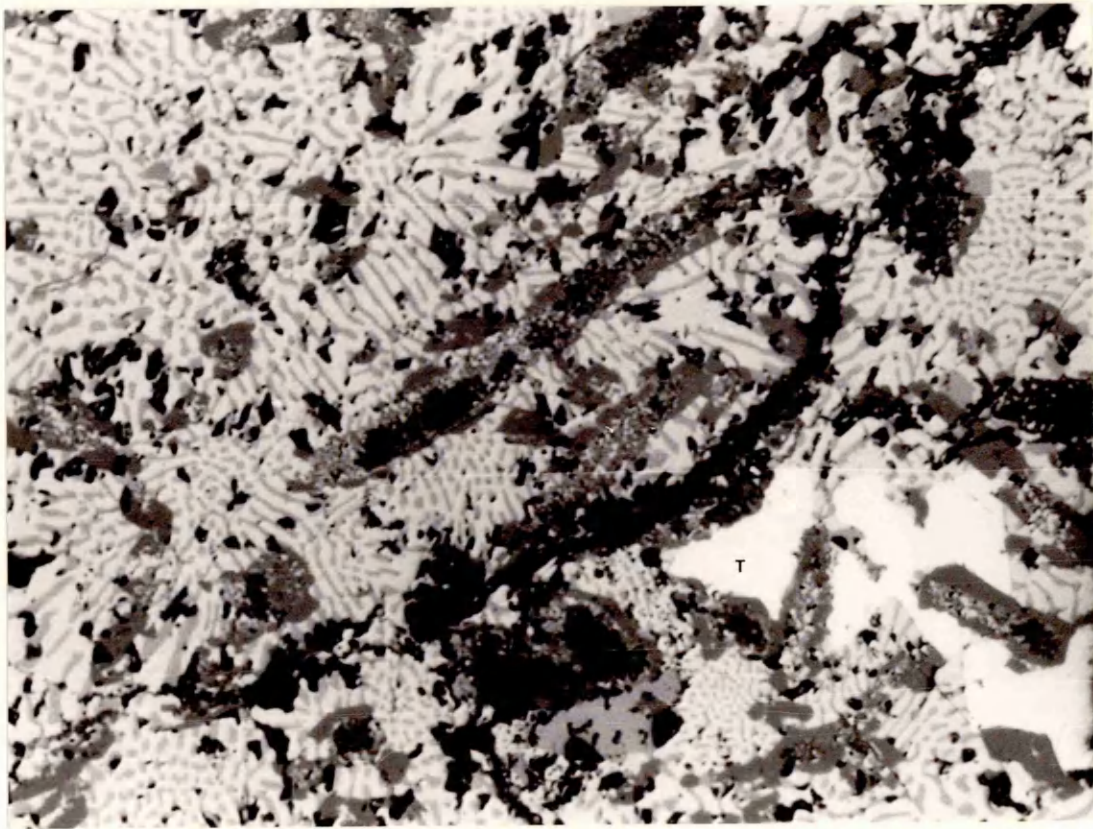
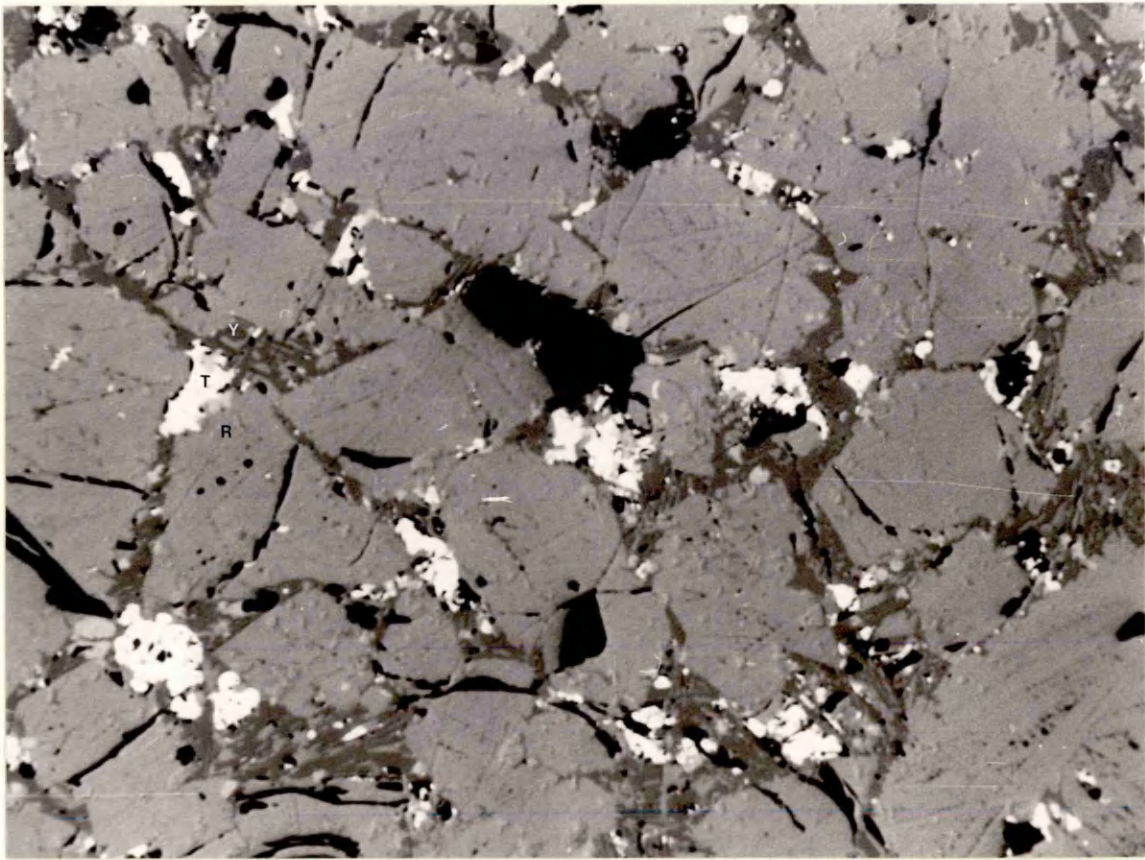


Plate 20 Surface Layers of Virtually Fully Reduced Acid Pellets after the High Temperature Test. (Sample Taken from Test Number 2). A Grain of Quartz (Q) is Visible within the Metallic Iron Grains (G).  
Magnification x 880.

Plate 21 Pellet Core of Virtually Fully Reduced Pellets after the High Temperature Test (Test Number 2). A Distinct Silicate Phase (P) can be seen between the Metallic Iron Grains (G).  
Magnification x 1760.

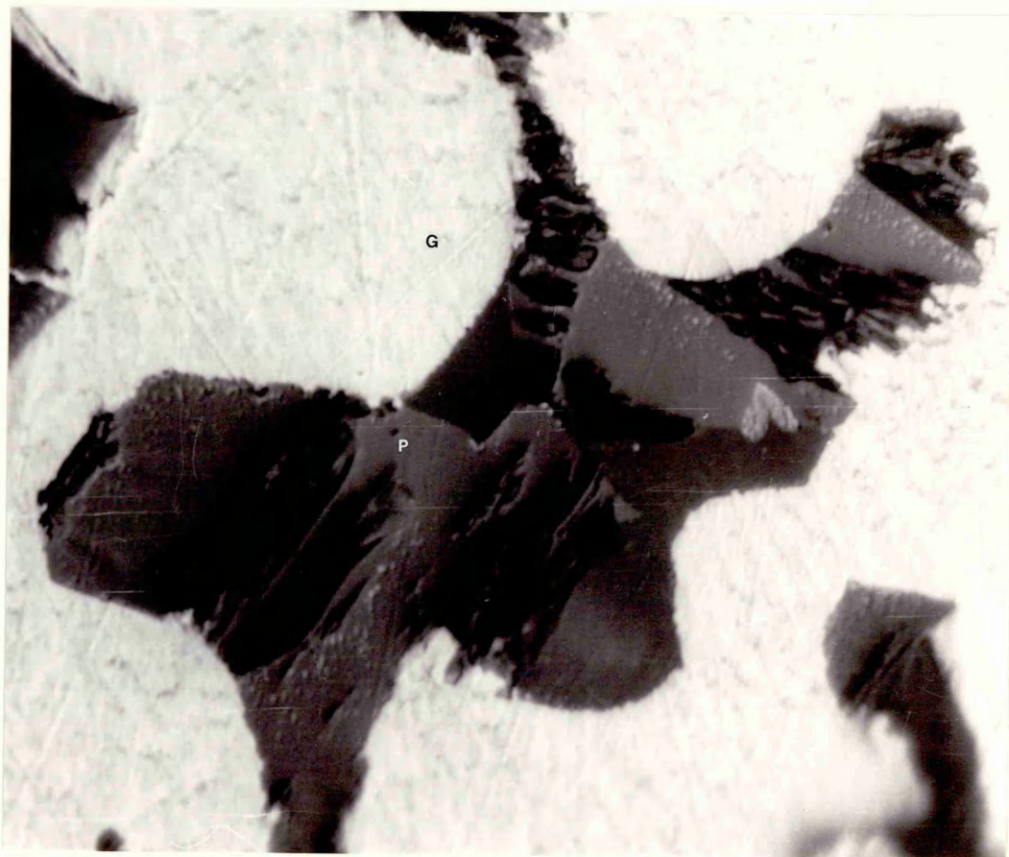
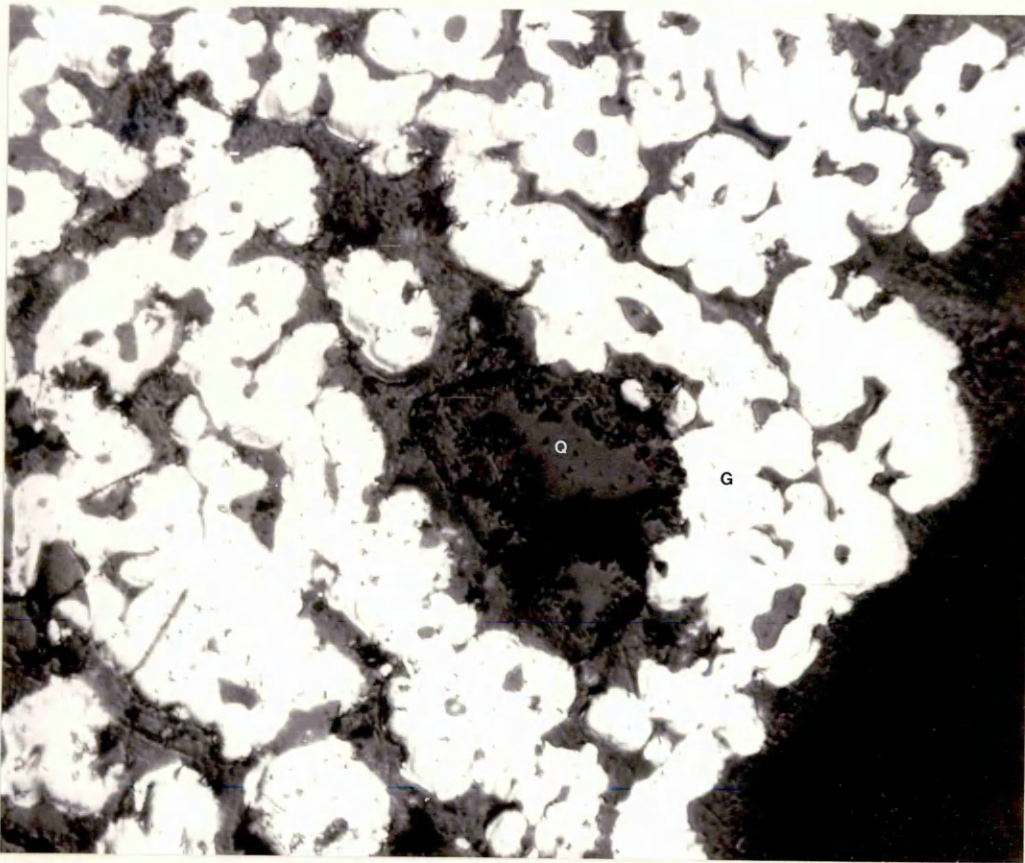


Plate 22 Virtually Fully Reduced Acid Pellets after the High  
Temperature Test (Test Number 2) Showing the Void  
between two Pellets and some Slag (S).  
Magnification x 220.



Plate 23    Slag Attacking a Quartz Grain in Acid Pellets  
During the High Temperature Test (Test Number 2).  
Quartz Grain (Q), Slag (S) and Metallic Iron Grains (G)  
Magnification x 880.

Plate 24    Structure of the Metallic Iron Grains in an almost  
fully Reduced Acid Pellet after the High Temperature  
Test (Test Number 2) after Etching in 2% Nital.  
Dark Needles of Iron Nitride are Visible in the  
Grains of Iron (White).  
Magnification x 880.

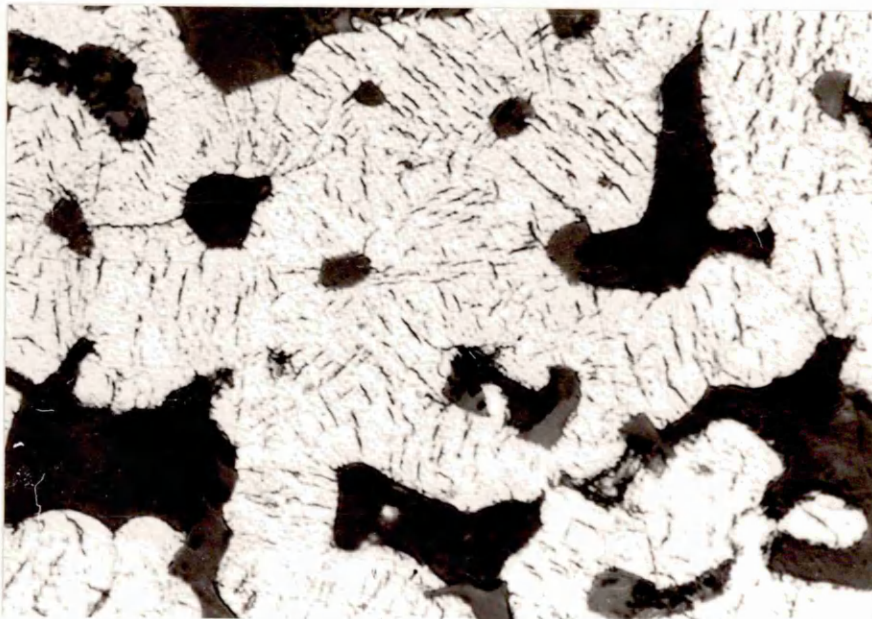
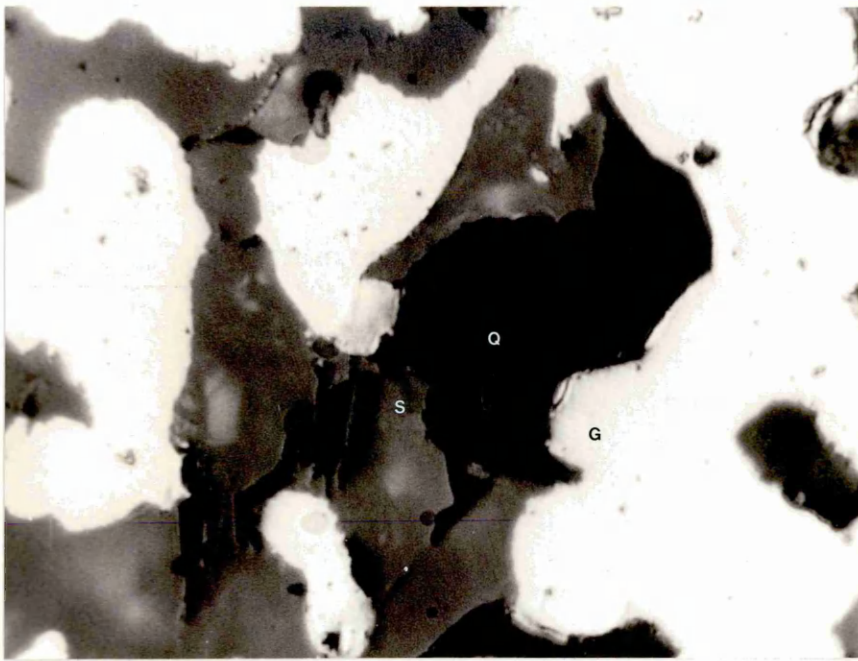


Plate 25 Pellet Core of a Semi-Reduced Acid Pellet after the  
High Temperature Test (Test Number 4) Showing  
Wustite Grains (W), Slag (S), Metallic Iron (M) and  
Voids (V).  
Magnification x 880.

Plate 26 Void between two Semi-Reduced Acid Pellets after the High Temperature Test (Test Number 4). Escape of Slag (S) into the Void is Clearly Visible. Metallic Iron Grains (M) and Dendrites of Wustite (D).  
Magnification x 220.

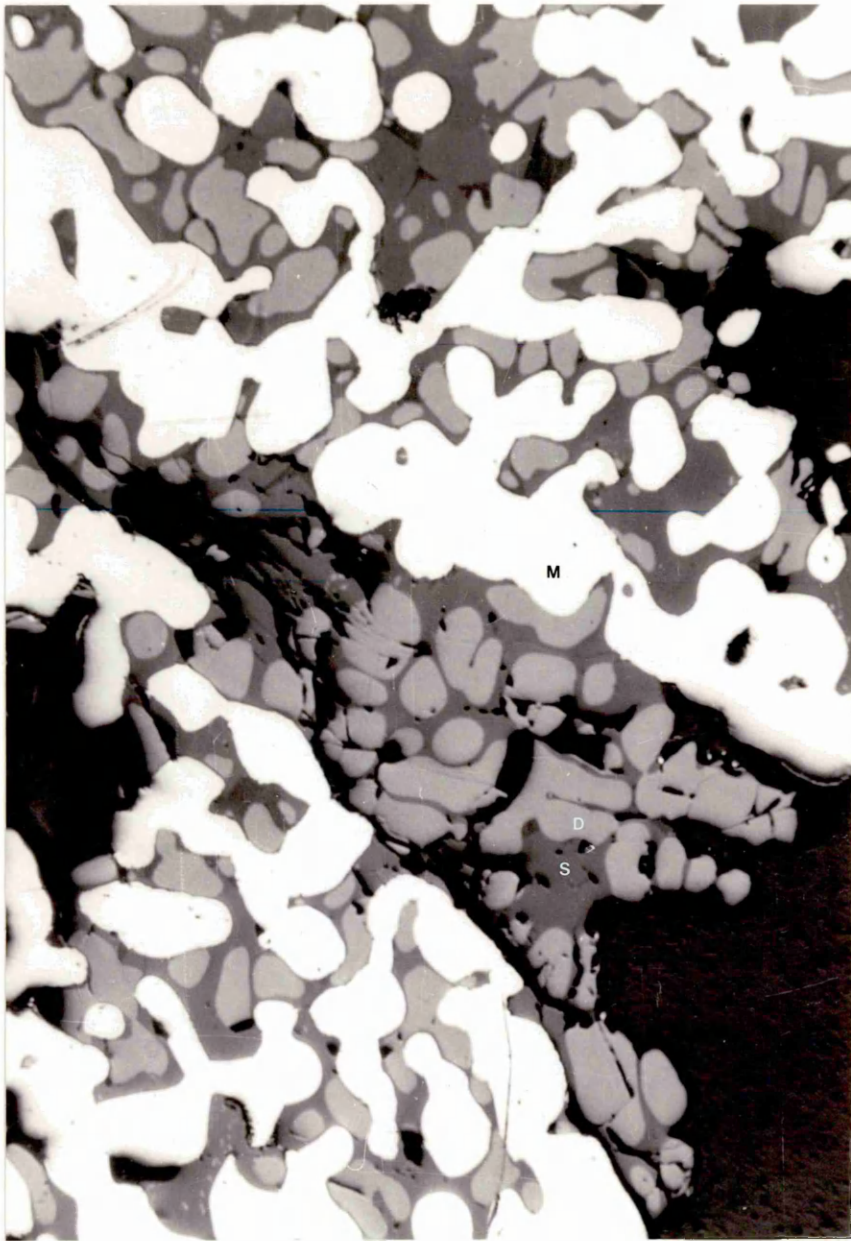


Plate 27    Semi-Reduced Acid Pellets after the High Temperature  
Test (Test Number 3) Showing Wustite (W), Slag (S)  
and Incompletely Formed Metallic Iron Grains  
(Mottled Appearance).  
Magnification x 220.

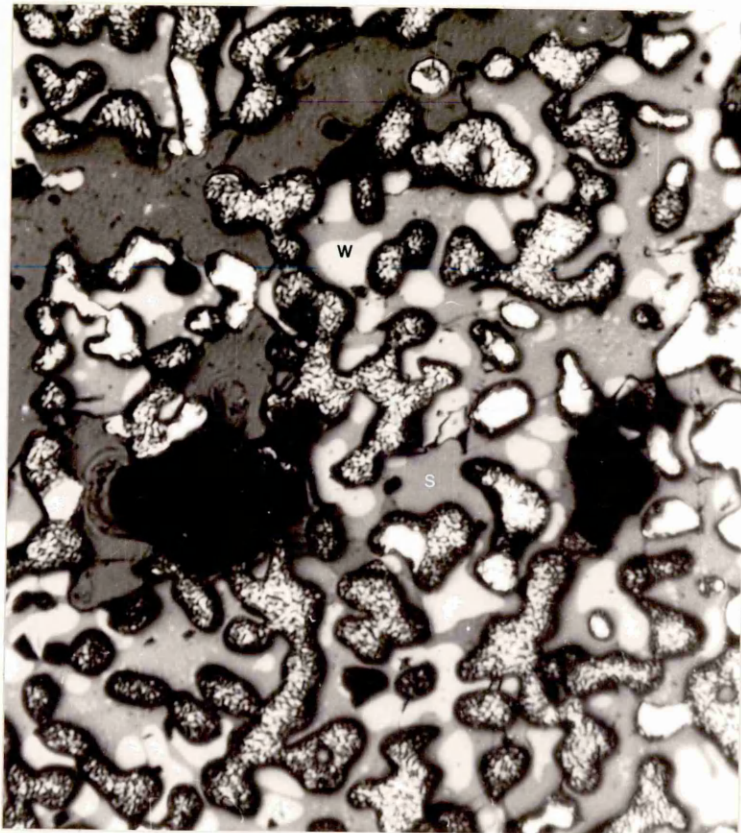


Plate 28 Acid Pellets after the High Temperature Test Showing Slag (S) Advancing Through a Reduced Region Towards the Pellet Surface. (Test Number 7). The Slag is Advancing Right to Left in the Photograph. Wustite (G) and Metallic Iron Grains (M).  
Magnification x 220.

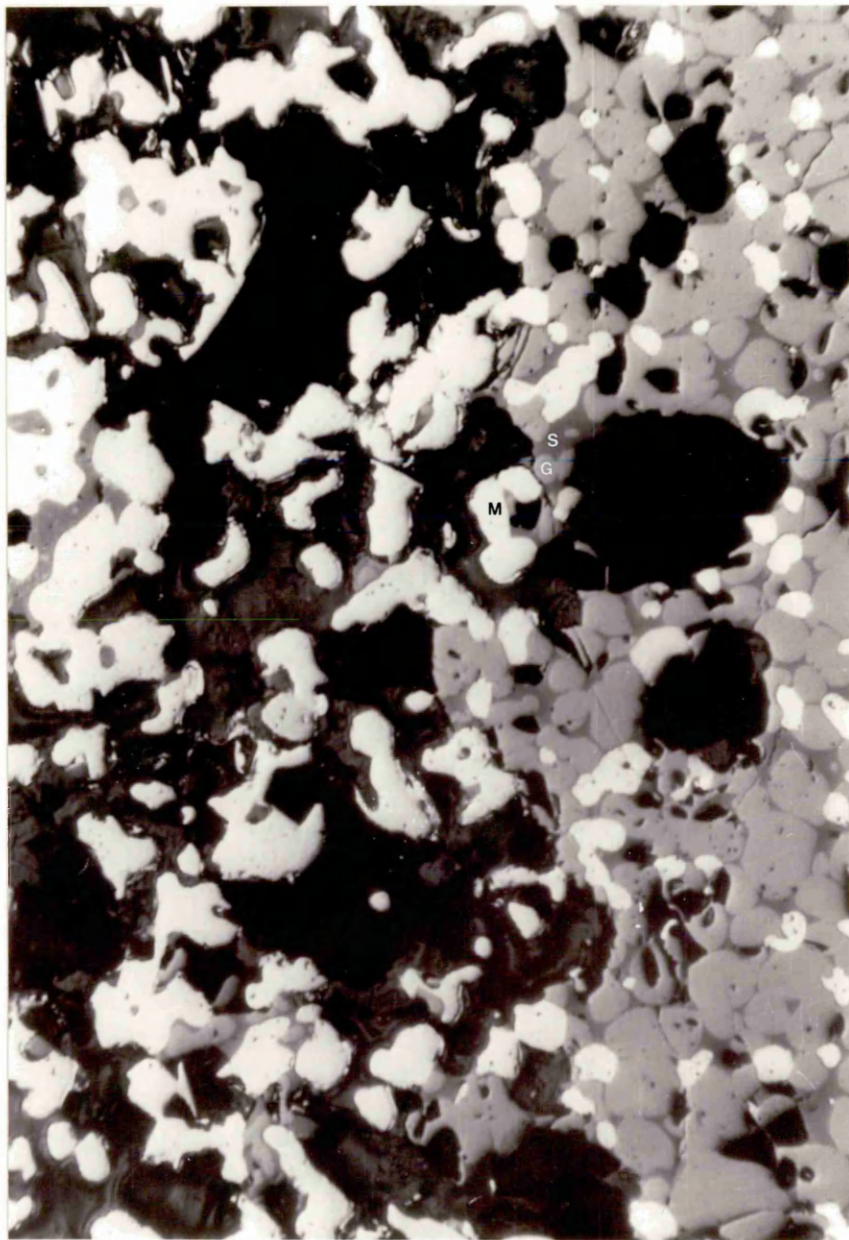


Plate 29 Solidified Molten Iron in Semi-Reduced Acid Pellets  
after the High Temperature Test (Test Number 4)  
Showing Cementite (C) at the Boundaries of the Iron  
Grains (F).  
Magnification x 220.

Plate 30 Solidified Molten Iron, after Etching in 2% Nital,  
in Semi-Reduced Acid Pellets after the High  
Temperature Test (Test Number 4) showing Cementite  
(C) and the Pearlite Eutectoid (E). Note this is  
not identical to the Region Shown in Plate 29, but  
in the same location.  
Magnification x 220.

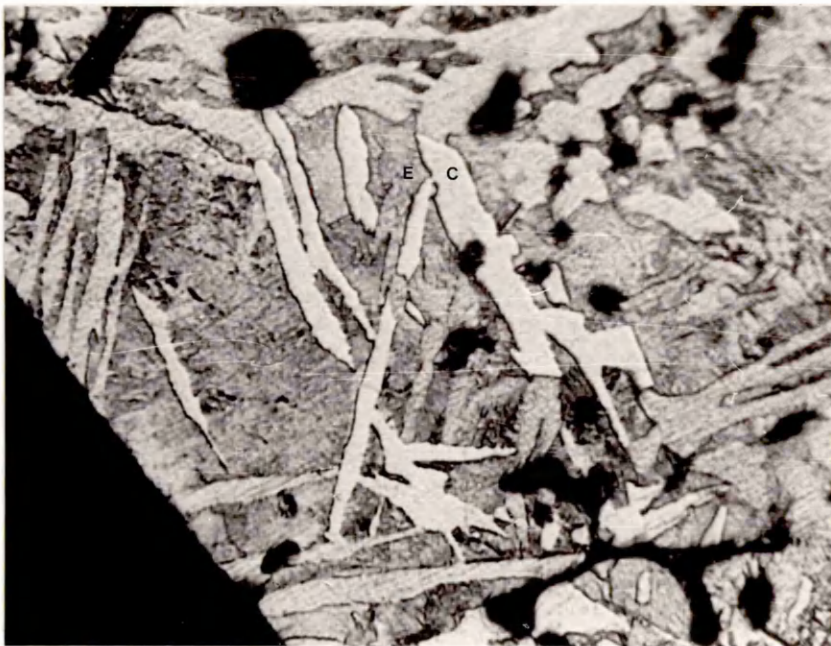
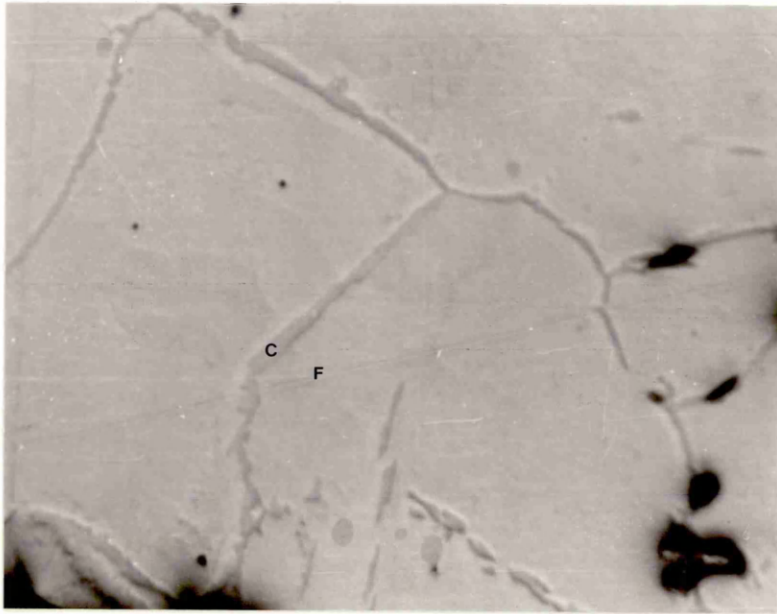


Plate 31    Core of the Acid Pellets, Pre-Reduced at 600°C,  
after the High Temperature Test (Test Number 13).  
Note the large amount of porosity (V) and the small  
quantity of Slag (S) amongst the Wustite Grains (W).  
Magnification x 220.

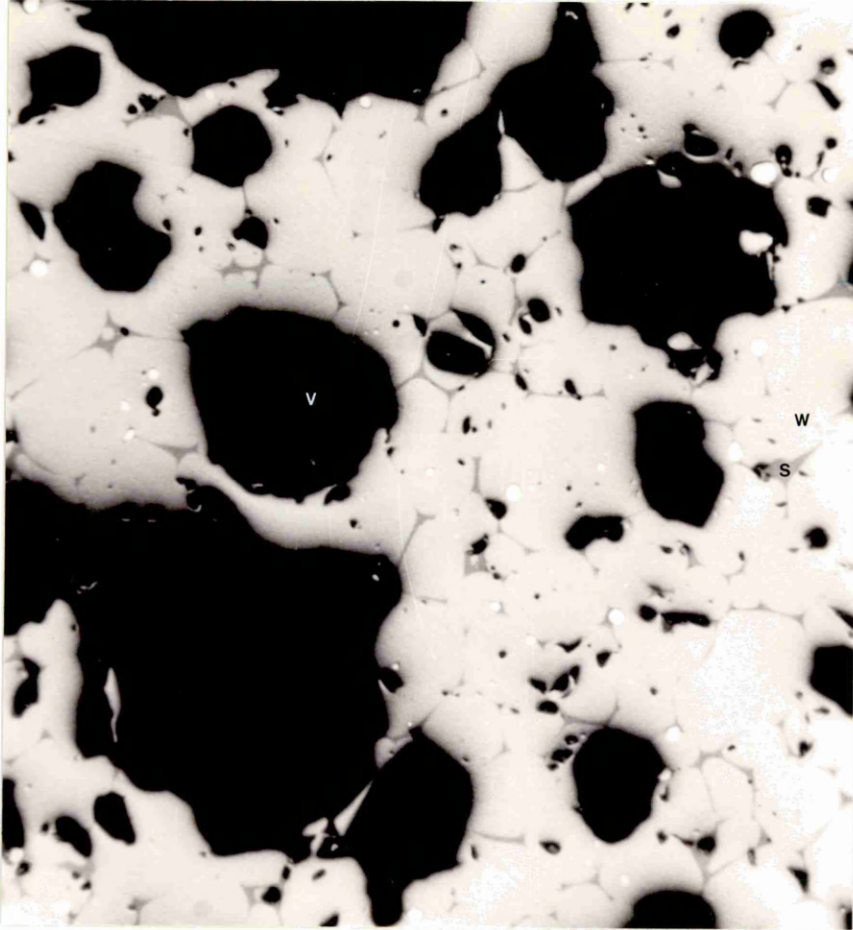


Plate 32 Surface of the Acid Pellets, Pre-Reduced at 600°C,  
after the High Temperature Test (Test Number 13)  
showing escape of Slag into the Void between two  
Pellets. Wustite Dendrites (D), Metallic Iron (M),  
Slag Phases (S and T).  
Magnification x 220.

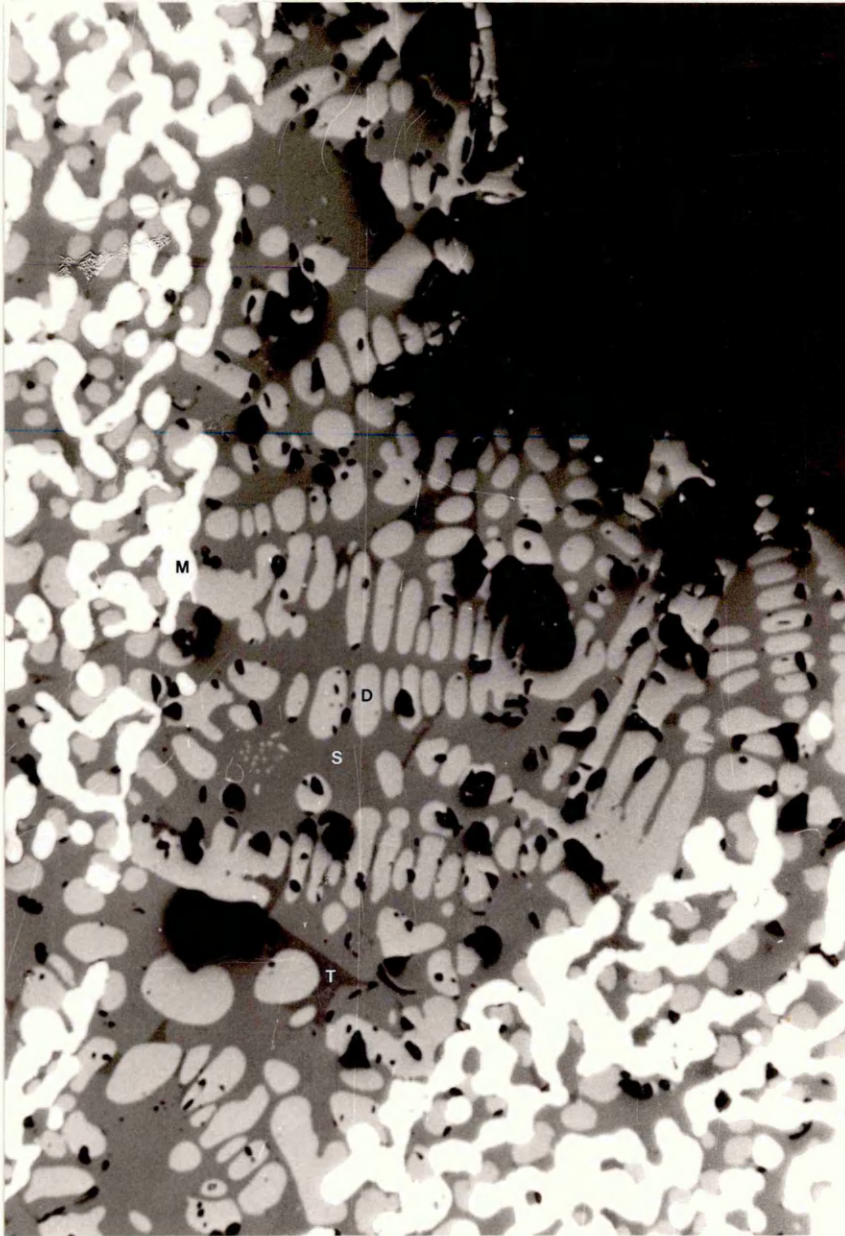


Plate 33    Acid Pellets after the High Temperature Test with Sulphur Addition (Test Number 15) Showing Metallic Iron (A), the Fe-S-O Eutectic Phase (E), Wustite (R) and two Slag Phases (T and U).  
Magnification x 1760.

Plate 34    Void between two Acid Pellets after the High Temperature Test with Sulphur Addition (Test Number 17). . Two Slag Phases (S and T) can be seen exuding from the Pellet surfaces, indicated by the Grains of Metallic Iron (B).  
Magnification x 220.

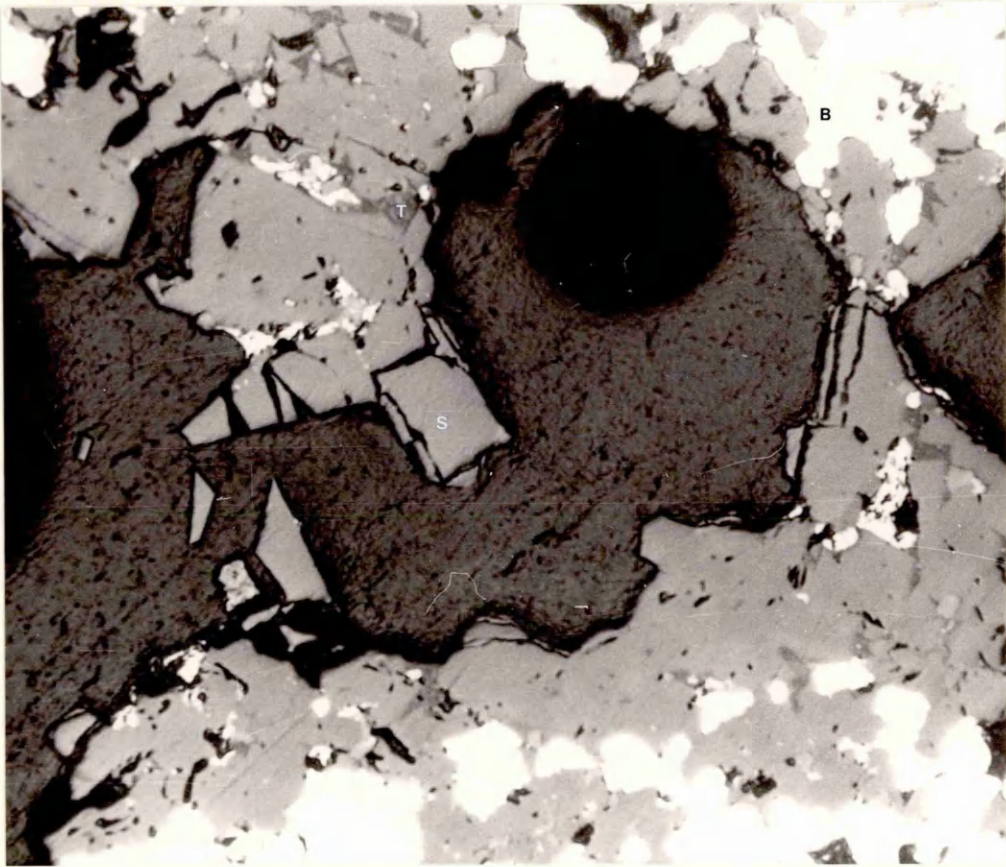
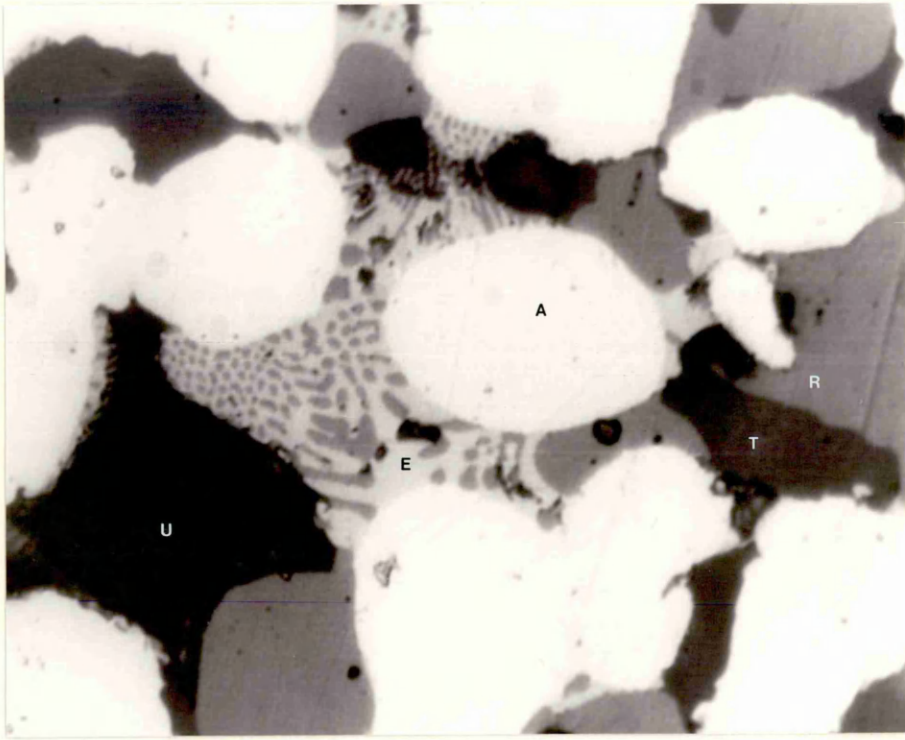


Plate 35(A)      Surface of Acid Pellets after the High Temperature  
Test with Alkali Vapour (Test Number 20).      Note  
the relative fineness of the Metallic Grains  
(white).      Also noticeable is the Olivine Crystals  
(O) precipitated in the Slag Phase between two  
Pellets along with the Dendrites of Wustite (D).  
Magnification x 220.

Plate 35(B)      Surface Layer of an Acid Pellet after the High  
Temperature Test (Test Number 4) without Alkali  
Vapour.      Note the relative coarseness of the  
Metallic Iron Grains (white).  
Magnification x 220.

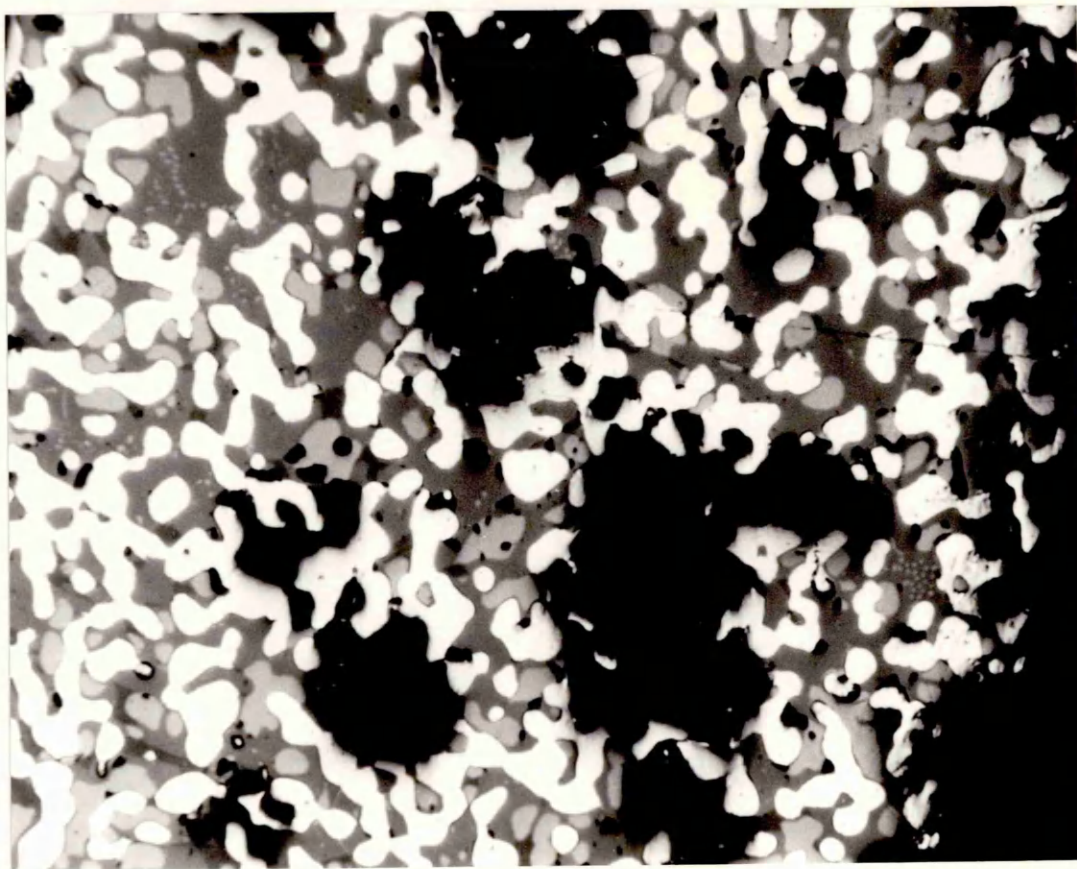


Plate 36 Semi-Reduced acid pellets after the interrupted high temperature test (Test Number 21) with alkali vapour.  
Note the non topochemical reduction mode. Wustite (W) and Metallic Iron (A).  
Magnification x 220.

Plate 37 Core of an acid pellet after the high temperature test (Test Number 20) with alkali vapour. Note the thin needle-like precipitates (N) in the Slag (P). Wustite (R)  
This particular structure was only observed at the highest alkali loading, at lower levels of addition the trend towards this structure was evident.  
Magnification x 220.

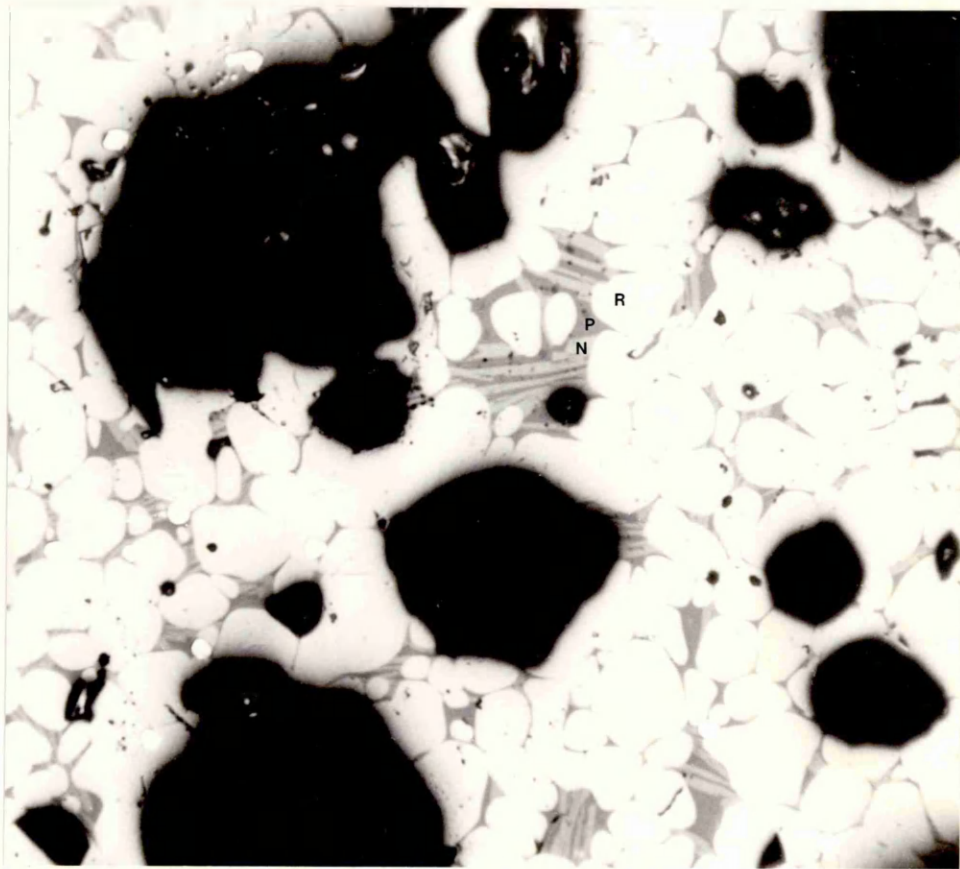
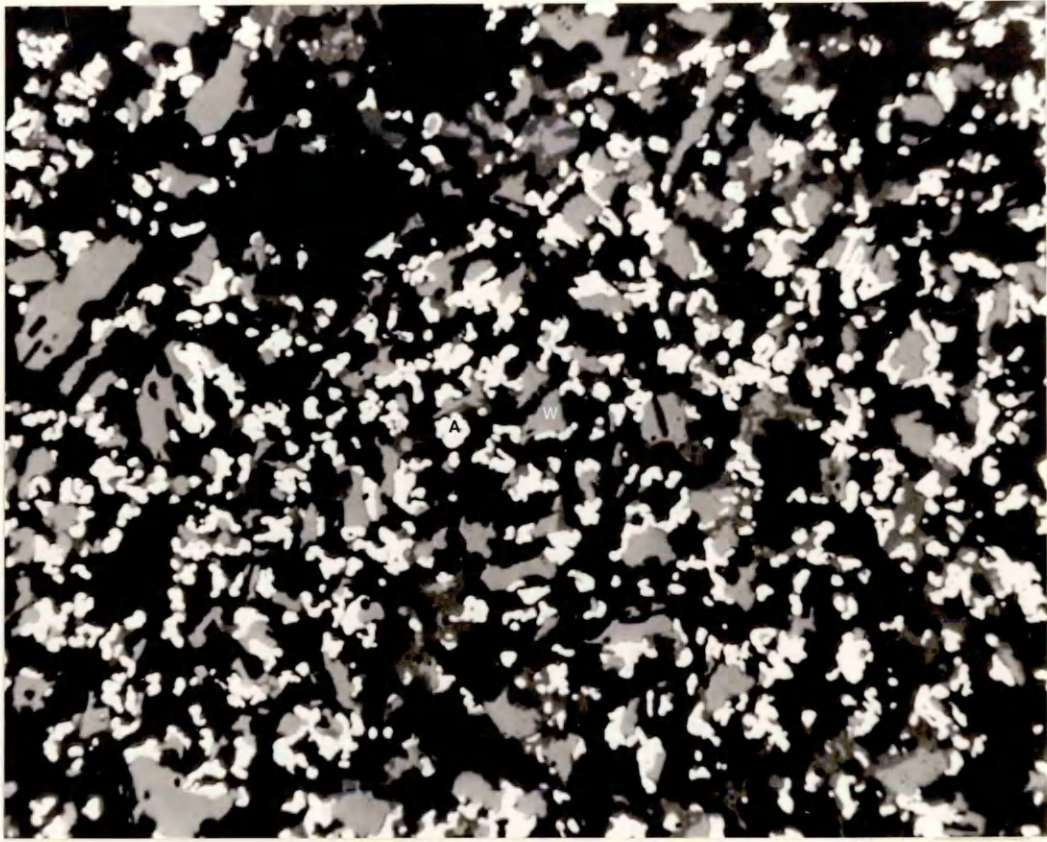


Plate 38 Partially reduced 1.8 CaO/SiO<sub>2</sub> sinter after the initial melting test showing melting of the semi-reduced calcium ferrites (C) and grains which were originally magnetite in the as-received state (R). Note that the latter shows no sign of melting.  
Magnification x 1760.

Plate 39 Partially reduced 1.4 CaO/SiO<sub>2</sub> sinter after heating to 1100°C in the initial slag formation test showing the wustite grains (G) being attacked by a slag phase (S). Iron grains (F).  
Magnification x 880.

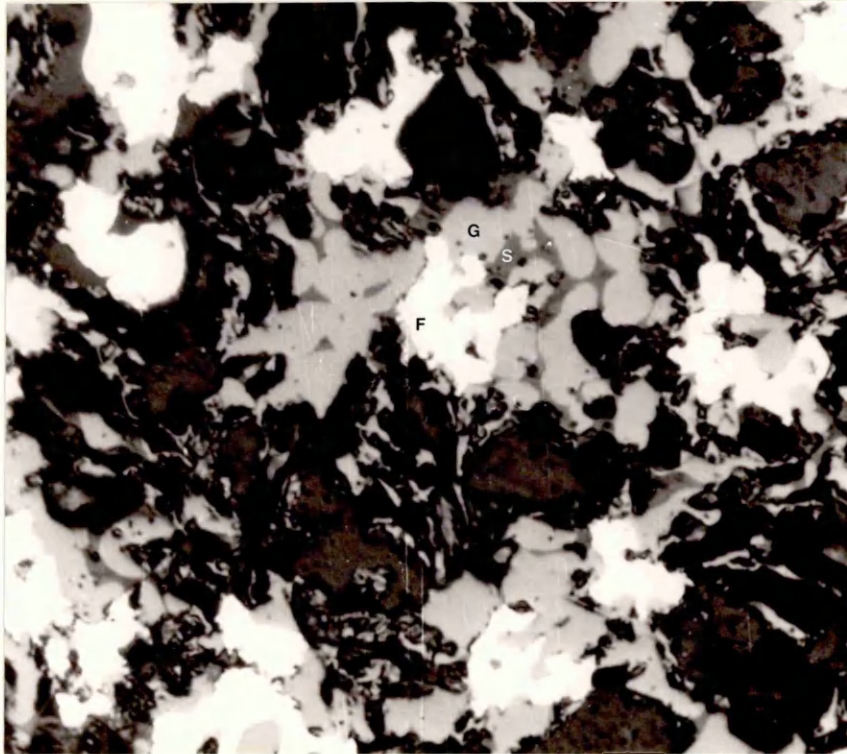
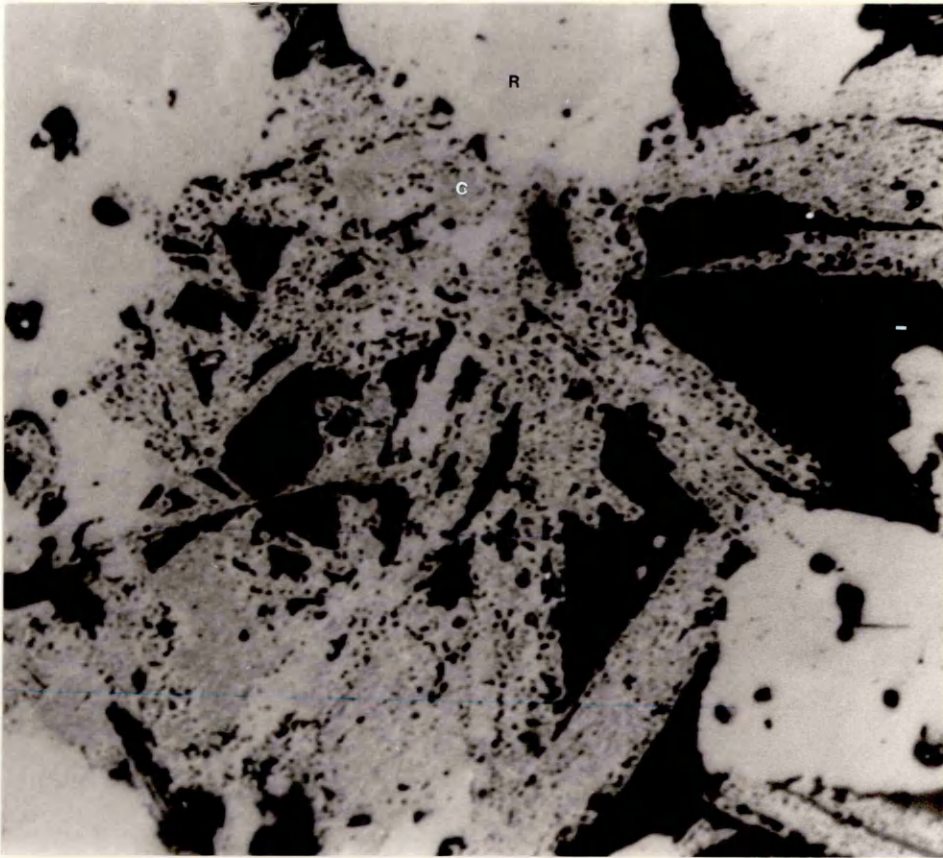


Plate 40 Surface of a sinter which displayed a high gas pressure drop during the high temperature test (Test Number 24).  
Note the slag (H) and wustite (W) filling the pores between the metallic iron grains (E).  
Magnification x 880.

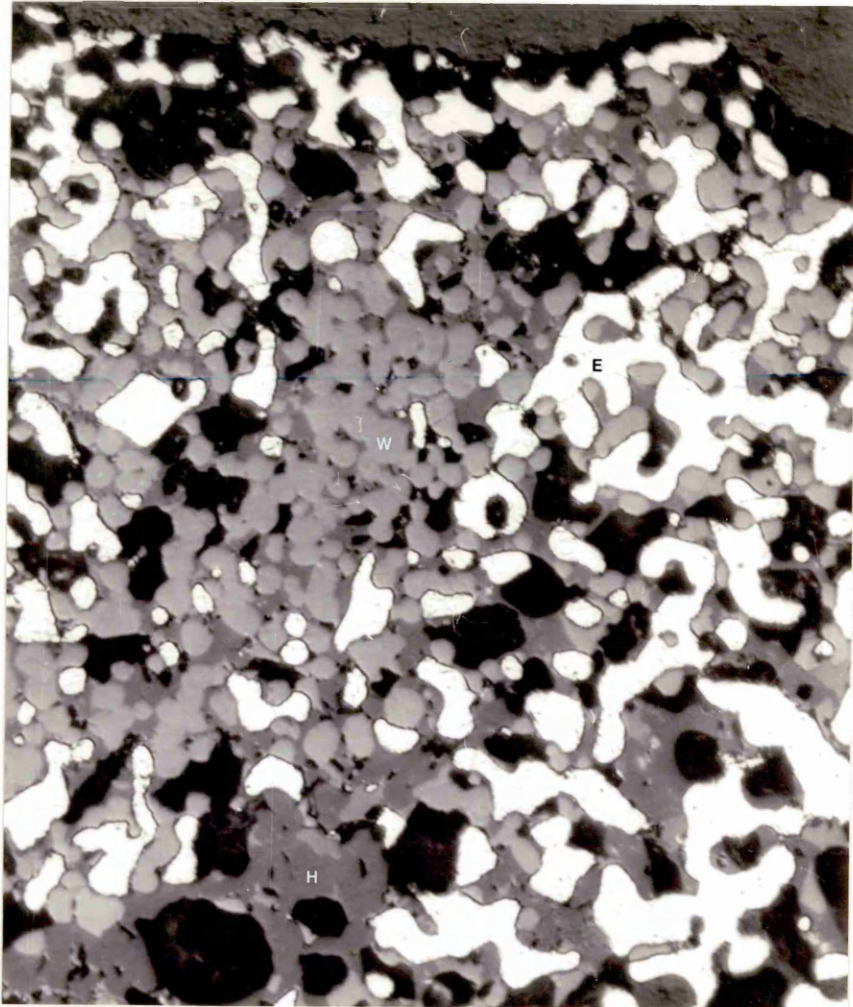


Plate 41 Core of an acid pellet in a sinter/pellet mixture  
after the high temperature test (Test Number 41)  
showing Wustite (T), Slag (S), Iron (V) & Voids (Black).  
Magnification x 220.

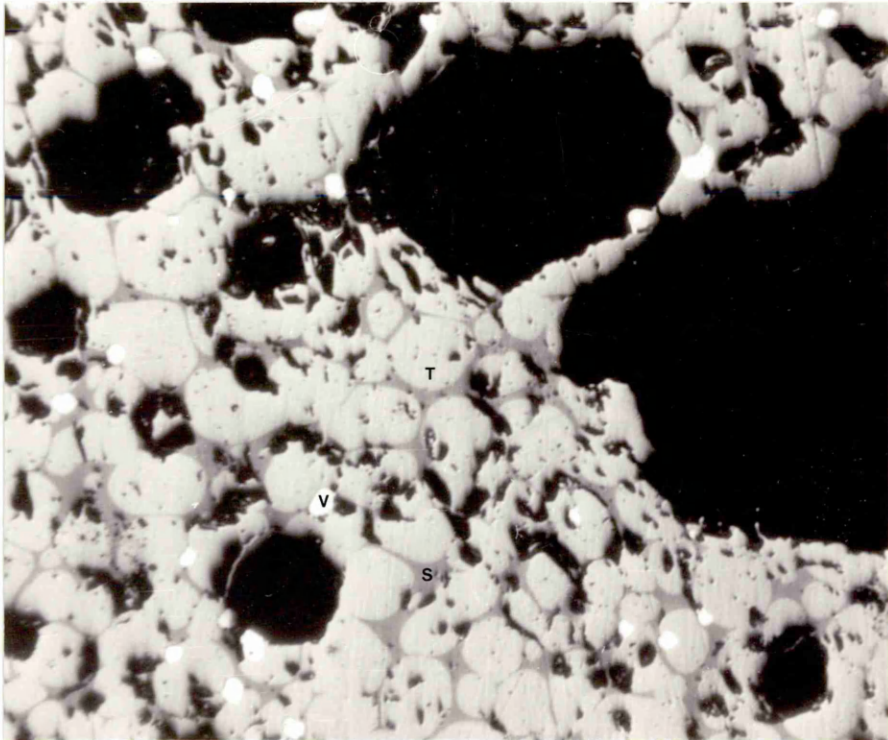


Plate 42 Well-reduced sinter particle in a sinter/pellet mixture after the high temperature test (Test Number 41) showing Slag (S) from the acid pellets advancing (from bottom right) through pores. Metallic iron in the sinter (H).  
Magnification x 220.

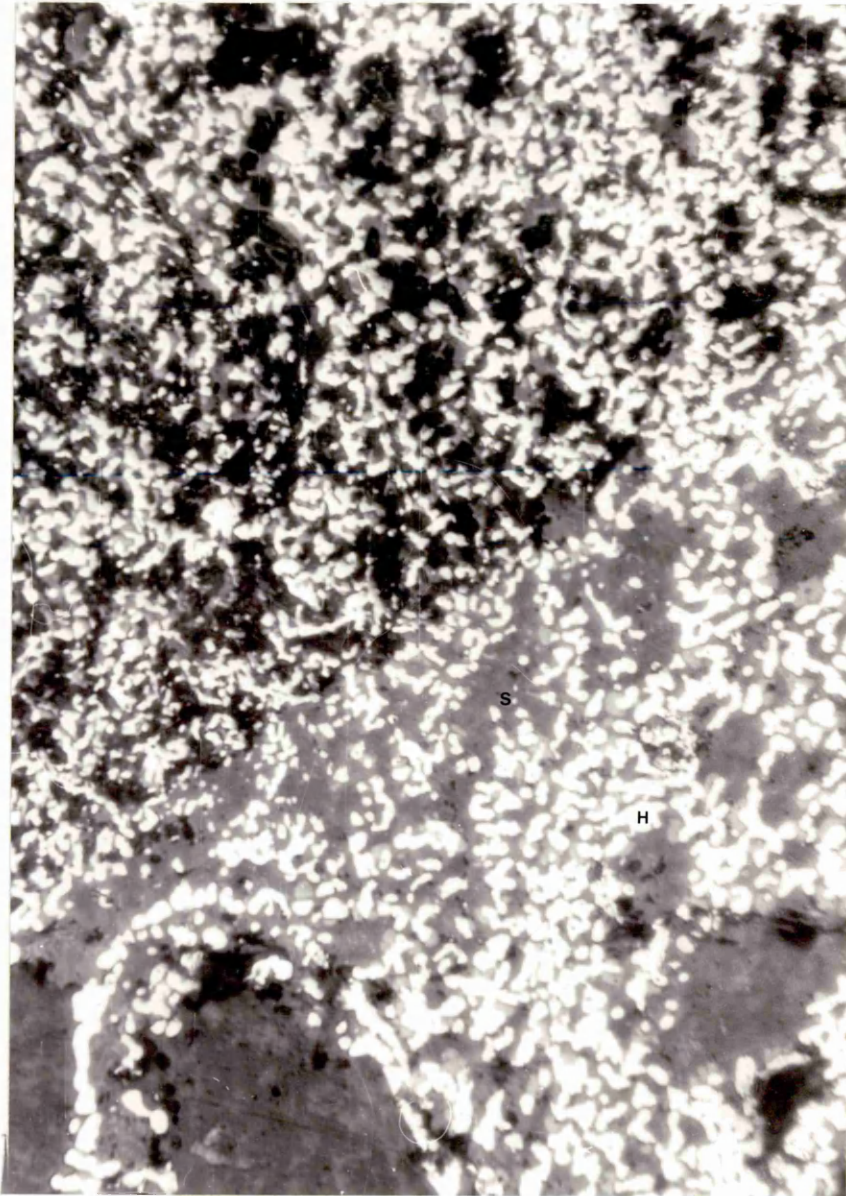


Plate 43 EDAX spectrum of the  
slag phase in fully  
oxidised pellets

Plate 44 EDAX spectrum of the  
main slag phase in  
partially reduced acid  
pellets (sample from  
initial melting test  
with 44% reduced pellets  
after heating to 980°C)

Plate 45 EDAX spectrum of the  
minor slag phase in  
partially reduced acid  
pellets (same sample  
as Plate 44)

Plate 46 EDAX spectrum of  
olivine crystals in  
the icicles

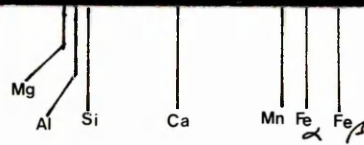
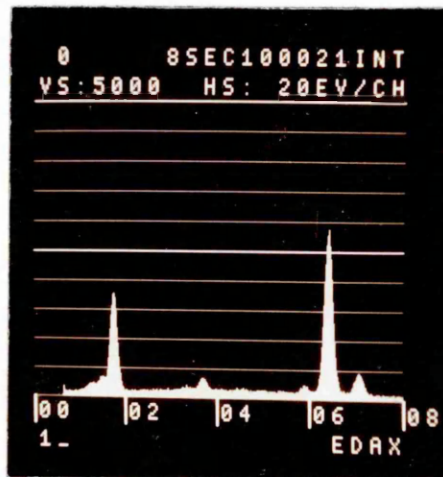
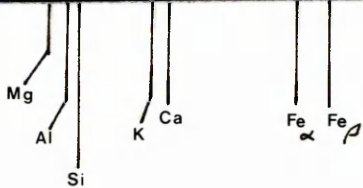
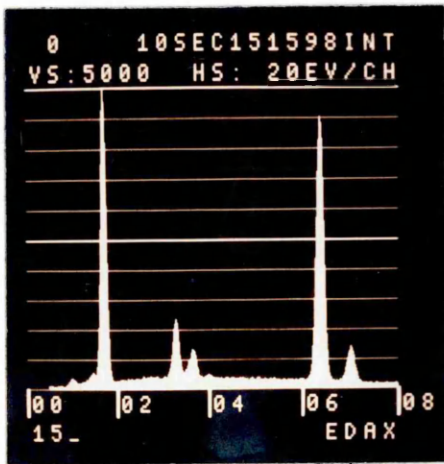
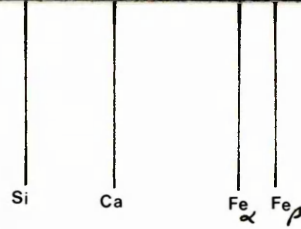
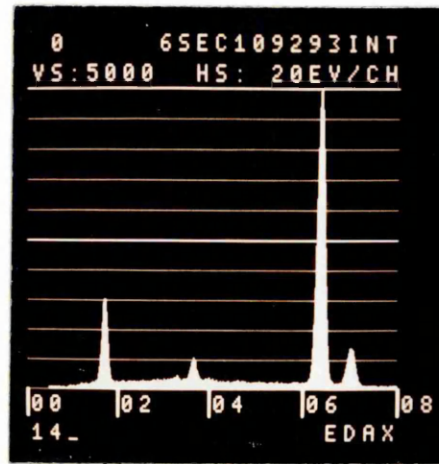
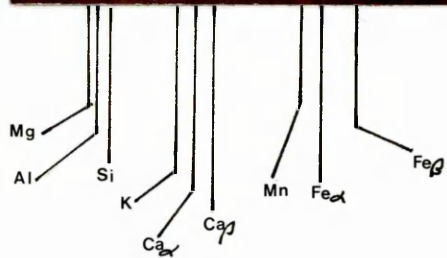
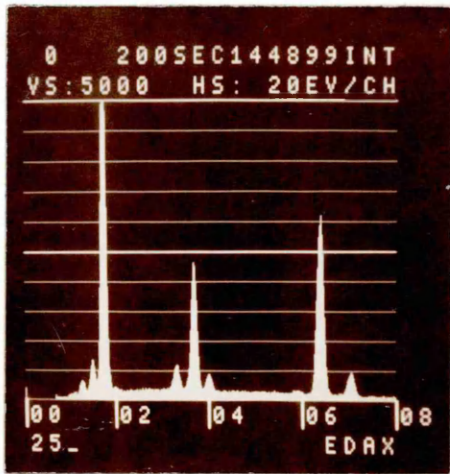
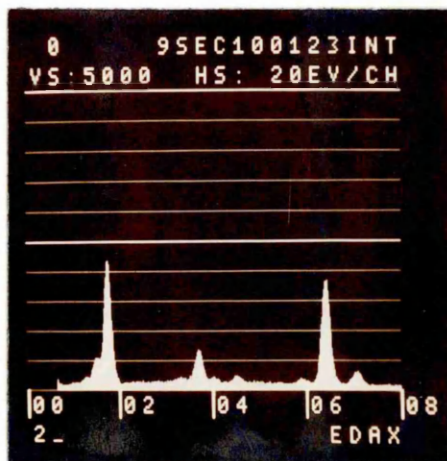


Plate 47 EDAX spectrum of the slag surrounding the olivine crystals in the icicles

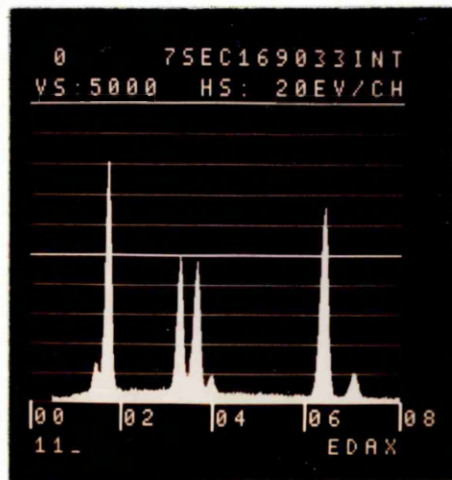
Plate 48 EDAX spectrum of the thin needle-like grains precipitated in the slag phase of acid pellets after a high temperature test with alkali vapour (Test Number 20)

Plate 49 EDAX spectrum of the olivine crystals precipitated in the slag phase of acid pellets after a high temperature test with alkali vapour (sample from same test as Plate 48).

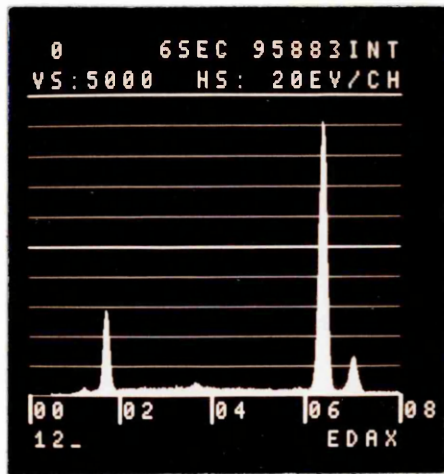
Plate 50 EDAX spectrum of the slag phase in acid pellets after the high temperature test with alkali vapour (sample from same test as Plates 48 and 49).



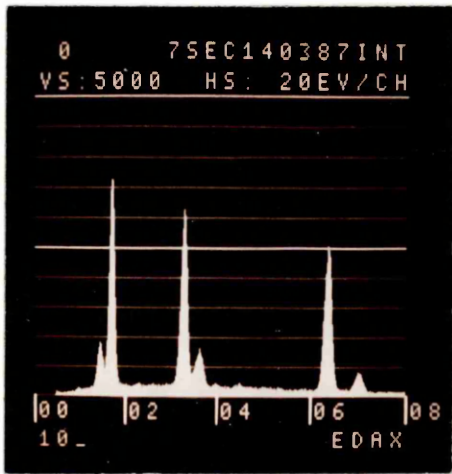
Al  
Si  
Ca  
Ti  
Mn  
Fe $\alpha$  Fe $\beta$



Al  
Si  
K $\alpha$   
K $\beta$   
Ca $\alpha$  Ca $\beta$   
Fe $\alpha$  Fe $\beta$



Mg  
Si  
Ca  
Fe $\alpha$  Fe $\beta$



Al  
Si  
K $\alpha$   
K $\beta$   
Fe $\alpha$  Fe $\beta$

## APPENDIX I

### EXPERIMENTAL ERRORS IN THE HIGH TEMPERATURE TEST PROCEDURE

The aim of this section is to highlight the sources of experimental error existing in the high temperature test procedure and to assess their influence upon the results obtained.

#### 1. Measurement of Sample Bed Temperature

The thermocouples used were of the inconel sheathed chromel/alumel variety having an accuracy of  $\pm 3^{\circ}\text{C}$  between 0 and  $400^{\circ}\text{C}$ . Above  $400^{\circ}\text{C}$  the accuracy was  $\pm \frac{1}{4}\% ^{\circ}\text{C}$ . Normally  $1200^{\circ}\text{C}$  is the limit of operation for thermocouples of this type, but in the experimental study this range was extended up to  $1350^{\circ}\text{C}$  in some instances, which produces an error of  $\pm 10^{\circ}\text{C}$  at  $1350^{\circ}\text{C}$ . Although reducing gas affects the calibration of chromel/alumel thermocouples<sup>1</sup>, this was not thought to be a major source of error because new thermocouples were used for each test. In the tests, which were terminated because of thermocouple failure, it was found that failure was caused by the thermocouples interacting either with the upper coke layer or the sulphur in the reducing gas. However, when sulphur was present in the gas, failure always coincided with the rapid rise in gas pressure drop which necessitated discontinuation of the test anyway.

A great deal of time and effort was expended ensuring that the temperature gradient within the sample bed was kept to a minimum. During commissioning of the high temperature apparatus a temperature difference of  $50^{\circ}\text{C}$  was obtained between

the top and bottom of the bed, but by adjusting the position of the individual 'turns' of the induction coil on a 'trial and error' basis this unacceptable temperature difference was reduced significantly. Another problem was that the samples from the commissioning tests displayed a large degree of surface melting created by the heating influence of the induction coil, but this was virtually eliminated by adjustment of the coil. The net result was that at the  $400^{\circ}\text{C}.\text{hr.}^{-1}$  heating rate the maximum temperature difference between the top and bottom of the bed was  $15^{\circ}\text{C}$ , although variation during a test and between individual tests occurred. The most likely causes of the variation were (a) channelling of the gas through the sample bed and (b) movement of the thermocouples into and out of small temperature gradients within the bed height as the sample was compressed. A check on the temperature profile across the bed was carried out and provided the temperature was measured within a distance, equivalent to one pellet diameter, from the crucible wall, then the temperature lay within the temperature range existing between the top and bottom of the bed. At a heating rate of  $200^{\circ}\text{C}.\text{hr.}^{-1}$  the temperature difference between the top and bottom of the bed was less than the  $15^{\circ}\text{C}$  found at the faster heating rate, probably due to the bed being closer to equilibrium conditions.

Finally, for control purposes the thermocouple at the bottom of the sample bed was used to monitor the heating rate for every test, but the temperature documented in the results is the average of that measured by the thermocouples at the top and bottom of the bed.

## 2. Applied Load and Sample Bed Contraction Measurement

The load on the sample bed was imposed by means of a pneumatic cylinder and the gas pressure, within the cylinder,

necessary to produce the required applied load on the sample bed was calculated with the following formula:-

$$P_r = P_p \cdot \frac{A_p}{A_r} \quad [1]$$

where,

$P_r$  = Pressure required to be exerted on sample bed,  $\text{k N.m}^{-2}$

$P_p$  = Gas pressure acting on piston of pneumatic cylinder,  $\text{k N.m}^{-2}$

$A_p$  = Area of piston exposed to pressurised gas,  $\text{m}^2$

$A_r$  = Area of ram pressing on sample bed,  $\text{m}^2$

Measurement of the gas pressure in the pneumatic cylinder was by means of a pressure gauge accurate to  $\pm 1\%$ .

Friction between the ram and the walls of the graphite crucible was eliminated by providing a clearance between the two surfaces of approximately 2 mm. The friction between the stainless steel connecting rod and the bronze bushes in the entry port was negligible because the ease of movement of the rod was such that it could move freely under its own weight. The ceramic fibre layer insulating the top of the ram and crucible was lightly placed on the surface and did not provide any frictional resistance.

Measurement of the extent of bed contraction was by means of a conventional scale and pointer technique capable of

measuring to an accuracy of 1 mm. It has been stated that the temperature at which 3% contraction of the bed occurred was selected as the start of the softening process because a 2 mm movement (equivalent to 3% contraction) was the first detectable change (Section 4.3.3.1.). Although the measurement of bed contraction was accurate to 1 mm, a 2 mm change at the start was chosen so that one could be certain that the softening process had definitely started.

### 3. Differential Gas Pressure Drop Across the Sample Bed

The differential gas pressure across the sample bed was measured by the use of two probes situated on either side of the bed. The lower probe was in the graphite tube whilst the upper pressure tapping was in the furnace shell, which was approximately 2.5 times the internal diameter of the graphite tube. Consequently the differential pressure measured was not an absolute value but the best that could be measured considering the complexity of the apparatus.

Another problem was that the gas pressure drop measured was not just over the sample bed, but over the entire graphite crucible, i.e. it included the base of the crucible, coke layers, graphite ram and the ceramic fibre. However, the change in gas pressure drop during a high temperature test was only caused by (a) the increased gas velocity, due to the increase in temperature, and (b) the contraction of the sample bed - the coke layers and the ceramic fibre did not show any indication of consolidation which would decrease their permeability. Consequently one can compare the form of the gas pressure drop-temperature curves for different materials, or experimental conditions, to assist with the evaluation of the reactions occurring within the bed.

Measurement of the differential gas pressure was made using a manometer graduated in mm water gauge and was readable to

the nearest mm.

4. Control of the Reducing Gas Flow and Gas Analysis Error

Gas flow was controlled with rotameters, previously calibrated at 15°C and 760 mm Hg by the manufacturer, having an accuracy of  $\pm 1\frac{1}{4}\%$  FSD<sup>3</sup>. To prevent the gas flow falling throughout the test as the permeability of the sample bed decreased, the rotameters were operated at a working pressure of 2.38 bar absolute which was well in excess of the back pressure created by the drop in bed permeability. Recalibration of the rotameters to cope with the increased working pressure was undertaken using the following formula quoted by the manufacturer<sup>3</sup> :-

$$V_t = V_m \sqrt{\frac{P_w}{P_a}} \quad \text{-----} \quad [2]$$

where,

$V_t$  = True flow rate,  $l.\text{min.}^{-1}$  (measured at 15°C and 760 mm Hg pressure)

$V_m$  = Flow rate indicated on the rotameters,  $l.\text{min.}^{-1}$  (at 15°C and an operating pressure of  $P_w$ )

$P_w$  = Absolute increased working pressure of the rotameter, bar

$P_a$  = Absolute original calibration pressure, bar

No temperature correction was made to the flow rate because the temperature of the gas did not alter significantly from the manufacturers calibration temperature of 15°C.

The pressure gauge used for measuring the working pressure of the rotameters was correct to  $\pm 1\%$ <sup>2</sup> which was equivalent to a variation of the gas flow of  $\pm 0.8\%$  at the working pressure. In total the error in gas flow is a maximum of  $\pm 1\frac{1}{4}\%$  rotameter error plus the  $\pm 0.8\%$  caused by pressure gauge error which is equal to  $\pm 2.05\%$ .

The infra red gas analysers used for analysing the inlet and outlet gas compositions were well within the accuracy of the standard gases used for their calibration<sup>4</sup>. Two calibration gases, in addition to nitrogen used for zeroing, were employed: (a) 18 vol.% CO<sub>2</sub>, 38 vol.% CO and 44 vol.% N<sub>2</sub> and (b) 8 vol.% CO<sub>2</sub>, 21 vol.% CO and 71 vol.% N<sub>2</sub> which were correct to  $\pm 5\%$ <sup>5</sup>, i.e. 38 vol.% CO could be 38  $\pm 1.9$  vol.%.

---

### References

1. BICC Pyrotenax Ltd. Private communication.
2. Budenberg Gauge Co. Ltd. Product literature.
3. G A Platon (Flowbits) Ltd. Product literature.
4. Grubb Parsons Ltd. Private communication.
5. Rank Precision Industries Ltd. (Analytical Division Hilger and Watts) Technical data sheet No.1-9D.

## APPENDIX II

### DETERMINATION OF THE REDUCTION DEGREE IN THE HIGH TEMPERATURE TEST

The change in the degree of reduction of the sample bed was determined by continuous measurement of the carbon monoxide and carbon dioxide levels in the inlet and outlet gases using Grubb Parsons infra red gas analysers. The experimental procedure during the initial stage of the high temperature test was to sample the inlet and outlet gases alternately and pass them through the analysers at a controlled flow rate of  $1 \text{ l.min.}^{-1}$ . This procedure allowed adjustment of the rotameters controlling the inlet gas composition until the desired composition was achieved. When the inlet gas composition was correct the analysers monitored the outlet gas only, with occasional checks of the inlet gas composition.

#### 1. Mass Balance

The principle of the reduction rate calculations was based on an oxygen mass balance of the system. Derivation of the relevant equations was made with reference to the following nomenclature:-

V = Volumetric flow rate of nitrogen in the inlet gas,  
 $\text{m}^3.\text{min.}^{-1}$ .

$\text{CO}_{(i)}$  = Volumetric flow rate of carbon monoxide in the  
inlet gas,  $\text{m}^3.\text{min.}^{-1}$ .

$\text{N}_2(i)$  = Nitrogen in the inlet gas.

- $\text{CO}_{(wi)}$  = Mass flow rate of carbon monoxide in the inlet gas,  $\text{g.min.}^{-1}$ .
- $\text{CO}_{(o)}$  = Volumetric flow rate of carbon monoxide in the outlet gas,  $\text{m}^3.\text{min.}^{-1}$ .
- $\text{CO}_{2(o)}$  = Volumetric flow rate of carbon dioxide in the outlet gas,  $\text{m}^3.\text{min.}^{-1}$ .
- $\text{N}_{2(o)}$  = Nitrogen in the outlet gas.
- $\text{CO}_{(wo)}$  = Mass flow rate of carbon monoxide in the outlet gas,  $\text{g.min.}^{-1}$ .
- $\text{CO}_{2(wo)}$  = Mass flow rate of carbon dioxide in the outlet gas,  $\text{g.min.}^{-1}$ .
- $\dot{m}$  = Net rate of oxygen flow out of the sample bed,  $\text{g.min.}^{-1}$ .
- $K$  = Nitrogen purge correction factor,  $\text{m}^3.\text{min.}^{-1}$ .
- $V_t$  = True total gas flow leaving the sample bed,  $\text{m}^3.\text{min.}^{-1}$ .
- $\text{CO}_{(ot)}$  = True volumetric flow rate of carbon monoxide in the outlet gas,  $\text{m}^3.\text{min.}^{-1}$ .
- $\text{CO}_{2(ot)}$  = True volumetric flow rate of carbon dioxide in the outlet gas,  $\text{m}^3.\text{min.}^{-1}$ .
- $\text{N}_{2(ot)}$  = True nitrogen in the outlet gas.
- $\%$  = In front of any gas converts it to volume %, e.g.  $\% \text{CO}_{(i)}$  signifies the vol.% of CO in the inlet gas.
- $t$  = Total time of reaction, minutes.

- PR = Degree of pre-reduction, wt.%.  
 $W_o$  = Original oxygen content of the sample, g.  
 $R_t$  = Degree of total reduction after t minutes, wt.%.  
n = Reaction time interval, minutes.

Notes: (a) All gas flows are at 15°C and 760 mm Hg pressure.

(b) The concentration of nitrogen in the gases was calculated by difference.

### 1.1 Consideration of the Inlet Gas

Now,  $CO_{(i)} = \frac{V}{\% N_2(i)} \cdot 100 \cdot \frac{\% CO(i)}{100} m^3 \cdot min^{-1}$  \_\_\_\_\_ (1)

$$CO_{(wi)} = \frac{V \cdot \% CO(i)}{\% N_2(i)} \cdot \frac{28 \cdot 10^3}{22.4} g \cdot min^{-1}$$
 \_\_\_\_\_ (2)

Hence, oxygen input =  $\frac{V \cdot \% CO(i)}{\% N_2(i)} \cdot \frac{28 \cdot 10^3}{22.4} \cdot \frac{16}{28} g \cdot min^{-1}$  \_\_\_\_\_ (3)

$$= \frac{V \cdot \% CO(i)}{\% N_2(i)} \cdot \frac{16}{22.4} \cdot 10^3 g \cdot min^{-1}$$
 \_\_\_\_\_ (4)

### 1.2 Consideration of the Outlet Gas

Now,  $CO_{(o)} = \frac{V \cdot 100}{\% N_2(o)} \cdot \frac{\% CO(o)}{100} \cdot m^3 \cdot min^{-1}$  \_\_\_\_\_ (5)

$$\text{CO}_{(wo)} = \frac{V.\% \text{CO}_{(o)}}{\% \text{N}_2(o)} \cdot \frac{28}{22.4} \cdot 10^3 \text{ g.min.}^{-1} \quad (6)$$

Hence, oxygen content of  $\text{CO}_{(wo)} = \frac{V.\% \text{CO}_{(o)}}{\% \text{N}_2(o)} \cdot \frac{28}{22.4} \cdot 10^3 \cdot \frac{16}{28} \text{ g.min.}^{-1}$  (7)

$$= \frac{V.\% \text{CO}_{(o)}}{\% \text{N}_2(o)} \cdot \frac{16}{22.4} \cdot 10^3 \text{ g.min.}^{-1} \quad (8)$$

Now,  $\text{CO}_2(o) = \frac{V.100}{\% \text{N}_2(o)} \cdot \frac{\% \text{CO}_2(o)}{100} \cdot \text{m}^3 \cdot \text{min.}^{-1}$  (9)

$$\text{CO}_2(wo) = \frac{V.\% \text{CO}_2(o)}{\% \text{N}_2(o)} \cdot \frac{44 \cdot 10^3}{22.4} \cdot \text{g.min.}^{-1} \quad (10)$$

Hence, oxygen content of  $\text{CO}_2(wo) =$

$$\frac{V.\% \text{CO}_2(o)}{\% \text{N}_2(o)} \cdot \frac{44 \cdot 10^3}{22.4} \cdot \frac{32}{44} \text{ g.min.}^{-1} \quad (11)$$

$$= \frac{V.\% \text{CO}_2(o)}{\% \text{N}_2(o)} \cdot \frac{32 \cdot 10^3}{22.4} \cdot \text{g.min.}^{-1} \quad (12)$$

### 1.3 Complete Balance

Combining equations (4), (8) and (12)

$$\dot{m} = \frac{V.\% \text{CO}_{(o)}}{\% \text{N}_2(o)} \cdot \frac{16}{22.4} \cdot 10^3 + \frac{V.\% \text{CO}_2(o)}{\% \text{N}_2(o)} \cdot \frac{32}{22.4} \cdot 10^3 - \frac{V.\% \text{CO}_{(i)}}{\% \text{N}_2(i)} \cdot \frac{16}{22.4} \cdot 10^3 \quad (13)$$

$$= \frac{V \cdot 16}{22.4} \cdot 10^3 \left[ \frac{\% \text{ CO}_{(o)}}{\% \text{ N}_2(o)} + \frac{2 \cdot \% \text{ CO}_2(o)}{\% \text{ N}_2(o)} - \frac{\% \text{ CO}_{(i)}}{\% \text{ N}_2(i)} \right] \text{ g. min.}^{-1} \quad (14)$$

An additional complication arose because the high temperature apparatus contained two nitrogen gas purge inlets. One of these was situated in the gas pre-heat section and entered at the side of the furnace - the purpose of this was to prevent any air entering and oxidising the outside of the graphite tube. The second purge was positioned at the entrance port of the pneumatic ram and maintained a slight positive pressure around the port, preventing any carbon monoxide escaping from the apparatus. The nitrogen from the pre-heat purge and some of the nitrogen from the other purge eventually mixed with the outlet gas, diluting the carbon monoxide and carbon dioxide levels. Allowance for the dilution effect was made by the introduction of a correction factor, K, into the equations derived for the outlet gas.

The value of K was different for each test and was selected in order to make the final % reduction calculated by gas analysis equal to that calculated by determining the weight loss of the sample after the test. Consequently K became a 'tuning factor'.

Incorporating K

$$V_t = \frac{(V + K)}{\% \text{ N}_2(o)} \cdot 100 \quad \text{m}^3 \cdot \text{min.}^{-1} \quad (15)$$

$$\text{Hence, } \% \text{ CO}_{(ot)} = \% \text{ CO}_{(o)} \cdot \frac{V_t}{(V_t - K)} \quad (16)$$

$$\text{and similarly, } \% \text{ CO}_2_{(ot)} = \% \text{ CO}_2(o) \cdot \frac{V_t}{(V_t - K)} \quad (17)$$

the true nitrogen content of the gas leaving the sample bed (i.e. influence of nitrogen purge eliminated):

$$\% N_{(ot)} = 100\% - \% CO_{2(ot)} - \% CO_{(ot)} \quad (18)$$

The values of  $N_{2(ot)}$ ,  $CO_{(ot)}$  and  $CO_{2(ot)}$  are substituted for  $N_{2(o)}$ ,  $CO_{(o)}$  and  $CO_{2(o)}$  respectively in equation (14) to calculate the oxygen loss from the system.

The degree of reduction after a reaction time of t minutes is

$$R_t = \frac{\dot{m}t}{W_o} \cdot 100 + PR, \text{ wt.}\% \quad (19)$$

After a further n minutes, the degree of reduction of the sample is:-

$$\frac{\dot{m}.n. 100}{W_o} + R_t + PR, \text{ wt.}\% \quad (20)$$

## 2. Estimation of the Quality of Direct Reduction

The technique used was based on the difference between the ratio of % CO/% N<sub>2</sub> of the inlet and outlet gases. When the following inequality occurred, direct reduction was judged to be definitely occurring:-

$$\frac{\% CO_{(ot)}}{\% N_{2(ot)}} - \frac{\% CO_{(i)}}{\% N_{2(i)}} > 0 \quad (21)$$

Equation (21) should contain a term for the carbon dioxide concentration, i.e. the first term should be  $[\% \text{CO}_{(\text{ot})} + \% \text{CO}_{2(\text{ot})}] / \% \text{N}_{2(\text{ot})}$ . However, the accuracy of the experimental readings were insufficient to be as absolute as this.

The derived equations were incorporated into a computer program for ease of calculation of (a) the degree of reduction, (b) the quantity of direct reduction and (c) McKewan's  $1-(1-R)^{1/3}$  term.

### 3. Assessment of Errors in the Calculation of the Degree of Reduction

Assessment of the errors in the mass balance was undertaken by determining the effect of changing (a) the gas flow rate and (b) the inlet gas composition using data obtained from a high temperature test with a sinter (Tables AI and AII). In Table AII the standard case is No.1, whilst cases 2-7 deal with changes in the inlet nitrogen gas flow, and hence the total gas flow, into the sample. Cases 8-13 deal with variations of the carbon monoxide content of the inlet gas whilst maintaining a constant gas flow. Case No.14 is where the nitrogen correction factor has been adjusted until the final degree of reduction, calculated from the mass balance, agrees with the degree of reduction determined by weight loss.

Considering the results presented in Table AII; it is apparent that deviations in the nitrogen flow rate (or the total flow rate) do not generate large errors in the calculated reduction values, e.g. a change of  $\pm 3 \text{ l.min.}^{-1}$  in the nitrogen flow rate alters the final degree of reduction to 81.7 or 90.4% compared to 86.0% obtained with the standard flow rate (cases 1, 4 and 7). A change in nitrogen flow rate of  $3 \text{ l.min.}^{-1}$  is

in excess of 8% and about four times the error that could be expected from the equipment (discussed in Appendix I, Section 4).

Inaccuracies in gas composition of the inlet gas on the other hand make themselves apparent in the calculated degree of reduction, e.g. at the standard nitrogen flow rate of  $36 \text{ l.min.}^{-1}$  an error of  $\pm 0.2\%$  in the 40.9 vol.% CO inlet value alters the final degree of reduction to 79.8% or 92.2%, compared with 86.0% calculated as standard (Cases 1, 8 and 11).

Appraisal of the error generated with a change in the initial oxygen content of the sample showed that errors from this source could be effectively ignored, e.g. Table AIII shows that a variation of just over 2.5% in the oxygen level alters the final degree of reduction to 84.7% or 87.4% from the original value of 86.0%.

	Time, Minutes							
	0 <sup>†</sup>	10	20	30	40	50	54	56
Vol.% CO*	35.0	35.4	36.9	38.0	39.2	40.5	40.9	41.1
Vol.% CO <sub>2</sub> *	6.0	5.3	4.0	2.8	1.8	0.8	0.6	0.5
Vol.% CO <sup>+</sup>	35.2	35.6	37.1	38.2	39.4	40.7	41.1	41.3
Vol.% CO <sub>2</sub> <sup>+</sup>	6.0	5.3	4.0	2.8	1.8	0.8	0.6	0.5

\* As analysed - data used for Case No.1 in Table AII

+ After correction factor used - data used for Case No.14 in Table AII

† At time zero the outlet composition is unknown, and arbitrary values have to be assigned for the purposes of the computer program, but these values do not enter into the mass balance.

Table AI     Carbon Monoxide and Carbon Dioxide Levels in the Outlet Gas During a High Temperature Test with a Sinter

Case No.	Vol.% CO (inlet)	N <sub>2</sub> flow <sub>-1</sub> 1.min.	% change in variable	N <sub>2</sub> correction factor	Calc. total flow 1.min. -1	Time, Minutes							
						0	10	20	30	40	50	54	56
1	40.9 <sup>+</sup>	36	0	0	60.9	33.8	49.9	63.0	71.5	77.9	82.8	84.9	86.0
2	40.9	35	-2.8	0	59.2	33.8	49.5	62.1	70.5	76.7	81.4	83.5	84.6
3	40.9	34	-5.6	0	57.5	33.8	49.0	61.3	69.4	75.5	80.1	82.1	83.1
4	40.9	33	-8.3	0	55.8	33.8	48.6	60.5	68.4	74.3	78.7	80.7	81.7
5	40.9	37	+2.8	0	62.6	33.8	50.4	63.8	72.6	79.2	84.1	86.3	87.5
6	40.9	38	+5.6	0	64.3	33.8	50.8	64.6	73.6	80.4	85.5	87.8	88.9
7	40.9	39	+8.3	0	66.0	33.8	51.3	65.4	74.7	81.6	86.9	89.2	90.4
8	40.7	36	-0.5	0	60.7	33.8	51.0	65.2	74.8	82.3	88.3	90.9	92.2
9	40.5	36	-1.0	0	60.5	33.8	52.1	67.3	78.1	86.7	93.2	96.7	98.3
10	40.3	36	-1.5	0	60.3	33.8	53.2	69.5	81.3	91.0	99.2	>100	>100
11	41.1	36	+0.5	0	61.1	33.8	48.8	60.7	68.2	73.5	77.3	78.9	79.8
12	41.3	36	+1.0	0	61.3	33.8	47.7	58.5	64.8	69.1	71.7	72.9	73.6
13	41.5	36	+1.5	0	61.5	33.8	46.6	56.3	61.5	64.6	66.1	66.9	67.3
14	40.9	36	0	0.35	60.9	33.8	51.4	65.8	75.8	83.6	89.7	92.4	93.8*

+ Measured vol.% CO inlet

\* Final degree of reduction determined by weight loss measurement

Table AII Review of Errors in the Mass Balance Used for Calculation of the % Reduction

Initial Oxygen content, g	% change in oxygen	Vol.% CO (inlet)	N <sub>2</sub> flow, l.min. <sup>-1</sup>	Final degree of reduction calculated from gas analysis, %
133.5*	0	40.9	36	86.0
137	+2.6	40.9	36	84.7
130	-2.6	40.9	36	87.4

\* Equivalent to Case No.1 in Table AII

Table AIII    Effect of Error in the Initial Oxygen Content  
Upon the Calculated Final Degree of Reduction

## APPENDIX III

### PUBLISHED PAPERS

During the course of the study two papers have been published and copies of them are included in this section. The two papers are:-

- (a) "Simulated Blast Furnace Reduction of Acid Pellets in the Temperature Range 950-1350°C". Ironmaking and Steelmaking 7 (1980), 68-75.
  
- (b) "Softening and Melting of Superfluxed Sinters and Acid Pellets". 39th meeting of the Ironmaking Proceedings of AIME held in Washington DC March 1980, 370-389. This conference was attended by the author.

reprinted from

# IRONMAKING & STEELMAKING

A joint publication of  
The Metals Society and the American Society for Metals



THE METALS SOCIETY  
1 CARLTON HOUSE TERRACE LONDON SW1Y 5DB

erating techniques has emphasized the fundamental significance of gas distribution. The profile and position of the melting zone, determined by this distribution, govern the entire operation of the unit and affect directly permeability, heat flows on the walls, and reduction efficiency.

In Solmer blast furnaces, where the gas-distribution control is ensured by means of a movable armour, the tests were carried out with a view primarily to protect the walls by decreasing the heat flow. At first, this result was achieved, but to the detriment of reduction efficiency and, consequently, of heat consumption. A new development in the charging method has now made it possible to keep the heat flow low with a considerable decrease in the fuel consumption, i.e. a saving of  $20 \text{ kg t}^{-1}$  of iron. The reduction efficiency of iron oxides becomes nearly ideal owing to good utilization of the gas reducing power from the centralized gas flow. This is characteristic of the presence of a sufficient quantity of sinter in that zone. This centralized flow should not be created only by a variation of coke/sinter ratio, but also by the use of size segregation.

These tests have been made possible by continuous analysis and follow-up of the operating conditions through the use of control means consisting essentially of an

important measuring device worked by a process computer in conjunction with the IRSID mathematical model.

#### ACKNOWLEDGMENTS

The authors wish to thank particularly all the staff of the Ironmaking Division of Solmer, whose strong support and close cooperation have made it possible for the authors to obtain these results, and IRSID, for its assistance and participation in the tests through necessary investigations for the understanding of the operating techniques.

#### REFERENCES

1. SOLMER: *Rev. Métall.*, 1974, **71**, (3), 193-317.
2. A. RIST and N. MEYSSON: *Proc. AIME Ironmaking Conf.*, 1966, **25**, 88-96.
3. K. KANBARA, M. SASAKI, Y. OKUNO, and T. KATAYAMA: *Proc. AIME Ironmaking Conf.*, 1974, **33**, 416-422.
4. Y. ISHIKAWA: *Rev. Métall.*, 1976, **73**, (3), 283-314.
5. M. HIGUCHI, K. KURODA, and G. NAKATANI: *Iron Steel Eng.*, 1974, **51**, (9), 44-50.
6. J. A. MICHARD: *Proc. Journées Int. de Sidérurgie*, Luxembourg, 1962, 346-363.
7. C. STAIB and J. A. MICHARD: *J. Met.*, 1965, **17**, (1), 1; (2), 165.
8. C. STAIB, N. JUSSEAU, J. VIGLIENGO, and J. C. COCHERY: *Proc. AIME Ironmaking Conf.*, 1967, **26**, 66.

## SECONDARY STEELMAKING

This volume contains the proceedings of an international conference organized by Activity Group Committee V of The Metals Society, and held at the Royal Lancaster Hotel, London, on 5-6 May 1977.

The papers in this volume cover ladle refining and secondary steelmaking techniques for bulk and special steels. The aim of this conference was to describe the progress of these techniques and discuss the implications of introducing another stage in the integrated production process. This volume contains 17 papers, together with 3 discussion sections.

vi+130 pp, illustrated (code 190) ISBN 0 904357 14 7 297×210 mm

**Price: UK £22.50 (Metals Society Members £18) post free**

**Overseas \$65 (Members \$52) post free**

Please send orders, quoting ordering code 190 and enclosing the correct remittance, to:

**Sales Department, The Metals Society, 1 Carlton House Terrace,  
London, SW1Y 5DB**

# Simulated blast-furnace reduction of acid pellets in temperature range 950°–1350°C

G. Clixby

The behaviour of a batch of acid pellets during athermal reduction in the temperature range 950°–1350°C has been studied experimentally. Melting of partially reduced pellets was found to be caused by a reaction between wüstite and the slag phase present in the fully oxidized pellets. This liquid slag phase then proceeds to attack the remaining wüstite and quartz grains as the temperature rises producing an increase in the quantity of slag. Whether a bed of acid pellets exhibits high or low permeability depends upon the extent of reduction. High levels of reduction maintain bed permeability whereas low levels of reduction produce an impermeable bed, caused by liquid slag filling the voids of the bed. The situation can be looked upon as a balance of the reduction and slag-forming reactions. If the former dominates the bed remains permeable, but dominance by the latter produces an impermeable bed. Using the experimental results and the evidence provided by the Japanese dissection studies on quenched blast furnaces, the reactions occurring and the types of structure obtained in the cohesive zone are explained. IS/342

©1980 The Metals Society. Manuscript received 13 March 1979. The author is with the British Steel Corporation, Teesside Laboratories, Middlesbrough.

The Japanese dissection studies revealed that the cohesive zone consists of several 'doughnut'-shaped structures, each of which originates from a layer of the furnace burden. These doughnuts are arranged in a cone-shaped stack in a centre-working high-productivity furnace, Fig. 1a. Cross-sections of two individual doughnuts from different locations within the cohesive zone are shown in Fig. 1b. The locations of these zones within the furnace are governed by the gas flow, materials distribution, and the softening-melting characteristics of the burden components. The high-temperature properties of burden materials depend upon the phases present and their proportions, which are related to the basicity and the degree of reduction, e.g. semireduced acid pellets at temperatures in excess of 1000°C consist essentially of metallic iron, wüstite, and a slag phase. One of the major influences on the behaviour of materials at high temperatures is the composition of the slag phase. A slag phase possessing a low melting point is detrimental in that the slag melts and impedes gaseous reduction of the iron oxide phases.

The structure of the cohesive zone has an important influence on the productivity and life of the furnace. For example, wall working leads to high wall temperatures and premature failure of the furnace lining. The dissection studies have revealed that furnace productivity is related to the height of the commencement of the cohesive zone (measured from tuyere level).<sup>6</sup> The higher the cohesive zone is up the furnace the greater the productivity. The best estimation, at present, of the temperature and reduction profiles existing within the cohesive zone is provided by the data from the quenched furnaces. In considering the reduction state of the burden, as measured, it must be recognized that the act of water quenching affects re-oxidation of the burden materials. Japanese workers<sup>1</sup> have derived a relationship between the initial reduction degree of sinter and the degree of reduction after water quenching. Using this relationship, they claim an improved estimate of the degree of reduction can be made for the burden under furnace operating conditions.

## EXPERIMENTAL TECHNIQUE

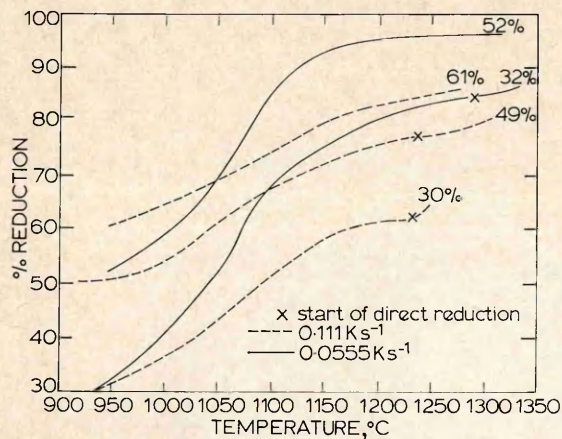
The published information arising from the dissection of Hirohata no.1 blast furnace has been examined to obtain an indication of the heating rates, and the degree of burden reduction within the cohesive zone, thus providing a basis for the experimental study.

Hirohata no.1 was known to be a centre-working furnace and had a production rate between 2580 and 3289 t d<sup>-1</sup>.<sup>2</sup> These production rates represent 1.83 and 2.34 t m<sup>-3</sup> d<sup>-1</sup>, respectively. The burden fed to this furnace was equivalent to 23.62 t of hot metal per charge. To obtain 2580 t d<sup>-1</sup> from the furnace, the furnace must have been charged at 13 min intervals and to obtain 3289 t d<sup>-1</sup> the furnace must have been charged at 10 min intervals. Consequently, one can look upon the distribution of the softening-melting layers as time intervals, allowing an estimation of the heating rate through the cohesive zone to be made. Using this technique the heating rates in Hirohata no.1 have been calculated as 0.083 K s<sup>-1</sup> near the apex of the cohesive zone and 0.053 K s<sup>-1</sup> near the base, at a production rate of 2.34 t m<sup>-3</sup> d<sup>-1</sup>. The experimental measurements of softening and melting characteristics of acid pellets described in this paper, span this calculated range of heating rates.

The experimental technique adopted was basically an athermal reduction under load procedure. The sample of pellets was first prerduced to the desired degree at 950°C using reducing gas of composition 40 vol.-% CO–60 vol.-% N<sub>2</sub> in a separate piece of apparatus. When cool the partially reduced sample was transferred to the high-

One of the most important zones existing within the blast furnace is the cohesive or softening-melting zone. Until fairly recently, very little was known of the structure of this zone, or of the reactions occurring within it, owing to the practical problems of removing samples from an operating blast furnace. Japanese workers in recent years have quenched several blast furnaces and systematically dissected them to reveal the nature of the cohesive zone.<sup>1-5</sup>





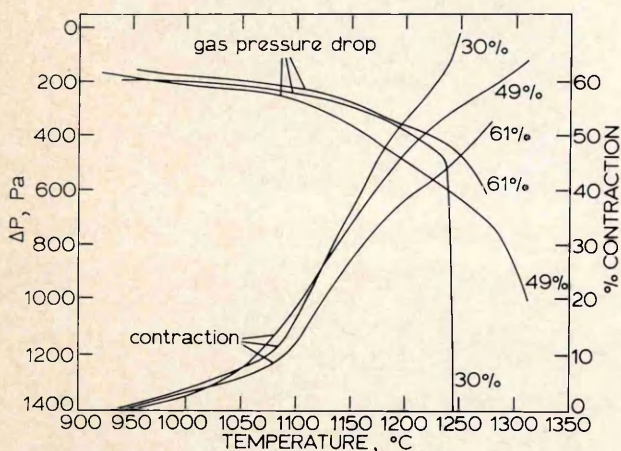
**3 Reduction v. temperature curves at both heating rates: numbers on curves are levels of pre-reduction**

contraction curves is that for both samples the early contraction follows a similar path.

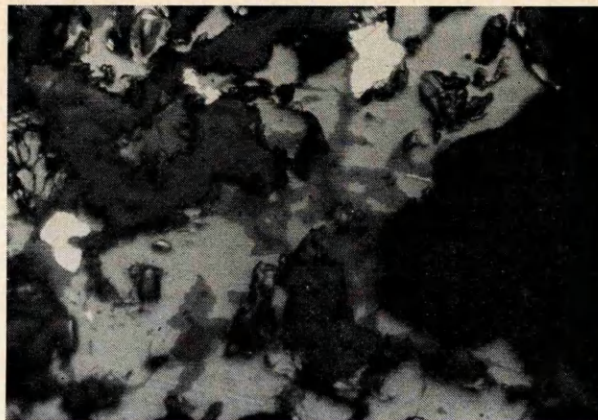
In these tests it was possible to detect the commencement of direct reduction, caused by a reaction between the sample and the coke, from the compositions of the inlet and outlet gases. The temperature at which this occurred is indicated on Fig.3 for the 32% pre-reduced sample. In the case of the 52% pre-reduced sample no such reaction was detected.

At a heating rate of  $0.111 \text{ K s}^{-1}$  the contraction v. temperature curves for pellets pre-reduced by 30, 49, and 61% oxygen removal show that softening commenced at similar temperatures to those obtained at the slower heating rate, namely  $985^{\circ}$ – $1010^{\circ}\text{C}$  (Fig.4). At the highest level of pre-reduction a gradual increase in gas pressure drop occurred, but at the lower levels of pre-reduction a dramatic increase occurred. The rapid rise of gas pressure drop of the 30% pre-reduced sample coincides with the commencement of direct reduction (Fig.3).

Four tests at a heating rate of  $0.111 \text{ K s}^{-1}$  were carried out using samples pre-reduced to 26, 44, 47, and 64%, but with a nitrogen atmosphere instead of the carbon monoxide-nitrogen gas mixture. The 3% contraction temperatures were in the same region as the tests using reducing gas. The gas pressure drop v. temperature curves are not shown, but the rapid rise of gas pressure drop occurred at  $1180^{\circ}$ ,  $1225^{\circ}$ ,  $1225^{\circ}$ , and  $1240^{\circ}\text{C}$  for the 26, 44, 47, and 64% pre-reduced samples, respectively.



**4 % contraction and gas pressure drop  $\Delta P$  at heating rate of  $0.111 \text{ K s}^{-1}$ : numbers on curves are levels of pre-reduction**



**5a Structure of pre-reduced pellets after heating to  $980^{\circ}\text{C}$ , dark phase in slag caused by segregation during cooling: iron white, wüstite light grey, slag grey, segregation of slag dark grey, pores black  $\times 100$**

The simple heating test using three pellets showed that at  $950^{\circ}\text{C}$  no melting occurred, but at  $980^{\circ}\text{C}$  melting was evident in isolated locations. As the holding temperature, rose the extent of melting also increased. Figures 5a and 5b show the microstructures of pellets heated to  $980^{\circ}\text{C}$ ; two slag phases are visible (caused by segregation of the liquid during cooling). The lighter shaded phase was qualitatively composed of  $\text{CaO}$ ,  $\text{SiO}_2$ , and  $\text{FeO}$ , while the darker shaded phase (the minor phase) was composed of  $\text{CaO}$ ,  $\text{SiO}_2$ ,  $\text{FeO}$ , and the other minor impurities, i.e.  $\text{K}_2\text{O}$ ,  $\text{Al}_2\text{O}_3$ ,  $\text{MgO}$ ,  $\text{MnO}$ , etc.

In the fully oxidized pellets the slag phase was found to be qualitatively composed of  $\text{Fe}_2\text{O}_3$ ,  $\text{SiO}_2$ , and  $\text{CaO}$  plus the minor constituents, i.e.  $\text{K}_2\text{O}$ ,  $\text{Al}_2\text{O}_3$ ,  $\text{MgO}$ , etc.

Some examples of the microstructure of the pellets after the high-temperature test are shown in Figs.6a–6c. Again, two slag phases are visible in some areas of Figs.6b and 6c which were found to correspond in composition to the two slags found in the pellets treated in the simple heating test.

## DISCUSSION MECHANISM OF INITIAL MELTING

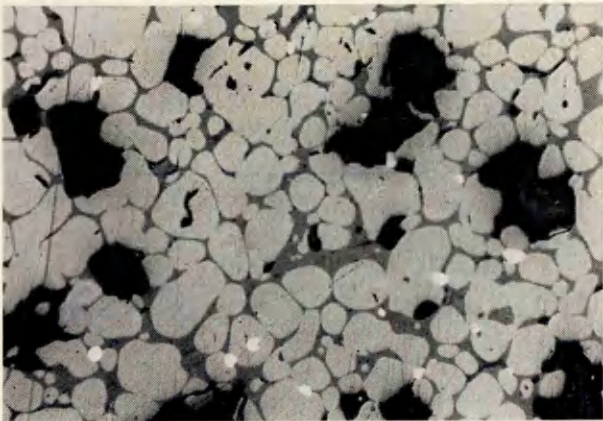
The simple heating tests showed that melting started at a temperature of  $980^{\circ}\text{C}$  caused by a reaction between



**5b Structure of pre-reduced pellets after heating to  $980^{\circ}\text{C}$ ; note metallic iron acting as barrier between wüstite and slag: iron white, wüstite light grey, slag grey, segregation of slag dark grey, pores black  $\times 400$**



**6a Microstructure of virtually fully reduced pellets after high-temperature test: iron white, quartz dark grey, pores black** ×100



**6b Core of pellet after high-temperature test at fast heating rate: iron white, wüstite light grey, slag grey, pores black** ×100



**6c Slag escaping from pellets during high-temperature test at fast heating rate; two pellet surfaces can be seen, dendrites originate from slag during cooling: iron white, wüstite light grey, slag grey, pores black** ×100

wüstite and the slag present in the fully oxidized pellets (termed residual slag in this paper). This is verified by the fact that the residual slag and the newly created liquid slag contain the same constituents: CaO, SiO<sub>2</sub>, iron oxide, and traces of K<sub>2</sub>O, Al<sub>2</sub>O<sub>3</sub>, MgO, etc. Evidently, the presence of alkalis in the residual slag serves to lower the melting

point of the liquid slag to ~980°C. A layer of iron surrounding a wüstite grain provides an effective barrier to the residual slag-wüstite reaction as illustrated in Fig.5b.

The results of the high-temperature test showed that the start of softening (3% contraction temperature) was between 985° and 1010°C and is in good agreement with the simple heating test findings.

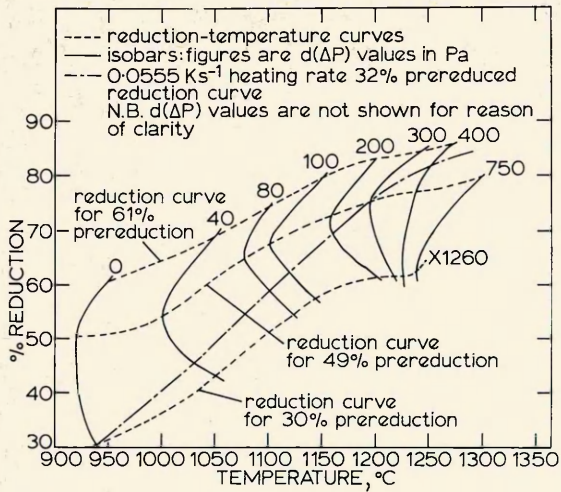
The nature of the reaction between wüstite and the residual slag (the fully oxidized state) leads to the conclusion that there is a level of reduction which leads to a maximum area of contact between the wüstite and the residual slag. If all the iron oxide were reduced to wüstite then the maximum number of points of contact would be obtained. However, the prereluction stage was carried out in an atmosphere of 40%CO-60%N<sub>2</sub>, which is capable of reducing the iron oxides to metallic iron. Consequently, topochemical reduction occurs producing a layer of metallic iron around some of the wüstite grains, which has been demonstrated to shield the residual slag from contact with the wüstite. This means that it is impossible to obtain the maximum number of contact points for the following reason. At low levels of reduction the core of the pellet is still in the hematite-magnetite stage, yet the edge shows signs of metallic iron. Intermediate locations along the pellet radius are at the wüstite stage, which can react with the residual slag. As the level of reduction rises the core approaches the wüstite composition while the thickness of the metallic shell of the pellet increases. The rise in the quantity of wüstite towards the core naturally increases the number of reaction sites, but acting against this is the increased quantity of inert metallic iron. The net effect is that the maximum number of reaction sites does not occur at 30% reduction, but at the higher levels of 40-50%. Workers at CRM<sup>7</sup> also found that the minimum softening temperature of sinters occurred at reduction levels of 40-50%. An additional point is that the metallic iron will strengthen the sample anyway and minimize the total level of contraction, but not the start of contraction.

Attempting to apply this hypothesis to the softening of pellets as they undergo reduction is difficult because the reduction state is constantly changing and the time for reaction between the wüstite and the residual slag is short. The tests with nitrogen gas only showed that the minimum 3% contraction temperature occurred at 44% reduction.

#### TEMPERATURE-REDUCTION-ISOBAR DIAGRAMS

Examination of the data from the gas pressure drop *v.* temperature and reduction *v.* temperature curves obtained using both heating rates showed that the gas pressure drop is a function of the degree of reduction and the temperature (Fig.7). This diagram has been constructed by plotting the % reduction *v.* temperature curves at the fast heating rate and superimposing on to them the increase in gas pressure drop, i.e. the total gas pressure drop at any temperature minus the total gas pressure drop at 950°C. These diagrams have been termed 'TRIB diagrams' (Temperature, Reduction, Isobars) and they illustrate a 'critical' area (or zone) of reduction and temperature where high gas pressure drops are encountered, i.e. where 'melt down' of the bed results in a loss of permeability. The critical area is where the isobars merge together, i.e. at 1200°-1250°C and 60-65% reduction. At the slow heating rate the reduction path of the 32% prerelucted sample bypasses the critical zone, avoiding the production of high gas pressure drops.

Naturally, in the area beneath the critical zone high gas pressure drops will also occur. Tests using nitrogen only with samples having prereluction levels between 26 and 64% showed that the melt-down temperature was proportional to the degree of reduction, the higher the degree



7 TRIB diagram at heating rate of  $0.111 \text{ K s}^{-1}$

of reduction the greater the melt-down temperature, e.g. at 26% reduction the melt-down temperature was  $1180^\circ\text{C}$  and at 64% reduction it rose to  $1240^\circ\text{C}$  (the latter being in good agreement with the temperature predicted from the TRIB diagram at 64% reduction).

The inflection in the TRIB diagram (Fig.7), i.e. the 49% pre-reduced sample exhibiting higher gas pressure drops than the other two samples at temperatures up to  $\sim 1150^\circ\text{C}$  can be explained as follows. Plotting the total gas pressure drop  $v.$  contraction for the three samples shows that, up to  $\sim 30\%$  contraction, the gas pressure drop is directly related to the contraction level. This point is equivalent to  $\sim 1140^\circ\text{C}$  in all cases. At this point divergence of the curves occurs.

Returning to the contraction  $v.$  temperature curves (Fig.4), it is apparent that between  $1050^\circ$  and  $1100^\circ\text{C}$  the 49% pre-reduced sample contracted more than the other two samples. As the gas pressure drop is related to the contraction level in this temperature range, it follows that the gas pressure drop must be higher, hence explaining the inflection. The reason for the increased contraction level is probably connected with the extent of slag formation, i.e. the quantity of molten slag was probably greater than that present in the other two samples in this temperature range. As the temperature rose the lowest pre-reduction sample (30%) produced a greater quantity of slag which resulted in increased contraction and an escape of the slag into the voids of the bed. Consequently, the inflection is smoothed out as the temperature rises.

#### THEORY OF REACTION MECHANISM IN ACID PELLETS DURING ATHERMAL REDUCTION WITH $\text{CO-N}_2$ GAS MIXTURE

The results of the experimental work has led to the establishment of a theory describing the reactions occurring and their influence upon the high-temperature properties of acid pellets during athermal reduction.

The mechanism of the initial liquid slag formation has been discussed above. The subsequent rise in temperature with time has two effects. First, it promotes further reactions between the wüstite, residual slag, quartz, and the newly created liquid slag producing an increase in the volume of liquid slag. Secondly, the degree of reduction increases, limiting the creation of liquid slag because of the decrease in the quantity of wüstite (provided the degree of reduction is in excess of the optimum mentioned above). Consequently, the situation existing can be looked upon as a competition between the liquid-slag-formation reaction and the reduction reaction; if the reduction reaction

dominates the quantity of liquid slag will be small. Should the slag-formation reaction dominate then the degree of gaseous reduction will be limited because of the slag forming an impermeable layer around the wüstite. A slow rate of temperature rise favours the gaseous reduction reaction and results in a highly reduced pellet coupled with a low gas pressure drop. Rapid heating rates favour the liquid-slag-formation reaction providing a low degree of gaseous reduction and a high gas pressure drop. These two contrasting effects can be seen by comparing the results of the 30% pre-reduced samples at the fast and slow heating rates (Figs.2-4).

The microstructural changes occurring within the pellets under rapid heating rate conditions are as follows. At the pellet surface the topochemical nature of the reduction reaction results in the rapid production of iron grains; consequently, the liquid-slag-formation reaction does not occur and the structure comprises metallic iron and unreacted quartz. (Figure 6a shows the structure of a virtually fully reduced pellet which is also identical to the microstructure of the surface of all pellets during reduction, irrespective of heating rate or degree of pre-reduction.) At the pellet core the wüstite enters into the slag-forming reaction and becomes enveloped in liquid slag which inhibits further gaseous reduction (Fig.6b). As the temperature increases the viscosity of the slag decreases and the slag starts to migrate towards the pellet surface, assisted by the squeezing action of the applied load. During its migration the slag dissolves any quartz grains in its path, further increasing the slag volume. Whether or not the slag escapes from the pellet into the voids of the bed depends upon the slag quantity and the thickness of the iron shell, the thicker the shell the greater the resistance to slag flow and the less the squeezing action because of the physical strength of the shell. If the slag escapes into the voids of the bed then the gas pressure drop will rise rapidly and the iron oxide in the slag will undergo direct reduction with the coke (Figs.3, 4, 6c).

At slow heating rates slag formation still occurs at the pellet core, but the decreased quantity of wüstite (which limits the volume of liquid slag) coupled with the thick iron shell makes escape of the liquid slag into the voids of the bed impossible and bed permeability is maintained.

#### REDUCTION-TIME-TEMPERATURE CONSIDERATIONS

The change of the degree of reduction with time for each sample has been plotted on the basis of McKewan's rate equation.<sup>8</sup> Making the assumption that the oxygen density and the particle size are constant, McKewan's rate equation simplifies to:

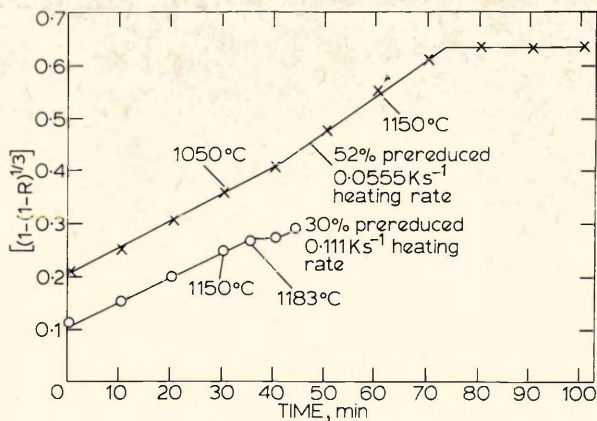
$$[1 - (1 - R)^{1/3}] = kt \quad \dots \dots \dots (1)$$

where

- $k = \text{a constant, s}^{-1}$
- $R = \text{fractional degree of reduction}$
- $t = \text{time, s.}$

An example of two plots is shown in Fig.8 for the 30% pre-reduced sample at the  $0.111 \text{ K s}^{-1}$  heating rate and the 52% pre-reduced sample at the  $0.0555 \text{ K s}^{-1}$  heating rate. The main feature of these plots is that the reduction procedure is athermal, yet the slope of the curve shows little change. Normally, the reduction rate depends upon the temperature of the reaction, yet in this case no such dependence is evident up to  $\sim 35$  min reduction time at both heating rates. After this point the  $0.111 \text{ K s}^{-1}$  test started to show a high gas pressure drop which naturally impeded gaseous reduction.

In the case of the  $0.0555 \text{ K s}^{-1}$  reduction test some divergence from linearity occurred, i.e. a new rate constant



8  $[1-(1-R)^{1/3}]$  v.  $t$  under athermal reduction conditions

came into play, although the change in slope of the curve cannot be termed dramatic. The conclusion is that in the temperature range studied, provided melt-down conditions are not encountered, the reduction-rate constant does not vary significantly, irrespective of the heating rate. The probable reason for this is that the rise in temperature provides an increase in the reaction kinetics, but acting against this is a decrease in the reaction driving force, as the ratio of  $CO/(CO+CO_2)$  in equilibrium with  $FeO$  and  $Fe$  approaches unity, producing the net result of a steady reaction rate in the temperature range studied.

**APPLICATION TO BLAST-FURNACE PROCESS**

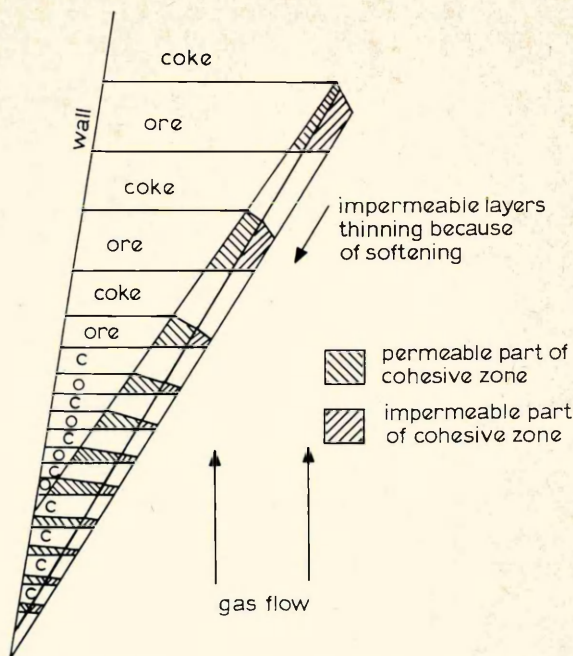
It has been demonstrated that material in the apex of the cohesive zone in a centre-working furnace undergoes an extremely fast rate of heating. Material in the base of the cone, on the other hand, is exposed to a relatively slow heating rate. The structure and degree of reduction of each portion of the cohesive zone are given in Fig.1b and Table 1, respectively. Considering the situation near the apex of the cone (G-5), it is apparent that the majority of material is only slightly reduced before entering the zone, i.e. portion D. (It must be remembered that some oxidation of the burden materials may have occurred on water quenching.) However, the small portion, C, has a high degree of reduction yet is still classed within the lumpy portion. It is highly reduced because it is exposed to lower temperatures and a high flowrate of reducing gas passing through the coke bed overhead.<sup>1</sup>

The boundary between the granular zone and the softening zone (X-X) can be thought to be the equivalent of the 3% contraction temperatures determined experimentally, i.e.  $\sim 985^\circ C$  for acid pellets. The temperature indicated by the Japanese data is  $\sim 1100^\circ C$  for furnaces operating predominantly on  $\sim 80\%$  sinter burdens. The journey of the burden through the cohesive zone is rapid

Table 1 Degree of reduction of iron ores of softening-melting layers of Hirohata no.1 blast furnace

Softening-melting layer	Portion*	Degree of reduction, %		
		Sinter	Lumpy ore	Pellet
G-5	B	65.6	65.0	79.3
	C	72.8	68.2	81.2
	D	11.5	12.3	14.6
G-19	D	35.4	36.6	41.3

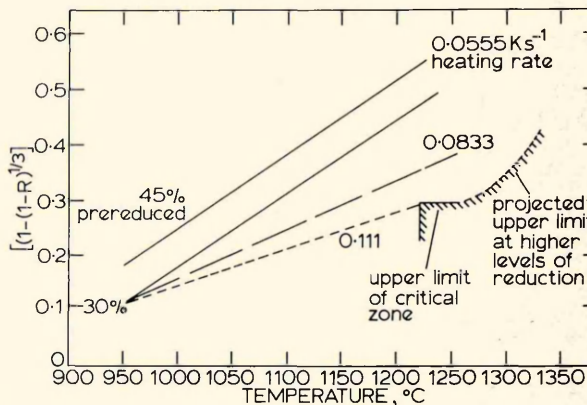
\*B=softening portion ; C and D=lumpy portion.



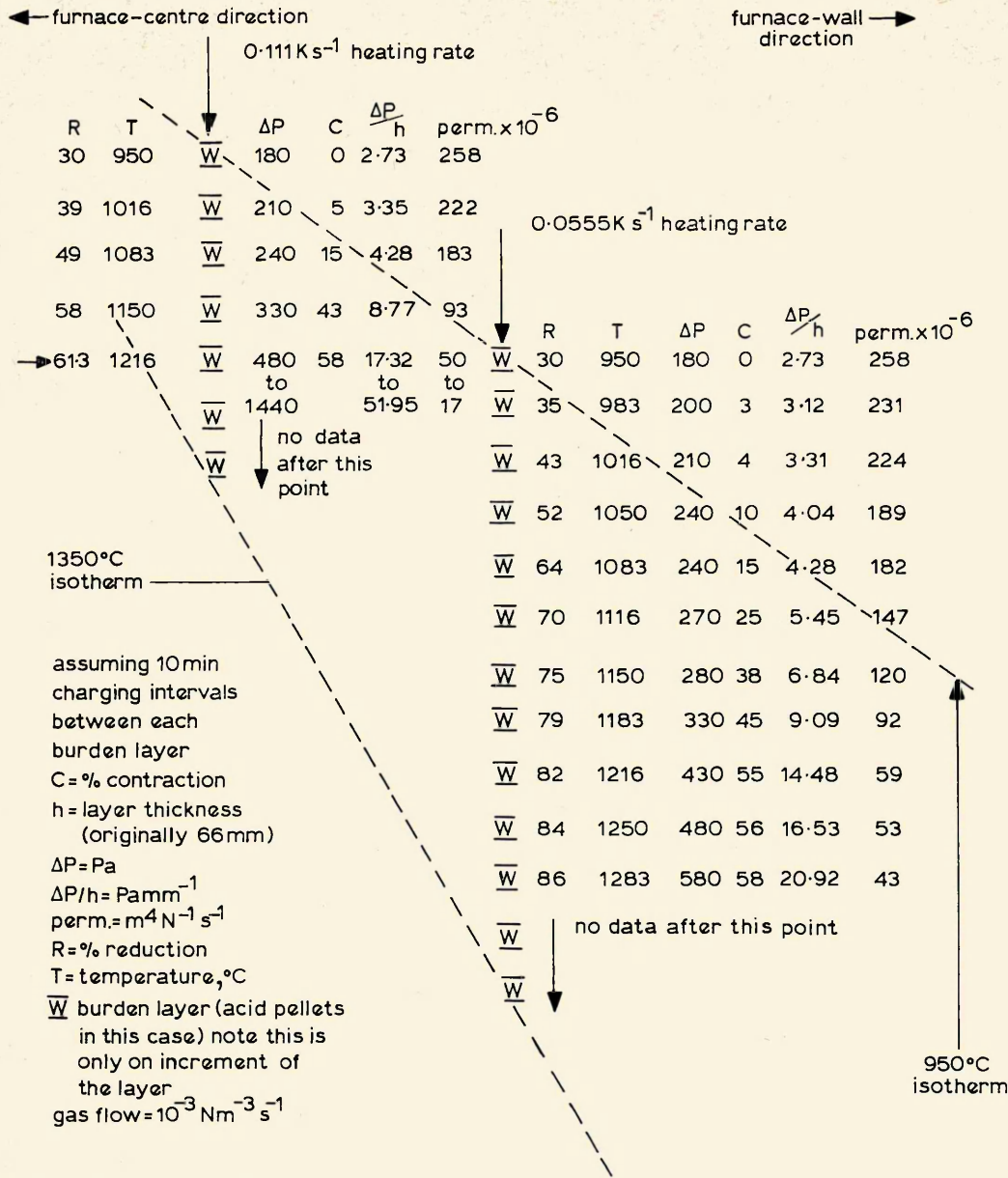
9 Schematic representation of the two parts of cohesive zone

and time for reduction of portion D materials is short. The effect of this is analogous to that shown experimentally with low prereduction samples at fast heating rates, i.e. blockage of the voids of the bed and the commencement of direct reduction. This stage is the boundary Y-Y. In portion A the slag starts to drip out into the underlying coke bed where it undergoes direct reduction. The metallic iron is left in portion A and subsequently melts. The small 'icicles' shown are hollow and consist of an iron shell with slag adhering to the inside wall.<sup>4</sup> Identical icicles have been obtained from the experimental apparatus during commissioning. The icicles emanated from a batch of acid pellets at  $\sim 60\%$  reduction and a temperature of  $\sim 1225^\circ C$ .

Considering the cohesive zone lower down the furnace (G-19), it is immediately apparent that the level of reduction of the materials entering the zone (portion D in Fig.1b) is higher (as shown in Table 1). This is because of the longer residence time in the furnace allowing an increased amount of reduction. Once in the beginning of the zone (bounded by X-X) the transit time through the zone is relatively longer than that of layer G-5, which allows the material to be reduced to a greater extent thus



10 Estimation of reduction path of acid pellets at different heating rates



11 Permeability data for acid-pellet burden layers

avoiding the production of vast quantities of liquid which fill the voids of the bed. In this situation portion A should be fairly permeable. Actual blockage of the voids will probably occur in the much smaller portion A' (bounded by Z-Z). The conclusion from the observations is that the cohesive zone consists of two distinct zones. The first is the zone between the 3% contraction temperature and the build-up of fluid in the voids. This zone is quite permeable and gaseous reduction proceeds readily. The second zone exists between the build-up of fluid in the voids and the melting of the metallic iron. This zone is not permeable. The relative extent of each zone depends upon the degree of reduction and the localized temperature. Low levels of reduction persisting up to high temperatures give rise to an extensive impermeable zone. High levels of reduction achieved at lower temperatures result in a decrease in volume of the impermeable zone. Some indication of the relative proportions of each zone has been attempted schematically in Fig.9.

As the value of *k* in equation (1) is fairly constant, irrespective of heating rate or the prereduction level, one

can use this equation to estimate the extent of reduction from 950°C up to the melt-down temperature at any selected heating rate. An example of this is shown in Fig.10 for acid pellets of 30% prereduction and at three heating rates. To use the diagram one simply estimates the heating rate in the area of the cohesive zone of interest and reads off the value of [1-(1-R)<sup>1/3</sup>] (which can be converted to % reduction) at the different temperatures. The values of % reduction and temperature are then converted to a gas pressure drop value by use of the TRIB diagram. The problem of different levels of prereduction is easily accommodated as alteration of this parameter moves the [1-(1-R)<sup>1/3</sup>] v. temperature curve up or down by a fixed amount as shown for the 45% prereduced situation at a heating rate of 0.0555 K s<sup>-1</sup>.

The gas pressure drop per unit of bed height can be calculated from the changes in gas pressure drop and contraction with increase in temperature. Naturally, it is necessary to scale-up the gas pressure drop values for the increased gas flow within the blast furnace, relative to that of the experimental work. Using this simple technique a

reasonable estimate of the permeability, % reduction, and temperature of the materials within the cohesive zone can be obtained. Such an estimation is depicted in Fig.11 for the two heating rates, intermediate rates lying in between. Although the author realizes the applied load in the furnace is unknown, its effect is simply to reposition the cohesive zone within the furnace, i.e. a higher load will move the impermeable zone to lower temperatures.

If a centre-working blast furnace is charged with two materials of substantially different high-temperature properties, e.g. acid pellets and superfluxed sinter\*, then to alleviate the problem of high gas pressure drops occurring at relatively low temperatures, the material with the least resistance to softening and melting should be charged towards the wall of the furnace. This allows the material (pellets in this situation) to be subjected to a slow heating rate allowing ample time for reduction to proceed, i.e. the critical area in the TRIB diagram is bypassed. The more resistant material should be charged towards the centre of the furnace as it is capable of withstanding the rapid heating rate. In a wall-working furnace the situation is reversed. Using this technique the gas pressure drop in the cohesive zone should decrease and the coke rate should also show a decrease, as the quantity of indirect reduction of the pellets increases.

Layering of the two components across the furnace should be avoided as the acid pellets under rapid heating rate conditions will soften and form an impermeable layer which may prevent gas flow in the adjoining sinter layer. Restrictions to gas flow in the sinter will certainly occur if the liquids from the pellets enter the voids of the sinter layer. If preferential charging of pellets towards the wall of a centre-driving furnace cannot be obtained, the best compromise would be to mix the pellets and sinter before charging. This dilutes the pellet bed with a stronger material and increases the melt-down temperature. The actual increase depends upon the quantity of pellets and sinter in the bed.

## CONCLUSIONS

1. The approximate heating rates of materials through the cohesive zone have been calculated using published data and applied experimentally to acid pellets.

\*Superfluxed sinters have been examined, although the results are not discussed in this paper. However, it can be stated that their melt-down temperatures are higher than that of acid pellets.

2. With acid pellets the first liquid slag formed during reduction is from the  $\text{CaO-FeO-SiO}_2$  (and  $\text{Fe}_2\text{O}_3$ ?) system caused by a reaction between wüstite and the residual  $\text{CaO-Fe}_2\text{O}_3\text{-SiO}_2$  slag present in fully oxidized pellets. Naturally, small amounts of  $\text{MgO}$ ,  $\text{K}_2\text{O}$ , and  $\text{Al}_2\text{O}_3$ , etc. are present in this slag which lowers the melting point.

3. The important parameters for controlling burden-material behaviour at elevated temperatures are the degree of reduction and the localized temperature. Materials possessing a high degree of reduction show low gas pressure drops at elevated temperatures, whereas materials of low levels of reduction at equivalent temperatures show extremely high gas pressure drops. This information has been summarized on temperature-reduction-isobar diagrams, which pinpoint critical areas of reduction and temperature.

4. The high-temperature properties of any material are determined by the relative rates of the reduction and the slag-forming reactions. If the reduction reaction is rapid then low gas pressure drops can be expected. If the slag-forming reaction dominates, high gas pressure drops and increased levels of direct reduction will occur.

5. The distribution of materials within the blast furnace should be thought of in terms of their high-temperature properties in order to minimize coke rates and move the high pressure drop region (melt down) to higher temperatures.

## FURTHER WORK

The study of pellets, sinters, and sinter-pellet mixtures is continuing. Additionally, it is hoped to examine the influence of sulphur and alkalis on the reactions occurring.

## ACKNOWLEDGMENTS

The author would like to thank Dr A. W. D. Hills and Dr G. Briggs of Sheffield Polytechnic Metallurgy Department and F. B. Traice of the British Steel Corporation for discussions, and the British Steel Corporation for permission to publish this work.

## REFERENCES

1. K. SASAKI *et al.*: *Trans. Iron Steel Inst. Jpn*, 1977, **17**, 252-261.
2. K. KANBARA *et al.*: *ibid.*, 371-380.
3. Y. SHIMOMURA *et al.*: *ibid.*, 381-390.
4. M. SASAKI *et al.*: *ibid.*, 391-400.
5. K. KOJIMA *et al.*: *ibid.*, 401-409.
6. Y. OMORI and Y. TAKAHASHI: 'Agglomeration 1977', (ed. K. V. S. Sastry), Vol.1, 286-305; 1977, New York, AIME.
7. P. LECOMTE *et al.*: *Met. Rep. CNRM*, 1969, (21), 21-28.
8. W. M. MCKEWAN: *Trans. AIME*, 1958, **212**, 791.

## CONTINUOUS CASTING OF STEEL

Proceedings of an international conference organized jointly by The Metals Society (UK) and IRSID (France), held at Biarritz, France, on 31 May-2 June 1976.

This volume contains more than forty papers presented at the conference on the subjects of: liquid metal preparation and refractories; machine maintenance related to maximum availability; quality; non-conventional and new techniques; plant experience - blooms and billets; and plant experience - slabs.

xii+324 pp, illustrated  
ISBN 0 904357 08 2

297×210 mm

Price: UK £36.00 (Metals Society Members £30.00) post free  
Overseas: \$90.00 (Members \$72.00) post free

Send orders with full remittance and quoting ordering code 184 to:  
Sales Department, The Metals Society, 1 Carlton House Terrace, London SW1Y 5DB

# Scrap preparation for bulk steelmaking

J. W. Harrington

An estimated 10.64 Mt of scrap is processed annually in the UK, the bulk of which is delivered to the consumer by only 5% of the 10000 or more registered dealers. Scrap consumption has not fluctuated significantly over the past few years; current trends show a slight increase in demand from steelworks and steel foundries, but a continued fall in demand from iron foundries. A widening gap between prices in the UK and in the EEC, however, has resulted in record exports during 1978.

The present supply pattern can be divided into three main categories: direct suppliers, i.e. those supplying the British Steel Corporation; non-direct suppliers, i.e. those supplying the private sector, direct suppliers, and foundries; and those delivering to direct suppliers, the private sector, and other major companies.

Scrap material can also be divided into three categories, namely, circulating scrap, process scrap, and capital scrap. Sorting is the most important step in the processing cycle as it is at that stage that a number of grades are identified before the five main processing operations: pressing, shearing, chipping, fragmentizing, and oxy-acetylene burning.

With respect to the future of the scrap industry, an increasing investment in more sophisticated plant will be necessary to meet the more exacting demands of modern steelmakers. To this end, investigations have already been made into the spheres of hot briquetting and cryogenics. Another factor which will have a growing influence on the competitiveness of the UK steel industry is the increasing capability of third world countries with their cheap ore and energy. This situation is offset only by the volume of indigenous scrap in the UK, an asset not to be lost through low-priced exports. IS/340SC

©1980 The Metals Society. This paper was presented at the conference 'Management of scrap for the electric arc furnace' held jointly by The Metals Society and the Sheffield Metallurgical and Engineering Association in Sheffield on 8 December 1978. The author is with George Cohen Sons and Co. Ltd, London.

**Table 1 Results of BRIC survey of BSF members 1977-78**

Annual quantity of scrap handled and processed, Mt	10.64
Capital investment (processing plant), £m	163
Capital investment (transport), £m	33
Number of employees	14300
Annual wage bill, £	50465000

## THE SCRAP INDUSTRY

The scrap industry is estimated to consist of over 10000 dealers registered with local councils, although not all are continuously active. About 95% of this number collect and deliver no more than 15% of the total tonnage to the main processors. Nearly all the 'bought-in' scrap, handled, sorted, processed, and delivered to the consumer is dealt with by the remaining 5% which is represented by the 538 full members of the British Scrap Federation (BSF). The British Reclamation Industries Confederation (BRIC) recently conducted a survey of BSF members with the results given in Table 1. On a normal basis of ten years depreciation on plant and five years on transport, the depreciation cost alone is £2.15 t<sup>-1</sup> and the average labour cost is £4.74 t<sup>-1</sup>. Added to these figures is the cost of transport into depot and from depot to consuming works, power, heat, light, consumables, financing, and all other overheads. The results obtained by the BSF in their recent survey showed that the average cost incurred by members on each tonne handled and processed was £11.65. The survey was based on operations in 1977-78 and therefore the costs have since risen and will continue to rise in the future. The given average cost per tonne excludes the expenses incurred by the itinerants who scour the towns and countryside collecting small quantities of scrap to supply to the processors, and also excludes the return required by the industry on its investment.

The average consumption of scrap in steelworks and foundries in the UK during 1975-77 is given in Table 2. It can be seen from Table 2 that the average annual tonnage supplied by the scrap industry as bought-in scrap was 8.56 Mt. Over the same period, average exports were 0.80 Mt/year, and the annual increase in merchant stocks was 0.10 Mt, making a total of 9.46 Mt. Added to this total will be the circulating scrap processed in merchants depots, any additions to consumers' stocks, wastage, punchings for road making, and scrap used for other special purposes.

The average stock of steel scrap held by the members of the BSF during 1975-77 was 780000t, while the consumption of home-bought scrap by steelworks and steel foundries over the same period was 6.11 Mt/year. Exports set aside, the stock held by merchants is theoretically

**Table 2 UK scrap consumption 1975-78**

Year	Home bought		Imported		Circulating		Total, Mt
	Mt	% of total	Mt	% of total	Mt	% of total	
Steelworks and steel foundries							
1975	5.94	53.71	0.10	0.90	5.02	45.39	11.06
1976	6.51	52.76	0.69	5.59	5.14	41.65	12.34
1977	5.87	52.80	0.08	0.68	5.17	46.52	11.12
Total	18.32	..	0.87	..	15.33	..	34.52
Average	6.11	53.08	0.29	2.25	5.11	44.40	11.51
1978	7.10	..	0.02	..	4.67	..	11.79
Iron foundries							
1975	2.50	65 (est.)	..	..	1.34	35 (est.)	3.84
1976	2.50	65 (est.)	..	..	1.35	35 (est.)	3.85
1977	2.36	65 (est.)	..	..	1.27	35 (est.)	3.63
Total	7.36	..	..	..	3.96	..	11.32
Average	2.45	65 (est.)	..	..	1.32	35 (est.)	3.77
1978	2.24	..	..	..	1.27	..	3.51

SOFTENING AND MELTING OF SUPERFLUXED  
SINTERS AND ACID PELLETS

George Clixby

British Steel Corporation  
Ironmaking Section  
Teesside Laboratories  
Middlesbrough  
Cleveland

Introduction

The softening and melting zone of the blast furnace has always been regarded as an important region of the ironmaking process. Unfortunately, because of the practical difficulty of examining the interior of an operating blast furnace, very little was known about this region until fairly recently. The quenching and dissection of several operating blast furnaces in Japan in the seventies produced a vast amount of information describing the internal state of the blast furnace<sup>(1-5)</sup>. This information highlighted the importance of the softening-melting or cohesive zone in the production of iron and also provided the data necessary to allow realistic experimental studies of the behaviour of blast furnace burden materials. This paper describes some of the studies performed and their relationship with blast furnace practice. The majority of the work described in this paper was undertaken specifically for the British Steel Corporation's 14m furnace at Redcar.

Experimental Technique

The test procedure was basically an athermal reduction-under-load technique carried out in the temperature range 950°C - 1350°C. The material under examination was pre-reduced to the desired degree, at 950°C, in a separate piece of apparatus by a 40 vol. % carbon monoxide/60 vol. % nitrogen atmosphere, and cooled in nitrogen. When cold the sample was transferred to the high temperature apparatus (Figure 1). The charging procedure adopted was to place a layer of coke into the crucible, followed by the sample and finally a second layer of coke. Thermocouples to measure the

sample temperature were embedded in the sample during the charging procedure. The coke layers served to protect the graphite crucible and ram from attack by the sample.

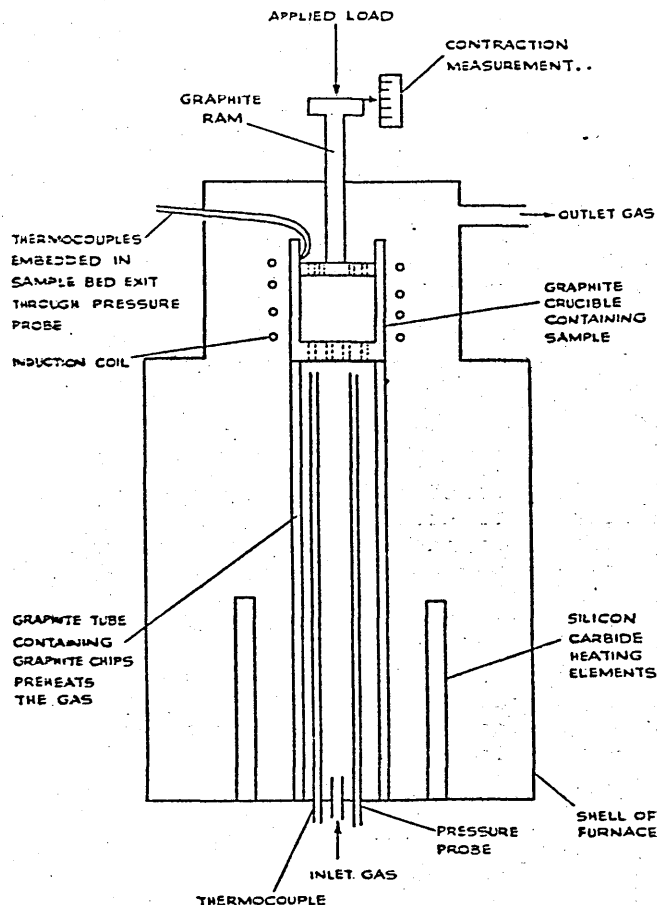


Figure 1 Schematic view of the apparatus

The sample was heated in nitrogen to 950°C and then a 40 vol. % carbon monoxide/60 vol. % nitrogen gas mixture was passed through the sample bed at a controlled flow rate. Simultaneously a load was applied to the sample and the temperature of the bed raised at a pre-determined rate. As the test proceeded the gas pressure drop across the bed and the contraction of the bed were measured. Termination of the test usually occurred when the rate of increase of the gas pressure drop became excessive or when the thermocouples measuring the bed temperature failed. Determination of the change in the degree of reduction of the bed was accomplished by analysis of the inlet and outlet gases. At the end of the test the sample was cooled in nitrogen, removed and weighed, enabling the reduction level calculated by gas analysis to be checked.

The test conditions used in these experiments are shown in Table I.

TABLE I - TEST CONDITIONS USED

Heating rate from 950°C:	200 or 400 deg. C. hr <sup>-1</sup>
Gas Flow:	3.6Nm <sup>3</sup> .hr <sup>-1</sup>
Gas Composition:	40 vol.% CO, 60 vol.% N <sub>2</sub>
Applied Load:	49 K.N.m <sup>-2</sup>
Bed Diameter:	90mm
Initial bed Height:	66mm
Bottom coke layer Depth:	40mm
Top coke layer Depth:	15mm
Particle Size Range:	10-12.5mm

The procedure for studying the influence of sulphur and alkalis contained in the reducing gas upon the softening-melting characteristics of the sample bed was fairly straight-forward. Sulphur was introduced as sulphur dioxide which was subsequently reduced by the graphite chips in the pre-heat stage to molecular sulphur. (Note: all sulphur concentrations stated in this paper are in elemental terms). The sulphur dioxide was admitted at the start of the test (950°C) and the flow rate maintained constant until the termination of the test.

Alkali was introduced by placing a small graphite crucible containing potassium carbonate in the pre-heat stage just beneath the crucible containing the sample. In some cases two crucibles were used in order to accommodate the necessary volume of carbonate. The potassium carbonate was reduced by the graphite and entered the reducing gas in the form of metallic vapour and potassium cyanide. Although there was no control of the vapour pressure of the alkali, the test conditions were identical in each test, hence the tests are comparative and the levels of alkali addition can be expressed as a loading, i.e. x kg/tonne of metal, or as a weight of potassium carbonate used. Such a test procedure obviously has flaws, one of which is the question, does the alkali vaporise rapidly over a short temperature range or reasonably uniformly throughout the reduction procedure? One test interrupted at 1125°C showed that just over half of the alkali had vaporised, yet complete tests terminating between 1250°C and 1300°C had 100% vaporisation of the carbonate.

This indicates that vaporisation is reasonably uniform throughout the test.

Selection of Heating Rate and Pre-Reduction Levels

In order to make the test procedure described realistic, it was necessary to determine (a) the heating rate of the burden through the cohesive zone, and (b) the degree of reduction of the burden prior to entry of the cohesive zone. As previously stated the majority of the test work was directed towards the 14m blast furnace at Redcar, which was scheduled to operate with a strong centre working practice. Hence the Japanese quenched furnace data was examined for a similar operating furnace, from which the necessary information could be extracted. Such a furnace was Hirohata No. 1.

The softening-melting layers (Figure 2) can be looked upon as time intervals, and knowledge of the charging frequency allows an estimation of the heating rate of burden materials in the cohesive zone to be made. Calculations showed that the heating rate near the apex of the cohesive zone was ~ 300 deg. C.hr<sup>-1</sup> and ~ 190 deg.C.hr<sup>-1</sup> near the base(6). Hence, for the experimental work two heating rates were selected: 400 deg.C.hr<sup>-1</sup> representing the central region of a centre working furnace and 200 deg.C.hr<sup>-1</sup> representing the condition near the walls of the furnace.

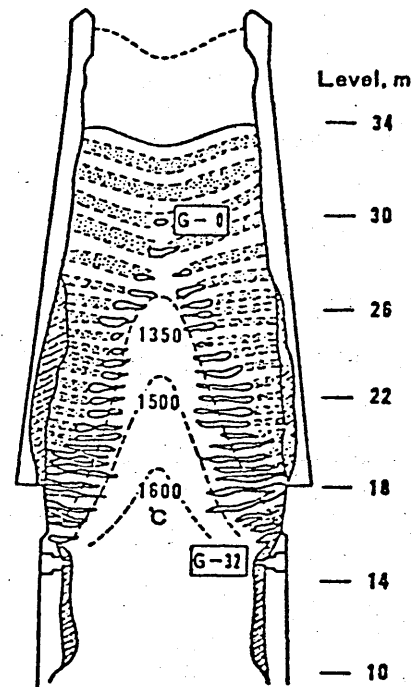


Figure 2 Formation of softening and melting layers (Hirohata No.1 B.F.)

Selection of the pre-reduction level for the testwork, from the quenched furnace data, was complicated by the possible reoxidation of burden materials during the quenching operation. Figure 3 shows the structure of two of the softening-melting layers, whilst Table II gives the reduction levels in the different regions of the layers. It is apparent that in the main lumpy portion (D) the reduction degree in the central region of the furnace is very low and even towards the walls it is only 35 to 41%. The smaller lumpy portion (C) in the central region has a much higher level of reduction, attributed to the slightly lower reduction temperature whilst in contact with coke<sup>(1)</sup>.

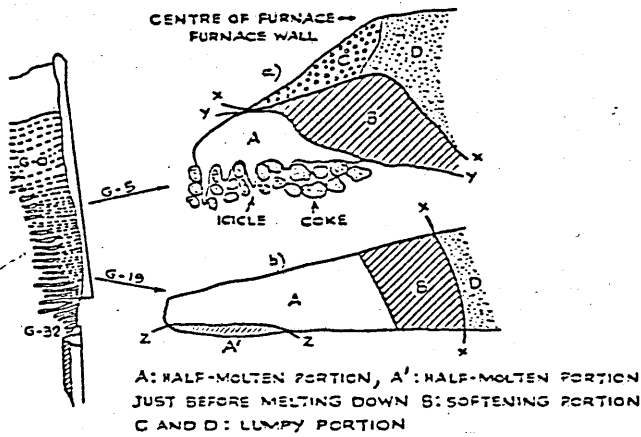


Figure 3 Structure of softening-melting layers (Hirohata No.1 B.F.)

Due to the doubt existing regarding the level of pre-reduction, the experimental procedure adopted was to carry out several tests, each at a different level of pre-reduction and to assess the results as a whole.

#### Materials Used in the Experimental Study

All the sinters examined were manufactured from the same blend of ores in a laboratory sinter pot. The CaO/SiO<sub>2</sub> ratio was varied from 1.6 to 2.4 by alteration of the proportions of ores used and by the addition of limestone (Table III).

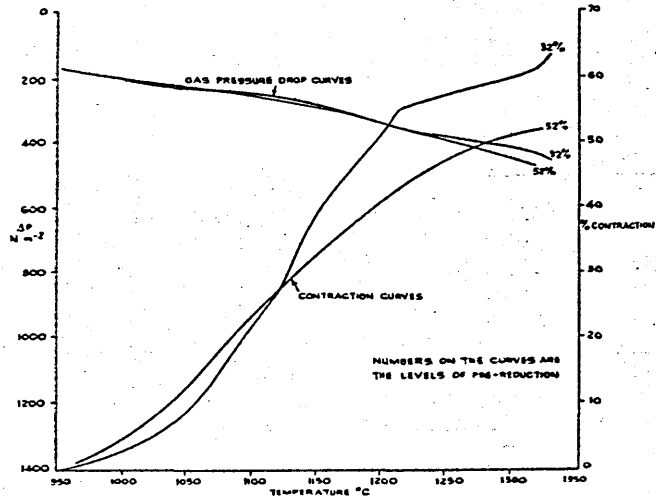


Figure 4 Contraction and gas pressure drop at the 200 deg.C.hr<sup>-1</sup> heating rate for Type A pellets

TABLE II REDUCTION DEGREES OF THE IRON ORES OF THE SOFTENING-MELTING LAYERS (HIRCHATA NO.1 BLAST FURNACE)

Softening-melting layer	Portion	REDUCTION DEGREE (%)		
		Sinter	Lumpy Ore	Pellet
G-5	B	65.6	65.0	79.3
	C	72.8	68.2	81.2
	D	11.5	12.3	14.6
G-19	D	35.4	36.6	41.3

B = Softening Portion,  
C and D = Lumpy Portion

The acid pellets were also manufactured in the laboratory using a grate-kiln pilot plant. Three types of acid pellets were examined, Type A were manufactured from one blend of iron ores, Type B were manufactured from a different blend and Type C were produced by adding a small quantity of limestone to the ore blend used for Type B pellets.

### Results

Acid pellets have a homogeneous structure compared to sinter and because of this the majority of the fundamental testwork was devoted to pellets. Sinters were found to be subject to identical trends in behaviour, i.e. the concepts developed from the experimental work with acid pellets were found to apply equally to sinters.

#### Acid Pellets

The change in the gas pressure drop across the bed and the contraction of the bed with rise in temperature is shown in Figure 4 for Type A pellets tested using the 200 deg.C.hr.<sup>-1</sup> heating rate. Figure 5 shows the increase in the degree of reduction with temperature for these two tests. The change in the gas pressure drop across the bed and the contraction of the bed with increase in temperature using the 400 deg.C.hr.<sup>-1</sup>

heating rate is illustrated in Figure 6; the corresponding reduction-temperature curves are shown in Figure 5. It was possible to detect the commencement of the process of direct reduction of the sample in some cases. (The start of direct reduction was calculated from the gas analyses). Where such a reaction was detected the temperature is marked on the reduction curves.

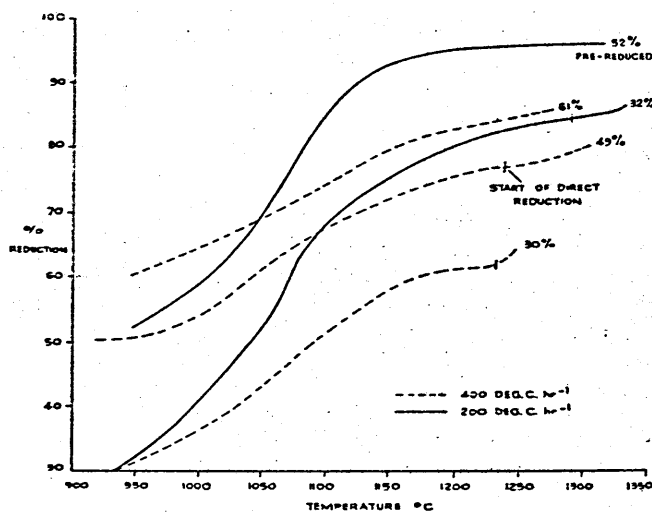


Figure 5 Reduction-temperature curves for Type A pellets at both heating rates

TABLE III CHEMICAL ANALYSES OF THE MATERIALS

Sinters	wt.%						
	CaO/SiO <sub>2</sub>	Fe	FeO	CaO	SiO <sub>2</sub>	Al <sub>2</sub> O <sub>3</sub>	MgO
	2.4	54.5	8.1	12.6	5.1	1.5	2.5
	2.1	56.5	8.2	11.1	5.1	1.8	2.5
	1.8	57.4	12.8	9.6	5.3	1.7	1.8
	1.6	56.9	16.8	9.6	5.9	2.0	2.9
Pellets							
A		66.3	-	0.03	4.60	0.40	0.50
B		64.8	-	0.10	5.10	1.30	0.20
C		64.6	-	1.02	5.16	1.31	0.21

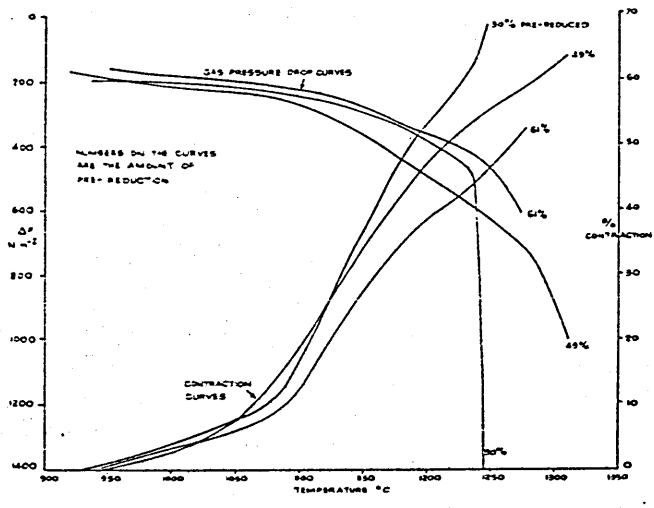


Figure 6 Contraction and gas pressure drop at the 400 deg.C.hr<sup>-1</sup> heating rate for Type A pellets

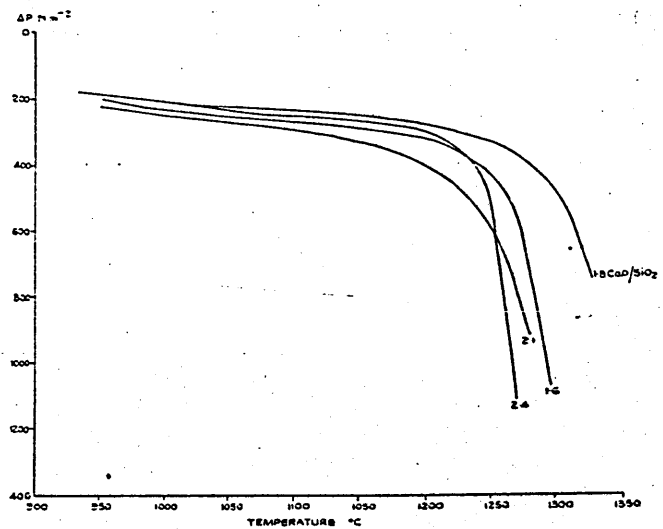


Figure 9 Gas pressure drop for sinters (in the as-received state) at the 400 deg.C.hr<sup>-1</sup> heating rate

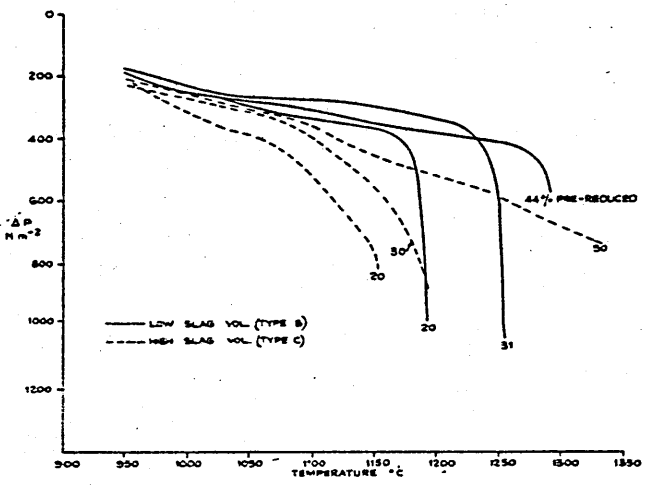


Figure 7 Influence of pellet slag volume on the gas pressure drop

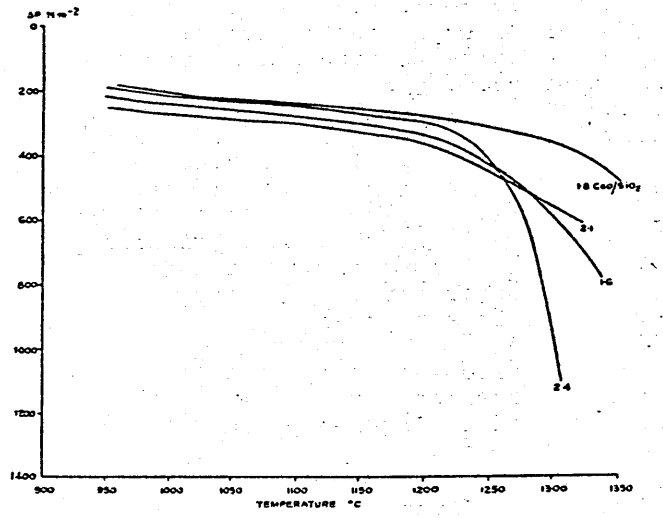


Figure 10 Gas pressure drop for sinters (30% pre-reduced) at the 400 deg.C.hr<sup>-1</sup> heating rate

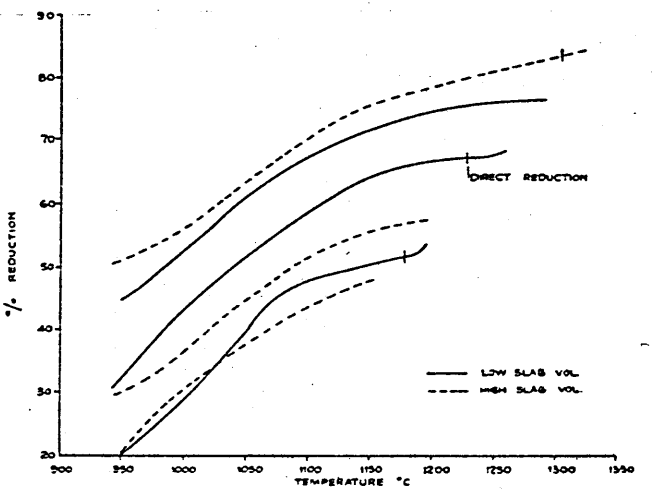


Figure 8 Influence of pellet slag volume on the % reduction

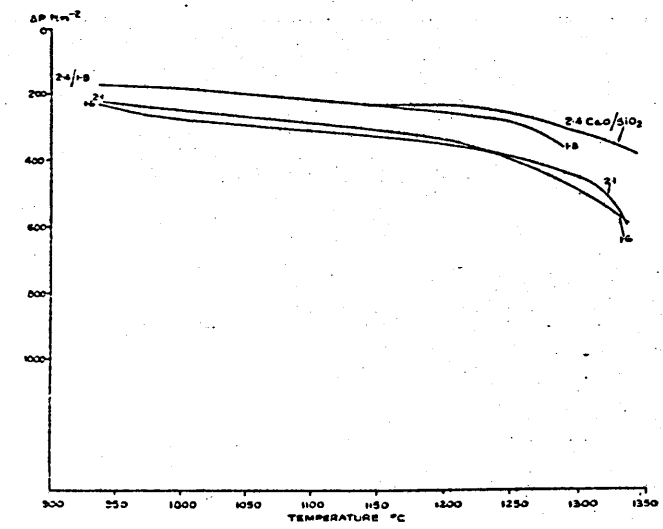


Figure 11 Gas pressure drop for sinters (45% pre-reduced) at the 400 deg.C.hr<sup>-1</sup> heating rate

Only the 400 deg.C.hr<sup>-1</sup> heating rate test procedure was used for the examination of Type B and Type C pellets. The rise in gas pressure drop across the bed with increase in temperature is shown in Figure 7, whilst Figure 8 shows the corresponding reduction-temperature curves. Although not shown graphically, the temperature at which 3% contraction of the bed occurred with both Type B and Type C pellets was similar to that of Type A pellets. (The significance of the 3% contraction temperature will be discussed later).

Quantitative analyses of the proportions of mineralogical phases present in the fully oxidised pellets was undertaken and are given in Table IV.

### Sinters

The sinter was tested using both the 200 and 400 deg.C.hr<sup>-1</sup> heating rates. For reasons explained later only the 400 deg.C.hr<sup>-1</sup> heating rate test results are presented. Figures 9, 10 and 11 show the gas pressure drop-temperature curves for the three levels of pre-reduction examined (as received, 30% and 45%). The reduction-temperature curves for the as-received and 30% pre-reduced samples are shown in Figures 12 and 13. The temperature at which 3% contraction of the bed occurred was ~ 1100°C in every case.

Quantitative analysis of the mineralogical phases present in the sinters, in their as-received state, was also undertaken (Table IV).

### Sinter/Pellet Mixtures

The softening-melting character-

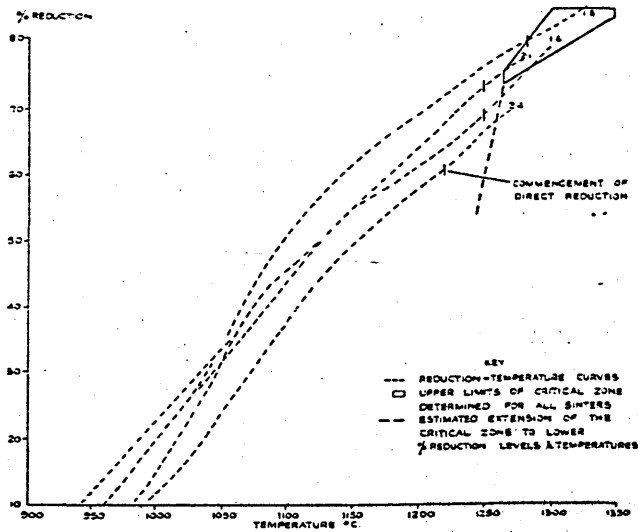


Figure 12 Reduction-temperature curves for sinters (in the as-received state) at the 400 deg.C.hr<sup>-1</sup> heating rate

istics of the sinter/pellet mixtures were examined using the 2.4 CaO/SiO<sub>2</sub> sinter and Type A acid pellets in the proportions 50 wt.% sinter/50 wt.% pellets. Additional tests were carried out to determine the influence of the proportion of pellets in a sinter bed upon the softening-melting characteristics of the bed. These tests were undertaken using the 1.8 CaO/SiO<sub>2</sub> sinter and Type B acid pellets.

Considering the 2.4 CaO/SiO<sub>2</sub> sinter and Type A acid pellets tests first; as the reducibilities of the two materials were different, the two materials were pre-reduced separately under identical conditions for the same

TABLE IV PHASE ANALYSES OF THE MATERIALS (VOLUME %)

Phase	Sinter CaO/SiO <sub>2</sub>				Pellets		
	1.6	1.8	2.1	2.4	A	B	C
Magnetite	48.2	21.6	22.2	21.4	4.4	-	-
Hematite	14.0	23.8	20.0	18.6	70.8	87.0	78.4
Slag	11.0	6.8	4.4	6.4	15.4	2.6	14.0
Ferrites	23.0	39.4	47.2	45.0	-	-	-
C <sub>2</sub> S	3.8	8.4	6.2	8.6	-	-	-
Quartz	-	-	-	-	9.4	10.4	7.6

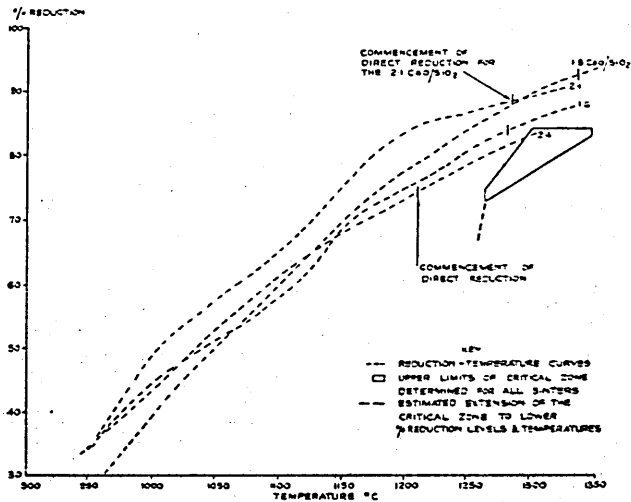


Figure 13 Reduction-temperature curves for sinters (30% pre-reduced) at the 400 deg.C.hr<sup>-1</sup> heating rate

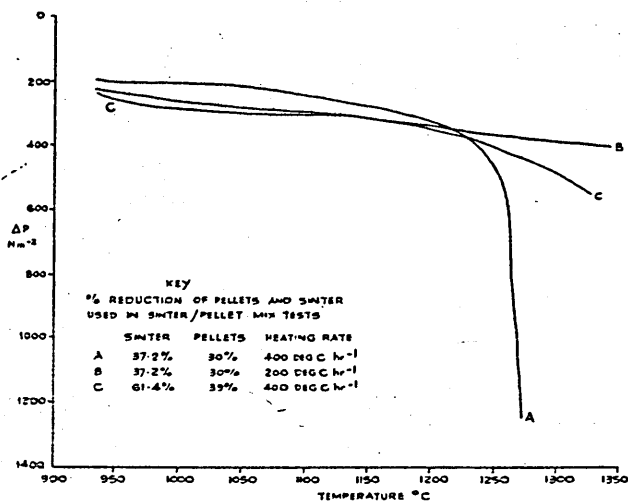


Figure 14 Gas pressure drop for mixtures of 2.4 CaO/SiO<sub>2</sub> sinter and Type A pellets

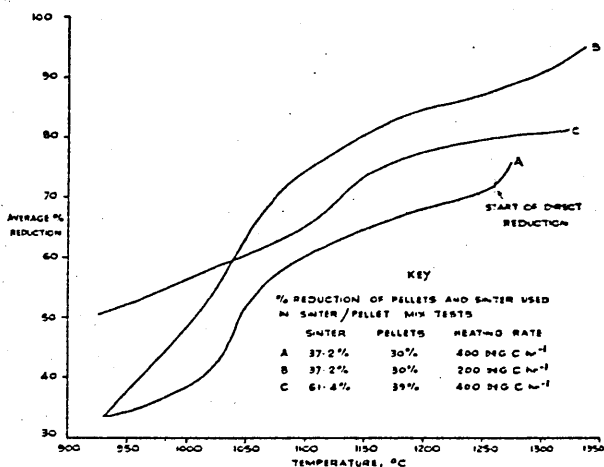


Figure 15 Reduction-temperature curves for mixtures of 2.4 CaO/SiO<sub>2</sub> sinter and Type A pellets

period of time and their degree of reduction determined. The materials were then mixed in proportions equivalent to 50/50 wt.% in the as-received state and tested in the high temperature apparatus. Two pre-reduction times and the two heating rates were used. Figure 14 shows the gas pressure drop-temperature curves for the three tests:-

Test A - Both materials pre-reduced for 30 minutes, then tested at the 400 deg.C.hr<sup>-1</sup> heating rate.

Test B - Both materials pre-reduced for 30 minutes, then tested at the 200 deg.C.hr<sup>-1</sup> heating rate.

Test C - Both materials pre-reduced for 60 minutes then tested at the 400 deg.C.hr<sup>-1</sup> heating rate.

It was not possible to determine the change in reduction of the individual components in the high temperature test, merely the change in the average reduction level of the sample bed (Figure 15).

In tests using the 1.8 CaO/SiO<sub>2</sub> sinter and Type B acid pellets; again both materials were pre-reduced under identical conditions for thirty minutes then mixed in the proportions equivalent to 25, 50 and 75 wt.% pellets in the mix in the as-received state. The pre-reduction levels of the sinter and pellets were 40.5 and 27.1% respectively. Testing of these mixtures was carried out at the 400 deg.C.hr<sup>-1</sup> heating rate; the gas pressure drop and reduction-temperature curves are shown in Figures 16 and 17 respectively.

#### Tests with Gaseous Sulphur in the Reducing Gas

These tests were carried out with Type A pellets and the 1.8 CaO/SiO<sub>2</sub> sinter. Two levels of sulphur loading were investigated: 0.28 and 0.75 vol.% calculated on an elemental basis. The influence of sulphur on the gas pressure drop and the degree of reduction of the pellets (pre-reduced by 30%) is shown in Figures 18 and 19. It was impossible to determine the reduction path of the acid pellets tested at the 200 deg.C.hr<sup>-1</sup> heating rate, for reasons discussed later.

The effect of 0.75 vol.% of sulphur dioxide in the reducing gas upon the gas pressure drop and the reduction path of the 1.8 CaO/SiO<sub>2</sub> sinter, also pre-reduced by 30%, at the 400 deg.C.hr<sup>-1</sup> heating rate is shown in Figure 20.

Chemical analyses of the materials

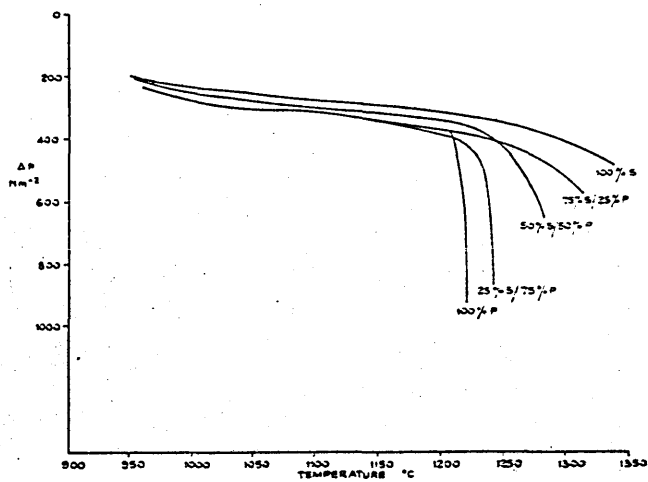


Figure 16 Gas pressure drop for mixtures of 1.8 CaO/SiO<sub>2</sub> sinter and Type B pellets

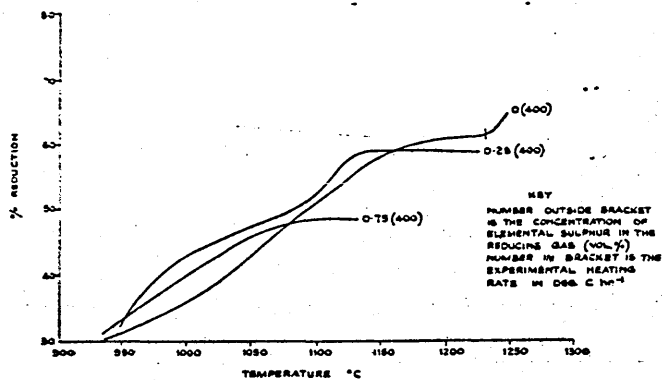


Figure 19 Influence of sulphur on the reduction of Type A pellets

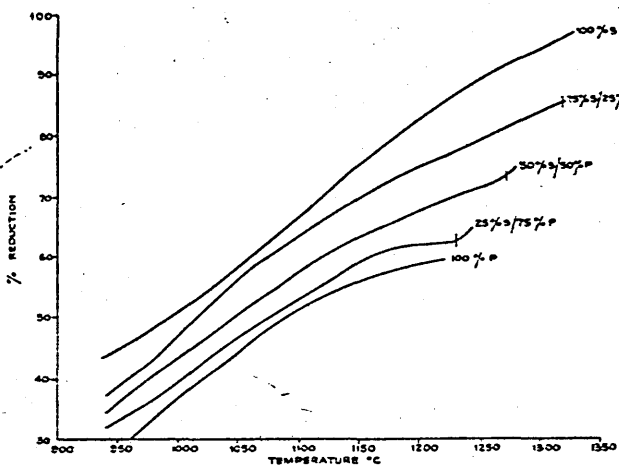


Figure 17 Reduction-temperature curves for mixtures of 1.8 CaO/SiO<sub>2</sub> sinter and Type B pellets

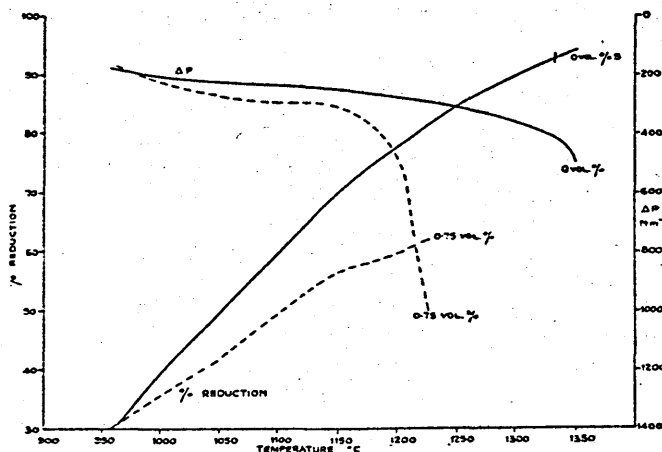


Figure 20 Influence of sulphur on the gas pressure drop and the reduction of 1.8 CaO/SiO<sub>2</sub> sinter

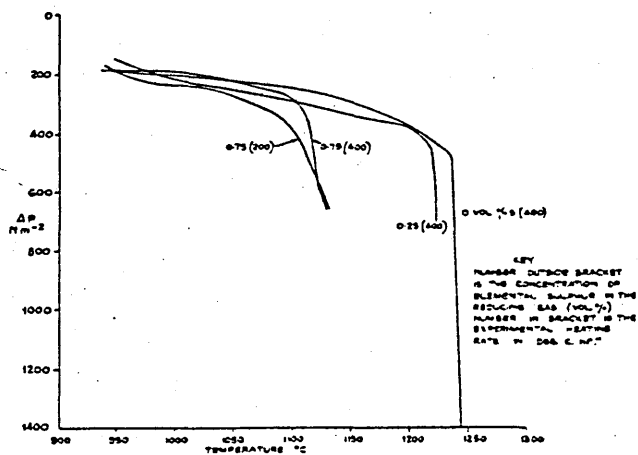


Figure 18 Influence of sulphur on the gas pressure drop of Type A pellets

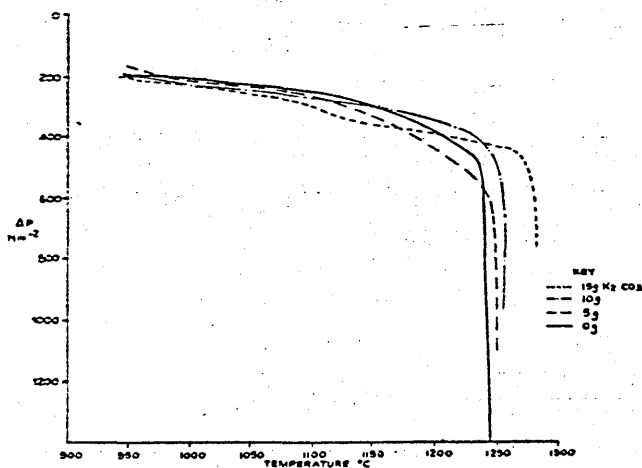


Figure 21 Influence of alkali on the gas pressure drop of Type A pellets

after the high temperature test are given in Table V.

### Influence of Alkali Vapour in the Reducing Gas

The alkali vapour tests were carried out with Type A acid pellets using an identical degree of pre-reduction and heating rate for each of the four tests (30% pre-reduction and the 400 deg.C.hr<sup>-1</sup> heating rate). Three levels of alkali loading were examined - 5 g K<sub>2</sub>CO<sub>3</sub>, 10 g and 15 g which is equivalent to 6 kg K<sub>2</sub>O/tonne of metal; 12 kg/tonne and 18 kg/tonne respectively, assuming that all the alkali was retained in the sample bed. The results of these tests are shown in Figures 21, 22 and Table V.

### Influence of Alkali Vapour and Sulphur in the Reducing Gas

This test was carried out at the 400 deg.C.hr<sup>-1</sup> heating rate using Type A pellets that had been pre-reduced by 30%. An alkali loading of 15 g K<sub>2</sub>CO<sub>3</sub> coupled with a sulphur concentration of 0.75 vol.% was used (Figures 23 and 24).

### Discussion

#### Type A Acid Pellets

Tests at a heating rate of 200 deg.C.hr<sup>-1</sup> showed that both samples started to contract at virtually the same temperature, namely 1010°C and 985°C for the 32% and 52% pre-reduced samples respectively. (The temperature at which 3% contraction of the bed occurred was arbitrarily selected as the start of softening). During the test both samples showed a steady rise in gas

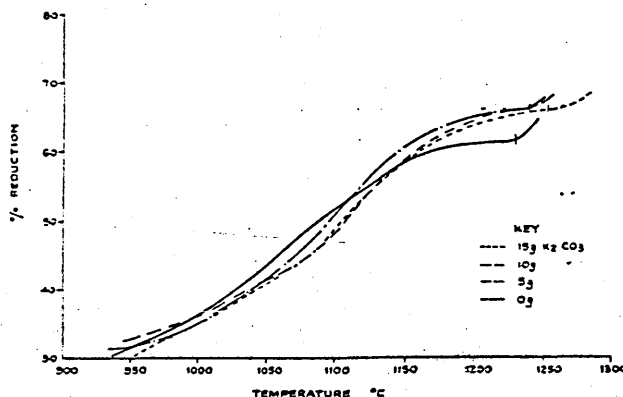


Figure 22 Influence of alkali on the reduction of Type A pellets

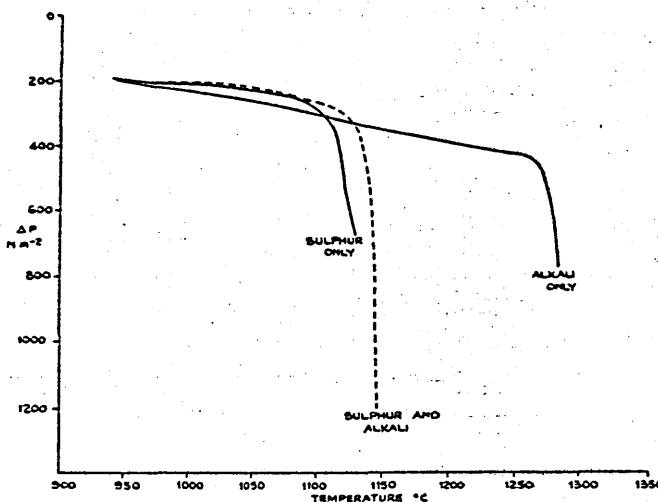


Figure 23 Influence of sulphur and alkali on the gas pressure drop of Type A pellets

TABLE V CHEMICAL ANALYSES AFTER SULPHUR AND ALKALI TESTS

Sample	Species	Concentration	Heating Rate	Wt. %					
				Met.Fe	FeO	Total Fe	Na <sub>2</sub> O	K <sub>2</sub> O	S
Pellets	Sulphur	0.28 vol. %	400 deg.C.hr <sup>-1</sup>	33.40	49.90	75.20	0.19	0.10	0.92
"	"	0.75	400	24.40	63.80	74.10	0.20	0.07	1.80
"	"	0.75	200	31.90	57.80	76.70	0.18	0.08	2.70
Sinter	"	0.75	400	29.20	42.80	62.80	-	-	3.70
Pellets	Alkali	5gK <sub>2</sub> CO <sub>3</sub>	400	40.90	41.20	76.90	0.17	0.38	0.04
"	"	10g	400	52.30	28.90	79.00	0.20	0.77	0.03
"	"	15g	400	49.90	31.60	78.20	0.21	0.70	0.03

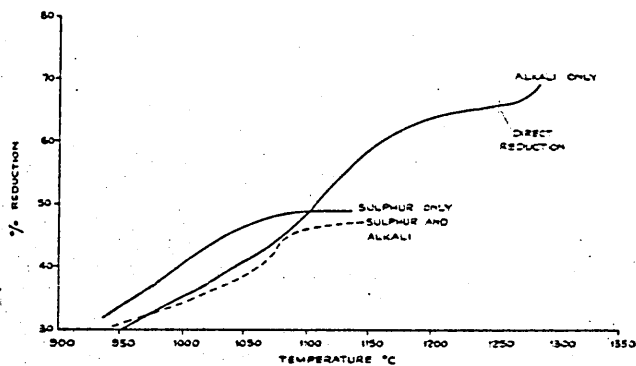


Figure 24 Influence of sulphur and alkali on the reduction of Type A pellets

980°C from the 1100°C of the CaO-SiO<sub>2</sub>-FeO eutectic.

The increase in gas pressure drop with rise in temperature at the fast heating rate was dramatic, especially at the lower levels of pre-reduction (Figure 6). The rapid rise in the gas pressure drop coincided with the commencement of direct reduction (Figure 5). This indicates that iron oxide rich liquid was filling the voids of the bed, causing the rapid rise in pressure, and the same liquid was reacting with the coke bed to cause the direct reduction reaction<sup>(6)</sup>. Hence the gas pressure drop is the most useful parameter for characterising the softening-melting properties of burden materials - measurement of the contraction of the bed is useful only for detecting the start of softening.

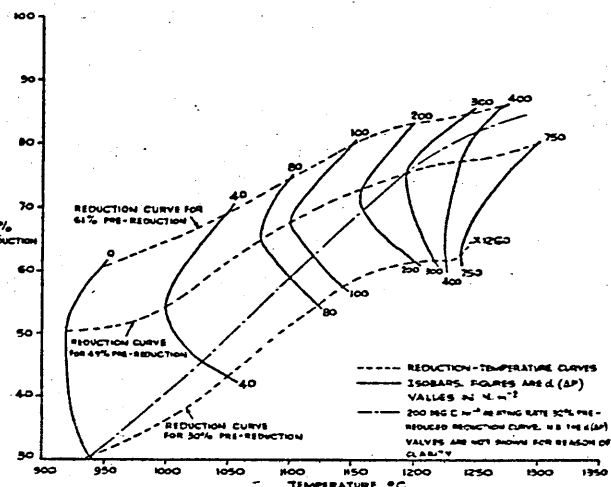


Figure 25 'TRIB diagram' for Type A pellets

A relationship was found to exist among the % reduction, temperature and the gas pressure drop, (Figure 25). This diagram has been constructed by plotting the % reduction against temperature for the tests carried out at the 400 deg.C.hr<sup>-1</sup> heating rate and superimposing onto the curves the change in the gas pressure drop, i.e. the gas pressure drop at any temperature minus the gas pressure drop at the starting temperature of the experiment (950°C). These type of diagrams have been termed 'TRIB diagrams' (Temperature, Reduction Isobars) and show the region of reduction and temperature in which high gas pressure drops, associated with 'melt-down' of the bed and liquids filling the voids, occur. The 'critical' region is where the isobars merge together; in this case 60-65% reduction and 1200 - 1250°C. Although not documented in this paper tests with pre-reduced samples using nitrogen only confirmed the 'melt-down' temperatures determined from the 'TRIB diagram' and also showed that at levels of reduction less than 60% the 'melt-down' temperature decreased<sup>(6)</sup>.

pressure drop and achieved a fairly high degree of reduction (Figures 4 and 5).

At a heating rate of 400 deg.C.hr<sup>-1</sup> the 3% contraction temperatures were identical to those obtained at the slower heating rate, i.e. 985°C for the 30% and 65% pre-reduced samples and 1010°C for the 49% pre-reduced sample. (Figure 6). Although not documented in this paper, tests with pre-reduced samples using nitrogen gas only also showed similar 3% contraction temperatures. The similar 3% contraction temperatures are due to a reaction between wustite and the slag present in the fully oxidised pellets (residual slag) producing a liquid slag which has a melting point of ~980°C. This liquid slag is composed essentially of CaO, SiO<sub>2</sub>, FeO and traces of MgO, Al<sub>2</sub>O<sub>3</sub> and alkali<sup>(6)</sup>. Evidently the alkali is responsible for the lowering of the melting point of the slag to

'TRIB diagrams' show the zone of temperature and reduction that must be avoided if high gas pressure drops occurring at relatively low temperatures are to be prevented. Both samples tested at the 200 deg.C.hr<sup>-1</sup> heating rate achieved levels of reduction in excess of the 'critical' resulting in the maintenance of a low gas pressure drop up to 1350°C.

A detailed description of the liquid slag forming reaction occurring within these particular pellets is given elsewhere<sup>(6)</sup>, but basically the liquid slag is formed at the pellet

core and migrates to the pellet surface, prompted by the squeezing action of the applied load and the increase in temperature (the latter lowering the slag viscosity). The factor determining whether the slag can escape from the pellet is the degree of reduction. A low degree of reduction produces a lot of slag and a thin metallic shell, which offers little resistance to the outflow of slag causing high gas pressure drops. A high degree of reduction minimises the slag volume and produces a thick metallic shell, offering a great resistance to the outflow of slag. This is a low gas pressure drop situation.

The situation existing can be looked upon as a competition between the slag forming reaction and the reduction reaction. If the slag formation reaction dominates, the extent of reduction is limited and the 'melt-down' temperature is low, coupled with a high gas pressure drop. Dominance by the reduction reaction raises the 'melt-down' temperature and maintains bed permeability. Fast heating rates favour the slag formation reaction whilst slow heating rates favour the reduction reaction.

#### Type B and C Pellets

Type B pellets although manufactured from a different ore blend to Type A pellets showed similar behaviour to Type A pellets. Compare the 31% pre-reduced Type B pellet with the 30% pre-reduced Type A pellet (Figures 5, 6, 7 and 8). Both underwent 'melt-down' at approximately the same temperature, but the Type B pellets were slightly more reducible than the Type A pellets.

Increasing the slag volume of Type B pellets, i.e. Type C pellets caused a marked deterioration in the softening-melting properties (Table IV and Figures 7 and 8). The increased slag volume allowed the liquid slag forming reaction between the wustite and the residual slag to proceed readily causing decreased levels of reduction and lower 'melt-down' temperatures relative to Type B pellets. It is apparent that the rapid 'melt-down' shown by the 30% pre-reduced Type B pellet did not occur with the corresponding Type C pellet, however, the gas pressure drop was higher with Type C pellets, until the Type B pellets underwent 'melt-down'. The reason for this is probably that although the slag forming reactions were occurring to a greater extent with Type C pellets, the temperature was too low to make the slag fluid enough to rapidly break out of the pellet and fill the

voids of the bed. The lack of any direct reduction reaction with the 20% and 30% pre-reduced samples of Type C pellets also points to the lack of fluidity of the slag, i.e. if the slag was sufficiently fluid then it would drip into the underlying coke layer, causing direct reduction. Some direct reduction was detected with the 50% pre-reduced Type C pellets, but at a higher temperature. Naturally, the higher the level of gaseous reduction, the less direct reduction that can occur because of the decreased liquid slag volume.

Although both Type A and Type C pellets have similar slag volumes, the softening-melting characteristics of Type A pellets are akin to Type B pellets, which have a smaller slag volume (Table IV). This indicates that although slag volume is important in acid pellets manufactured from the same blend, the introduction of other blends of similar slag volume can have a marked effect. The exact mineralogical reason for this is not clear at this stage, but seems unlikely to be associated with the melting point of the slag formed by the wustite/residual slag reaction because the 3% contraction temperatures are similar. A tentative explanation may be the differing reduction modes between the three different types of pellets. Type A pellets during the pre-reduction stage showed topochemical reduction and very little swelling. Types B and C swelled and cracked considerably showing non-topochemical reduction behaviour of the wustite grains. It may be that the protective iron shell around the wustite formed by topochemical reduction prevented a lot of the slag formation reactions occurring, especially at the lower temperatures<sup>(6)</sup>. Non-topochemical reduction would not produce a protective iron shell, thus the liquid slag formation reactions could still occur.

#### Superfluxed Sinters

Micro-examination of semi-reduced sinters showed that two distinct mechanisms of slag formation were operating:-

- (i) In lime deficient regions a reaction between wustite (originating from the original hematite or magnetite grains) and the surrounding slag to form essentially a CaO-SiO<sub>2</sub>-FeO liquid slag.
- (ii) In lime rich regions the semi-reduced ferrites underwent internal melting to produce a FeO-CaO liquid slag.

All the sinters tested in the as-received state at the 400 deg.C.hr<sup>-1</sup> heating rate showed a rapid rise of gas pressure drop and 'melt-down' of the bed. (Figure 9). This is an analogous situation to that occurring with acid pellets. The testing of samples in the as-received state is obviously not directly applicable to blast furnace operation, however, such tests provided useful information at the lower level of final reduction. At a pre-reduction level of 30% and at the 400 deg.C.hr<sup>-1</sup> heating rate only the 2.4 and the 1.6 CaO/SiO<sub>2</sub> sinter underwent a rapid rise of gas pressure drop. The other two sinters showed little sign of 'melt-down', (Figure 10). At 45% pre-reduction and the 400 deg.C.hr<sup>-1</sup> heating rate none of the sinters entered into the 'melt-down' condition, (Figure 11). Although not documented in this paper, no sinters tested in the as-received condition using the 200 deg.C.hr<sup>-1</sup> heating rate underwent 'melt-down'.

The concept of 'TRIB diagrams' was introduced using Type A acid pellets as an example. 'TRIB diagrams' were constructed for each of the sinters covered in this paper and for some other sinters of lower basicity also manufactured from the same blend. (The latter sinters are not discussed in this paper). Although the individual 'TRIB diagrams' differed the 'critical' zone of reduction and temperature in which the rapid build-up of gas pressure drop occurred was very similar for all the sinters. Consequently it was possible to determine a region of reduction and temperature within which all the 'critical' zones of the individual sinters lay. The entry of the reduction path into this zone, or the underlying region causes the rapid build-up of gas pressure and 'melt-down' of the bed. Figure 12 shows that the reduction paths of all the sinters tested in the as-received state using the 400 deg.C.hr<sup>-1</sup> heating rate entered either into the zone or the underlying region, which should cause 'melt-down' of the bed. This is verified by the gas pressure drop temperature curves (Figure 9). At 30% pre-reduction and the 400 deg.C.hr<sup>-1</sup> heating rate the reduction paths of the 1.8 and 2.1 CaO/SiO<sub>2</sub> sinters by-passed the zone by a good margin, whilst the reduction path of the 2.4 CaO/SiO<sub>2</sub> sinter entered the zone and the reduction path of the 1.6 CaO/SiO<sub>2</sub> sinter just avoided the zone (Figure 13). This situation should lead to the 1.8 and 2.1 CaO/SiO<sub>2</sub> sinters avoiding 'melt-down' in the temperature range studied, and the 2.4 and 1.6 CaO/SiO<sub>2</sub> sinters undergoing 'melt-down'. This hypothesis is verified by the gas

pressure drop-temperature curves (Figure 10).

At 45% pre-reduction and the 400 deg.C.hr<sup>-1</sup> heating rate the level of reduction attained by all the sinters was almost 100%, by-passing the 'critical' zone by a large margin. Consequently 'melt-down' of the bed did not occur up to the limit of the apparatus (Figure 11).

The factor that determines whether a burden material has a high or low 'melt-down' temperature is the reducibility. Simply, the more reducible the material the higher the 'melt-down' temperature. Hematite and calcium ferrites are the most reducible phases (an exception is dicalcium ferrite), and the greater the proportion of these phases the more reducible the sinter should be. The reduction-time curves have been analysed in terms of McKewan's rate equation and assuming the oxygen density and particle radius are constant for each material his equation simplifies to:-

$$1-(1-R)^{\frac{1}{3}} = kt \text{ ————— (1)}$$

It is worth mentioning that there has been considerable debate concerning the mechanism of the reduction reaction and its relationship to McKewan's rate equation. It is not the intention of the author to enter into this sphere of debate, but merely to use McKewan's equation as a tool, irrespective of the rate controlling mechanism.

It was found that the reduction-time curves conformed to this equation irrespective of the heating rate and the degree of pre-reduction(6). The rate constants for the four sinters were calculated and are given in Table VI. As a comparison the sinters were subjected to the standard ISO reducibility test and the reduction-time curves treated using equation (1). In the ISO reducibility test the maximum reduction rate occurred at 2.1 CaO/SiO<sub>2</sub> ratio, but in the high temperature test the 1.8 CaO/SiO<sub>2</sub> had the maximum reduction rate, the latter corresponding to the maximum 'melt-down' temperature.

Evidently there is a balance between the reduction reactions and the slag forming reactions, i.e. as the proportion of ferrites in the sinter increases the reducibility increases (at 2.4 CaO/SiO<sub>2</sub> it is possible that the less reducible dicalcium ferrite was present, accounting for the decrease

in reduction rate determined by the ISO reducibility test), but the slag formation reaction, caused by the internal melting of the partially reduced ferrites also increases. The net result is that the high temperature reduction rate is a maximum at 1.8 CaO/SiO<sub>2</sub>.

#### Sinter/Pellet Mixtures

2.4 CaO/SiO<sub>2</sub> sinter/Type A acid pellets: In test A (low pre-reduction and fast heating rate) the sample exhibited the 'melt-down' condition, indicated by the rapid rise in gas pressure drop (Figure 14). As found with other materials, notably Type A acid pellets, the temperature at which 'melt-down' commenced coincided with the start of direct reduction (Figure 15). It is interesting to note that the 'melt-down' temperature of this sinter/pellet mixture is intermediate between that of Type A pellets and the 2.4 CaO/SiO<sub>2</sub> sinter tested at similar levels of pre-reduction and an identical heating rate. This indicates that the pellets weakened the bed or conversely the sinter strengthened the bed. Micro-examination of the sample bed at the conclusion of the test revealed that the iron silicate slag from the acid pellets was advancing through the bed, filling the pores of the sinter particles and the voids of the bed.

At the low level of pre-reduction and the slow heating rate (Test B), the gas pressure drop showed a steady increase with no sign of 'melt-down' occurring (Figure 14). The final level of reduction was very high, in excess of 90% (Figure 15). With the high level of pre-reduction and the fast heating rate again no sign of a 'melt-down' situation occurred and a fairly high degree of reduction was reached (Figures 14 and 15).

The situation with sinter/pellet mixtures is analogous to that of sinter or pellets alone, i.e. fast heating rates and a low level of pre-reduction cause premature 'melt-down' of the bed. Slow heating rates and a low level of pre-reduction or a fast heating rate with a high degree of pre-reduction are conditions that maintain bed permeability, produce a large amount of gaseous reduction and a high 'melt-down' temperature.

1.8 CaO/SiO<sub>2</sub> sinter/Type B acid pellets: It was desirable to determine the ratio of sinter:pellets at which the 'melt-down' temperature of a bed was significantly different from a bed of sinter alone. It has been demonstrated that the 1.8CaO/SiO<sub>2</sub> sinter has the highest 'melt-down' temperature of all the burden materials examined. Hence this series of tests were carried out using this sinter and Type B acid pellets. It has also been shown that the most demanding test conditions are a fast heating rate coupled with a low degree of pre-reduction. If a material behaves well under these conditions then it will perform even better under less demanding conditions. Hence the reason for selecting a low degree of pre-reduction and the 400 deg.C.hr<sup>-1</sup> heating rate for these tests.

As the sinter and pellets were pre-reduced for thirty minutes rather than to a set weight loss, the materials achieved pre-reduction levels slightly different to the levels used for the tests on the individual materials. Consequently the gas pressure drop and reduction curves for the separate materials have been estimated from the relevant 'TRIB diagram'.

Introducing pellets into the sinter bed altered the properties of the bed by

TABLE VI VALUES OF K DETERMINED FOR THE ISO REDUCIBILITY TEST AND THE HIGH TEMPERATURE TEST

Sinter CaO/SiO <sub>2</sub>	ISO Reducibility Test	High Temperature Test
2.4	C.0052min <sup>-1</sup>	0.0063 min <sup>-1</sup>
2.1	C.0058	0.0075
1.8	C.0047	0.0080
1.6	C.0045	0.0067

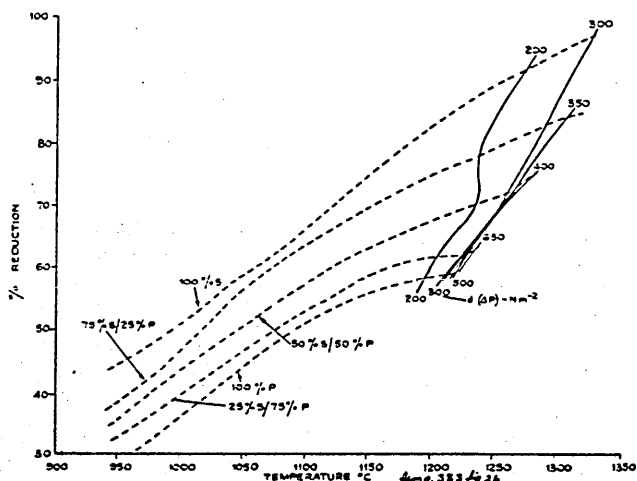


Figure 26 'TRIB diagram' for mixtures of 1.8 CaO/SiO<sub>2</sub> sinter and Type B pellets

the introduction of the 'melt-down' situation. Figure 16 shows that 25 wt.% pellets in the bed provided the beginning of a 'melt-down' situation. At 50 wt.% and above the characteristic rapid rise in gas pressure drop associated with 'melt-down' and direct reduction of the bed occurred (Figure 17).

It was experimentally difficult to make minor adjustments to the proportions of pellets and sinter in the bed and the problem of determining the influence of small variations in the relative proportions were solved by the construction of a 'TRIB diagram' (Figure 26). This diagram shows that the 'melt-down' region occurs at relatively low temperatures with 50% or greater pellets in the bed and to achieve a higher 'melt-down' temperature the pellet proportion must be decreased.

#### Influence of Gaseous Sulphur in the Reducing Gas

Hills<sup>(7)</sup> postulated that sulphur is the cause of melting in the blast furnace due to the formation of a low melting point Fe-S-O eutectic phase. This phase eventually separates into the respective metal and slag phases.

It was estimated that the concentration of gaseous sulphur, calculated on an elemental basis, in the tuyere region of a blast furnace was of the order of 0.28 vol. % (assuming complete gasification of all the sulphur in the oil and the coke at the tuyere). The test with Type A pellets at the fast heating rate with 0.28 vol. % sulphur showed that the

'melt-down' temperature decreased by ~15 deg.C (Figure 18). The rate of reduction actually accelerated before reaching a plateau beneath the reduction level attained without sulphur in the reducing gas (Figure 19).

To account for recirculation of sulphur inside the blast furnace, which acts to increase the concentration, a second test was carried out using a concentration of sulphur in elemental terms of 0.75 vol. %. This produced a decrease in the 'melt-down' temperature of ~150 deg. C, (Figure 18). The reduction rate still accelerated in the early stages before reaching a plateau below the 0.28 vol. % sulphur test, (Figure 19). Takahashi et al<sup>(8)</sup> also found that injection of sulphur dioxide into the reducing gas caused an acceleration of reduction rate, although they offered no explanation of the phenomena.

Micro-examination of the samples after the test revealed the presence of the low melting point Fe-S-O eutectic phase, the proportion of which was related to the lowering of the 'melt-down' temperature. The presence of substantial quantities of liquid in the bed will obviously hinder the reduction of wustite; but the initial acceleration in the reduction rate may be caused by the more favourable kinetics of oxygen removal from the bed, i.e. a change from a solid/gas reaction to a liquid/gas reaction. As the quantity of liquid increases it effectively seals the pores, causing the rise in the gas pressure drop and limits diffusion of gas into the sample, thus stopping the reduction reaction.

The presence of the low melting point Fe-S-O eutectic phase is evidently responsible for the lowering of the 'melt-down' temperature and it was thought that a slower heating rate would allow the sample to reduce more prior to 'melt-down', hence increasing the 'melt-down' temperature. The results of such a test, however, shows that the 'melt-down' temperature actually decreased (Figure 18). The reduction rate in this case could not be calculated because of the extensive loss of molten material from the sample bed, but the occurrence of direct reduction during the test was evident from the high level of carbon monoxide in the outlet gas. Chemical analysis of the sample after the test indicated that the degree of reduction had increased relative to the other two samples, but the proportion of sulphur also increased (Table V). This indicates that a mass effect is dominating the reduction, i.e. at the 200 deg.C.hr<sup>-1</sup>

heating rate the mass of sulphur entering the sample bed in a given temperature span is twice that entering at the 400 deg.C.hr<sup>-1</sup> heating rate.

The 1.8 CaO/SiO<sub>2</sub> sinter has been shown to have the highest 'melt-down' temperature of all the materials examined and it was interesting to study the effect of gaseous sulphur upon this sinter, especially in the light that the high basicity may influence the melting by the formation of calcium sulphide, i.e. the presence of calcium sulphide may minimise the quantity of Fe-S-O eutectic. Figure 20 shows that the presence of sulphur decreased the amount of gaseous reduction. The acceleration of reduction rate detected with acid pellets did not occur, but the presence of sulphur introduced a 'melt-down' condition, which was absent in the test without sulphur in the gas.

Optical and electron probe microscopy of the sample after the test showed that in some regions wustite grains were surrounded by a sulphur rich iron phase within which were precipitated needles of calcium silicate (containing some iron). This indicates that during the test some of the iron oxide grains remained solid whilst a molten sulphur rich phase was formed, within which calcium silicate needles precipitated, either during the test or on cooling. Although requiring further study it may be that the kinetics of calcium silicate formation are more favourable than calcium sulphide formation. Calcium silicate formation effectively removes the beneficial calcium from the system and may account for the introduction of the 'melt-down' stage below 1350°C. Consequently it may be that because of calcium silicate formation the presence of calcium in the burden is of little value in preventing premature 'melt-down' caused by sulphur. However, this statement is tentative and requires further experimental work.

#### Influence of Alkali Vapour in the Reducing Gas

Figures 21 and 22 show that the effect of alkali vapour in the reducing gas was to raise the 'melt-down' temperature and the final level of reduction. That is an improvement in properties rather than the deterioration which may have been expected due to the formation of a low melting point slag. Takahashi et al(8) also found that alkali vapour caused an improvement in reducibility during isothermal tests. Blefuss(9) attributed the increase in reduction rate of burden materials in

the presence of alkali to the non-topochemical reduction reaction leaving exposed large areas of oxide to the reducing gas. Khalafalla and Weston(10) verified experimentally that alkali acted as a catalyst and found that there was an optimum alkali level producing the maximum reducibility, increases above which caused the reducibility to drop because of slag formation.

In the work discussed in this paper, non-topochemical reduction was evident along with the production of a relatively fine grained iron shell around the pellets. The nature of the iron shell was such that it imparted considerable physical strength to the bed, minimising the extent of bed contraction and acting as a barrier to the flow of liquid slag from the pellet core. This is the reason for the rise in 'melt-down' temperature with increase of the alkali loading. Further work is necessary to determine if an optimum alkali loading exists above which extensive slag formation limits the reduction rate.

It is obvious from the chemical analyses (Table V) that the alkali is entering the slag phase, but it cannot significantly increase the volume of the slag nor the initial melting point (as alkali is already inherent in the residual slag and it would require a considerable alkali pick-up to further lower the melting point by a marked amount).

Although only one material has been examined with alkali vapour in the reducing gas, the choice of acid pellets was reasonable because alkali is more likely to be absorbed by siliceous material than basic material. These tests have shown that alkali in the proportions used, can be beneficial to the softening-melting characteristics. Consequently other materials should not be affected detrimentally, indeed an improvement as found in this work may occur. One problem that may occur especially at lower temperatures is pellet swelling, which was not encountered with Type A pellets.

It is interesting to contrast the effect of the two major recirculating phases in the blast furnace, namely sulphur and alkalis. Sulphur has been shown to be detrimental by lowering the 'melt-down' temperature and the degree of gaseous reduction; alkalis have been shown to be beneficial due to their influence upon the rate of reduction and the production of a fine iron shell which restrains fluid flow and imparts a high physical strength. It is difficult to see alkali having a marked influence

upon the slag formation process unless present in considerable quantities. The alkali inherent in the burden material is most likely the important species, if this level is high then the initial melting point of the slag phase will be low and the liquid slag will limit gaseous reduction at relatively low temperatures. Alkali vapour species in the gas would appear to only accelerate the gaseous reduction reaction although they do enter into the slag with apparently no ill effects.

Sulphur forms a low melting point Fe-S-O eutectic phase which is an additional liquid phase to the liquid slag already present (from the wustite/residual slag reaction). Naturally the two slags will eventually merge together to form one slag, but the slag volume will be increased in this case compared with the situation without sulphur. This increased slag volume and the lack of an accelerating influence upon the reduction rate causes the deterioration in 'melt-down' temperature and a decrease in the extent of gaseous reduction.

The joint sulphur and alkali test showed that the 'melt-down' temperature is between the two extremes of sulphur and alkali only (Figure 23). It is interesting to observe that although the gas pressure drop curve is closer to the sulphur-only curve, the reduction-temperature curve is more akin to the alkali-only curve up to 1075°C (Figure 24). This indicates that the alkali is definitely influencing the reduction mechanism, but the dominance of the detrimental sulphur eventually shows.

#### Iron Carburisation

Throughout the experimental studies it was possible to observe the mechanism of carbon pick-up by the iron. Iron reduced from iron oxide by gaseous means which did not come into contact with coke or graphite had a negligible carbon content, only iron nitride being present. Metallic iron that was in contact with coke contained a lot of carbon, generally in the form of cementite and pearlite, i.e. a typical white cast iron structure caused by a fast cooling rate and/or a low silicon content. (No silicon was detected in the iron). The melting point of such iron is 1147°C and the micro-structure provided substantial evidence that the iron had been molten. It is likely that the solid iron (zero carbon) makes contact with the coke and the carbon diffuses in, eventually reaching a concentration sufficient to lower the

melting point to the pertaining temperature. Once molten the rate of carbon pick-up will accelerate rapidly. In general carburisation of the iron occurred at the point of contact with coke rather than at a graphite interface, indicating that coke is the more reactive of the two carbon sources. A second mechanism was that liquid iron oxide rich slag contacted the coke causing direct reduction and the formation of metallic iron which subsequently carburised.

In some instances molten iron dripped from the bed into the graphite crucible. This iron had a micro-structure typical of grey cast iron, symbolic of cast iron that was slow cooled or had a high silicon content, (again no silicon was detected in the iron).

#### Application to the Blast Furnace Process

The burden passing through the apex of the cohesive zone in a centre working furnace is exposed to a rapid heating rate. Material near the walls on the other hand is exposed to a much slower rate of heating. Consider the situation at the apex of the zone (layer G-5 in Figure 3). It is obvious that the material is only slightly reduced prior to entry of the cohesive zone because of the relatively short transit time from the stockline to the start of the cohesive zone (Table II). The boundary between the lumpy and the softening zone (X-X in Figure 3) can be thought of as the equivalent of the 3% contraction measured in the experimental tests, i.e. 985°C for Type A acid pellets and ~1100°C for all the sinters examined. The temperature indicated by the Japanese dissection studies is ~1100°C for furnaces operating on ~80% sinter burdens. The journey of the burden through the cohesive zone is rapid and time for reduction is limited, which is analogous to the situation with materials tested experimentally having a low degree of pre-reduction and at the fast heating rate. Tests of this nature lead to blockage of the voids of the bed and the replacement of indirect reduction by direct reduction. This stage is equivalent to the boundary Y-Y in Figure 3.

In portion A the metal and slag starts to drip out into the underlying coke bed where the latter undergoes direct reduction. The icicles found by the Japanese dissection studies are of particular interest, consisting of a metallic shell with slag adhered to it and a hollow interior<sup>(4)</sup>. Identical



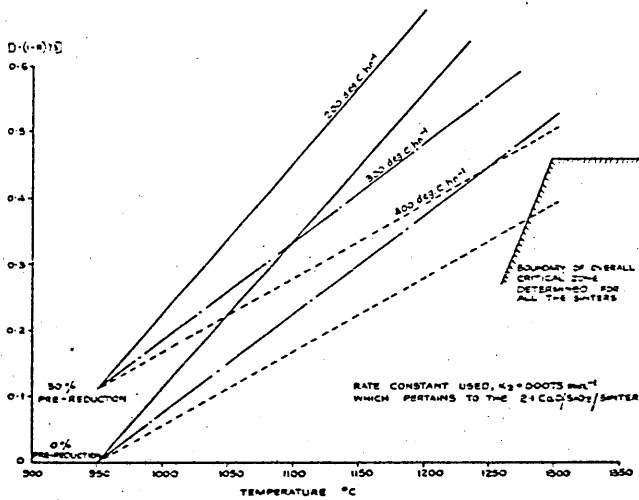
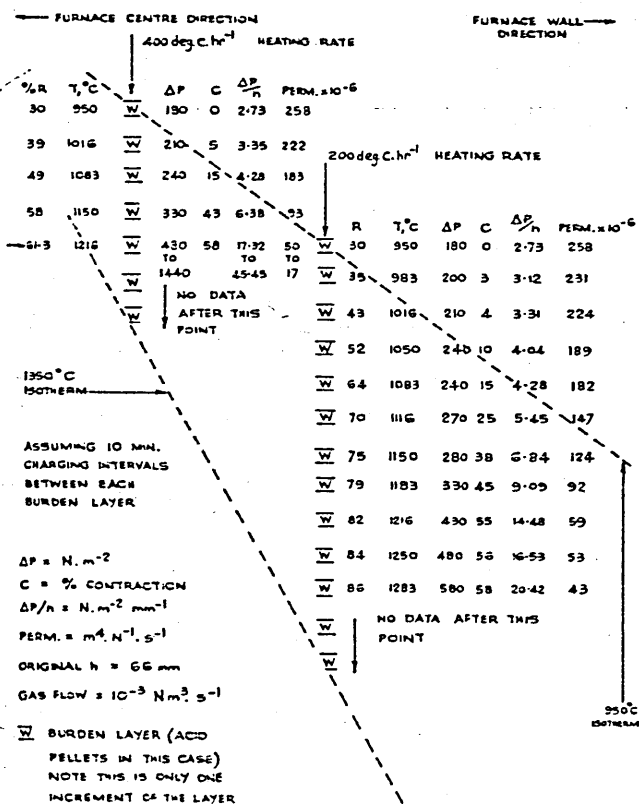


Figure 28 Influence of pre-reduction and heating rate upon entry into the critical zone



lower the CaO/SiO<sub>2</sub> ratio of the sinter and decrease the proportion of acid pellets in the burden as the new burden may possess a higher 'melt-down' temperature than the original 50/50 pellet/sinter burden. Obviously it would be necessary to carry out the appropriate experimental work or estimate the effect of such a change using the existing data.

One method that should be avoided is the layer charging of acid pellets and superfluxed sinter as the pellets will become impermeable in the central region of a centre working furnace. These impermeable layers might restrict the gas flow in the sinter layers decreasing the extent of gaseous reduction.

Gaseous sulphur lowers the 'melt-down' temperature of both acid pellets and sinter by a considerable margin with less than 1 vol. % of sulphur in the reducing gas. The experimental work although clearly demonstrating the detrimental effect is not typical of the situation occurring in the blast furnace, i.e. in the experimental work the concentration of sulphur in the reducing gas was maintained constant yet in the blast furnace the concentration gradually increases as the temperature rises. (The Japanese dissection studies show that the maximum sulphur level in the burden occurs just prior to 'melt-down'). Such a gradual increase of sulphur would benefit high temperature properties because the oxygen content would be decreased before the sulphur level became sufficient to produce large volumes of the Fe-S-O eutectic. The Japanese dissection studies show that the 'melt-down' temperature is ~1500°C near the walls and 1350°C in the central region of Hirohata No.1 (Figure 2). In contrast the 1.8 CaO/SiO<sub>2</sub> sinter tested had a 'melt-down' temperature of 1200°C, but if the sulphur level had been subject to a gradual increase during the test than the 'melt-down' temperature would have been greater.

Alkali vapour has proved to be beneficial to the softening-melting properties of acid pellets (a burden material that is commonly held to be prone to the 'detrimental influence' of alkali). The information from the Japanese dissection studies<sup>(4)</sup> shows that the alkali level of the burden in the cohesive zone is in good agreement with the alkali concentrations in the experimental tests. Consequently it is difficult to see alkali that is not inherent in the burden having a detrimental influence on the softening-melting properties.

## Conclusions

1. The factors that determine the 'melt-down' temperature of burden materials are the degree of reduction and the temperature. A low degree of reduction persisting up to a high temperature produces an impermeable bed and a relatively low 'melt-down' temperature coupled with an appreciable quantity of direct reduction. A high level of reduction, achieved at low temperatures, produces a relatively high 'melt-down' temperature coupled with a permeable bed and a high degree of gaseous reduction. This information has been conveniently summarised on 'Temperature-Reduction-Isotherm diagrams'.
2. Whether a material has a high or a low 'melt-down' temperature depends on the balance between the reduction and the slag formation reactions. If the former dominates bed permeability is maintained and the 'melt-down' temperature is high. Domination by the slag forming reaction makes the bed impermeable and lowers the 'melt-down' temperature. Fast heating rates favour the slag forming reaction and slow heating rates favour the reduction reaction. Slow heating rates do not cause problems in terms of the high temperature properties of burden materials.
3. In the range of sinter basicity studied the maximum 'melt-down' temperature and the maximum degree of gaseous reduction occurred at 1.8 CaO/SiO<sub>2</sub>.
4. Introducing acid pellets into a sinter bed lowers the 'melt-down' temperature and the proportion of gaseous reduction. This is especially noticeable at 50% or more of pellets in the bed.
5. Sulphur in the reducing gas has a dramatic detrimental influence upon the permeability of the bed due to the formation of the low melting point Fe-S-O eutectic.
6. Alkali vapour has proved to be beneficial to the high temperature properties of acid pellets causing an increase in reducibility and a rise in 'melt-down' temperature due to the formation of a fine grained iron shell around the pellets which effectively prevents flow of slag into the voids of the bed.

### Nomenclature

- k = a rate constant, mm  
t = time of reaction, minutes  
R = fractional reduction

### Acknowledgements

The author would like to thank Dr A W D Hills and Dr G Briggs of Sheffield Polytechnic and Mr F B Traice of the British Steel Corporation for their advice and discussions during the course of this work.

Finally, I would like to thank the British Steel Corporation for granting their permission to publish this paper.

### References

1. Sasaki, K, et. al. Trans. ISI Jap. vol. 17, 1977, 252-261.
2. Kanbara, K, et. al. *ibid*, 371-380.
3. Shimomura, Y, et. al. *ibid*, 381-390.
4. Sasaki, M, et.al. *ibid*, 391-396.
5. Kojima, K, et.al. *ibid*, 401-409.
6. Clixby, G, to be published in Ironmaking and Steelmaking.
7. Hills, A W D, Heat and Mass Transf in Process Metallurgy. Institute Mining and Metallurgy, London 1967, 39-77.
8. Takahashi, R, et.al. "Effects of gaseous components within blast furnace on softening-melting behaviour of agglomerates". AIME Ironmaking Proceedings, Chicago 1978, 78-87.
9. Bleifuss, R L, "Single particle studies applied to direct reduction and blast furnace operations" Blast Furnace Technology Science and Practice. Proceed. of the CC Furnes Memorial Conference on Ironmaking Technology, Buffalo, October 1970.
10. Khalafella, S E and Weston Jnr, P L Trans. AIME, vol. 239, October 1967 1494-1499.
11. Moon J T and Walker R D, Ironmaking and Steelmaking 1975, 2(1), 30-35.